eman ta zabal zazu

Universidad del País Vasco

Euskal Herriko Unibertsitatea

Departamento de Fisiología
Facultad de Medicina y Odontología

Role of TREM2 receptor during the progression of liver disease; from acute liver injury, to chronic liver disease and the development of hepatocellular carcinoma (HCC)

Tesis presentada por
AITOR ESPARZA BAQUER

San Sebastián
2018

Role of TREM2 receptor during the progression of liver disease; from acute liver injury, to chronic liver disease and the development of hepatocellular carcinoma (HCC)

Tesis presentada por
Aitor Esparza Baquer

Para la obtención del título de doctor en
Investigación Biomédica **por la**
Universidad del País Vasco/Euskal Herriko Unibertsitatea

Tesis dirigida por
Dra. Dña. María Jesús Perugorria Montiel
Dr. D. Luis Bujanda Fernandez de Piérola

This study was funded by the University of the Basque Country (UPV/EHU) (PIF2014/11) and by the short-term training fellowship Andrew K. Burroughs (European Association for the Study of the Liver, EASL).

ACKNOWLEDGEMENTS

The development of a doctoral thesis is a long and laborious path in which we try to overcome the obstacles, problems and difficulties we find, not always with success. But, fortunately, I have shared this path with people who have helped and encouraged me to keep walking it and to whom today I would like to thank their friendship, support and affection.

First of all, I would like to thank my PhD directors for giving me the opportunity to develop this doctoral thesis. Dr. María Jesús Perugorria, Matxus, thank you very much for selecting me to carry out this thesis and for always teach me. I will never forget the hours working together in the animal facility and in the cell culture room isolating cells. Thank you very much for showing me how is excellent science done and also how the scientific world works. I would like to thank my PhD director Dr. Luis Bujanda for his constant support, and because you are always ready to help us.

I would like to take this opportunity to thank Dr. Jesús Bañales, Txus, for all the ideas you have given me during all these years and for your constant effort in promoting all the members of the group, you have created an excellent research group.

I would like to specially thank all the members of the liver disease group "hepato". For their constant support, friendship, collaboration and the good atmosphere. I will always be grateful for putting me up during all these four years of PhD, for being there in the good times and also in the bad ones. We have shared laughter, tears, anger and endless conversations in which we fixed the world (or at least we tried). I also want to thank the coffee hour, all the catchy songs we have invented, that summer of 2015, which was so important for us and also to the last of the Philippines, which always closed the lab. In short, I thank you for forming such an incredible human team!

Aiii Ibone, how many moments we have shared together! Since I came here, you have been my main support. Working with you is so amazing that it will be really strange not working beside you... I will always remember all the frustrations that we have shared (chronic animal models, 4-HNE ELISA, reviews...), thanks to you they were far easier. Fortunately we have also shared a lot of good moments; I will specially miss the confidences we had when working on the hood. For all this and because I cannot think about a better person to share a work project with, I would like to thank you all the help and support you gave me through all these years, MANY THANKS! I am sure you will have a promising future.

Oihane, thank you very much, because when I really needed and without asking it, you helped me a lot with the SOX revision. For me, you have been the reference of the lab, you

have taught me thousand techniques and how to organize the experiments and I will always be always grateful for that.

To Ander, we miss you a lot in the lab! Fortunately, Paris is not far away and we see you quite often. Thank you very much for everything you have taught me, for all the good times we had in the lab and outside it and also for your pistachios!
To Pedro, although you have only been with us for half a year, it seems you have been here from the beginning; I would like to thank you because you put a lot of energy and effort in all you do. You are a very good scientist and a better "pintxo-pote" partner.

Ainhoa, because this group would miss a lot without you. Your joy and sense of humor are essential for the group, never change! Paula, you know everything, you are a great researcher and a better person, in short, thank you for being as you are. Álvaro, you help us every day with your good sense of humor and with your jokes, which are as bad as funny, thanks for being always there when needed. Laura, I would like to thank you for being the voice of sanity and for organizing everything in the lab, because you are a great person and you always want to improve the laboratory and the group. To Javi, because although I deeply hate the scares you give me, with your joy and humor you cheer up the group every day. You are almost there!

To Elisa and Mirian, thank you very much for being part of this group, the six months you were here were probably the best of my thesis, in part thanks to you. I will always remember the good atmosphere you generated, how fun was to give you Basque lessons and also all the songs we invented. I hope you all the best, because you deserve it. Patri, I want to thank you for all the techniques you taught me, this laboratory is what it is thanks to you. Thank you very much Maite, although you left the lab years ago, you are always present. Many thanks to Puyi, for giving me the opportunity to improve my English and also for giving me the honour to be the coffee master in your absence. I hope you all the best. Also, I do not want to forget the new members and the people who left the lab: Nuno, Nerea, Aloña, Anne, Leire, Maider ... I wish you the best in your scientific career.

I would like to thank the contribution of the people from the Biodonostia Institute. Many thanks also to Mikel, Tatiana, Claudia, Jaione, Junkal… and to all the researchers of the Biodonostia Institute, because you are always willing to help, both with your scientific advice and for all the kits and lab material we take from you, always with permission, throughout these years, this has greatly facilitated my thesis, thank you! Particularly, I would like to thank Leire, it seems that we live parallel lives; we met each other working at the University in the marmota monax project and we met again here at Biodonostia. We have

shared so many moments together and now we are about to separate... I would like to give you a thousand thanks for everything you taught me, for all the moments we have experienced together and hope you all the best with your research career, I am sure that you will do a fantastic viva!

I am very grateful to the people from the Newcastle Fibrosis Research Group, especially to Prof. Derek Mann and Prof. Jelena Mann for giving me the opportunity to stay in the group. To Prof. Fiona Oakley, for helping and supporting me with this project. To Hanna, Julia, Michelle, Arianna, William, Marco… thank you very much for helping me with the experiments and with everyday life in the lab. Also, I would like to thank the Spanish team: Laura, Marina and Alicia, thank you very much for everything, for the beers, the coffees, the parties, the trips… I am also very grateful to the people from the Medical University of Vienna, and especially to Dr. Omar Sharif, for his constant help and support.

And since not everything in the thesis is the laboratory life, I also want to thank all the people with whom I have lived and made plans during these four years. To the "pintxo-potes" of Amara, to the "desayuno con diamantes" and to the "pisukides". To the people from Bilbo, to Ana, Carlos, Esti ... I have passed almost more weekends in Bilbo than in Donostia, we have made so many plans, hikes, trips to Japan, New York, the way of Santiago... To my friends from Iruñea, even though we are all scattered, we will always be the "kuadrilla". I promise that after the viva I will resume my social life with you. Thank you very much for all the encouragement during these years and for helping me when I am down. Thanks a lot!

Finally, I reserve the last thanking words to the most important people in my life, my family. Thank you very much for always being there, for unconditionally supporting me in all the adventures I decide to take, I love you. To my mother, you are the referent of my life, a natural born-fighter. To Unai and Cris, thank you for always being there, for all the support and for understanding me. To my grandmother, the rest of the family and those who are no longer here, thanks for everything you taught me and for all the support, thank you. Finally, I would like to thank Xabi for all the help and support you gave me during the last two years. Because we have had a great time together and because a lot more will come, many thanks. Although it is difficult, you understand the moments of stress and anxiety that I had and thanks to the happiness, joy, good humor, positivism and support I received from you I was been able to carry out this thesis. I will compensate you for all the food that you have cooked for me from January onwards. I love you.

ABBREVIATIONS

4-HNE	4-hydroxynonenal
A1CF	APOBEC1 complementation factor
AACS	Acetoacetyl-CoA synthetase
Abx	Antibiotics
ACTA2	Actin alpha 2, smooth muscle
AD	Alzheimer’s disease
ALD	Alcoholic disease
ALF	Acute liver failure
ALT	Alanine aminotransferase
APAP	Acetaminophen
APC	Antigen presenting cells
αSMA	Alpha smooth muscle actin
AST	Aspartate aminotransferase
ATP	Adenosine triphosphate
ATP5H	ATP synthase subunit d, mitochondrial
AU	Arbitrary units
BAMBI	BMP and activin membrane bound inhibitor
Bax	B-cell lymphoma 2 associated X
Bcl2	B-cell lymphoma 2
Bcl2l1	B-cell lymphoma 2-like 1
BCLC	Barcelona clinic staging cancer
BDL	Bile duct ligation
BHA	Butylated hydroxyanisole
BM	Bone marrow
BMDM	Bone marrow-derived macrophages
BrdU	5’-bromo-2’-deoxyuridine
BSA	Bovine serum albumin
CC50A	Cell cycle control protein 50A
CCl_4	Carbon tetrachloride
CCR2	Chemokine (C-C motif) receptor 2
CEEA	Comité ético de experimentación animal
CFU	Colony-forming unit
cDNA	Complementary deoxyribonucleic acid
CID	Collision-induced dissociation
COL1A1	Collagen type 1 alpha 1
Cybb	Cytochrome b-245 beta
Cxcl1	C-X-C motif ligand 1
DAB	3,3-diaminobenzidine
DAMPs	Damage-associated molecular patterns
DAP-12	DNAX-activation protein 12
DAVID	Database for annotation, visualization and integrated discovery
DEN	Diethylnitrosamine
DHR123	Dihydrorhodamine 123
DILI	Drug-induced liver injury
DMEM	Dulbecco's modified eagle medium
DNA	Deoxyribonucleic acid
dNTPs	Deoxy-nucleotide-triphosphate
ECM	Extracellular matrix
E. coli	Escherichia coli
EDTA	Ethylenediaminetetraacetic acid

EGF	Epidermal growth factor
EGFR	Epidermal growth factor receptor
ELISA	Enzyme-linked immunosorbent assay
EMA	European medicines agency
EMT	Epithelial-mesenchymal transition
ENTP5	Ectonucleoside triphosphate diphosphohydrolase 5
ERK1/2	Extracellular signal-regulated kinases ½
FADS2	Fatty acid desaturase 2
FBS	Fetal bovine serum
FCCP	Carbonyl cyanide-4-(trifluoromethoxy)phenylhydrazone
FCS	Fetal calf serum
FDA	Food and drug administration
FGF	Fibroblast growth factor
FGFR	Fibroblast growth factor receptor
FITC	Fluorescein isothiocyanate
GAPDH	Glyceraldehyde 3-phosphate dehydrogenase
GFP	Green fluorescent protein
γH2AX	Phospho-histone H2A.X
GNA1	Glucosamine 6-phosphate N-acetyltransferase
GO	Gene ontology
H&E	Hematoxylin and eosin
DCF	2'-7'-dicholodihydrofluorescein diacetate
H_2O_2	Hydrogen peroxide
HAV	Hepatitis A virus
HBsAg	Hepatitis B surface antigen
HBSS	Hanks' balanced salt solution
HBV	Hepatitis B virus
HCC	Hepatocellular carcinoma
HCV	Hepatitis C virus
HEPES	4-(2-hydroxyethyl)-1-piperazineethanesulfonic acid
HEV	Hepatitis E virus
HGF	Hepatocyte growth factor
HIV	Human immunodeficiency virus
Hmox1	Heme oxygenase 1
HRP	Horseradish peroxidase
HSC	Hepatic stellate cell
HSDL2	Hydroxysteroid dehydrogenase-like protein 2
Hspa1b	Heat-shock family member 1b
IBD	Inflammatory bowel disease
i.e.	Latin: id est (it is)
IFNγ	Interferon γ
IGFBP1	Insulin like growth factor binding protein 1
IgG	Immunoglobulin G
IgG2B	Immunoglobulin gamma 2b chain
IHC	Immunohistochemistry
IKK	IκB kinase
IL	Interleukin
IL1B	Interleukin 1B
IL1BR	Interleukin 1B receptor
IL6	Interleukin 6

IL6R	Interleukin 6 receptor
IL8	Interleukin 8
IRGM1	Immunity-related GTPase family M protein
1ITAM	Immunoreceptor tyrosine-based activation motif
ITIM	Immunoreceptor tyrosine-based inhibition motif
IU	International units
IVC	Inferior vena cava
JNK	C-Jun N-terminal kinase
KC	Kupffer Cell
LC-MS	Liquid chromatography - mass spectrometry
LDL	Low density lipoprotein
LPS	Lipopolysaccharide
LSEC	Liver sinusoidal endothelial cell
MAPK	Mitogen-activated protein kinases
MCP1	Monocyte chemoattractant protein 1
Mip-1β (CCL4)	C-C motif chemokine ligand 4
MMPs	Matrix metalloproteases
mRNA	Messenger ribonucleic acid
MS	Mass spectrometry
Myd88	Myeloid differentiation primary response gene 88
NAFLD	Non-alcoholic fatty liver disease
NAPDH	Nicotinamide adenine dinucleotide phosphate
NAPQI	N-acetyl-p-benzoquinone imine
NASH	Non-alcoholic steatohepatitis
NEEA	Non-essential amino acids
NF-κB	Nuclear factor kappa B
NK	Natural killer
NKT	Natural killer T cell
NT	Not tested
NU1M	NADH-ubiquinone oxidoreductase chain 1
O.Oil	Olive oil
OCR	Oxygen consumption rate
PAMPs	Pathogen associated molecular patterns
PBS	Phosphate buffered saline
PCNA	Proliferating cell nuclear antigen
PD-1	Programmed death receptor 1
PerCP	Peridinin chlorophyll protein complex
PHx	Partial hepatectomy
PLOSL	Polycystic lipomembraneous osteodysplasia with sclerosing leukoencephalopathy
PPAR	Peroxisome proliferator-activated receptor
PROD	Proline dehydrogenase 1, mitochondrial
PRRs	Pattern recognition receptors
qHSC	Quiescent hepatic stellate cell
qRT-PCR	Quantitative real-time polymerase chain reaction
RANTES (CCL5)	C-C motif chemokine ligand 5
RIPA	Radio-immunoprecipitation assay
RNA	Ribonucleic acid
ROS	Reactive oxygen species
RPMI	Roswell park memorial institute medium 1640

RT	Reverse transcription
SAPK	Stress-activated protein kinases
SD	Standard deviation
SDS-PAGE	Sodium dodecyl sulfate polyacrylamide gel electrophoresis
SEM	Standard error of the mean
SGPL1	Sphingosine-1-phosphate lyase 1
SIRS	Systemic inflammatory response syndrome
STAT3	Signal transducer and activator of transcription 3
sTREM	Soluble triggering receptor expressed on myeloid cells
T-TBS	Tris buffered saline with 0.1% Tween 20
TCGA	The cancer genome atlas
TERT	Telomerase reverse transcriptase
TGF	Transforming growth factor
Tgfb1	Transforming growth factor beta-1
TGFBR	Transforming growth factor beta receptor
TIMPs	Tissue inhibitors of metalloproteases
TLR	Toll-like receptor
TNF	Tumor necrosis factor
TNFR1	Tumor necrosis factor receptor 1
TREM	Triggering receptor expressed on myeloid cells
TREML	Triggering receptor expressed on myeloid cells like
UPLC	Ultra performance liquid chromatography
VEGF	Vascular endothelial growth factor
WNT3	Wnt family member 3
WNT7A	Wnt family member 7A
WT	Wild type
Z3SF	Zone 3 sinusoidal fibrosis

INDEX

INTRODUCTION

I.1 The liver

The liver is the largest internal organ of the human body and one of the most important organs for the maintenance of the metabolic homeostasis in our body. The liver performs vital functions including the synthesis, metabolism, storage and redistribution of nutrients. In addition, due to its localization, the liver is exposed to a variety of toxic compounds, the detoxification and neutralization of these toxins is one of the vital functions that the liver performs (1, 2).

I.1.1 *Anatomy*

The liver is arranged in hexagonal subunits named hepatic lobules (**Figure I.1**). The hepatic lobule is organized around a central vein and is structured by the confluence of the hepatic sinusoids. The hepatic sinusoids drain the blood from one branch of the portal vein and from another branch of the hepatic artery. Between the hepatic sinusoids are located the hepatocytes, these cells are arranged radially forming rows around the central vein. In the vertex of the hepatic lobules is located the portal triad, which is formed of connective tissue and contains a branch of the hepatic artery, a branch of the portal vein and a bile duct. To the latter reaches the bile produced by hepatocytes through a network of canaliculi (1, 2) (**Figure I.1**).

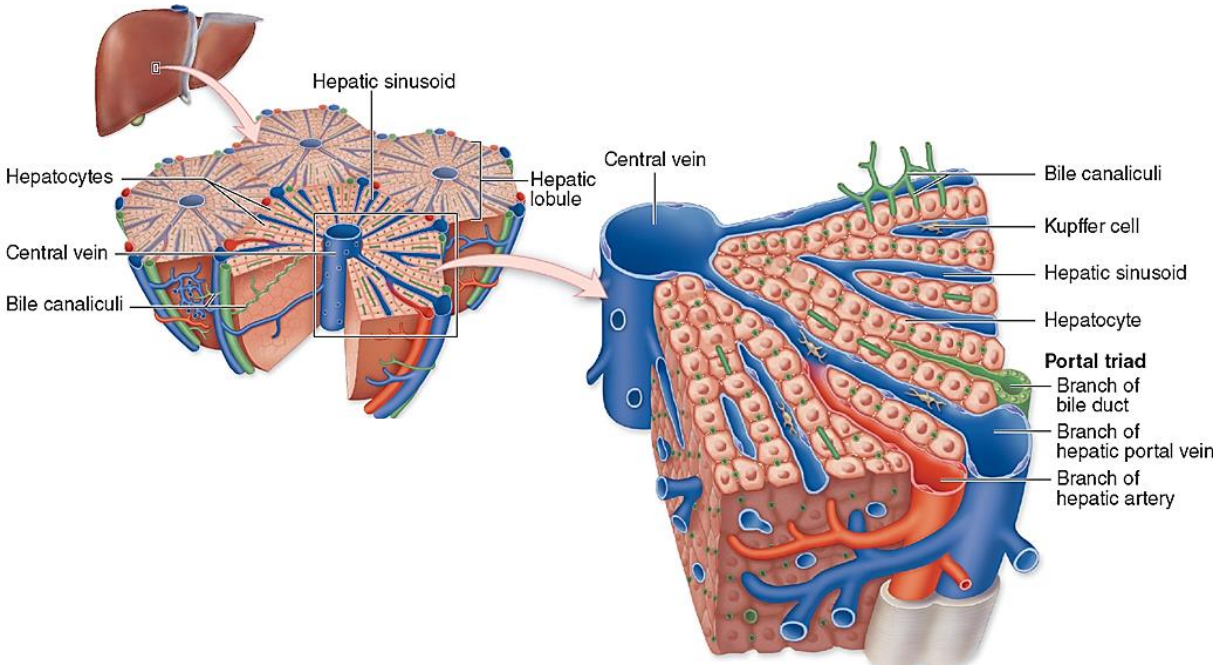

Figure I.1. Structure of the liver and the hepatic lobule. The liver is structured in hexagonal hepatic lobules which are arranged around a central vein. (Adapted from Mescher et al, 2013).

The perisinusoidal space or space of Disse is located between the hepatic sinusoids and the hepatocytes and contains a network of reticular fibers and blood plasma. In the perisinusoidal space takes place the metabolic exchange between the hepatocyte and the plasma (1, 2).

I.1.2 Microscopic anatomy of the liver

The liver consists of two types of epithelial cells, hepatocytes and cholangiocytes. About 70-80% of the liver volume is occupied by parenchymal hepatocytes which are large cuboidal or polyhedral epithelial cells that are often binucleated. These cells are responsible of performing the majority of the metabolic functions of the liver (1, 2).

The non-parenchymal liver cells of the liver include populations of cholangiocytes, liver sinusoidal endothelial cells (LSECs), hepatic stellate cells (HSCs), Kupffer cells (KCs) and intrahepatic lymphocytes. Cholangiocytes are the epithelial cells that line-up the biliary duct, they only represent the 3-5% of the liver cells but they carry out important functions in bile modification and transport (3-5). HSCs are present in the space of Disse, these cells store vitamin A, produce extracellular matrix (ECM) and are the main pro-fibrogenic cells (6). The liver sinusoids are lined with two types of cells, sinusoidal endothelial cells and phagocytic KCs. KCs are the resident macrophages in the liver, they have cytokine-producing phagocytic activity and together with lymphocytes form part of the immune system in the liver (7). In addition, LSECs perform an important function in filtering metabolites. For that, these cells have small fenestrations that allow the free diffusion of many substances between the blood and the hepatocytes (8) (**Figure I.1**).

I.1.3 Physiological functions of the liver

The liver is responsible for multiple functions and plays a central role in metabolism. For that, hepatocytes contain thousands of enzymes that are able to perform key metabolic functions such as the oxidative energy metabolism, carbohydrate metabolism, lipid metabolism, amino acid and nitrogen metabolism, bile formation and secretion and the metabolism of xenobiotics. In addition, the liver also serves as a reservoir of glucose, lipids, iron and vitamin A (in HSCs) and other vitamins. Among other functions that the

liver carries out are also the synthesis and secretion of albumins, apolipoproteins, transferrins, fibrinogen and other plasma proteins to the blood (2).

I.2 Liver injury

The liver plays an important role in the detoxification of drugs, xenobiotics and toxic metabolites and thus, due to its constant exposure to harmful agents is susceptible to damage and the development of liver disease. Etiologic factors include the chronic infection with hepatitis B virus or hepatitis C virus (HBV or HCV), chronic alcohol intoxication, poisoning, obesity and metabolic-syndrome associated non-alcoholic steatohepatitis (NASH), genetic alterations such as hemochromatosis and α1-antitrypsin deficiency or immune-type damage (9-19). The maintenance of the hepatic function is of paramount importance at a systemic level; if liver function is lost it causes a great impact on the body and may result in the death of the organism (20).

I.2.1 *Acute liver failure*

Acute liver failure (ALF) is a life-threating disease with an increasing incidence in the developing world (20). ALF often occurs without a pre-existing liver disease as commonly arises in healthy adults and may be caused by drug overdose, such as acetaminophen, alcohol overdose, viral hepatitis (especially A, B or E), acute fatty liver of pregnancy or poisoning by *Amanita phalloides* and other amatoxin-producing fungus among others. Clinically, ALF manifests hepatic dysfunction with alterations in the biochemical values of the liver and coagulopathy. It may also cause encephalopathy and organ failure, ultimately leading to death in about 50% of ALFs (**Figure I.2**) (13, 20).

In the developing world ALFs are mostly related to hepatitis viral infection, whereas in the USA and Western Europe viral infection-mediated ALFs are decreasing and drug-induced liver injury (DILI) is now the most common cause of ALFs (**Figure I.2**) (21).

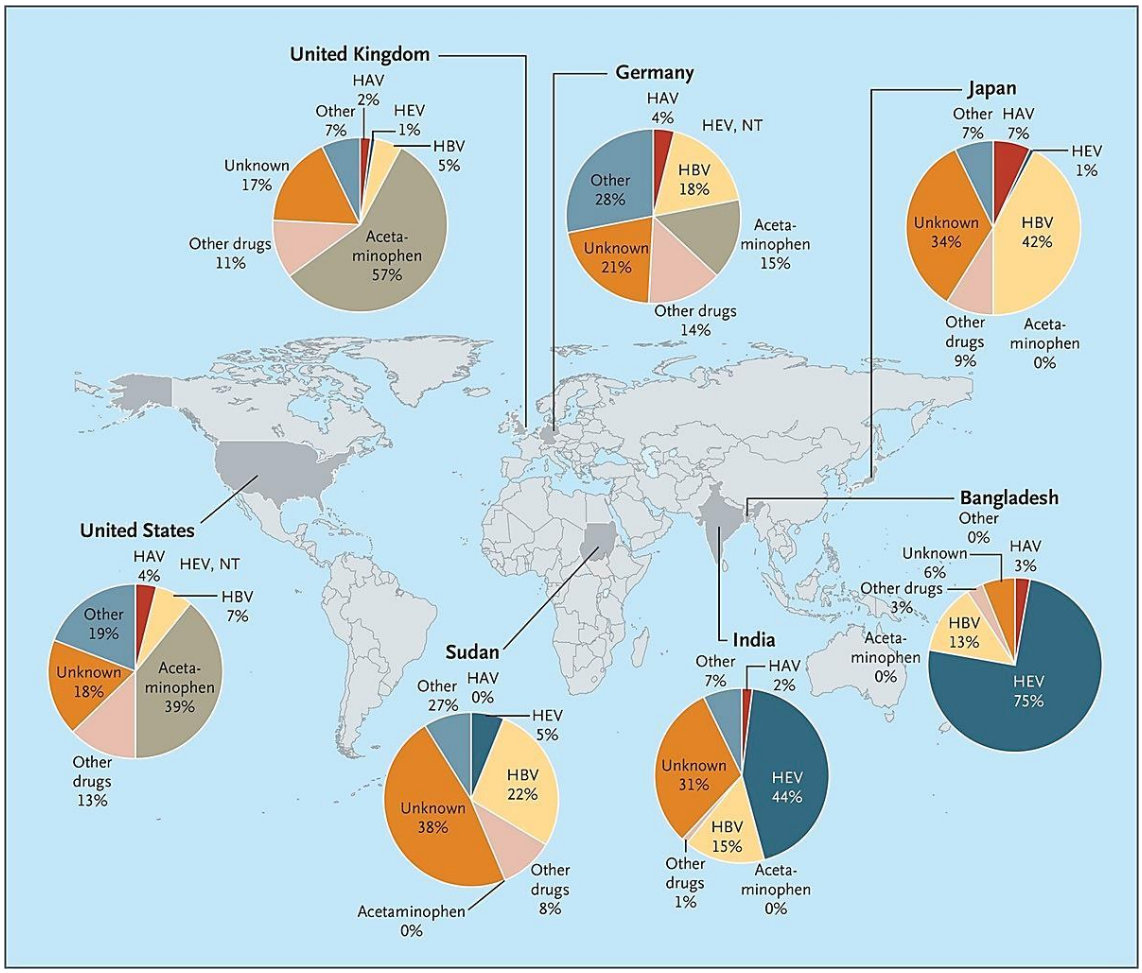

Figure I.2. Acute liver failure cases worldwide. HAV; hepatitis A virus, HBV; hepatitis B virus, HEV; hepatitis E virus NT, not tested. (Adapted from Bernal W and Wendon J, 2013).

I.2.1.1 DILI

DILI is the most common ALF in the developed world with an estimation incidence of 10-15 cases per 100000 inhabitants (13). However, due to the difficulties in the diagnosis, DILI cases may be largely under-estimated (13). Of note, one of the main reasons for the discontinuation of developing and already approved drugs is DILI (22). Acetaminophen (APAP) overdose is the most common DILI and it may represent more than half of all ALFs in some countries of the developed world, up to 70% of the APAP intoxications being reported as suicidal intents (**Figure I.2)** (20).

APAP hepatotoxicity is well established and is caused by N-acetyl-p-benzoquinone imine (NAPQI), which is a highly reactive intermediate metabolite (13). At therapeutic dosage, acetaminophen is mainly metabolized by sulfation and glucuronidation in the liver, while a small part is metabolized by CYP2E1 and CYP3A4 isoenzymes that form NAPQI that is conjugated by glutathione. However, when APAP intoxication occurs,

sulfation and glucuronidation mechanisms are overwhelmed and acetaminophen is oxidized by CYP2E1 and CYP3A4 isoenzymes forming high amounts of NAPQI that cannot be detoxified as the glutathione pool is diminished. NAPQI generates reactive oxygen species (ROS), causes distortions in the nuclear and mitochondrial function, covalently binds to intracellular proteins and may lead to apoptosis and necrosis (13). Importantly, alcohol abuse and obesity have been reported to be risk factors of acetaminophen-mediated ALF (23, 24).

As mentioned earlier, half of ALFs result in death. However, the liver has an extraordinary capacity of regeneration and therefore, if the injury is not fatal, liver regeneration will be triggered in order to recover the lost liver mass and function (25, 26).

I.3 Mechanisms of liver regeneration

After a liver injury, the architecture and function of the liver are compromised and as a consequence, liver regeneration is triggered. A central event in this scenario is the death of the hepatocyte. The death of this parenchymal liver cell triggers a powerful inflammatory and regenerative response that tries to restore the lost liver tissue (27, 28). Liver regeneration involves several molecular and cellular mediators, such as cytokines, chemokines and growth factors and the involvement of different cell-types including resident macrophages. Liver regeneration is triggered immediately after the injury and is fundamental for the activation of the proliferation of viable hepatocytes and therefore, for the recovery of the liver mass and its function (25, 29).

For the study of liver regeneration animal models such as partial hepatectomy (PHx) in rodents are widely used (30). These animal models have helped us to gain knowledge about the early responses that trigger the regenerative process after a liver resection (29, 30). The immune system plays a very important role in the normal liver regeneration. In this sense, interleukin 6 (IL6) is a cytokine that orchestrates the early phases or priming phase of liver regeneration, as it seems to regulate almost 40% of all the genes that are deregulated immediately after PHx (31, 32). IL6 binds to its receptor in hepatocytes activating the extracellular signal-related kinase 1 and 2 (ERK1/2) and signal transducer and activator of transcription 3 (STAT3) pathways. Another important cytokine is tumor necrosis factor (TNF) which is rapidly upregulated after PHx, and binds to TNF receptor 1 primarily in Kupffer cells, leading to nuclear factor kappa B (NF-κB) activation and IL6 production. In addition, components of the innate immunity such as

lipopolysaccharide (LPS), C3a and C5a also bind to their receptors in Kupffer cells and promote liver regeneration (26, 32, 33) (**Figure I.3**).

After the priming phase orchestrated by cytokines, growth factors are upregulated during the proliferative phase. Among these growth factors, hepatocyte growth factor (HGF) seems to play a key role; HGF is paracrinally secreted from HSCs to induce hepatocyte proliferation. Besides HGF, other growth factors are also implicated in liver regeneration, such as the epidermal growth factor (EGF), vascular-endothelial growth factor (VEGF) and transforming growth factor (TGF). All these growth factors contribute to the normal regeneration of the liver after PHx (**Figure I.3**) (32, 33).

To restore the lost parenchymal structure, the participation of ECM producing cells is also essential. These fibrogenic cells are activated by inflammatory mediators and have their origin primarily from the activation of periportal fibroblasts and HSCs (6). At the beginning of liver regeneration the ECM is degraded in order to help the proliferation of hepatocytes. However, about 3-4 days after PHx HSCs produce ECM and the normal liver architecture is reconstructed, by properly reconnecting hepatocytes and the sinusoidal epithelium (**Figure I.3**) (26, 34).

However, in a chronic injury the regenerative capacity of the liver is severely impaired due to the excessive inflammation and fibrosis (25, 29).

Figure I.3. Liver regeneration after PHx. Liver regeneration is divided in 3 different phases;

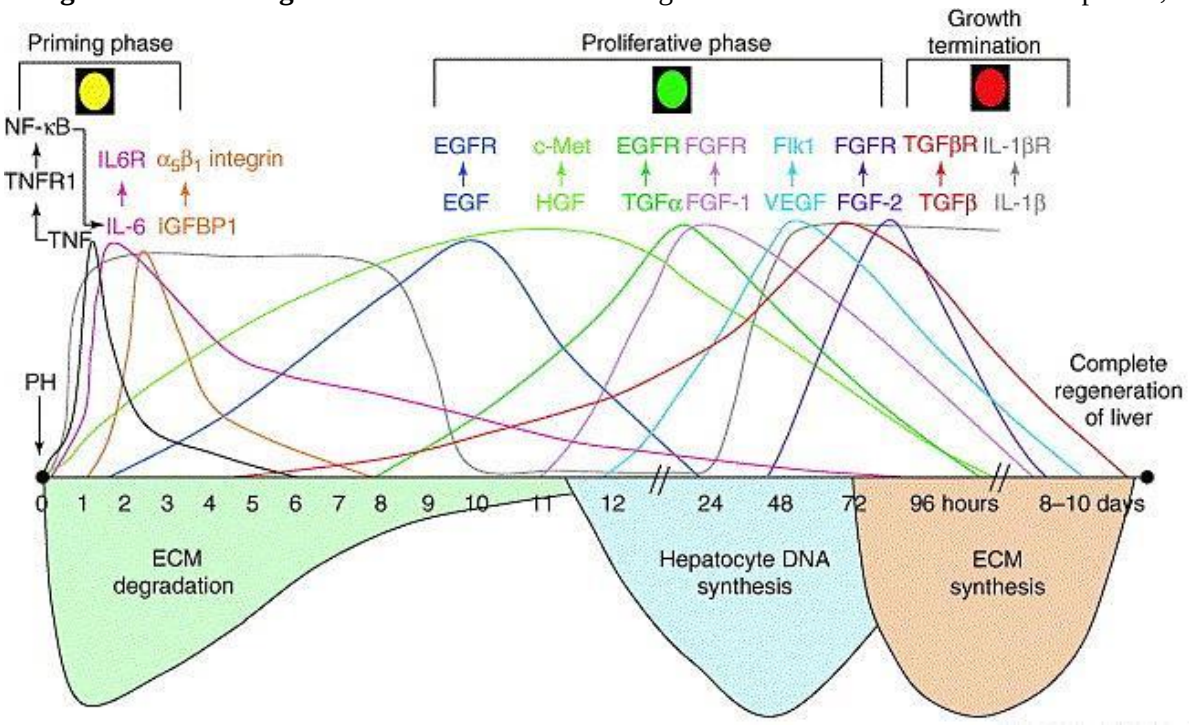

the priming phase, in which inflammatory cytokines are induced right after the surgery and ECM is degraded, the proliferative phase, in which growth factors are upregulated and hepatocytes proliferate and the growth termination phase, in which proliferation ends and the ECM is synthesized. ECM, extracellular matrix; EGF, epidermal growth factor; EGFR, epidermal growth factor receptor; FGF, fibroblast growth factor; FGFR, fibroblast growth factor receptor; HGF, hepatocyte growth factor; IGFBP1, insulin like growth factor binding protein 1; IL1β, interleukin 1 β; IL1βR, interleukin 1 β receptor; IL6, interleukin 6; IL6R, interleukin 6 receptor; NF-κB, nuclear factor kappa B; PH, partial hepatectomy; TGF, transforming growth factor β; TGFβR, transforming growth factor β receptor; TNF, tumor necrosis factor; TNFR1, tumor necrosis factor receptor 1; VEGF, vascular endothelial growth factor. (Adapted from Mohammed F and Khokha R, 2005.)

I.4 Chronic liver injury and progression of the disease

As mentioned earlier, liver injury occurs as a result of the exposure to different potentially harmful agents and when liver injury persists on time it becomes chronic. Interestingly, the progression of liver injury shares virtually common features regardless of the underlying cause (**Figure I.4**) (18).

As aforementioned, in a context of an acute liver damage the death of liver parenchymal cells after an injury triggers an inflammatory and regenerative process to restore the lost liver tissue, following a normal regenerative process of controlled healing (25, 26, 29). However, when the liver injury persists and becomes chronic, the inflammatory response is perpetuated and a chronic hepatitis is developed. Moreover, the

liver parenchyma will be progressively replaced by fibrotic tissue, developing liver fibrosis. If the injury is severe and persists on time, the hepatocellular parenchyma is progressively lost, the normal architecture of the liver is replaced by regenerative hepatocytes surrounded by fibrous septa, the function of the liver is compromised and liver cirrhosis is developed. In the cirrhotic liver complications such as ascites and hepatic encephalopathy may appear, and ultimately, renal failure, liver failure and the development of hepatocellular carcinoma (HCC) (**Figure I.4**) (35-38).

All these evidences support the idea that the progression of the liver injury includes the development of fibrosis and its evolution to cirrhosis and that this progression results largely from the chronic and uncontrolled activation of physiological mechanisms of tissue repair and regeneration.

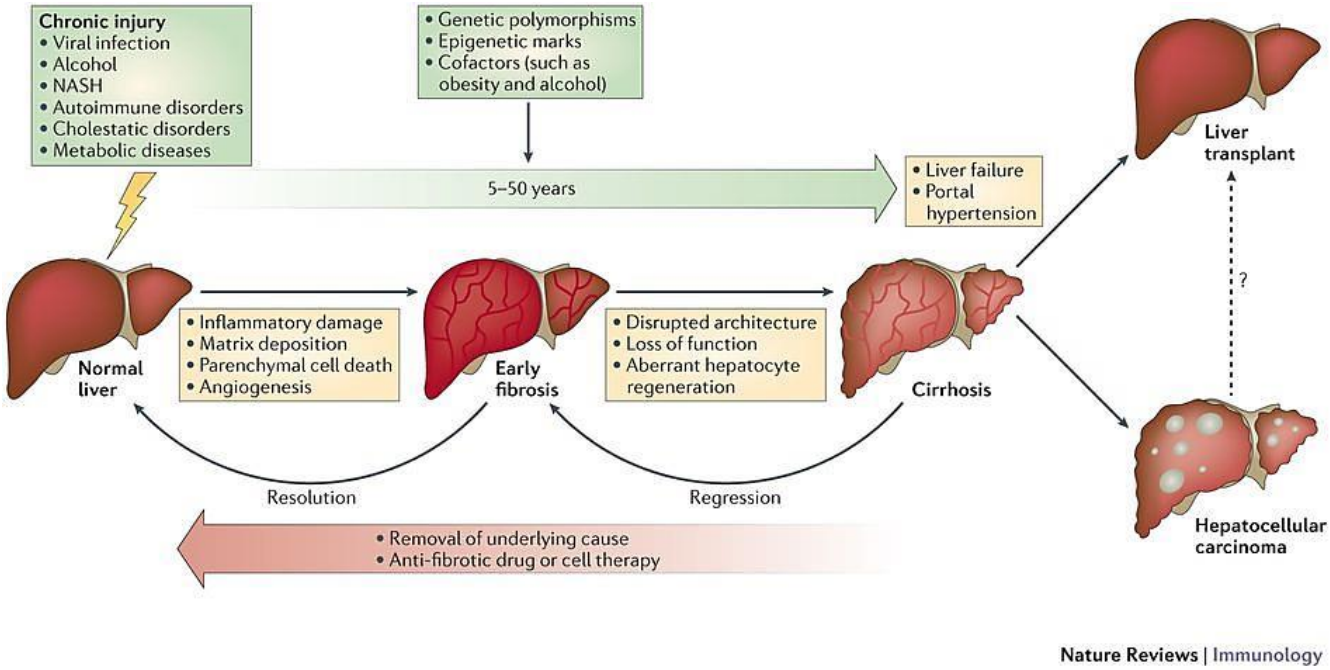

Figure I.4. Progression of liver injury. Chronic liver injury regardless of its aetiology produces inflammatory damage, matrix deposition, cell death and angiogenesis leading to liver fibrosis which is reversible. However, if the injury persist the liver losses its architecture and function and becomes cirrhotic, that may regress but not resolve. At this point, HCC and other complications may appear. HCC, hepatocellular carcinoma; NASH, non-alcoholic steatohepatitis. (Adapted from Pellicoro et al, 2014).

I.4.1 *Liver fibrosis*

Liver fibrosis results from a process of scarring of the liver which is characterized by an excessive accumulation of ECM proteins that occurs in a chronic liver damage (18). The

ECM production and accumulation is termed liver fibrogenesis, which is characterized by several key features: i) chronic persistent damage to parenchymal liver cells; ii) chronic inflammation; iii) activation of ECM producing cells and iv) qualitative and quantitative changes in the composition of the ECM (39).

After a hepatic injury the hepatocyte damage provokes the recruitment and stimulation of inflammatory cells, including the activation of the macrophages resident in the liver (i.e KCs) (40, 41). These inflammatory cells, together with the damaged and regenerative hepatocytes secrete inflammatory mediators and growth factors that promote the activation of HSCs, the main fibrogenic cells that transdifferentiate into myofibroblasts (42, 43). Myofibroblasts secrete and deposit collagen and other ECM proteins, ECM accumulates in the space of Disse and causes several changes in different cell types; hepatocytes lose their microvilli and endothelial cells lose their fenestrations (44-46). All these, dramatically affects the normal function of the liver (**Figure I.5**) (18).

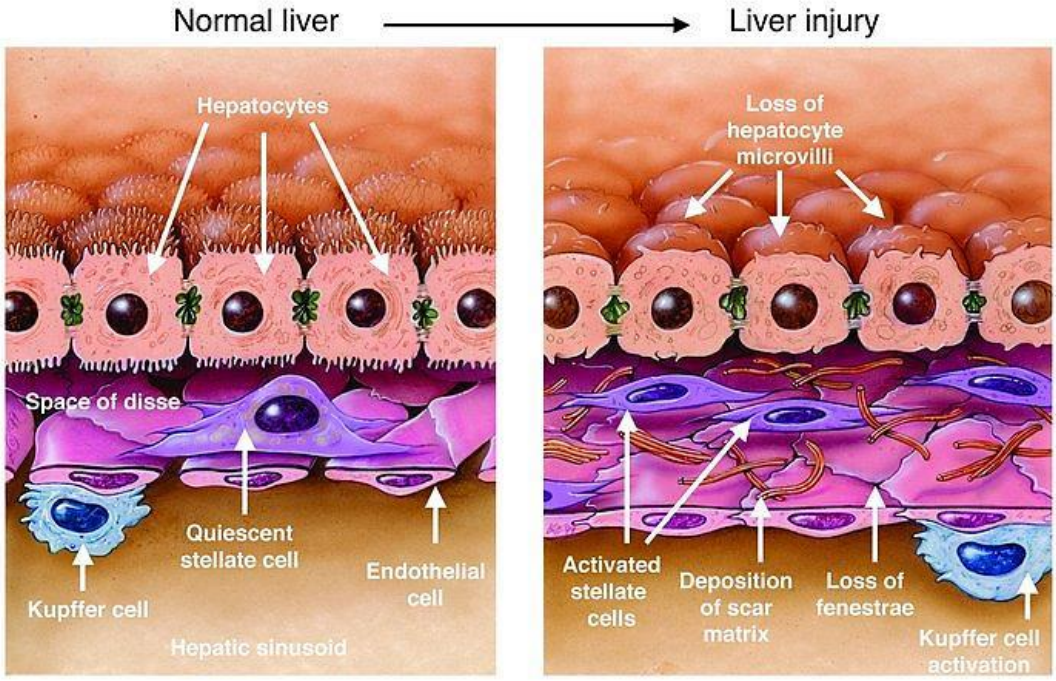

Figure I.5. Changes occurring in the hepatic sinusoid in liver fibrosis. During fibrosis activated HSCs secrete ECM in the space of Disse, as a consequence, hepatocytes lose their microvilli and endothelial cells lose their fenestrations compromising the normal function of the liver. ECM, extracellular matrix; HSC, hepatic stellate cell. (Adapted from Friedman SL et al., 2005).

I.4.1.1 *HSCs: Main pro-fibrogenic cells*

HSCs are the main pro-fibrogenic cells as they are the main producers of ECM during liver fibrosis (43). HSCs reside in the space of Disse and are responsible of the storage of vitamin A in the normal liver. However, after a liver damage, HSCs activate or

transdifferentiate into myofibroblasts constituting one of the most important events during fibrogenesis. Myofibroblasts then migrate and accumulate in tissue repair sites secreting large amounts of ECM and regulating ECM degradation (47). For that, the activated HSCs or myofibroblasts acquire proinflammatory, proliferative, fibrogenic and contractile properties (47, 48) Apart from collagen, HSCs also secrete matrix metalloproteinases (MMPs) that serve to degrade the ECM. Besudes, HSCs also secrete the tissue inhibitors of metalloproteinases (TIMPs), the inhibitors of MMPs (49).

The discovery of the activation of HSCs was a milestone in the research of liver fibrosis, gaining key knowledge for the bases of liver fibrogenesis (6, 50). However, myofibroblasts are a complex cell population and HSCs are not the only cells contributing to myofibroblast population, Moreover, activation pathways and the overall contribution of fibrogenic cells to myofibroblasts during liver damage may be very different (42, 51). Depending on the aetiology of liver disease, myofibroblasts not only derive from resident HSCs, but may also be derived from portal fibroblasts, from circulating fibrocytes and from bone marrow derived cells (42, 51). In addition, cell-fate studies showed that neither hepatocytes nor cholangiocytes contribute to the myofibroblast population (**Figure I.6**) (42, 51-55).

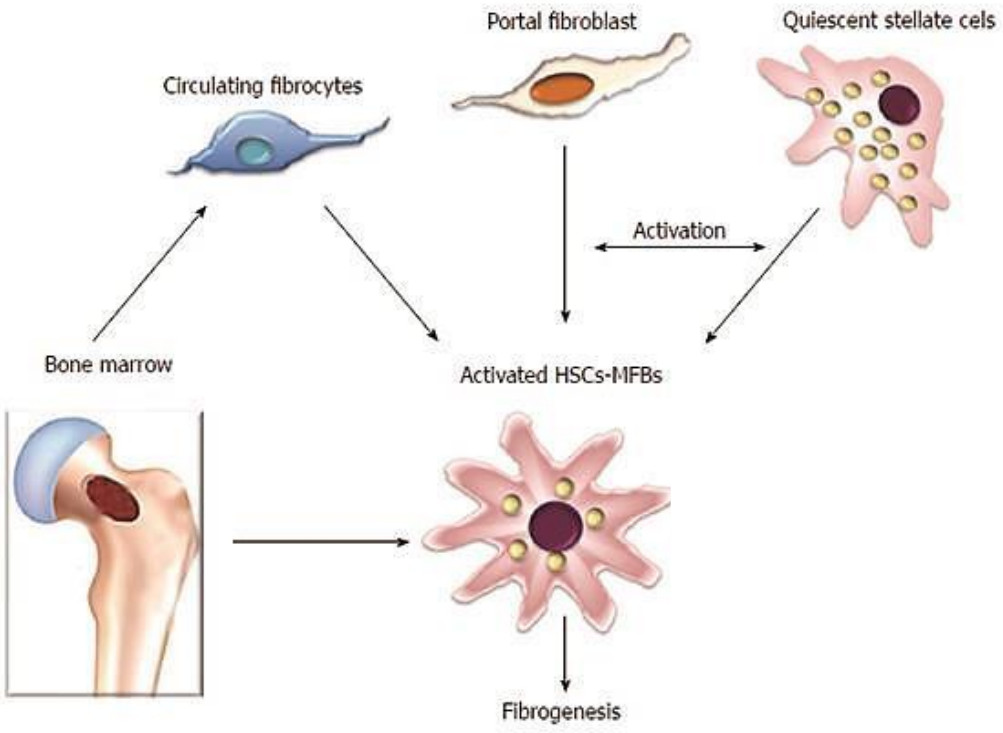

Figure I.6. Contribution of HSCs and other cells to liver myofibroblasts. Different cell types may transdifferentiate into myofibroblasts and promote fibrosis, HSCs being the main contributors to myofibroblast population. HSC, hepatic stellate cell. (Adapted from Elpek GO et al., 2014).

The activation of HSCs is a complex but highly programmed event. The initiation or pre-inflammatory stage is associated with a rapid gene induction, resulting from paracrine stimulation of inflammatory cells and hepatocytes or cholangiocytes, and early changes in the composition of the ECM (42). Oxidative stress is one of the early determinants of HSC activation. The main intermediates of ROS are hydrogen peroxide, superoxide anion, hydroxyl radicals and also 4-hydroxy-2,3-nonenal and 4-hydroxy-2,3-alkenal, the main end products of lipid peroxidation and can be derived from hepatocytes, macrophages, HSCs and other inflammatory cells (6, 56). In addition to oxidative stress, early changes in ECM composition, such as the production of fibronectin by endothelial cells, can stimulate the activation of HSCs (57). Besides, Wnt/β-catenin pathway is activated during HSC activation and Wnt3A ligand activates HSCs in culture and promotes their survival (58). In addition, Wnt4, Wnt5a and Wnt6 ligands are expressed in rat HSCs, modulating HSC activation and survival through non-canonical Wnt/β-catenin (59, 60).

The classic stimulus of inflammation and fibrogenesis is necrosis. However, apoptosis is now viewed as a pro-fibrogenic response for HSCs (27). These cells are able to phagocytose apoptotic bodies making HSC more activated and pro-fibrogenic (61-63). In the last decade, the role of innate immunity in HSC activation has gained attention. In this regard, HSCs express different Toll-like receptors (TLRs) that may respond to components of bacteria translocated from the gut, the so called gut-liver-axis. In this line, LPS has been shown to increase the fibrogenic activity in HSCs through TLR4. TLR4 activation upregulates cytokines and chemokines and also the levels of TGFβ by downregualting the expression of BMP and activin membrane bound inhibitor (BAMBI) (64).

Activated HSCs may be maintained an amplified due to a mechanism of perpetuation. This implies autocrine and paracrine stimulation of growth factors, as well as the accelerated remodeling of the ECM. In this scenario, HSCs acquire new functions such as proliferation, fibrogenesis, chemotaxis, contractility and the production of various enzymes, growth factors and receptors. One of the main features of HSC activation is the

de novo expression of alpha smooth muscle actin (αSMA). HSCs are the main source of ECM production and are key players in the development of fibrosis (47).

The resolution of hepatic fibrosis has been demonstrated in animal models and in humans and can be therefore considered a potentially bidirectional and reversible process. In this sense, the remodeling of the ECM and the regression of fibrosis are always associated with the interruption of the chronic damage. In addition, one of the most relevant characteristics of the hepatic fibrosis resolution process is the decrease of the myofibroblast pull. For that, myofibroblast may reverse to quiescent HSCs, entering into senescence or apoptosis (65, 66). During a chronic liver damage, apoptosis of activated HSCs is impeded, however, when the deleterious stimulus is removed, the loss of survival factors leads to the apoptosis of the activated HSCs, which facilitates the process of remodeling the matrix by eliminating the main source of collagen and TIMPs (67, 68). Nevertheless, the loss of activated HSCs is not sufficient to allow the remodeling of the collagen excess. The degradation of this collagen must also occur, and for that the increase in the activity of collagen degrading MMPs is necessary. In this regard, macrophages play an important role in fibrosis resolution; they produce different MMPs, such as MMP12 and MMP13. Both MMPs being key players in the degradation of the excessive ECM (65, 69, 70).

I.4.2 *Liver cirrhosis*

Liver fibrosis and its final stage, cirrhosis, represent the final common consequence of almost all chronic liver diseases. They are a serious global health problem; the incidence of death in patients with cirrhosis is high and is also the optimal physiopathological context for the development of HCC. Therefore, a better understanding of the mechanisms responsible of this pathology and its evolution towards HCC and other complications is necessary in order to develop novel therapeutic strategies against liver fibrosis and cirrhosis (35, 71-73).

Cirrhosis is a pathology characterized by the massive synthesis of ECM by myofibroblasts, which occupies the parenchymal space and gives the liver a scar-like appearance. This process is accompanied by a decrease in the functional capacity of hepatocytes, which lose the expression of key genes in the maintenance of the hepatocellular phenotype, causing their de-differentiation (35, 71).

Thus, progressively, liver architecture and functionality is lost and due to the massive accumulation of ECM hepatic blood vessels are obstructed causing portal hypertension, which is the underlying cause of most complications of cirrhosis and the subsequent mortality in cirrhotic patients. In the same way, the lobular organization of the liver is replaced by regeneration nodules surrounded by fibrotic tissue, with zones composed of proliferating hepatocytes (74). These nodules may contain phenotypically altered hepatocytes that can lead to neoplastic nodules. Moreover, within the regenerating hepatocytes, new monoclonal cell populations can arise that derive from cells that could have accumulated genetic alterations, with an increase in proliferation and a proportional decrease in apoptosis, which is associated with an increased risk of developing HCC (35, 49, 75).

I.4.3 *HCC*

HCC is the sixth most common cancer worldwide, the third leading cause of cancer mortality and accounts for more than 80% of malignant primary liver tumours (76). Risk factors are well established in HCC as up to 80% of all HCCs develop in a background of cirrhotic liver (76). Chronic liver disease, caused by viral infections by HBV or HCV, alcohol consumption, obesity, or a combination of the above are the most common trigger factors of HCC (77, 78).

The distribution of HCC in the world population is not homogeneous, its prevalence is increasing and is especially high in areas of East Asia and Sub-Saharan Africa; In East Asia the main causative agent is viral infection by HBV, whereas in Africa HBV infection and food intoxication with aflatoxin B1 are the main causatives of HCC. In contrast, in industrialized regions such as Europe, North America and Japan HCC incidence is mainly caused by chronic HCV infection (**Figure I.7**). Other risk factors associated with the development of HCC include chronic genetic conditions such as hereditary hemochromatosis, α1-antitrypsin deficiency and non-alcoholic fatty liver disease (NAFLD) and NASH, the latter being especially relevant in countries with increasing rates of obesity such as in the USA and Europe (76, 79, 80).

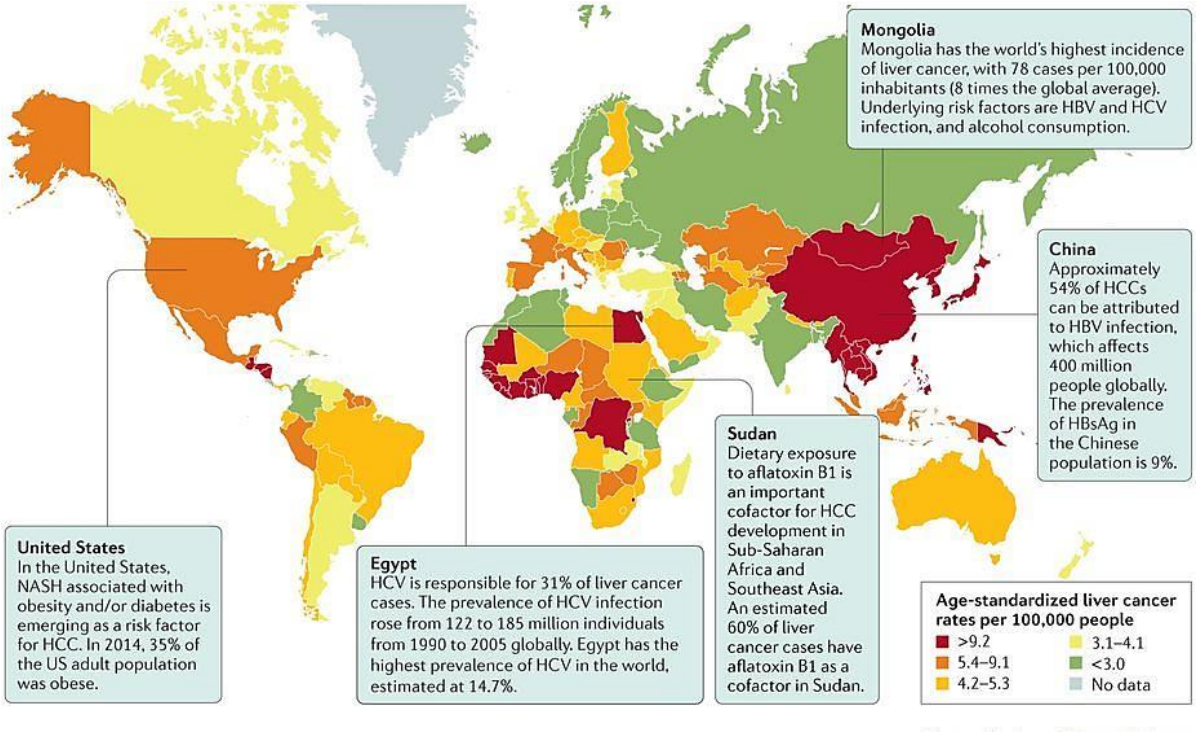

Figure I.7. HCC rates worldwide. HCC rates are high in East Asia and Africa. The HCC causatives are different, HBV being high in China, HCV in Egypt, and both HCB and HCV and also alcohol consumption in Mongolia, having the world's highest HCC incidence. In the USA and other developed countries HCC associated to NASH and metabolic syndrome is increasing whereas in African countries such as Sudan poisoning with aflatoxin B1 is an important co-factor in the development of HCC. HBsAg, hepatitis B surface antigen; HBV, hepatitis B virus; HCC, hepatocellular carcinoma; HCV, hepatitis C virus; NASH, non-alcoholic steatohepatitis. (Adapted from Llovet JM et al, 2016).

HCC shows a very poor prognosis, with almost similar number of new cases of HCC diagnosed and deaths. This is in part due to the high resistance of HCC to chemotherapy, the deleterious state of the liver in which most of the HCC develop and the lack of reliable diagnostic markers. Because of this, intense research efforts are being made to understand the cellular and molecular mechanisms of HCC development to uncover novel therapeutic strategies to tackle this disease (81).

I.4.3.1 *Mechanisms involved in the development of HCC*

HCC is a clear example of inflammation-related cancer, as HCC is a type of tumour that slowly unfolds on a background of chronic inflammation, mainly triggered by exposure to infectious agents or toxic compounds (82). HCC development is a multistep process, characterized by chronic inflammation, fibrogenesis and hepatocyte death and regeneration (79). HCC develops in a cirrhotic background and the risk of developing

HCC increases while liver function is impaired. Like other tumours, HCC is developed as a consequence of somatic mutations. Genetically, HCCs exhibit a high heterogeneity, with numerous mutations in diverse genes. However, some genes appear to be frequently mutated in HCC, such as *telomerase reverse transcriptase* (*TERT*) (60%), *TP53* (25-30%), *CTNNB1* (18%), *AXIN1* (8%), *CDKN2A* (2-12%), *CCND1* (7%), *RB1* (3-8%) and *ARID2* (3-18%) (79, 83, 84).

Mutations in the promoter of *TERT* are very common in HCC but *TERT* is not usually expressed in hepatocytes, however, during HCC development its expression in becomes re-activated. Telomerase activation happens in up to 90% of HCCs, whereas in precancerous nodules telomerase activation occurs in 6-20% of cases. Therefore, telomerase activation is important for the transformation and for the promotion of uncontrolled proliferation of hepatocytes (84, 85). Wnt/β-catenin pathway is an embryogenic pathway that is also commonly re-activated in HCC (20-35%) and a significant proportion of HCCs have mutations in key genes of this pathway, such as *CTNNB1* and *AXIN1* (86, 87). As a consequence, β-catenin stabilizes in the cytoplasm and translocates to the nucleus promoting the transcription of genes associated to an increased proliferation, migration and metastasis, such c-Myc and cyclin D1 (87, 88). Inactivation of p53 and cell-cycle related alterations are a common feature in various cancers and also in HCC, especially in HCCs related to HBV infection or to aflatoxin B1 poisoning. Other key pathways altered during HCC are the ras/raf/MEK/ERK pathway, PI3K/Akt/mTOR, NF-κB and JAK/STAT pathways. In addition, chromatin remodelling complexes and epigenetic regulators and oxidative stress are other key processes altered in HCC (75, 79, 89-94).

Apart from these common mechanisms, according to the different aetiological agents the hepatocarcinogenic process may have relevant differences. In the case of the deoxyribonucleic acid (DNA) virus HBV, the integration of viral DNA into the host cell genome may cause genomic instability. Commonly, HBV viral genome inserts in *TERT* promoter and other oncogenes, In addition, both HBV and HCV viral proteins may also promote HCC: HBV protein HBx and HCV proteins NS3, NS5A and NS5B have been shown to be oncogenic and are associated to tumour promotion (95-97). In alcohol-mediated HCC two main factors co-exist. One of the factors includes the direct damage produced in hepatocytes due to oxidative stress and lipid peroxidation produced when ethanol is metabolized by the enzyme Cyp2E1. In addition, when ethanol is metabolized, the carcinogenic primary metabolite acetaldehyde is produced. Acetaldehyde promotes

adduct formation, that causes DNA damage, alters the function of key proteins and as a consequence may provoke mutagenesis and HCC. On the other hand, these two factors, combined with the inflammatory and fibrotic environment in alcohol consumption-mediated cirrhotic liver ultimately cause the development and promotion of HCC (98).

In addition to the direct oncogenic activity of hepatitis B and C viruses and the chronic consumption of alcohol, these agents can also cause liver tumours through an indirect action. This involves the accumulation and fixation of mutations in the hepatocyte genome during the compensatory proliferation that is triggered by the loss of parenchymal cells and the chronic inflammation that occurs during fibrogenesis and cirrhosis (99-101). This scenario of chronic inflammation and regeneration appears to be essential for the complete development of the neoplastic phenotype, facilitating the accumulation of genetic alterations in a large population of progenitor cells (102, 103). This hyper-proliferative state found in the chronically affected liver is in part due to over-expression of mitogenic factors for hepatocytes, such as HGF. What initially is part of the endogenous defence of the damaged liver for a proper regeneration in response to the loss of parenchymal cells of the liver, its perpetuation in a chronic setting of liver damage may enhance the hepatocarcinogenic process establishing autocrine mechanisms for self-sustained cell growth (99-101).

Therefore, despite the molecular and aetiological heterogeneity of HCCs, there are common features that characterize the early stages of liver cancer development. Including the alteration of the normal expression of specific genes of the liver and the persistence of an inflammatory and regenerative environment guided by a complex interaction of cytokines and growth factors (75, 100).

I.4.3.2 *Current therapies for HCC*

HCC staging is very important for the correct management of HCC patients, in this regard, several staging systems have been proposed, including the tumour, node, metastasis (TNM) staging, which is used in most cancers and the Barcelona clinic liver cancer (BCLC) staging, that has been extensively validated and is the most widely used for HCC (76). The BCLC algorithm does not only take into account the tumour stage, but also incorporates other factors such as the liver function impairment with the Child-Pugh classification and the existence of cancer-related symptoms with the ECOG Performance Status, which are strongly associated to the prognosis of HCC. Importantly, the BCLC

staging system is classified in 5 different HCC stages which are paired with the best therapeutic option (76).

Current therapies are divided in three main categories: surgical treatments, locoregional therapies and systemic therapies. Surgical treatments are considered at very early or early BCLC stages and are based on the resection of the tumour tissue or in liver transplantation. Yet after tumour resection recurrence is common as the underlying cirrhosis is still present and liver transplantation in selected patients remains the best therapy for HCC. However, this approach is limited as there is a low availability and compatibility of organs to transplant. Regarding locoregional treatments, tumour ablation is indicated in early HCC stages when tumour resection and liver transplant are not possible. Other locoregional treatments such as transarterial chemoembolization and radioembolization are indicated in intermediate BCLC stages, for asymptomatic patients with multinodular tumours and a preserved liver function (76).

Regarding systemic therapies, HCC is a tumour that is highly resistant to conventional treatments based on nonspecific cytotoxic drugs and so far, there is no convincing evidence that systemic chemotherapy improves the overall survival of patients with HCC (76, 104). Even though major progress has been made during the last decade, due to the complex scenario in which HCC develops with the underlying liver cirrhosis, to date, there is no effective therapy to treat and cure this cancer. Thus, the development of novel therapeutic strategies is an urgent need (76, 104-106). Targeted therapies aiming to treat HCC have been shown modest beneficial effects (104) (107, 108). In this regard, sorafenib, a multikinase inhibitor drug, was the first food and drug administration (FDA) approved first-line treatment for HCC showing improved progression-free survival and overall survival (109, 110). Recently, Lenvatinib, another multikinase inhibitor was also approved as first-line and also as a second-line treatment for HCC after showing non-inferior to sorafenib overall survival improvement (111). In addition, regorafenib, another multikinase inhibitor drug, has been approved as a second-line treatment after sorafenib (112). In addition, a number of drugs are currently in Phase III trial and it is expected to enter in the clinics soon (107, 108). However, many phase II and III clinical trials result in the discontinuation of drugs because they are clinically unsuccessful (104).

Immunotherapy has emerged as a promising therapeutic approach for cancer treatment (113). Immunotherapy consists on the modulation of the immune system to tackle cancer, and may be achieved through different strategies, such as the use of monoclonal antibodies to modulate proteins of the immune system, treatment vaccines

and adoptive cell transfer among others. However, this field is still in its infancy and efforts should be made in order to learn how cancer cells evade the immune system surveillance (113). Currently there is only one FDA approved immunotherapy based drug for HCC as a second-line treatment; nivolumab, a programmed death receptor-1 (PD-1) blocking antibody. PD-1 is expressed in T cells and suppresses T cell inflammatory response promoting their apoptosis. PD-1 blockade by nivolumab is able to reverse the suppression of T cells, activating and helping them fight cancer cells (108, 114, 115). However, nivolumab has not yet been approved by the European medicines agency (EMA).

In view of these, the development of new therapeutic approaches to treat HCC is of paramount importance, and for that, a better understanding of the molecular mechanisms in the progression of liver diseases and HCC is necessary.

I.5 Innate immune system in the liver

The innate immune system plays a key role in liver homeostasis and disease. The liver is continually exposed to pathogens from the blood and acts as a barrier being the first line defence against pathogens derived from the gut. In this sense, the liver is able to detect and respond to pathogens due to its anatomical location and to the immune cells population (7, 116). The immune resident cells are located in the sinusoidal lumen and in the space of Disse and comprise a cell network of immune sentinels and effector cells (7, 116). The interaction of the resident immune cells with the pathogens is facilitated by the low pressure of the blood and the endothelial cells' fenestrae. This way, immune cells directly detect and destroy circulating pathogens (8).

In the liver, different adaptive and innate immune cells are present, including the antigen presenting cells (APC), lymphoid cells and myeloid cells (7, 116). These resident immune cells play important roles in the maintenance of the liver homeostasis and also during liver disease. Interestingly, the liver contains the greatest densities of natural killer cells (NK) and natural killer T cells (NKT) and the largest macrophages population (resident KCs) (8). Yet, the full liver resident immune cell populations are not clear (7, 116).

I.5.1 *The role of KCs in innate immunity*

As above mentioned KCs are the resident macrophages of the liver and comprise the largest population of resident macrophages in the organism (7). Although resident KCs have a prenatal origin and are generated from the yolk sac and/or fetal liver, during liver injury, circulating $Ly6C^+$ monocytes are recruited to the injured liver in a Monocyte *c*hemoattractant protein 1 / chemokine (C-C motif) receptor 2 (MCP1/CCR2) dependent manner, where they can contribute to injury (117-119). KCs are key players in the innate immune response in the liver, for that, they localize strategically in the hepatic sinusoids allowing them to phagocytise pathogens, especially the ones entering from the gut through the portal vein. Therefore, KCs act as components of the gut barrier by serving as a first line of defence in the liver for gut derived immunoreactive material. Thus, due to their phagocytic and inflammatory activity, KCs play a major role clearing the blood entering from the gut from pathogens, and preventing them from travelling past the hepatic sinusoid (120). In addition, KCs are specialized in phagocytising apoptotic bodies from the hepatic parenchyma, as well as dying erythrocytes from the systemic circulation (121-123). The phagocytic activity of KCs can be mediated by phagocytic pseudopodia, pinocytosis vesicles, vacuoles, and invaginations (124). Particles can be detected and phagocytised by specific receptors such as Fc and C3 receptors (124). In addition, opsonizing agents such as plasma fibronectin also facilitates the phagocytic activity of KCs. These cells also express CD14, a co-receptor that forms a complex with TLR4 and MD-2 to recognize bacterial-derived LPS (125, 126).

KCs also play a role in the metabolism of lipoproteins. Specifically, KCs are responsible of the metabolism of oxidized low density lipoproteins (LDL), which are metabolized in the liver also by endothelial cells (127, 128). For that, KCs express scavenger receptors such as CD36 and SR-A which are able to phagocytise and destroy the circulating oxidized LDLs (129, 130). This is particularly important in NASH, where the uptake of circulating oxidize LDLs triggers activation of KC promoting inflammation in the liver (130, 131).

I.5.1.1 *Activation of KCs*

KCs are activated by binding different molecules such as LPS, complement factor C5a, growth factors, TNF or interferon γ (IFNγ). Besides, KCs can also be activated by phagocytised particles such as apoptotic bodies, LDLs or pathogens (120, 124). Once

activated KCs secrete a number of inflammatory mediators such as cytokines, TGFβ, IFNs, growth factors and ROS among others (122). These inflammatory mediators are secreted in an autocrine-paracrine manner, affecting them and nearby cells in the hepatic sinusoid. In addition the phagocytic capacity of activated KCs increases and also these cells become more proliferative (122). Moreover, KCs show an important plasticity, as other macrophages, they are able to polarize into different inflammatory-state cells termed M1 or M2, M1 being the classic pro-inflammatory macrophages, involved in inflammatory processes, while M2 being anti-inflammatory macrophages, involved in the resolution of injury and wound healing and also related to tumorigenic processes. In addition, there are also different states termed as M2-like phenotypes which are involved in immunoregulation and can also promote tumorigenesis (120, 132).

KCs play an important protective role in the liver as they are important mediators of liver injury and repair (122). After liver injury KCs activate and help in the resolution of the liver damage (133). However, KCs may also play a deleterious role in the liver, as a change in the functional activity of these cells is associated with a number of liver diseases. Besides, deregulation of KCs may promote chronic inflammation which contributes to a number of diseases such as NASH, alcoholic liver disease (ALD) and insulin resistance and is also associated with the progression of liver injury and HCC (120, 134).

I.5.2 *The gut-liver axis*

As aforementioned, the liver due to its anatomical location is the first organ that encounters portal venous blood from the gut, an organ consisting of vast numbers of micro-flora. Blood from the portal vein mixes with oxygenized blood from the hepatic artery and drains through the sinusoids, allowing a rapid exchange of nutrients with hepatocytes and the elimination of immunoreactive molecules. Thus, the liver is capable of tolerating these immunogenic agents and at the same time responds efficiently to pathogens and infections (116).

The primary aim of the innate immune response is the rapid elimination of pathogens before they multiply, spread systemically and invade tissue. This prevents excessive inflammation that can result in immuno-pathology and organ failure. A variety of pattern recognition receptors (PRRs), including those of the TLR family are expressed by innate immune effector cells including KCs and dendritic cells. PRRs recognize

pathogen associated molecular patterns (PAMPs), conserved in microbes and trigger innate immune responses which shape adaptive immunity. PRRs also recognise damage associated molecular patterns (DAMPS) which recognize biomolecules that are exposed by damaged endogenous cells (120, 135, 136).

Recently, the role of bacterial flora and TLRs in the pathogenesis of fibrosis has been demonstrated. The gut-liver axis plays a significant role in liver injury and in the diseased state; the normal tolerogenic liver is exposed to bacteria and bacterial products including LPS, which is recognized by TLR4 (137). Moreover, polymorphisms in TLRs are associated with complications in cirrhosis (138). TLRs including TLR4 are expressed on KCs and also on hepatocytes (albeit at a low level) and on HSCs and as aforementioned, HSCs are extremely important in the synthesis of ECM, collagen and consequently the development of fibrosis (139, 140) (**Figure I.9**).

There is increasing evidence showing that TLRs play an important role in hepatic injury and liver disease. Mechanistically, gut microbiota are believed to be one of the main players, with the current idea being that liver injury causes altered intestinal permeability that ultimately results in induction of inflammatory responses which impact on the disease process (135, 141). Thus, it seems logical that the liver similar to the intestine would require mechanisms to control the intensity and duration of TLR driven cytokine production, which can contribute to the pathogenic process in various types of chronic and acute liver disease (142-144). By using genetic and molecular approaches it has been shown that LPS through TLR4 is able to increase the fibrogenic activity of TGFβ in HSCs (64). By the same means, TLR4 has been shown to promote the development of HCC (145). In line with this dogma, treatment of mice with antibiotics or probiotics attenuates various forms of liver injury including; carbon tetrachloride (CCl_4), bile duct ligation (BDL), NASH and HCC development (64, 145-148). Indeed, *Tlr4* deficient mice are protected from the aforementioned insults to the liver (145, 147, 148) (**Figure I.8**).

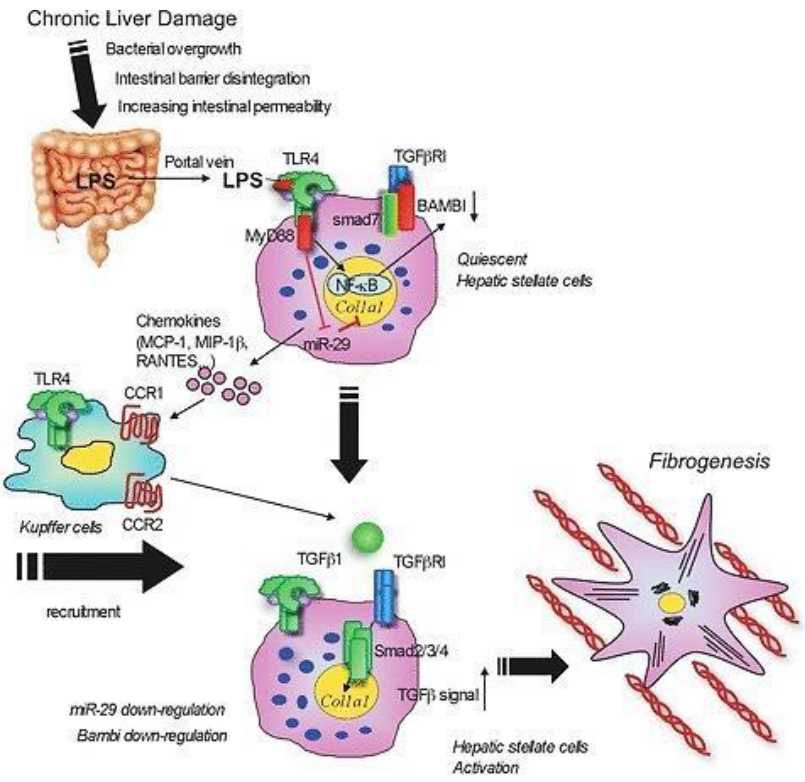

Figure I.8. Gut-liver axis and chronic liver disease progression. During chronic liver damage the gut epithelia is also damaged; the intestinal barrier disintegrates, and the intestinal permeability increases. In this scenario, bacterial products derived from the gut microbiota translocate to the liver promoting TLR signaling in KCs and HSCs and, eventually, promoting inflammation, fibrosis and chronic liver disease progression. BAMBI, BMP and activin membrane bound inhibitor; CCR, chemokine (C-C motif) receptor; COL1A1, collagen type 1 alpha 1; MAPK, mitogen-activated protein kinases; MCP1, monocyte chemoattractant protein 1; Mip-1β (CCL4), C-C motif chemokine ligand 4; Myd88, myeloid differentiation primary response gene 88; NF-κB, nuclear factor kappa B; LPS, lipopolysaccharide; RANTES (CCL5), C-C motif chemokine ligand 5; TGFβ, transforming growth factor β 1; TGFβR, transforming growth factor β receptor; TLR, toll-like receptor. (Adapted from Seki E et al, 2012).

I.6 Triggering receptor expressed on myeloid cells (TREM) family

The TREM family of genes are encoded on human chromosome 6p21.1 and are composed by *TREM1* and *TREM2*, the TREM-like genes *TREML1*, *TREML2* and *TREML4* and also the pseudogenes *TREML3P* and *TREML5P*. In mice, this family is encoded in chromosome 17C and are composed by *Trem1*, *Trem2*, *Trem3*, *Treml1*, *Treml2* and *Treml4* (Gene database from the NCBI, https://www.ncbi.nlm.nih.gov/gene) (**Figure I.9**). These genes encode a single V-type extracellular immunoglobulin-like domain, a trans-membrane domain and a short cytoplasmic tail. However, human and mouse TREM1 and TREM2 and mouse TREM3 lack any signalling motif. For that, they couple to the immunoreceptor tyrosine-based activation motif (ITAM) of DNAX-activation protein-12 (DAP-12) which becomes tyrosine phosphorylated and modulate cells

involved in immune innate responses (149). Regarding TREM-like genes, they also encode a V-type single variable type immunoglobulin domain and a transmembrane domain, but in the case of human *TREML1* and mouse *Treml1*, *Treml2* and *Treml4* they also have a cytoplasmic immunoreceptor tyrosine-based inhibitory motif (ITIM) domain and in the case of human *TREML2* a SH3 binding domain for their signalling (150). Interestingly, soluble forms of TREM receptors exist, either by alternative splicing or by cleavage soluble forms of TREM1, TREM2, TREML1 and TREML2 (sTREM1, sTREM2, sTREML1 and sTREML2) exist and although their role is still not clear they seem to negatively regulate their signalling by competing with the full form of the receptors (149).

TREM receptors are expressed on myeloid cells and also in other cells such as platelets and endothelial cells (149). TREM1 receptor was first described as a pro-inflammatory receptor whereas TREM2 has been described as an anti-inflammatory receptor (149). However, this may be cell-type specific and ligand-dependent (151, 152). By contrast, TREM-like proteins function is less clear and they may be involved in the negative regulation of TREM1 and TREM2 (149, 150).

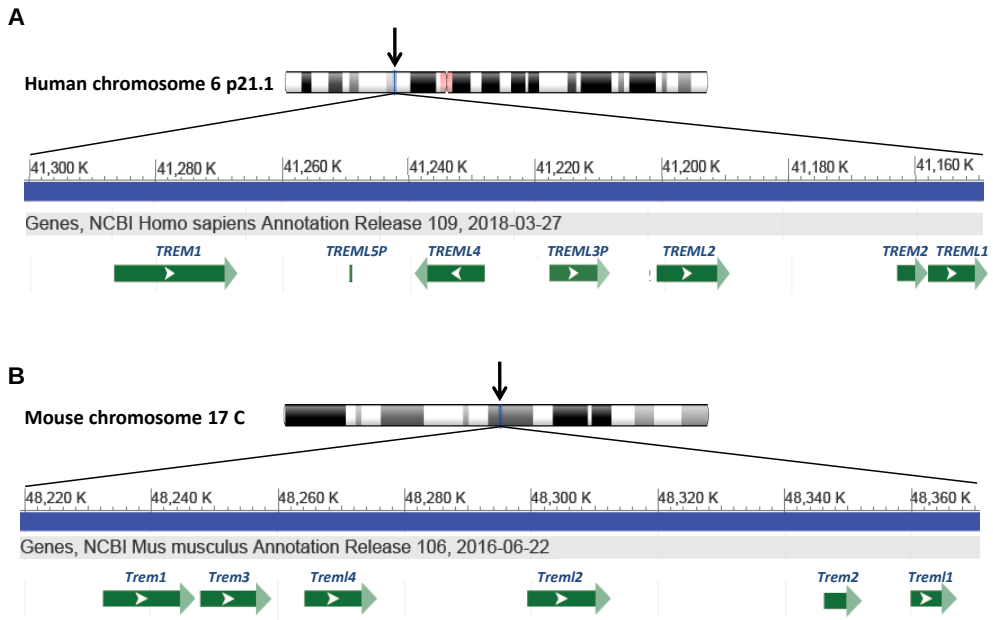

Figure I.9. The TREM family of genes. (**A**) The TREM family of genes is a gene cluster encoded on human chromosome 6 and composed by *TREM1*, *TREM2*, *TREML1*, *TREML2*, *TREML4* genes and *TREML3P* and *TREML5P* pseudogenes. (**B**) In mouse, they are encoded on chromosome 17

and are composed by *Trem1*, *Trem2*, *Trem3*, *Treml1*, *Treml2* and *Treml4*. TREM, triggering receptor expressed on myeloid cells; TREML, triggering receptor expressed on myeloid cells like. (Figure adapted from the Gene database from the NCBI, https://www.ncbi.nlm.nih.gov/gene).

I.6.1 *TREM1 and TREML members*

TREM1 was the first TREM family member being described (153). TREM1 is a pro-inflammatory receptor that acts as an enhancer of TLR mediated inflammation (153). TREM1 has been implicated in a number of diseases, including sepsis atherosclerosis, inflammatory bowel disease and many cancers such as intestinal, lung and liver cancer (154-165). Regarding the liver, TREM1 has been shown to be expressed in LSECs, KCs, HSCs and also in HCC cells (163-165). TREM1 promotes liver injury and HCC progression in mice; *Trem1*$^{-/-}$ mice are protected from diethylnitrosamine (DEN)-mediated tumourigenesis and *Trem1*$^{-/-}$ KCs have diminished activation with less activation of p38, ERK1/2, c-Jun N-terminal kinase (JNK), mitogen activated protein kinase (MAPK) and NF-κB pathways and a decreased expression of inflammatory markers (163). Moreover, TREM1 is associated with lower survival and faster time to recurrence in human HCC (164, 165). In addition, another study reported that activated HSCs show augmented levels of sTREM1 when cultured with HCC cells. Importantly, TREM1 was associated with migratory effects in HCC cells (165).

Considering the other members of the TREM family, TREML1 is expressed in megakaryocytes and platelets (166), contains an ITIM signalling motif and has been reported to regulate Ca^{+2} influx (167). TREML1 and its soluble form sTREML1 induce platelet aggregation interacting with fibrinogen (168-170). Interestingly, sTREML1 show high homology with TREM1 and is able to block TREM1-mediated inflammation (171). In this regard, sTREML1 has been reported to dampen TREM1-mediated leukocyte activation during sepsis by competing with TREM1 ligands (168). Moreover, serum levels of sTREML1 during sepsis are increased and could be used to differentially diagnose sepsis from non-infectious systemic inflammatory response syndrome (SIRS) (172). Of note, a TREML1 transcript variant is able to inhibit TREM2-mediated osteoclastogenesis (173).

Regarding TREML2, it has been reported to be expressed in macrophages, neutrophils and in B and T lymphocytes (174). TREML2 expression was shown to promote T cell activation, which was mediated by direct interaction with B7-H3 (175). Moreover, B7-H3 was shown to augment the function of tumor infiltrating $CD8^{+}$ T

expressing TREML2 cells (176). However, two more studies did not found any association between TREML2 and B7-H3 and the role of both TREML2 and B7-H3 in T cell activation remains controversial (177, 178). In addition, TREML2 promotes neutrophil activation (174, 179) and engulfment of apoptotic bodies by macrophages (180).

I.6.2 *TREM2*

TREM2 is a TREM family member expressed in dendritic cells, alveolar, liver and intestinal macrophages and endothelial cells among others (151). This receptor is a type 1 membrane glycoprotein, and as previously mentioned can be cleaved forming the soluble protein sTREM2. Cleavage is mediated by α-secretases ADAM10 and ADAM17, then γ-secretase cleaves the remaining C-terminal amino acids (181, 182).

TREM2 was first described as performing opposite functions to TREM1 being an anti-inflammatory receptor that negatively regulates TLR mediated inflammatory responses while TREM1 acts to augment TLR induced inflammation (154). In this sense, similar to IRAK-M and A20 null macrophages, *Trem2*$^{-/-}$ macrophages exhibit augmented cytokine responses to TLR ligands (183, 184). In this regard, TREM2 signals via the ITAM motif of the adaptor protein DAP-12, which becomes tyrosine phosphorylated leading to increases in intracellular calcium and ERK1/2 phosphorylation (185) (**Figure I.10**). However, TREM2 signalling is cell-type specific and may be ligand specific too, as it may exert pro-inflammatory effects under certain circumstances (151, 152, 186).

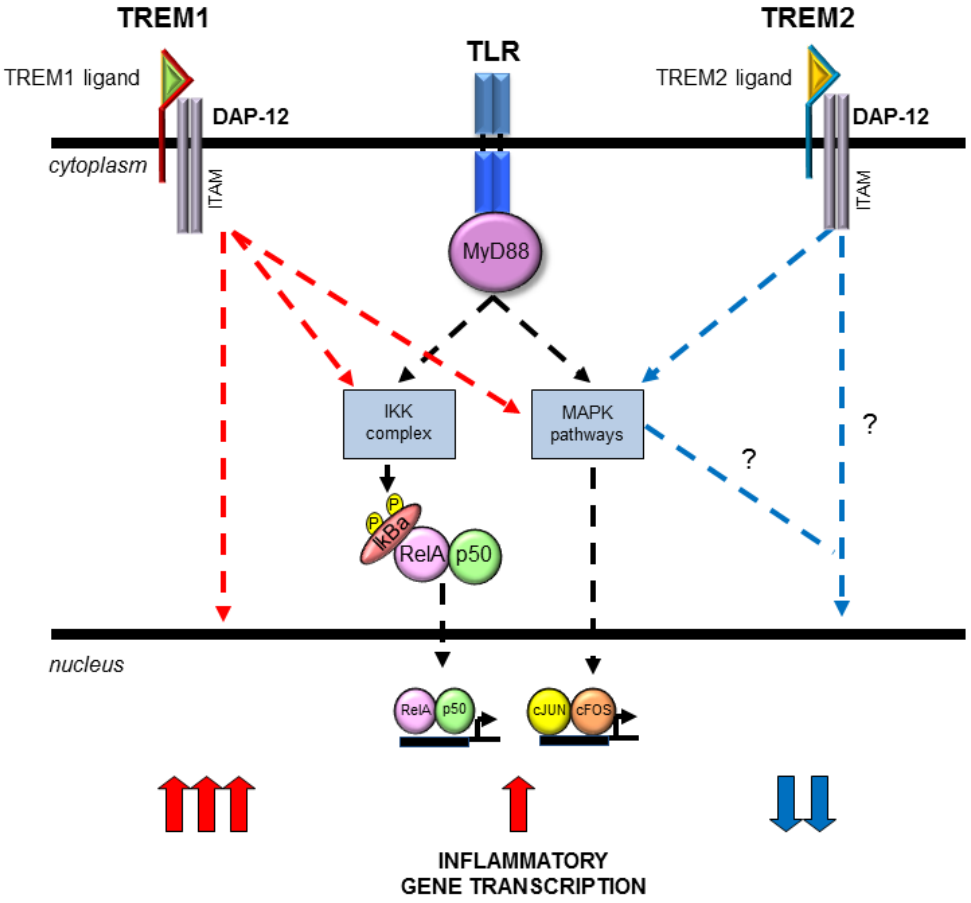

I.10. TLR-mediated signaling of TREM1 and TREM2. TREM1 and TREM2 both lack any signaling motif and therefore signal through ITAM motifs of DAP-12. TREM1 induces TLR signal amplification promoting the transcription of inflammatory genes. By contrast, TREM2 inhibits TLR-derived signaling reducing the transcription of inflammatory genes. These signals are further enhanced by non-TLR signalling. DAP-12, DNAX-activation protein 12; IKK, IκB kinase; ITAM, immunoreceptor tyrosine-based activation motif; MAPK, mitogen-activated protein kinases; Myd88, myeloid differentiation primary response gene 88; TLR, toll-like receptor; TREM, triggering receptor expressed on myeloid cells.

Importantly, TREM2 was described as a phagocytic receptor. In this regard, TREM2 has been shown to promote phagocytosis of apoptotic bodies by microglia (187, 188). However, a recent study showed that TREM2 was not involved in phagocytosis of apoptotic cells in the 5XFAD Alzheimer's disease (AD) model (189). In addition, TREM2 has been shown to promote bacterial clearance by peritoneal macrophages, bone marrow-derived macrophages (BMDM) and neutrophils (190, 191). However, surprisingly, *Trem2* deficient alveolar macrophages showed an increased phagocytosis of

bacteria (192), therefore, showing that TREM2-mediated phagocytosis may be cell-type specific.

TREM2 was first linked to a degenerative disease termed Nasu–Hakola, also known as polycystic lipomembranous osteodysplasia with sclerosing leukoencephalopathy (PLOSL) (193). PLOSL is a rare disease that is associated with bone cysts and fractures and dementia. Importantly, PLOSL patients have loss of function mutations in TYROBP (encoding DAP-12) or TREM2 (194). TREM2 was also associated to osteoclast differentiation from myeloid cells as osteoclast differentiation is impeded in patients-derived myeloid cells with mutations in *TREM2* (195).

More recently, TREM2 has attracted considerable interest due to its potential role in AD and other neurodegenerative diseases. In 2013, the TREM2 variant R47H (rs75932628) substitution was strongly associated to an increased predisposition to AD (196, 197). Since then, the role of TREM2 especially in microglia, the resident immune cells of the brain, has been extensively investigated (198), showing that TREM2 modulates the metabolism of microglia, via mTOR regulating the function of these cells (199). Moreover, TREM2 was shown to act as a sensor of lipids in microglia, such as phosphatidylcholine and sphingomyelin while the TREM2 variant R47H impaired the recognition of these lipids which was associated with β-amyloid accumulation and neuronal loss (189). Interestingly, human TREM2 transgene is able to restore the amyloid-β-induced microgliosis and microglial activation in the 5XFAD AD mice model (200). In addition, a missense variant of TREML2 was associated with protection to AD (201) and a recent study demonstrated that TREM2 and TREML2 have opposing roles in microglia activation (202).

The function of TREM2 has also newly been described in the gut, where it drives epithelial proliferation and stem cell replacement in crypts via the regulation of cytokine expression profile (203). Moreover, TREM2 levels are increased during inflammatory bowel disease (IBD) and TREM2 promotes mucosal inflammation during experimental colitis in mice (186). In addition, TREM2 is also expressed in alveolar macrophages, where it regulates opsonin secretion and bacterial phagocytosis (192). Besides, the expression of TREM2 has been found upregulated in lung cancer, gastric cancer, glioma, and renal cell carcinoma (204-207).

By contrast, the role of TREM2 in liver disease progression is largely unknown. TREM family expression in KCs and LSECs was analysed and TREM2 expression is suggested to be inhibited following LPS in both cell types (208). In addition, TREM2

expression in KCs was demonstrated to limit malaria parasite expansion in hepatocytes and *Trem2*$^{-/-}$ KCs showed an M2-like phenotype compared to WT KCs (209). Moreover, given that TREM2 attenuates TLR4-mediated inflammation and has previously been shown to be important in injury responses in the colon (203) and brain (188), we proposed that this receptor could play an important role in liver injury, inflammation, regeneration and cancer.

HYPOTHESIS AND OBJECTIVES

As TREM2 plays a role in various forms of injury our interest is centered on the analysis of the possible role of this receptor in the liver. Therefore, this dissertation aims to explore the potential implication of this receptor in different forms of liver disease, including acute and chronic liver injury and the development of HCC. Thus, we propose the following objectives to evaluate:

1. **Role of TREM2 in liver injury.**
    1.1. Gene expression analysis of *TREM2* in samples from healthy patients and from cirrhotic human tissue samples and in mouse models of liver injury.
    1.2. Analysis of TREM2 expression in liver cells.
    1.3. Determination of the role of this receptor in chronic liver injury.
    1.4. Characterization of the role of this receptor in acute liver injury.
    1.5. TREM2-mediated molecular mechanisms in liver injury.

2. **Role of TREM2 in liver regeneration.**
    2.1. Characterization of the potential role of TREM2 in the hepatic regenerative process and in hepatocyte proliferation.

3. **Role of TREM2 in HCC.**
    3.1. Gene expression analysis of *TREM2* in samples from healthy patients and from HCC human tissue samples and correlation with inflammation and fibrosis.
    3.2. Study of the role of the TREM2 receptor in the hepatocarcinogenic process.
    3.3. Mechanistic insights of TREM2 in hepatocarcinogenesis.

MATERIALS AND METHODS

M.1 Human liver tissue samples

M.1.1 San Sebastian cohort of patients

To carry out gene expression analysis at mRNA level, liver tissue from control individuals and patients with liver cirrhosis and HCC of different aetiology was obtained. Patient characteristics and liver-injury related serology are described in **Table M.1** and **Table M.2**. To perform TREM2 expression analysis by immunohistochemistry (IHC) 1 control sample and 5 cirrhotic liver samples were also used (**Table M.3**). Control liver tissue samples were obtained from non-neoplastic liver tissue resected specimens for colorectal metastasis and selected sections were located furthest away from tumour mass lesions. Samples for this study were provided by the Basque Biobank and were processed according to standard procedures approved by the Clinical Research Ethics Committees of the Basque Country and the Donostia University Hospital. An informed consent was obtained from all subjects.

Table M.1. Patient characteristics and parameters of liver-injury related serology of cirrhotic samples.

Parameters		**Controls***	**Cirrhotic**
Cases, n		21	23
Sex, n	Male	16	22
	Female	5	1
Age, n (±SD)		65.5 (±7.1)	60.8 (±8.7)
Aetiology, n	Alcoholic	-	9
	HCV	-	7
	HBV	-	2
	HCV, HBV	-	2
	HCV, HBV, HIV	-	1
	HCV, Alcoholic	-	1
	Idiopathic	-	1
Serum ALT, IU/L		20.85 (±7.10)	54.60 (±36.82)
Serum ALT, IU/L		23.52 (±5,85)	47.04 (±24.67)

Data are shown as median ± SD.

ALT, alanine aminotransferase; AST, aspartate transaminase; HBV, hepatitis B virus; HCV, hepatitis C virus; HIV, human immunodeficiency virus; IU, international units; SD, standard deviation.

* Background normal liver from resection specimens of colorectal liver metastasis.

Table M.2. Patient characteristics and parameters of liver-injury related serology of HCC samples.

Parameters		Controls*	HCC
Cases, n		21	35
Sex, n	Male	16	33
	Female	5	2
Age, n (±SD)		65.38 (±7.28)	62.80 (±9.13)
Aetiology, n			
	Alcoholic	-	10
	HCV	-	10
	HBV	-	2
	HCV, HBV	-	3
	HCV, HBV, HIV	-	1
	HCV, Alcoholic	-	1
	Hemochromatosis	-	1
	Idiopathic	-	7
Serum ALT, IU/L		21.19 (±7.32)	44.74 (±32.62)
Serum ALT, IU/L		23.19 (±6.19)	40.54 (±23.21)

Data are shown as median ± SD.

ALT, alanine aminotransferase; AST, aspartate transaminase; HBV, hepatitis B virus; HCC, hepatocellular carcinoma; HCV, hepatitis C virus; HIV, human immunodeficiency virus; IU, international units; SD, standard deviation.

* Background normal liver from resection specimens of colorectal liver metastasis.

Table M.3. Patient characteristics and parameters of liver-injury related serology used for histological analysis.

Parameters		Control*	Cirrhotic
Cases, n		1	5
Sex, n	Male	-	4
	Female	1	1
Age, n (±SD)		49	58.6 (±10.6)
Aetiology, n			
	HCV	-	1
	HBV	-	1
	HCV, HIV	-	1
	HCV, Alcoholic	-	1
	Fatty liver disease	-	1
Serum ALT, IU/L		33	87.8 (±51.20)
Serum ALT, IU/L		32	97.66 (±56.36)

Data are shown as median ± SD.

ALT, alanine aminotransferase; AST, aspartate transaminase; HBV, hepatitis B virus; HCC, hepatocellular carcinoma; HCV, hepatitis C virus; HIV, human immunodeficiency virus; IU, international units; SD, standard deviation.

* Background normal liver from resection specimens of colorectal liver metastasis.

M.1.2 *The cancer genome atlas (TCGA) cohort of patients*

TREM2 expression in 366 HCC and 49 surrounding normal tissue samples was also analysed in the obtainable RNAseq data of the TCGA. *TREM2* expression was also correlated to tumour stage.

M.1.3 *Human samples for hepatic myofibroblast isolation*

Isolation of human hepatic myofibroblasts was performed from livers of adult male patients after surgical resection with the approval of the Newcastle and North Tyneside Local Research Ethics Committee, subject to patient consent (10/H0906/41).

M.2 Experimental mouse models of liver injury and carcinogenesis

Animal experiments were performed in age-matched male C57BL/6 [wild type (WT)] and *Trem2* knockout (*Trem2*$^{-/-}$) mice bred at Biodonostia Research Institute or Medical University of Vienna. *Trem2*$^{-/-}$ mice backcrossed onto a >98% C57BL/6 background were obtained from Marco Colonna (Washington University) (184).

All procedures were approved by the Animal Experimentation Ethics Committee (CEEA) of the Biodonostia Research Institute as well as the Animal Care and Use Committee of the Medical University of Vienna and the Austrian Ministry of Sciences.

After the indicated treatments mice were sacrificed by cardiac puncture under general anaesthesia, body weight was recorded and blood was collected. Liver was extracted, weighted and processed as follows: 3 liver pieces (~50 mg) of different lobules from each mouse were fixed in paraformaldehyde 4% (Merck) for histological analysis. 2 liver pieces (~25 mg each, for mRNA and protein extraction) were collected from all mice and stored at -80ºC for further processing. The rest of the liver was also stored at -80ºC. Serum was extracted by centrifugation at 1500 g for 20 minutes at 4ºC. Alanine aminotransferase (ALT) and aspartate aminotransferase (AST) levels in serum were measured at the Donostia University Hospital in a Cobas 8000 c702 (Roche) analyser.

M.2.1 *CCl_4-induced acute liver injury model*

2 µl/g body weight CCl_4 (Sigma-Aldrich) was mixed 1:1 vol:vol with olive oil (Sigma-Aldrich) and intraperitoneally injected to 8-10 week old male WT mice. Mice were

sacrificed 24, 48 and 72 hours after for the analysis of *Trem2* expression. Similarly, the same model was carried out in 8 week old male WT and *Trem2*$^{-/-}$ mice, which were injected with CCl_4 and sacrificed after 6, 12 and 24 hours. Controls were injected with olive oil.

M.2.2 *Acute CCl_4 treatment and gut sterilization with antibiotics (Abx)*

6 week old WT and *Trem2*$^{-/-}$ male mice were treated for 4 weeks with a combination of antibiotics: 1 g/l ampicillin (Sigma-Aldrich), 1 g/l neomycin (Gibco), 1 g/l metronidazole (Acros Organics) and 500 mg/l vancomycin (Pfizer) in drinking water. After the antibiotic treatment, mice were intraperitoneally injected with CCl_4 at 2 µl/g body weight (CCl_4:olive oil at 1:1 [vol:vol]) and sacrificed after 12 hours. To determine intestinal permeability, all animals were gavaged with 4 kDa fluorescein isothiocyanate (FITC)-dextran (Sigma-Aldrich; 800 mg/kg body weight) four hours before the sacrifice. FITC-dextran was measured in 100 µl of mice serum by fluorimetry with an excitation wavelength of 485 nm and an emission wavelength of 535 nm using the Fluoroskan Ascent® fluorometer (Labsystems).

M.2.3 *CCl_4-induced chronic liver injury model*

8 week old WT male mice were intraperitoneally injected with CCl_4 at 2 µl/g body weight mixing it with olive oil 1:3 (vol:vol). Mice were injected twice per week during 12 weeks and sacrificed after 1, 3, 7 and 10 days for the analysis of *Trem2* mRNA expression as described (210). In the same way, a similar model was performed in 8 week old male WT and *Trem2*$^{-/-}$ mice, which were injected with CCl_4 twice per week during 8 weeks and sacrificed after 1 and 5 days. Controls were injected with olive oil.

M.2.4 *Bone marrow (BM) transplantation*

To perform BM transplantation *Trem2*$^{-/-}$ mice were crossed on a C57BL/6 background mice that ubiquitously express green fluorescent protein (GFP) (WT/GFP^{+}) to generate *Trem2*$^{-/-}$/Ub-GFP^{+} mice. BM was isolated from *Trem2*$^{-/-}$/Ub-GFP^{+} or WT-GFP^{+} expressing mice, while 8-10 week-old male WT and *Trem2*$^{-/-}$ mice were irradiated administrating γ irradiation (9 Gy). Mice were immediately reconstituted by intravenous injection of $2x10^6$ isolated BM cells to generate WT mice (WT/WT), *Trem2*$^{-/-}$ mice (*Trem2*$^{-/-}$/*Trem2*$^{-/-}$) or chimeric mice (WT/*Trem2*$^{-/-}$) and (*Trem2*$^{-/-}$/WT) mice (recipient

mouse and donor mouse, respectively). To control the efficiency of irradiation, 1 mouse of each genotype was left without reconstitution. Mice were kept under sterile conditions for 8 weeks after which repetitive CCl_4 injury was performed. BM reconstitution was confirmed by flow cytometry for GFP^+ blood leukocytes.

M.2.5 *BDL-induced cholestasis liver injury model*

WT male mice were surgically bile duct ligated and were sacrificed after 14 or 21 days. In short, mice were anesthetized, the abdomen was opened and bile duct was exposed. Afterwards, two surgical knots were performed on the bile duct using 5-0 non-absorbable sutures (**Figure M.1**). Finally, the peritoneum was sewed with 5-0 sutures and the skin with a 3-0 suture. Controls were sham operated.

M.2.6 *APAP-induced acute liver injury model*

APAP model was performed in 8-10 week old WT and *Trem2*$^{-/-}$ male mice (25-30 g). Mice were overnight starved, intraperitoneally injected with 300 mg/Kg or 500 mg/kg APAP (Sigma-Aldrich) dissolved in saline (Braun) and sacrificed 24 hours after. Controls were injected with saline.

M.2.7 *APAP-induced ALF*

For survival studies WT and *Trem2*$^{-/-}$ mice were injected with a lethal dose (750 mg/kg) of APAP and survival was monitored every hour during the first 30 hours and after that, it was monitored every day for the following days.

M.2.8 *DEN-induced liver carcinogenesis*

For studies of liver tumour development, 15 day-old WT and *Trem2*$^{-/-}$ mice were intraperitoneally injected with a single dose of DEN (Sigma-Aldrich) diluted in saline at a dose of 30 mg/kg body weight. Mice were sacrificed 30 or 40 weeks after DEN administration and tumours were manually counted and size was recorded. Control mice were injected with saline.

M.2.9 DEN-induced liver carcinogenesis and treatment with the anti-oxidant diet butylated hydroxyanisole (BHA)

Another group of WT and *Trem*2$^{-/-}$ mice were DEN treated in the same way and 15 weeks post-DEN injection were fed a diet supplemented with the antioxidant BHA (0,7% w/w) (Sigma-Aldrich). Mice were fed this diet for another 15 weeks and were sacrificed 30 weeks after DEN injection.

M.2.10 DEN-induced acute liver injury model

For short-term studies to asses DEN-induced hepatic injury and inflammatory response, experiments were performed in 8-10 week old male WT and *Trem2*$^{-/-}$ mice. Mice were intraperitoneally injected with a DEN dose of 100 mg/kg to induce liver DNA damage and mice were sacrificed 6, 24 and 72 hours after DEN administration. Control mice were injected with saline.

M.2.11 PHx model of liver regeneration

PHx was performed according to the method of Higgins and Anderson surgically removing ~70% of the liver (211). Adult male WT mice were used for the analysis of *Trem2* expression and animals were sacrificed 2, 4, 24, 48 and 72 hours after PHx. Similarly, PHx was performed in WT and *Trem*2$^{-/-}$ mice and these were sacrificed 6, 36, 72 hours and 5 days after the operation. In addition, Mice were injected intraperitoneally with 150 mg per kg of body weight of 5'-bromo-2'-deoxyuridine (BrdU; Sigma-Aldrich) two hours before culling to analyse proliferating hepatocytes.

M.3 Primary liver cell isolation, culture and treatments

M.3.1 In situ mouse liver perfusion for primary cell isolation

Liver perfusion was performed to digest the liver. In short, mice were anesthetized with 5% isoflurane (abbvie) in inhaling oxygen, then the abdomen was opened and the internal organs were exposed. Afterwards, the portal vein was cannulated with a 22G cannula (BD Insyte), the infusion tubing of the perfusion pump (Bio-Rad) was connected to the catheter and the inferior vena cava (IVC) was cut below the liver, which allows solutions to perfuse the liver and exit the IVC. Meanwhile, the liver was flushed with a perfusion buffer [10 mM 4-(2-hydroxyethyl)-1-piperazineethanesulfonic acid (hepes), 2.7 mM

KCl, 135 mM NaCl and 250 µM HNa_2PO_4 (all from Sigma-Aldrich)] to wash the liver at a flow of 5-7 ml/minute. After, 150 µl of liberase (Roche), which is a collagenase mixture, at 7 mg/ml and 10 mM $CaCl_2$ was added to the perfusion buffer and the liver was flushed at 3 ml/minute to achieve digestion of the liver. During this step, the IVC was clamped above the diaphragm in order to direct the solutions through the liver and to prevent the perfusion of other organs. To isolate HSCs and KCs, an additional intermediate digestion step with a solution containing Pronase was carried out, before the collagenase digestion. In this case, 100 µl of pronase (Roche) at 200 mg/ml were added to 50 ml of F-12 media (Gibco) and the liver was flushed at 3 ml/minute. Finally, the liver was carefully removed. For HSC isolation a minimum of 3 mouse livers are necessary to yield enough cells and in this case, livers were kept in ice until all the livers were perfused.

M.3.2 *Isolation of mouse hepatocytes*

After liver perfusion, livers were homogenized, filtered through a 70 µM cell strainer (Falcon) to eliminate undigested tissue remnants. Liver cell suspension was washed three times with William's medium E (Sigma-Aldrich) supplemented with 10% heat-inactivated foetal bovine serum (FBS) (Gibco), 1% penicillin-streptomycin (Gibco) and 1% MEM Non-essential amino acids (NEAA) (Gibco), by centrifugation at 800 g for 6 minutes at 4ºC. Hepatocytes were then resuspended in 25 ml of supplemented William's medium E. Next, a Percoll (Sigma-Aldrich) containing density gradient solution was prepared by adding 2.4 ml of phosphate buffered saline (PBS) 10X to 21.6 ml Percoll and adding the cells on top of this solution. Then, the gradient was centrifuged for 10 minutes at 1500 g at 4ºC without brake. Isolated hepatocytes were cultured in William's medium E supplemented with 10% FBS, 1% penicillin-streptomycin and 1% NEAA.

M.3.2.1 *Hepatocyte cell viability assay*

Hepatocytes isolated from WT and Trem2-/- mice were plated for 3 hours at 104 cells/well in opaque 96-well plates (Thermo fisher scientific). Afterwards, media was changed to William´s E Medium with 0.5% FBS, 1% penicillin-streptomycin and 1% NEAA. Hepatocytes were treated with 5 mM or 10 mM APAP for 24 hours after which the CellTiter-Glo® Luminescent Cell Viability Assay (Promega) was used to measure cell viability according to the manufacturer´s instructions. Briefly, the CellTiter-Glo® substrate was resuspended with the CellTiter-Glo® buffer and incubated for 30 minutes

at room temperature. Meanwhile, cells were also incubated for 30 minutes at room temperature. After the incubation, 100 µl of the resuspended mix was added to each well and the plate was incubated for two minutes shaking at room temperature. Finally, the plate was incubated for another 10 minutes at room temperature and luminometry was measured in a PHERAstar luminometer (BMG Labtech).

M.3.3 *Isolation of rodent non-parenchymal liver cells: KCs and HSCs*

After the *in situ* liver digestion, livers were further digested *in vitro* for 30 minutes at 37ºC in F-12 media supplemented with 10 µl pronase at 200 mg/ml and 50 µl DNase (Roche) at 2 mg/ml. Livers were homogenized, filtered through a 70 µM cell strainer and washed twice by centrifugation at 800 g for 6 minutes at room temperature. Subsequently, liver cell suspensions were subjected to density gradient centrifugation with Nycodenz (Sigma-Aldrich) (11% over 16.5%) at 1500 g at RT for 22 minutes without brake. KCs are collected in the 16.5% layer while HSCs are present in the 11% layer. KCs were plated at 10^6 cells/ml in 6 well dishes (Corning) in roswell park memorial institute medium 1640 (RPMI) (Gibco) supplemented with 10% FBS and 1% penicillin-streptomycin, and HSCs in Dulbecco's modified eagle medium (DMEM) (Gibco) supplemented with 10% FBS and 1% penicillin-streptomycin. KCs were plated for 20 minutes to allow them to adhere, and plates were then washed thoroughly to remove the contaminating endothelial cells. Purity of KCs was established by measuring liver cell type specific markers and all the experiments were carried out one or two days after the isolation. Purity of HSCs was assessed by autoflorescence one day after the isolation and was always higher than 95%. Experiments in activated HSC were carried out by culturing these cells on tissue culture plastic for 7 days at 37ºC and 5% of CO_2. Both KCs and HSCs were stimulated with $2x10^7$ cells/ml heat-killed *Escherichia coli* (*E. coli*) (O18:K1), 100 ng/ml LPS (Sigma-Aldrich), 10 ng/ml IL1β (Peprotech) or 10 ng/ml TNFα (Peprotech) for various time-points. Following treatment, cells were processed for RNA extraction or immunoblotting and stored at -80ºC, or supernatant was harvested and stored at -20ºC for cytokine measurements.

Activated HSCs from rat livers injured by BDL for 10 days or chronically injured with CCl_4 for 3 weeks were isolated as described (212).

Human hepatic myofibroblasts were isolated as described (213), were cultured in DMEM supplemented with 2 mM L-glutamine (Gibco), 16% FBS and 1% penicillin-streptomycin and were maintained at 37°C and at 5% CO_2.

M.3.4 *Isolation of liver cells for flow cytometry*

Liver mononuclear cells were isolated from chronic CCl_4-injured mice. Livers were first perfused with Hanks' Balanced Salt solution (HBSS) (Gibco) and then homogenised and digested for 1 hour at 37ºC in RPMI supplemented with 0.05% collagenase and dispase and 0.01% trypsin inhibitor (Gibco). The digested liver was then filtered through a 40 µM cell strainer (Falcon), centrifuged at 800 g for 10 minutes at 4ºC and resuspended with 10 ml RPMI media. A Percoll gradient was done by overlaying the resulting cell suspension in 15 ml of 33% (vol/vol) Percoll solution and centrifuging it for 30 minutes at room temperature without brake. Erythrocytes were lysed by adding 2 ml of red blood lysis buffer for 4 minutes to the cells. Cells were washed twice with RPMI and finally resuspended in PBS 1X with 2% of FCS. Total cell number per liver was counted using a hemocytometer and death cells were stained using fixable viability dye eFluor 780 (eBioscience). Fc receptors were blocked with CD16/CD32, clone 93 antibody (eBiosceince) and mononuclear cells were incubated with antibodies (**Table M.4**). Cells were washed, resuspended in PBS 1X and analysed by flow cytometry (BD LSR Fortessa). Neutrophils were identified as $CD45^+CD11b^+Ly6C^+Ly6G^+F4/80^-$ cells, whereas macrophages were identified as $CD45^+CD11b^+Ly6C^+Ly6G^-F4/80^+$ cells. Cell number was normalized with the total cell count and the liver weight. Blood staining was performed by the addition of antibodies for 30 minutes to 50 µl of sample. Cell lysis was performed by the addition of 140 µl of ADG lysis buffer (Andergrub Bioresearch) for 10 minutes and 3.5 ml of H_2O was added for another 7 minutes. Cells were washed, resuspended in PBS 1X and analysed by flow cytometry.

On the other hand, hepatocytes, KCs and HSCs were isolated as previously mentioned (**M.3.2** and **M.3.3**) and were analysed by flow cytometry following standard procedures. Cells were stained with APC-conjugated anti-mouse TREM2 antibody or an isotype control (**Table M.4**).

Table M.4. Antibodies used for flow cytometry.

Antibody	Company	Reference
Monoclonal rat anti-CD16/CD32, clone 93	eBioscience	14-0161-81
V500 monoclonal rat Anti-Mouse CD45, clone 30-F11	BD Horizon	561487
PE monoclonal rat anti-Ly-6G, clone 1A8	BioLegend	127607
PE/Cy7 monoclonal rat anti-Ly-6C, clone HK1.4	BioLegend	128017
PerCP/Cy5.5 monoclonal rat anti-F4/80, clone BM8	Invitrogen	45-4801-80
Alexa Fluor/700 monoclonal rat anti-CD11b, clone M1/70	Invitrogen	56-0112-82
Monoclonal rat anti-mouse TREM2 APC-conjugated	R&D	FAB17291A
Monoclonal rat IgG2B APC-conjugated	R&D	IC013A

IgG2B, Ig gamma 2b chain; PerCP, peridinin chlorophyll protein complex; TREM2, triggering receptor expressed on myeloid cells 2.

M.4 Isolation of BMDMs

BMDMs were isolated by flushing the femurs and tibias of mice with RPMI following a protocol previously described (214). BMDMs were differentiated in RPMI supplemented with 1% penicillin-streptomycin, 10% foetal calf serum (FCS) (Gibco) and 10% L-929 conditioned media for 7 days.

M.5 TREM2 overexpression in human hepatic stellate LX-2 cells

$3x10^5$ LX-2 cells were plated in 6 well plates in DMEM/F-12 supplemented with 2% of FBS and 1% penicillin-streptomycin. Cells were transfected using 1 μg of human TREM2 expression plasmid (Sino Biological Inc, HG11084-UT) or untagged negative control vector (Sino Biological Inc, CV011) with Fugene HD (Promega). In short, a mix with 1 μg of control or TREM2 plasmid per well was mixed with 100 μl of DMEM supplemented with 10 mM of hepes per well. Next, 6 μl of Fugene HD per well was added to the transfection mix and was incubated for 15 minutes at room temperature. Meanwhile media was changed and 875 μl of fresh DMEM/F-12 media supplemented with 2% of FBS and 1% penicillin-streptomycin was added to the cells. After 15 minutes of incubation, 100 μl of transfection mix was added to each well in a drop-wise manner. Transfection media was removed 8 hours after and replaced by DMEM/F-12 supplemented with 2% of FBS and 1% penicillin-streptomycin. 24 hours after, cells were treated for 3 hours with 100 ng/ml LPS and RNA was extracted for quantitative real-time polymerase chain reaction (qRT-PCR). In the same manner, LX-2 transfected cells and media were collected at different time-points post-transfection for qRT-PCR analysis and enzyme-linked immunosorbent assay (ELISA) respectively.

M.6 Culture of HCC spheroids with conditional media from HSCs

TREM2 was experimentally overexpressed in HSCs as previously mentioned. Twenty-four hours post-transfection, the cell culture supernatant was collected and incubated with the HCC spheroids. To generate the HCC spheroids, a total of 3000 Hep3B or PLC/PRF human HCC cells were seeded in a droplet of 20 µl of 10% FBS containing DMEM/F-12 media hanging in the lid of a petri dish for 7 days. Then, HCC spheroids were transferred to droplets of 20 µl of LX-2-conditioned media (i.e., media of LX-2 cells transfected with control plasmid or overexpressing TREM2) and were incubated hanging in the lid of a petri dish. Pictures of the HCC spheroids were taken at baseline (0 hours) and after 72 h using a Nikon eclipse TS100 microscope, and the spheroid size was measured with the Image J software. In addition, LX-2 cells or Hep3B spheroids were treated with 0.1 µM of the Wnt ligand secretion inhibitor IWP-2 (Sigma-Aldrich) and Hep3B spheroids were treated with the 5 µM of the Wnt/β-catenin inhibitor IWR-1 (Sigma-Aldrich).

M.7 Liver histology and staining

Tissue samples were collected and fixed in 4% paraformaldehyde for 24 hours, tissues were processed using the MTM tissue processor (Slee Medical GmbH), embedded in paraffin (Thermo fisher scientific) and cut using the HM355S microtome (Thermo fisher scientific) in sections at a thickness of 4-5 µm.

M.7.1 *Haematoxylin and eosin (H&E) staining*

H&E staining was performed to analyse tissue morphology as previously described (213). Human and mouse paraffin-embedded tissue samples were cut and then de-paraffined by incubating at room temperature in xylene (VWR) two times for 5 minutes. Slides were hydrated with solutions of decreasing alcohol concentration [100%, 96%, 70% and 50% ethanol (VWR)] for 2 minutes and finally with PBS 1X. Slides were incubated in Harris Haematoxylin (Merck) for 5 minutes. Then samples were washed with tap water and were incubated with eosin (Merck) for 5 minutes at room temperature. Next, samples were washed again with tap water and dehydrated with increasing grade alcohol solutions (50%, 70% and 100% ethanol). Finally, slides were incubated with xylene for 5 minutes at room temperature two times and were mounted with Pertex (Sigma-Aldrich).

M.7.2 *Sirius red staining*

Sirius red staining was performed for the determination of collagen deposition in liver tissue. Samples were de-parafinned and hydrated as previously described. Next, slides were stained for 2 minutes using 0.2% phosphomolybdic acid (Sigma-Aldrich). After that, samples were washed with distilled H_2O and incubated with 0.1% Sirius Red F3BA (Gibco) for 3 hours. Finally, slides were incubated with 0.01 N HCl (Merck) for 2 minutes and slides were dehydrated and mounted as previously mentioned.

M.7.3 *Liver histology and scoring*

Liver tissue samples were formalin-fixed, embedded in paraffin, cut in 5 μm thick sections and stained with H&E or Sirius red as previously described. All sections were blindly assessed by an experienced hepatopathologist.

Inflammation severity (scored 0-3, 0=none, 1=mild, 2=moderate, 3=severe), extent of necrosis (score 0-3, 0=none, 1=focal, 2=moderate, 3=extensive), acinar topography, type of inflammatory cells involved, and type of necrosis (zone 3, central-central bridging necrosis) were recorded. Hepatocyte injury, in the form of ballooned hepatocytes and apoptotic (oxyphilic) bodies, was also semi-quantitatively evaluated (score 0-3, 0=none, 1=few, 2=several, 3=many), and acinar involvement (zone 3 or both zones 3 and 2) was recorded. The presence, type and topography of hepatocyte steatosis were also recorded.

Fibrosis was evaluated based on the characteristic topography of fibrosis in chronic CCl_4-related liver damage (0=no significant fibrosis, 1=mild zone 3 sinusoidal fibrosis (Z3SF), 2=prominent Z3SF, 3=Z3SF plus central-central (C-C) fibrous septa, 4=advanced bridging fibrosis with C-C and few central-portal fibrous septa, 5=as per 4 plus occasional fully circumscribed nodules, 6=cirrhosis).

Damaged area in the acute DEN model was measured calculating the mean damaged area per field in 15 10X fields in each slide using NIS-Elements software (Nikon) in an Eclipse 80i (Nikon) microscope.

M.7.4 *IHC and image analysis*

IHC was performed in formalin-fixed and paraffin embedded mouse and human liver tissue sections. Mouse and human liver tissue sections were de-paraffinized in xylene and rehydrated in graded ethanol as previously described followed by 3% H_2O_2 (Sigma-

Aldrich) in methanol (Applichem Panreac) treatment for 15 minutes to block endogenous peroxidases. Thereafter, sections were subjected to antigen-retrieval and slides were blocked using the Avidin/Biotin Blocking Kit (Vector laboratories) after which slides were blocked with appropriate blocking buffers. Primary antibodies (**Table M.5**) were incubated at 4ºC overnight and the next day antibodies were washed with PBS 1X and slides were incubated with appropriate biotinylated secondary antibodies (**Table M.5**). Vectastain ABC Reagent (Vector laboratories) followed by 3,3-diaminobenzidine (DAB) peroxidase substrate Kit (Vector laboratories) was used for antigen visualization. Slides were counterstained with Mayer's haematoxylin (Sigma-Aldrich), dehydrated and mounted as previously described. Immunostained cells were manually counted in 15 high power fields (20X) of each slide and the mean number of positive cells was calculated. On the other hand, image analysis of 15 fields (20X) per slide was performed using NIS-Elements software for F4/80. Pictures were taken with NIS-Elements. Representative pictures were taken in an Eclipse 80i (Nikon) microscope using the Digital sight DS-U2 camera controller (Nikon).

An experienced hepatopathologist evaluated the IHC for human TREM2 by recording the type and topography of immunostained cells and evaluated the intensity of TREM2 specific cytoplasmic immunostaining as mild, moderate or severe compared to the immunostaining intensity of neutrophils in control liver sections.

For BrdU staining, IHC was performed in a similar way. Briefly, slides were de-waxed in xylene and hydrated in decreasing methanol concentration (100% and 70% methanol). Endogenous peroxidases were blocked; antigen retrieval was performed and primary antibody was incubated overnight at 4ºC. The next day slides were washed and incubated with a FITC-conjugated secondary antibody for 2 hours wrapped in foil. Next, slides were washed and incubated with a tertiary anti-FITC horseradish peroxidase (HRP) conjugated antibody. Antigen visualization, haematoxylin counterstaining, dehydration and mounting were performed as previously mentioned.

Table M.5. Antibodies used for IHC.

Antibody	Company	Reference	Dilution	Antigen retrieval
Rabbit polyclonal anti-4-HNE	Abcam	ab46545	1/200	citrate buffer pH6.0 (Vector laboratories)
Rat monoclonal anti-CD3	Serotec	MCA1477	1/100	1 mM pH8.0 EDTA (Sigma-Aldrich)

Rat monoclonal anti-F4/80	Abcam	ab6640	1/100	20 μg/ml proteinase K (Macherey-Nagel GmbH)
Rabbit Monoclonal anti-γH2AX	Cell Signalling	9718	1/100	1 mM pH8.0 EDTA
Rat monoclonal anti-Ly-6G	BD Pharmingen	551459	1/70	citrate buffer pH6.0
Rat monoclonal anti-NIMP.R14	Abcam	ab2557	1/100	citrate buffer pH6.0 followed by 2% trypsin in PBS 1X
Rabbit polyclonal anti-PCNA	Abcam	ab18197	1/6000	citrate buffer pH6.0
Rabbit polyclonal anti-TREM2	Sigma-Aldrich	HPA010917	1/200	citrate buffer pH6.0
Mouse monoclonal anti-BrdU	BD Biosciences	347580	1/10	citrate buffer pH6.0
Rabbit polyclonal anti-FITC conjugate	Inverness	F0313	1/100	-
Polyclonal Rabbit anti-FITC HRP conjugate	Dako	P5100	1/200	-
Swine anti-rabbit IgG biotinylated secondary antibody	Dako	E0353	1/200	-
Goat anti-rat IgG biotinylated secondary antibody	Serotec	STAR80B	1/200	-

4-HNE, 4-hydroxynonenal; BrdU, 5'-bromo-2'-deoxyuridine; BSA, bovine serum albumin; EDTA, ethylenediaminetetraacetic acid; FITC, fluorescein isothiocyanate; γH2AX, phospho-histone H2A.X; HRP, horseradish peroxidase; IgG, immunoglobulin G; IHC, immunohistochemistry; PCNA, proliferating cell nuclear antigen; TREM, triggering receptor expressed on myeloid cells.

M.8 Label free proteomic analysis

***M.8.1** In solution digestion*

Protein from DEN-induced WT and *Trem2*$^{-/-}$ tumour tissue was extracted using 7 M urea, 2 M thiourea, 4% CHAPS. Samples were incubated for 30 minutes under agitation at

room temperature and digested following the filter-aided FASP protocol as described (215). Trypsin was added to a ratio of 1:10 (trypsin:protein) and the mixture was incubated at 37^{o}C overnight, dried out in a RVC2 25 speedvac concentrator (Christ), and resuspended in 0.1% FA.

M.8.2 *Mass spectrometry (MS) analysis*

500 ng of each sample was submitted to liquid chromatography - mass spectrometry (LC-MS) label free analysis. Peptide separation was performed on a nanoACQUITY ultra performance liquid chromatography (UPLC) System (Waters) connected to an LTQ Orbitrap XL mass spectrometer (Thermo Electron). An aliquot of each sample was loaded onto a Symmetry 300 C18 UPLC Trap column (180 µm x 20 mm, 5 µm (Waters)). The precolumn was connected to a BEH130 C18 column (75 µm x 200 mm, 1.7 µm; Waters), and equilibrated in 3% acetonitrile and 0.1% FA. Peptides were eluted directly into an LTQ Orbitrap XL mass spectrometer (Thermo Finnigan) through a nanoelectrospray capillary source (Proxeon Biosystems), at 300 nl/minutes and using a 120 minutes linear gradient of 3-50% acetonitrile. The mass spectrometer automatically switched between MS and MS/MS acquisition in data-dependent acquisition mode. Full MS scan survey spectra (m/z 400-2000) were acquired in the orbitrap with mass resolution of 30000 at m/z 400. After each survey scan, the six most intense ions above 1000 counts were sequentially subjected to collision-induced dissociation (CID) in the linear ion trap. Precursors with charge states of 2 and 3 were specifically selected for CID. Peptides were excluded from further analysis during 60 seconds using the dynamic exclusion feature.

M.8.3 *Progenesis LC-MS software analysis*

Progenesis LC-MS (version 2.0.5556.29015, Nonlinear Dynamics) was used for the label free differential protein expression analysis. One of the runs was used as the reference to which the precursor masses in all other samples were aligned to. Only features comprising charges of 2+ and 3+ were selected. The raw abundances of each feature were automatically normalised and logarithmised against the reference run. Samples were grouped in accordance to the comparison being performed, and an ANOVA analysis was performed. A peak list containing the information of all the features was generated and

exported to the Mascot search engine (Matrix Science Ltd.). This file was searched against a Uniprot/Swissprot database restricted to *Mus musculus* entries, and the list of identified peptides was imported back to Progenesis LC-MS. Protein quantitation was performed based on the three most intense non-conflicting peptides (peptides occurring in only one protein), except for proteins with only two non-conflicting peptides. The significance of expression changes was tested at protein level, and proteins with a p-value ≤0.05 were selected for further analyses. Protein abundances were loaded onto Perseus software (216) and log2 transformed for the generation of the heatmaps.

M.8.4 *Functional analysis*

Gene ontology (GO) enrichment analysis of the differentially expressed proteins was carried out using the database for annotation, visualization and integrated discovery (DAVID) online tool (http://david.abcc.ncifcrf.gov/summary.jsp) (217). DAVID is a GO Term annotation and enrichment analysis tool used to highlight the most relevant GO terms associated with a given gene list. A Fisher Exact test was used in order to determine whether the proportion of genes considered into certain GO term or categories differ significantly between the dataset and the background. Biological Process, Molecular Function and Cellular Component categories were assessed, and only GO Terms enriched with a p-value <0.05 were considered for comparison and discussion.

M.9 Determination of protein expression by immunoblot

M.9.1 *Protein extraction from liver tissue*

Liver tissue (~20 mg) was homogenised in 400 µl of radio-immunoprecipitation assay (RIPA) lysis buffer which contains: 50 mM Tris pH 7.5 (Applichem Panreac), 150 mM NaCl (Sigma-Aldrich), 1% triton X100 (Sigma-Aldrich), 0.1% Sodium dodecyl sulfate (SDS) (Applichem Panreac), 0.5% sodium deoxycholate (Sigma-Aldrich), phosphatase inhibitors [1 mM sodium orthovanadate (Sigma-Aldrich), 10 mM NaF (Sigma Aldrich), 100 mM β-glycerophosphate (Sigma-Aldrich)] and protease inhibitors [Complete (Roche)]. Homogenised tissue was placed in a rotator (Stuart) for 30 minutes at 4ºC. Next, samples were sonicated (JP Selecta) two times for 15 seconds and centrifuged for 15

minutes at 18000 g at 4ºC. Supernatant was placed in a new tube for cell debris removal and total protein was quantified.

M.9.2 *Protein extraction from culture cells*

~2-3x10^5 cells were plated in 6-well plates and cultured in their corresponding media. Cells were washed with PBS 1X and 80 µl of RIPA was added to the plates. After scrapping, cells were collected and centrifuged for 15 minutes at 18000 g at 4ºC. Supernatant was placed in a new tube for cell debris removal and total protein was quantified.

M.9.3 *Determination of protein concentration*

Pierce Bicinchoninic acid (Thermo fisher Scientific) was used to measure total protein concentration in both tissue and cells. An aliquot of each sample was diluted 1/5 for cells or 1/40 for tissue, with distilled H_2O and placed in a 96-well plate (Corning). A standard curve was also prepared using bovine serum albumin (BSA). A and B reagents were mixed in a proportion 1:50 and 200 µl of the mixture was added to each sample. The plate was incubated 30 minutes at 37ºC in darkness and protein concentration was measured at 570 nm in a Multiskan Ascent® spectrophotometer (Thermo fisher Scientific)

M.9.4 *SDS polyacrylamide gel electrophoresis (SDS-PAGE) and immunoblotting*

To perform the SDS-PAGE, 30-60 µg of total protein was fractioned by 12.5% SDS-PAGE and then transferred onto nitrocellulose membranes (Bio-Rad). Blots were blocked in Tris-buffered saline with 0.1% Tween-20 (T-TBS) containing 5% BSA or 5% skim milk powder (all from Sigma-Aldrich) for 1 hour. Primary antibodies (**Table M.6**) were incubated overnight at 4ºC diluted in 5% BSA or 5% milk at 1:1000 dilution. The next day membranes were washed 3 times with T-TBS and incubated for 1 hour with appropriate HRP-conjugated secondary antibodies at 1:5000 dilution (**Table M.6**). Blots were washed and antigen was detected by ECL HRP Chemiluminiscent Substrate Reagent Kit (Invitrogen). β-actin was used as a protein loading control.

Table M.6. Antibodies used for immunoblot.

Antibody	Company	Reference	Dilution

Polyclonal rabbit anti-phospho-p44/42 MAPK (Erk1/2) (Thr202/Tyr204)	Cell signalling	9101	1/1000
Polyclonal rabbit anti-p44/42 MAPK (Erk1/2)	Cell signalling	9102	1/1000
Polyclonal rabbit anti-phospho-p38 MAPK (Thr180/Tyr182)	Cell signalling	9211	1/1000
Polyclonal rabbit anti-p38 MAPK	Cell signalling	9212	1/1000
Polyclonal rabbit anti-phospho-SAPK/JNK (Thr183/Tyr185)	Cell signalling	9251	1/1000
Polyclonal rabbit anti-SAPK/JNK	Cell signalling	9252	1/1000
Monoclonal rabbit anti-phospho-NFκB p65 (Ser536)	Cell signalling	3033	1/1000
Monoclonal mouse anti-NF-κB p65	Santa cruz	sc-8008	1/1000
Polyclonal rabbit anti-IκB-α (C-21)	Santa cruz	sc-371	1/1000
Polyclonal rabbit anti-PCNA	Abcam	ab2426	1/1000
Polyclonal rabbit anti-GAPDH	Abcam	Ab22555	1/1000
Monoclonal mouse anti-TREM2 (B-3)	Santa Cruz	Sc373828	1/100
Monoclonal mouse anti-β-Actin	Sigma-Aldrich	A5316	1/1000
Anti-rabbit IgG HRP-linked Antibody	Cell signalling	7074	1/5000
Anti-mouse IgG HRP-linked Antibody	Sigma-Aldrich	A4416	1/5000

Erk1/2, extracellular signal-regulated kinases 1/2; HRP, horseradish peroxidase; JNK , c-Jun N-terminal kinase; MAPK, mitogen-activated protein kinases; NF-κB, nuclear factor kappa B; PCNA, proliferating cell nuclear antigen; SAPK, stress-activated protein kinases;

M.10 ROS Measurement

M.10.1 *ROS measurement in liver tissue*

ROS levels were analysed in mouse liver tissue homogenising 20 mg of liver tissue in 500 µl PBS 1X. The lysate was sonicated and centrifuged for 10 minutes at 3200 g at 4ºC. The supernatant was transferred to a new tube and 50 µl of supernatant was incubated with 50 µl of 2′,7′-dichlorodihydrofluorescein diacetate (DCF) (Thermo fisher scientific) in opaque 96-well plates at a final concentration of 10 µM for 30 minutes at room temperature in darkness. Fluorescence was measured at excitation and emission wavelengths of 492 nm and 535nm respectively, in a Fluoroskan Ascent® spectophotometer.

M.10.2 *ROS measurement in cells*

Intracellular ROS was measured using the dye dihydrorhodamine 123 (DHR123) (Invitrogen). 10^6 cells/ml of WT and *Trem2*$^{-/-}$ BMDMs or KCs were plated in 24 well plates (Corning), treated for 3 hours with 100 ng/ml LPS and incubated 10 minutes with

the dye. Cells were washed with PBS 1X and ROS levels were analysed by flow cytometry.

M.11 Oxygen consumption assay

Oxygen consumption was analysed in KCs and BMDM plated in XF 24-well plates (Seahorse Bioscience). Cells were treated with 100 ng/ml LPS for 3 hours, media was replaced with 600 µl of buffer free Assay Medium (Seahorse Bioscience) and cells were incubated in a CO_2 free incubator at 37°C for 1 hour. Cells were transferred to XF24 Flux Analyzer (Seahorse Bioscience) and oxygen consumption was measured following the protocol. Briefly, 1 µM oligomycin was added to inhibit adenosine triphosphate (ATP) synthase, 3 µM trifluoromethoxyphenylhydrazone (FCCP) was used for mitochondrial uncoupling and 1 µM rotenone/antimycin was added to shut down the electron transport.

M.12 ELISA

M.12.1 *Cytokine and chemokine detection by ELISA*

The supernatant of isolated WT and *Trem2*$^{-/-}$ KCs and HSCs treated with *E. coli* or LPS was analysed by ELISA. C-X-C motif chemokine ligand 1 (CXCL1), MCP1 and IL6 were analysed with specific ELISAs following the manufacturer's instructions (R&D Systems).

Supernatant of LX-2 transfected cells was collected and ELISA of MCP1 and TNF was performed according to the manufacturer's instructions (Peprotech).

M.12.2 *Quantification of 4-hydroxynonenal (4-HNE) levels in liver tissue by ELISA*

OxiSelect™ HNE Adduct Competitive ELISA (Cell Biolabs) was used to measure 4-HNE protein adducts in liver tissues of WT and *Trem2*$^{-/-}$ mice following manufacturer´s instructions. Briefly, wells were coated with HNE conjugate by adding 100 µl of 1X conjugate diluent and 1 µg/ml HNE conjugate mixed at 1:1 ratio and incubated overnight at 4ºC. The next day, liquid was removed from the wells, 200 µl of assay diluent was added and incubated for 1 hour at room temperature, after which they were kept at 4ºC prior its use. Next, a standard curve of HNE-BSA was prepared ranging from 0 to 200 µg/ml. Then, the assay diluent was removed and 50 µl of sample or HNE-BSA standard curve was added to the wells and they were incubated for 10 minutes in an orbital shaker.

After that, 50 µl of anti-HNE antibody was added to each well and they were incubated for 1 hour at room temperature in an orbital shaker. Wells were washed 3 times and 100 µl of secondary antibody HRP conjugated was added for 1 hour at room temperature in an orbital shaker. After 3 washes, wells were incubated with 100 µl of substrate solution for ~5-10 minutes at room temperature in an orbital shaker. Finally, once the colour of the wells changed, 100 µl of stop solution was added and absorbance was measured at 450 nm in a Multiskan Ascent® spectrophotometer.

M.13 RNA isolation and qRT-PCR analysis

M.13.1 *Total RNA isolation*

RNA was isolated by homogenising small tissue samples (~20 mg) or cells in culture in 1 ml Tri-Reagent® (Sigma-Aldrich). 200 µl of chloroform (Merck) was added to the tubes and after vortexing, tubes were incubated at room temperature for 15 minutes and then centrifuged for another 15 minutes at 18000 g at 4ºC. The upper phase was transferred to a new tube and 500 µl of 2-propanol (AppliChem Panreac) was added. Tubes were mixed by inverting them several times, incubated 10 minutes at room temperature and centrifuged for 15 minutes at 18000 g at 4ºC. Supernatant was discarded and 1 ml of 75% ethanol was added. After a brief vortex tubes were again centrifuged for 15 minutes at 18000 g at 4ºC, the supernatant was discarded and the pellet was left to dry. Finally, pellets were resuspended in Ultrapure™ DNase/RNase-free distilled water (Gibco). RNA was quantified with NanoDrop® ND-1000 apparatus (Thermo fisher Scientific).

M.13.2 *Reverse transcription (RT) of RNA from human tissue samples*

The *SuperScript® VILO™ cDNA Synthesis Kit* (Life technologies) was used for human tissue RNA RT following manufacturer´s instructions. 2 µl of 10X SuperScript® Enzyme Mix, 4 µl of 5X VILO™ Reaction Mix and DNase/RNase-free distilled water to a total volume of 20 µl was added to 500 ng of total RNA of each sample.

RT was performed in a Verity 96 well thermal cycler (Applied biosystems) using a three step protocol: i) 10 minutes at 25ºC, ii) 1 hour at 42ºC, and iii) 5 minutes at 85ºC. DNase/RNase-free distilled water was added to the newly synthetized complementary deoxyribonucleic acid (cDNA) for a 12.5 ng/µl final concentration.

M.13.3 *RT of RNA from cell culture*

1 µg of extracted RNA was subjected to DNase treatment to remove genomic DNA by adding 1 µl of DNase I Amplification Grade (Invitrogen) and 1 µl of 10X DNase I Reaction Buffer (Invitrogen) and incubating for 20 minute at 37°C to enable the reaction. Next, 1 µl of 25 mM ethylenediaminetetraacetic acid (EDTA) (Invitrogen) was added and samples were incubated 10 minutes at 65°C, 1 minute at 90°C and kept at 4°C to chelate magnesium and stop DNase I reaction. Afterwards, to synthetize the cDNA, 30 µl of RT Mix (8 µl Buffer 5X, 4 µl Random primers 100 ng/µl, 4 µl Deoxy-nucleotide-triphosphate mix (dNTPs), 2 µl DTT, 1.2 µl RNase OUT, 1.2 µl M-MLVRT (all from Invitrogen) and 9.6 µl DNase/RNase-free distilled water) were added to the samples and reaction was performed by incubating the tubes 37°C for 60 minutes, 95°C for 1 minute and cooled at 4°C. Finally, obtained cDNA was diluted to a concentration of 12.5 ng/µl with DNase/RNase-free distilled water.

M.13.4 *Gene expression analysis by qRT-PCR*

For gene expression analysis, a mix was prepared with 10 µl of iQ™ SYBR® Green Supermix (Bio-Rad) 0.6 µl of 10 µM forward and reverse primers (**Table M.7**) and DNase/RNase-free distilled water to a final volume of 17 µl per sample and were added to Hard-Shell PCR plates 96-well (Bio-Rad). Afterwards 3 µl of each cDNA sample at 12.5 ng/µl were added and CFX96 apparatus (Bio-Rad) was used to detect DNA amplification using a iQ™ SYBR® Green Supermix standard protocol: i) cDNA denaturation and enzyme activation were performed by heating for 10 minutes at 95°C, ii) for DNA amplification 40 cycles of 3 steps consisting in 95°C for 15 seconds, 60°C for 30 seconds (primer binding) and 72°C for 45 seconds (extension) were carried out, iii) an incubation of 15 seconds at 95°C and iv) a dissociation curve was obtained by gradually increasing the temperature from 60°C to 93ºC. *Glyceraldehyde-3-phosphate dehydrogenase* (*GAPDH*) expression was used as a housekeeping control. Gene expression was determined using the ΔCT calculation and mRNA levels are expressed as arbitrary units (AU).

Table M.7. Primer sequences used for qRT-PCR.

Gene (human)	Forward primer (5' → 3')	Reverse primer (3' → 5')
ACTA2	CGGGACTAAGACGGGAATCCT	GTCACCCACGTAGCTGTCTT
COL1A1	GATGGCTGCACGAGTCACAC	AACGTCGAAGCCGAATTCCT
GAPDH	CCAAGGTCATCCATGACAAC	TGTCATACCAGGAAATGAGC
IL1B	AGCTACGAATCTCCGACCAC	CGTTATCCCATGTGTCGAAGAA
IL6	AAAGAGGCACTGGCAGAAAA	AGCTCTGGCTTGTTCCTCAC
IL8	GTGCAGTTTTGCCAAGGAGT	ACTTGTCCACAACCCTCTGC
MCP1	CAGCCAGATGCAATCAATGCC	TGGAATCCTGAACCCACTTCT
TNF	CCTGCTGCACTTTGGAGTGA	CAGCTTGAGGGTTTGCTACA
TREM2 1	ACGAGATCTTGCACAAGGCA	GGTAGAGACCCGCATCATGG
TREM2 2	CAAGATTCTAGCAGCCAGCG	CTCAGCCCTGGCAGAGTTTG
WNT3	ACAGCCTGGCCATCTTTGG	TATGATGCGAGTCACAGCCG
WNT7A	GCCCGGACTCTCATGAACTT	AAACTGTGGCAGTGTGGTCC
WNT8A	GCATTCAGTGCCTCTGCCT	ACTGGAACTTGCACTCCTCG
Gene (mouse)	**Forward primer (5' → 3')**	**Reverse primer (3' → 5')**
Acta2	TCAGCGCCTCCAGTTCCT	AAAAAAAACCACGAGTAACAAATCAA
Bax	TGAAGACAGGGGCCTTTTTG	AATTCGCCGGAGACACTCG
Bcl2	GTCGCTACCGTCGTGACTTC	CAGACATGCACCTACCCAGC
Bcl2l1	GACAAGGAGATGCAGGTATTGG	TCCCGTAGAGATCCACAAAAGT
Col1a1	TTCACCTACAGCACGCTTGTG	GATGACTGTCTTGCCCCAAGTT
Cxcl1	CTGGGATTCACCTCAAGAACATC	CAGGGTCAAGGCAAGCCTC
Cybb	TGTGGTTGGGGCTGAATGTC	CTGAGAAAGGAGAGCAGATTTCG
Gapdh	GCACAGTCAAGGCCGAGAAT	GCCTTCTCCATGGTGGTGAA
Hgf	ATGTGGGGGACCAAACTTCTG	GGATGGCGACATGAAGCAG
Hmox1	AAGCCGAGAATGCTGAGTTCA	GCCGTGTAGATATGGTACAAGGA
Hspa1b	GAGATCGACTCTCTGTTCGAGG	GCCCGTTGAAGAAGTCCTG
Il1b	GCAACTGTTCCTGAACTCAACT	ATCTTTTGGGGTCCGTCAACT
Il6	TAGTCCTTCCTACCCCAATTTCC	TTGGTCCTTAGCCACTCCTTC

Mcp1	TTAAAAACCTGGATCGGAACCAA	GCATTAGCTTCAGATTTACGGGT
Mmp13	CTTCTTCTTGTTGAGCTGGACTC	CTGTGGAGGTCACTGTAGACT
Nos2	GTTCTCAGCCCAACAATACAAGA	GTGGACGGGTCGATGTCAC
Tgfb1	CTCCCGTGGCTTCTAGTGC	GCCTTAGTTTGGACAGGATCTG
Tnf	CCCTCACACTCAGATCATCTTCT	GCTACGACGTGGGCTACAG
Trem2	TTGCTGGAACCGTCACCATC	CACTTGGGCACCCTCGAAAC
Gene (rat)	**Forward primer (5' → 3')**	**Reverse primer (3' → 5')**
Gapdh	TGTGAACGGATTTGGCCGTA	ATGAAGGGGTCGTTGATGGC
Trem2	AAGATGCTGGAGACCTCTGG	GGATGCTGGCTGTAAGAAGC

Acta2, actin alpha 2, smooth muscle; *Bax*, B-cell lymphoma 2 associated X, *Bcl2*, B-cell lymphoma 2; *Bcl2l1*, B-cell lymphoma 2-like 1; *COL1A1*, collagen type 1 alpha 1; *Cybb*, cytochrome b-245 beta; *Cxcl1*, C-X-C motif ligand 1; *GAPDH*, glyceraldehyde 3-phosphate dehydrogenase; *HGF*, hepatocyte growth factor; *Hmox1*, heme oxygenase 1; *Hspa1b*, heat-shock family member 1b; *IL*, interleukin; *MCP1*, monocyte chemoattractant protein 1; *MMP13*, matrix metalloprotease 13, *Nos2*, nitric oxide synthase 2; *tgfb1*, transforming growth factor beta-1; *TNF*, tumor necrosis factor; *TREM2*, triggering receptor expressed on myeloid cells 2; *WNT3*, Wnt family member 3; *WNT7A*, Wnt family member 7A; *WNT8A*, Wnt family member 8A.

M.14 Statistical analysis

GraphPad Prism 6.00 (GraphPad Software) was used to perform the statistical analysis. Data following a normal distribution were compared using a Student's T test and data not following a normal distribution were compared using Mann Whitney Test. When more than two groups were compared one-way analysis of variance with Tukey's post hoc test or Kruskal-Wallis test followed by Dunn's multiple comparison test for individual subgroup comparison were used. For correlation analysis non-parametric Spearman's correlation test was used. Data are expressed as mean ± standard error of the mean (SEM). Statistically significant data is represented in figures where *, **, ***, **** denote a *P* value of <0.05, <0.01, < 0.001 and < 0.0001 respectively.

RESULTS

R.1 Role of TREM2 in liver injury

R.1.1 *TREM2 expression is upregulated during chronic liver injury in humans*

First, the mRNA levels of *TREM2* in human liver tissue were analysed in a cohort of 21 control liver samples and 23 cirrhotic samples of different aetiologies, including HBV and/or HCV virus infection, HBV/HCV/HIV virus co-infection and alcoholics (**Table M.1**). Interestingly, we could observe upregulated *TREM2* transcript levels in diseased versus healthy liver (**Figure R.1A**). Moreover, *TREM2* mRNA levels correlated with liver injury markers ALT and AST, the inflammation markers *IL6* and *IL8* and collagen levels (**Figure R.1B-D**).

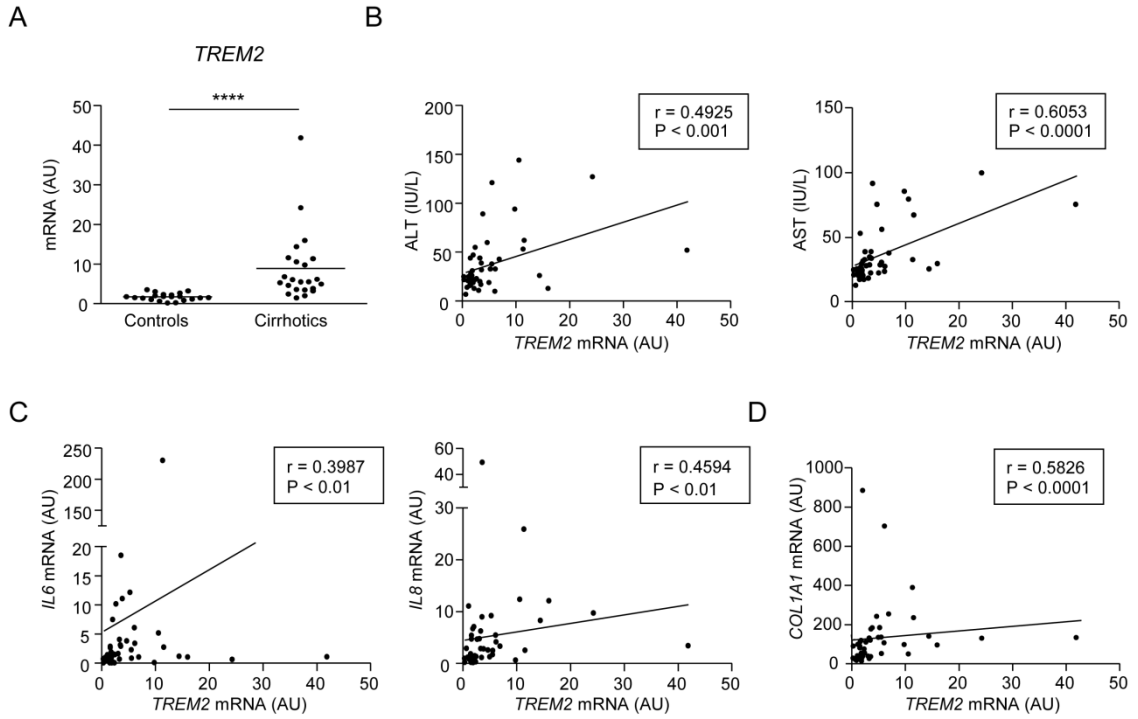

Figure R.1. *TREM2* mRNA expression in human liver disease. (**A**) *TREM2* mRNA expression analysis in 21 control livers and 23 cirrhotic tissue samples. (**B-D**) Correlation between *TREM2* expression and markers of liver injury and expression of inflammatory (*IL6* and *IL8*) and fibrotic markers (*COL1A1*). (**A**) Non-parametric Mann Whitney test was used. (**B-D**) Non-parametric Spearman's correlation test was used. ALT, alanine aminotransferase; AST, aspartate aminotransferase; AU, arbitrary units; *COL1A1*, collagen type 1 alpha 1; *IL*, interleukin; IU, international units; *TREM2*, triggering receptor expressed on myeloid cells 2.

Next, TREM2 expression was analysed by IHC in an independent cohort consisting of control liver and cirrhotic liver tissue samples of different aetiology (**Table M.2** and **Figure R.2**). The analysis of TREM2 immunostaining confirmed that TREM2 expression was more prominent in cirrhotic compared to control livers. In the control liver, mild cytoplasmic staining in monocytes and KCs was observed whereas no expression was detected in endothelial cells or lymphocytes. However, in cirrhotic samples TREM2 staining was observed in neutrophils, monocytes and macrophages in the fibrous septa, within sinusoids and in parenchymal inflammatory foci. Sirius red staining was also performed and collagen deposition was confirmed in fibrous septa (**Figure R.2**).

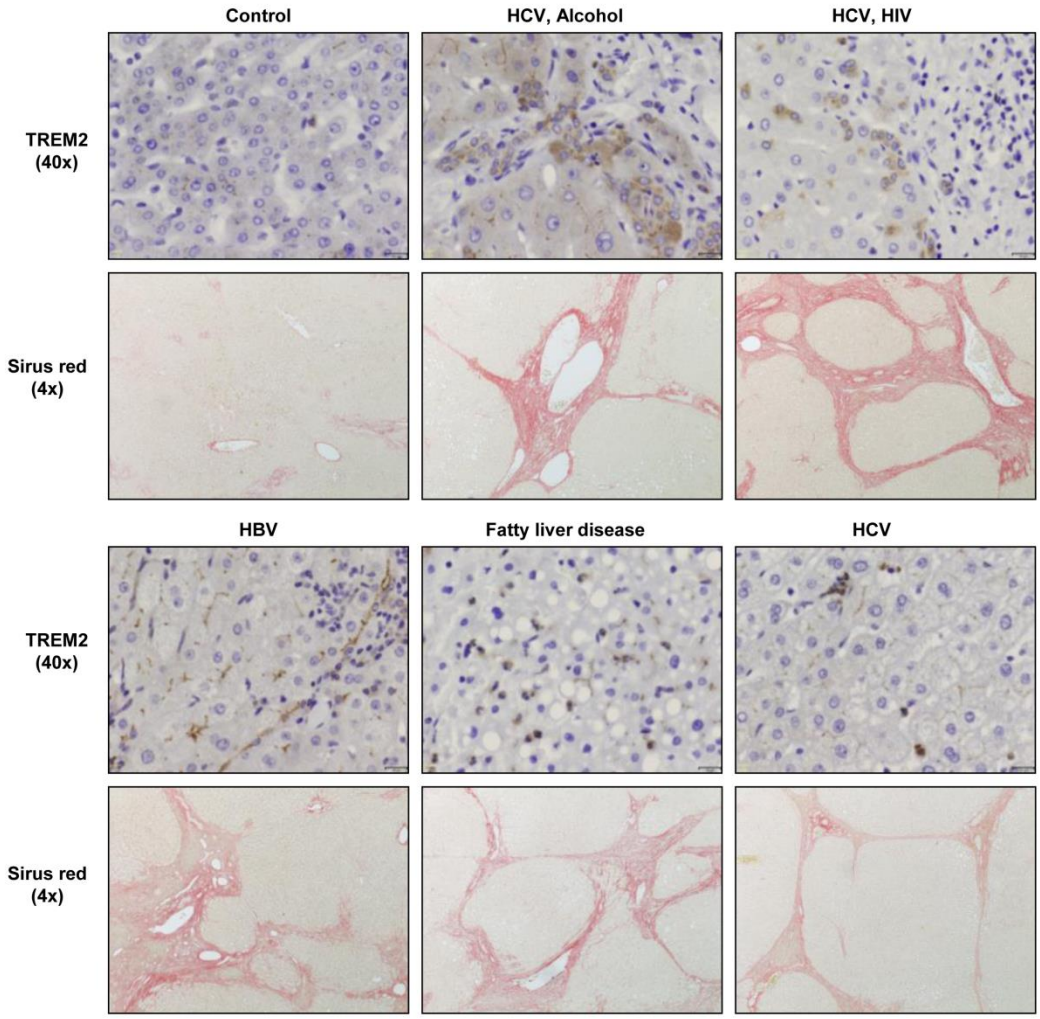

Figure R.2. TREM2 protein expression in human liver disease. TREM2 IHC staining and sirius red staining in a control liver tissue sample and 5 cirrhotic tissue samples of different aetiologies. HBV, hepatitis B virus; HCV, hepatitis C virus; HIV, human immunodeficiency virus; TREM2, triggering receptor expressed on myeloid cells 2.

Altogether, these data demonstrate that TREM2 expression increases during liver injury in humans and suggest that it could serve to dampen hepatic inflammation and injury.

R.1.2 *Trem2 expression is upregulated during acute and chronic liver injury in mice*

As in humans, *Trem2* expression was also upregulated during liver injury in mice (**Figure R.3)**. *Trem2* was induced during both CCl_4 mediated acute and chronic liver injury compared to olive oil treated controls (**Figure R.3A-B)**. Of note, after cessation of liver injury in the chronic CCl_4 model, levels of *Trem2* gradually descended but after 10 days of recovery remained slightly higher than olive oil injected mice (**Figure R.3B)**. Similarly, *Trem2* was upregulated during chronic cholestatic liver injury after BDL compared to sham operated mice (**Figure R.3C)**.

We conclude that during liver injury and recovery in mice *Trem2* expression is induced, indicating a potential role of this receptor in liver wound repair.

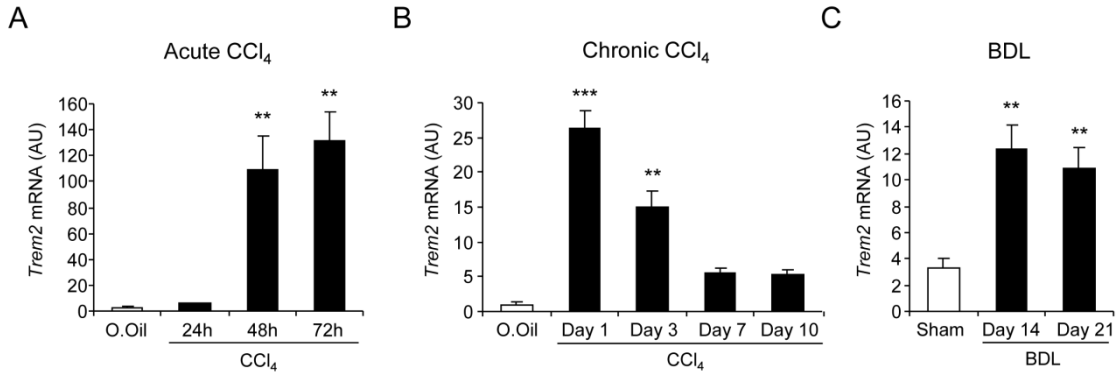

Figure R.3. Expression of *Trem2* during liver injury in mice. (**A**) *Trem2* mRNA expression was analysed in mice liver tissue after 24, 48 and 72 hours of CCl_4 administration (n=3). (**B**) CCl_4 was administered for 12 weeks and *Trem2* mRNA expression was measured 1, 3, 7 and 10 days after the last CCl_4 injection (n=3-5). (**A**-**B**) Olive oil was administered as control. (**C**) BDL surgery was performed and *Trem2* expression was measured after 14 and 21 days (n=4-5). Mice were sham operated as controls. One-way analysis of variance, followed by Tukey's posthoc test was used, data represent mean ± SEM and ** and *** denote a P value of <0.01 and <0.001, respectively versus O.Oil or sham mice. AU, arbitrary units; BDL, bile duct ligation; CCl_4, carbon tetrachloride; O.Oil, olive oil; *Trem2*, triggering receptor expressed on myeloid cells 2.

R.1.3 *TREM2 is expressed on non-parenchymal liver cells and its expression is induced during HSC activation*

The expression of TREM2 was analysed by flow cytometry in different mouse liver cell populations, demonstrating its expression in KCs and quiescent HSCs while no expression in hepatocytes was observed (**Figure R.4A**). These results were also confirmed by qRT-PCR (**Figure R.4B**), demonstrating that TREM2 is expressed in non-parenchymal liver cells. Next, *TREM2* expression during HSC activation was analysed by culturing freshly isolated quiescent HSCs in plastic for 7 days. *TREM2* was found strongly induced not only in mouse but also in rat and human activated HSCs compared to quiescent HSCs, showing a conserved upregulation during HSC trans-differentiation *in vitro* (**Figure R.4C**). We next compared the activation status of mouse HSCs in both genotypes, for that WT and *Trem2*$^{-/-}$ HSCs were isolated and the markers of HSC activation αSMA and α1(I)procollagen which are encoded by *Acta1* and *Col1a1* respectively were examined. However, no differences were observed in *Acta1* and *Col1a1* (**Figure R.4D**), suggesting that TREM2 does not affect the activation status of HSCs. We then focussed on HSC activation *in vivo* and for that, we isolated activated HSCs from chronic CCl_4 injured or BDL operated rats. Similarly, *Trem2* expression was significantly induced in HSCs isolated from chronic injured rat livers (**Figure R.4E**).

In conclusion, we demonstrated that TREM2 is expressed on non-parenchymal liver cells and during HSC activation.

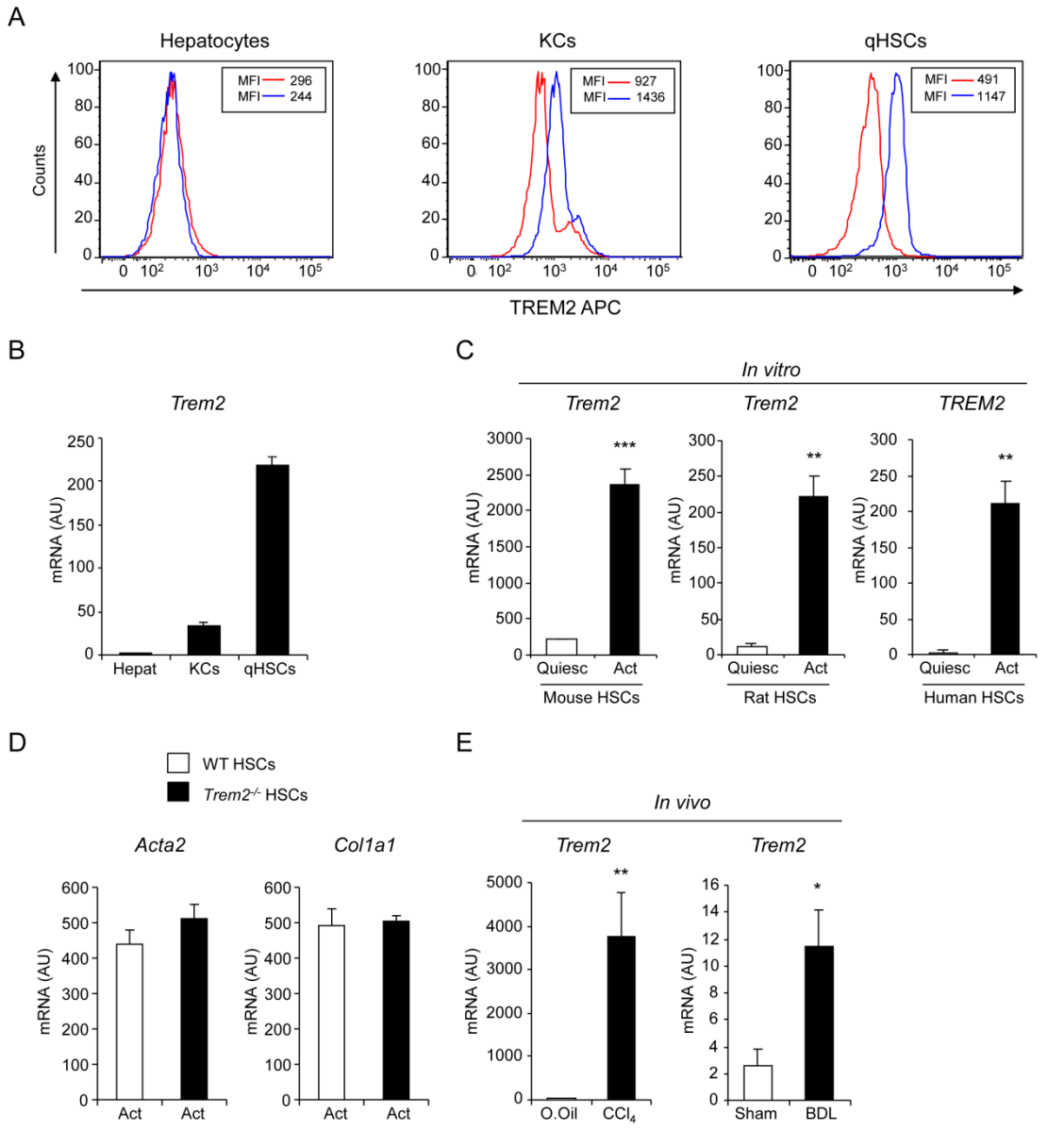

Figure R.4. TREM2 expression in liver cells and in activated HSCs during liver injury. (**A**) TREM2 expression in primary mouse liver cells (hepatocytes, KCs and qHSCs) detected by flow cytometry. Red line depicts the isotype and blue line depicts TREM2 antibodies. (**B**) *Trem2* mRNA expression in mouse hepatocytes, KCs and qHSCs (n=4-10). (**C**) *Trem2* mRNA expression in quiescent and activated mouse, rat and human HSCs (n=3). (**D**) mRNA levels of *Acta2* and *Col1a1* in WT and *Trem2*$^{-/-}$ mice isolated HSCs (n=3). (**E**) *Trem2* expression of activated HSCs isolated from rats treated with CCl_4 or BDL. Controls were treated with olive oil or sham operated (n=4-5). Parametric unpaired Student's t-test was used, data represent mean ± SEM and *, ** and *** denote a P value of <0.05, <0.01 and <0.001, respectively versus quiescent HSCs or O.Oil or sham mice. *Acta2*, Actin alpha 2, smooth muscle; AU, arbitrary units; BDL, bile duct ligation; CCl_4, carbon tetrachloride; *Col1a1*, collagen type 1 alpha 1; HSCs, hepatic stellate cells; KCs, Kupffer cells; O.Oil, olive oil; qHSC, quiescent HSC; *Trem2*, triggering receptor expressed on myeloid cells 2; WT, wild type.

The fact that *TREM2* expression was induced in a conserved manner during the activation of HSCs, suggested that TREM2 expression could play a role during chronic liver injury, a process where HSCs are key fibrogenic effectors as well as mediators of the cross-talk with other cell types, including liver resident and infiltrating cells, during hepatocellular injury.

R.1.4 *TREM2 halts chronic liver injury and inflammation*

We thus decided to study the role of TREM2 during chronic liver injury. For that purpose, we used WT mice and *Trem2*$^{-/-}$ mice and performed a model of chronic liver injury based on the administration of CCl_4 during 8 weeks. Mice were sacrificed 1 day (peak injury) or 5 days (recovery) after CCl_4 administration and serum transaminases were checked and histology as well as qRT-PCR analysis in the liver of these mice were performed.

We first analysed serum transaminase levels in these mice and found that they were significantly augmented during peak injury in *Trem2*$^{-/-}$ mice compared to WT mice (**Figure R.5A**) suggesting an increase in hepatocyte damage and death in *Trem2*$^{-/-}$ mice. In line with this, histologic analysis revealed increased apoptosis and necrosis in *Trem2*$^{-/-}$ livers and a non-significant tendency towards an increase in liver fibrosis in *Trem2*$^{-/-}$ mice (**Figure R.5B-C**).

We then analysed the mRNA expression of key inflammatory and fibrogenic mediators. The mRNA levels of monocyte chemoattractant protein 1 (*Mcp1*) and matrix metalloproteinase 13 (*Mmp13*) were induced 1 day after the last administration of CCl_4 in WT and *Trem2*$^{-/-}$ mice and recovered to almost basal levels after 5 days (**Figure R.6A**). Interestingly, *Trem2*$^{-/-}$ mice showed significantly elevated levels of *Mcp1* and *Mmp13* at peak injury compared to WT mice while no differences were recorded at recovery phase (**Figure R.6A**). In addition, mRNA expression of genes related to cellular stress and apoptosis were analysed and the stress marker *heat-shock family member 1B* (*Hspa1b*) and the anti-apoptotic marker *B-cell lymphoma 2-like 1* (*Bcl2l1*) were found upregulated at peak injury in *Trem2*$^{-/-}$ mice compared to WT mice (**Figure R.6B**).

We conclude that TREM2 is able to protect the liver from excessive injury in the context of iterative hepatotoxic damage.

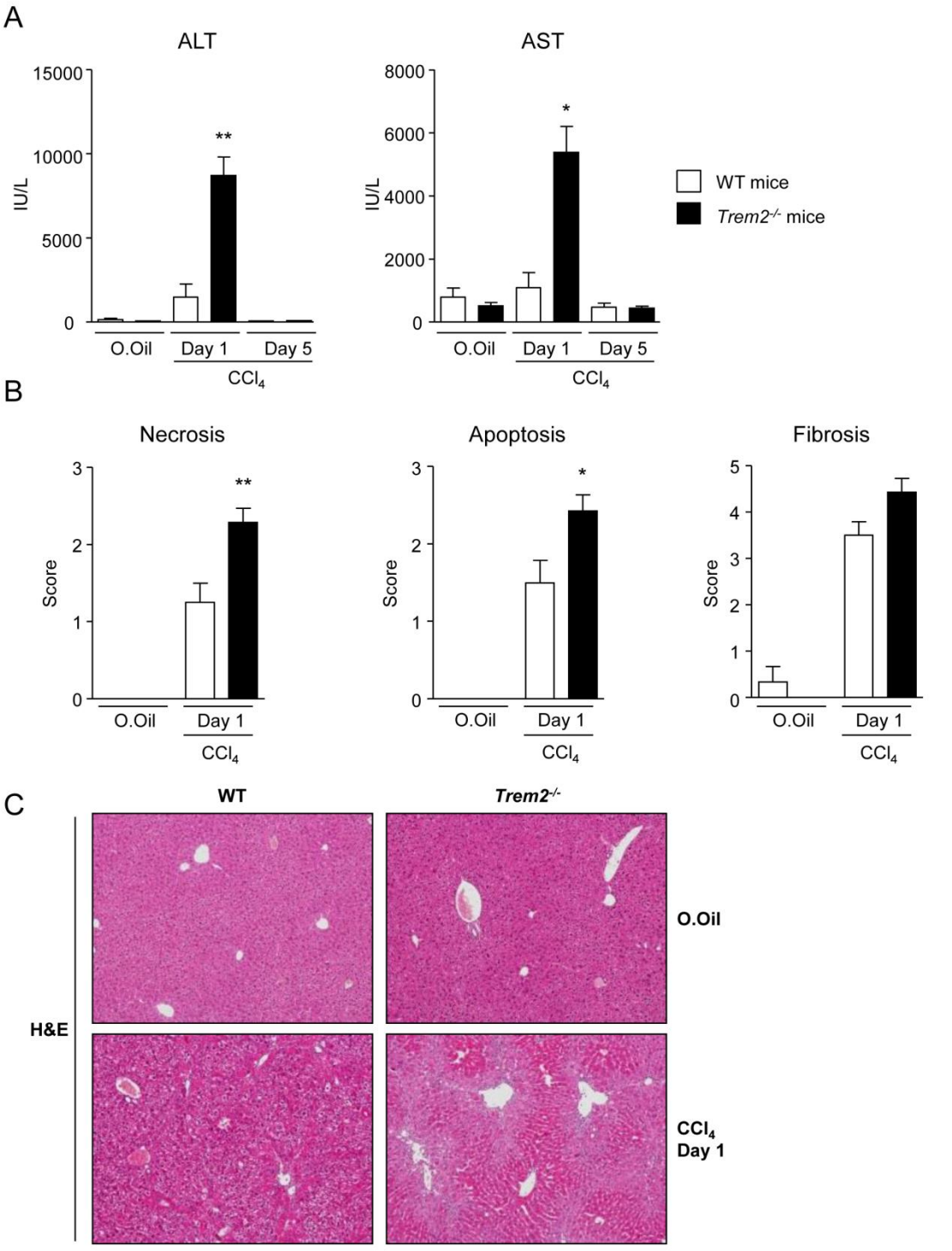

Figure R.5. TREM2 has a marked effect in chronic CCl_4-induced liver injury. WT and *Trem2*$^{-/-}$ mice were injected chronically for 8 weeks with CCl_4 and mice were sacrificed 1 and 5 days after the last injection (n=4-8). Controls were treated with olive oil (n=3). (**A**) ALT and AST levels were determined. (**B**) Histology was analysed for necrosis, apoptosis and fibrosis and (**C**) representative H&E (10X) from day 1 are shown. Non-parametric Mann Whitney test was used, data represent mean ± SEM and * and ** denote a P value of <0.05 and <0.01, respectively versus WT mice. ALT, alanine aminotransferase; AST, aspartate aminotransferase; CCl_4, carbon tetrachloride; H&E, haematoxylin and eosin; IU, international units; O.Oil, olive oil; *Trem2*, triggering receptor expressed on myeloid cells 2; WT, wild type.

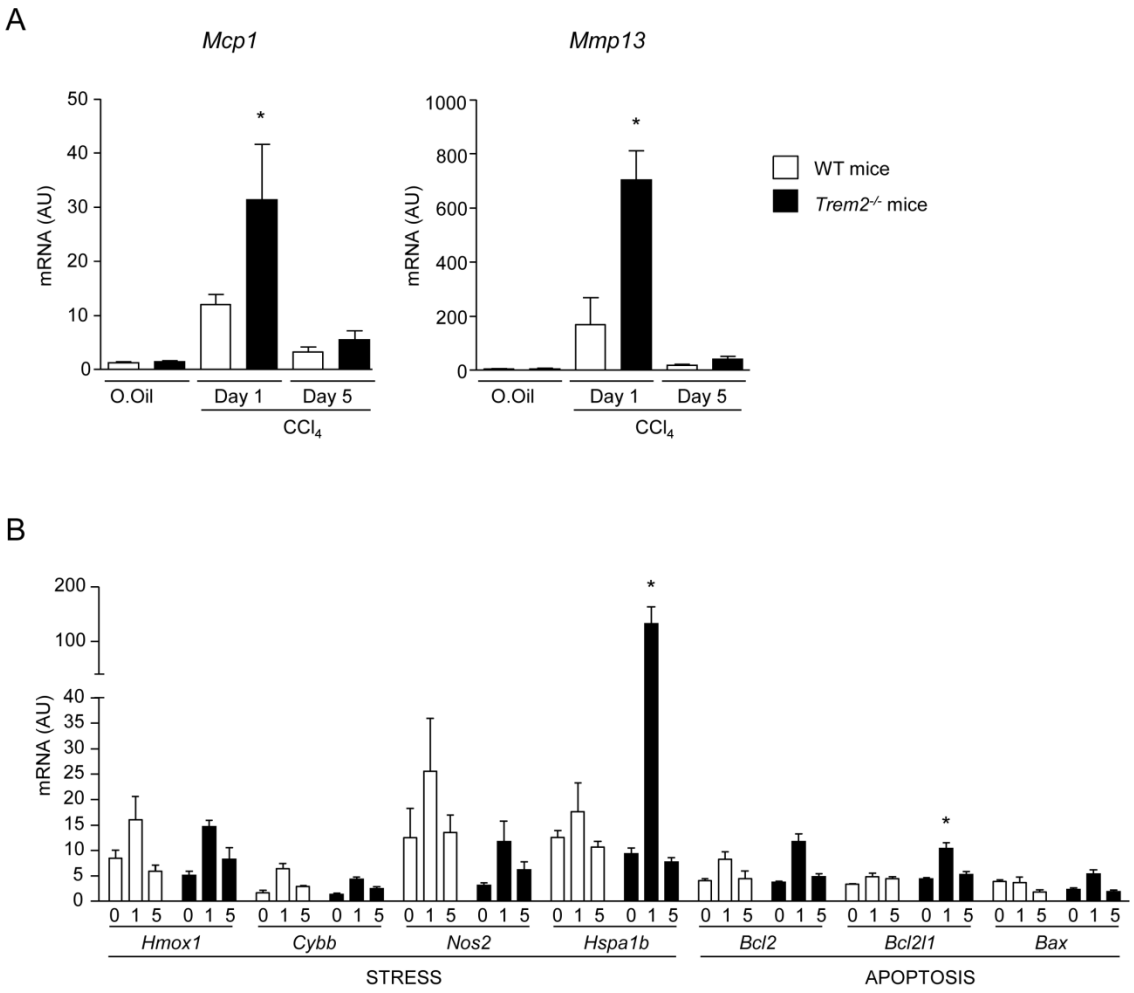

Figure R.6. mRNA expression analysis of key inflammatory, fibrogenic and injury mediators in the liver of WT and *Trem2*$^{-/-}$ mice after chronic CCl_4 administration. WT and *Trem2*$^{-/-}$ mice were injected chronically for 8 weeks with CCl_4 and mice were sacrificed 1 and 5 days after the last injection (n=4-8). Controls were treated with olive oil (n=3). (**A**) mRNA expression analysis of liver *Mcp1* and *Mmp13* and (**B**) stress and apoptosis-related genes was performed. Non-parametric Mann Whitney test was used, data represent mean ± SEM and * denotes a P value of <0.05. AU, arbitrary units; *Bax*, B-cell lymphoma 2 associated-X protein; *Bcl2*, B-cell lymphoma 2; *Bcl2l1*, B-cell lymphoma 2-like 1; CCl_4, carbon tetrachloride; *Cybb*, cytochrome b245 heavy chain; *Hmox1*, heme oxygenase 1; *Hspa1b*, heat-shock family member 1B; *Mcp1*, monocyte chemoattractant protein 1; *Mmp13*, matrix metalloproteinase 13; *Nos2*, nitric oxide synthase 2; O.Oil, olive oil; *Trem2*, triggering receptor expressed on myeloid cells 2; WT, wild type.

Intriguingly, when we checked the mRNA expression of other markers of inflammation, such as *Il6* and *Il1b*, *Tnf* and *transforming growth factor beta-1* (*Tgfb1*) no differences were observed between genotypes (**Figure R.7A-B**). In addition, although there was a tendency, towards having more *Acta2* and *Col1a1* mRNA levels in the livers *Trem2*$^{-/-}$ mice, Sirius red staining confirmed minor effects of TREM2 in liver fibrosis at peak injury (**Figure R.7C-D**).

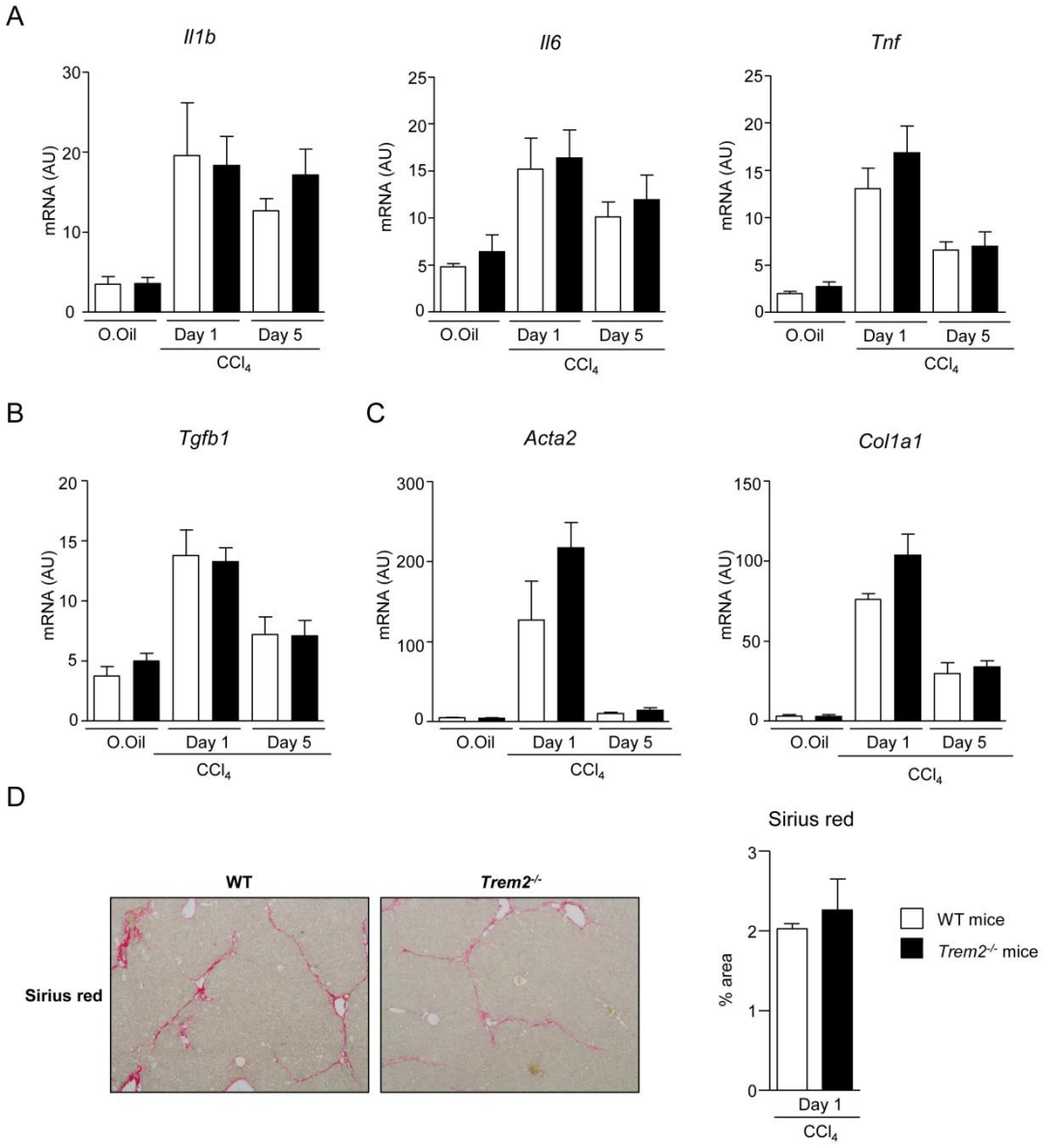

Figure R.7. No differences in inflammation and fibrosis in the liver of WT and *Trem2*$^{-/-}$ mice after chronic CCl_4 administration. Mice were treated as in **Figure R.4** and mRNA levels of (**A**) *Il1b*, *Il6* and *Tnf* cytokines and (**B**) *Tgfb1* and (**C**) *Acta2* and *Col1a1* were determined. (**D**) Representative sirius red stained image and quantifications are shown (4X) (n=3-8). Non-parametric Mann Whitney test was used, data represent mean ± SEM. AU, arbitrary units; CCl_4, carbon tetrachloride; *Il*, interleukin; O.Oil, olive oil; *Tgfb1*, transforming growth factor beta-1; *Tnf*, tumour necrosis factor; *Trem2*, triggering receptor expressed on myeloid cells 2; WT, wild type.

R.1.5 *Combined effect of resident liver cells and infiltrating immune cells is required for TREM2 to dampen chronic liver injury*

In order to elucidate which cells are contributing to TREM2-mediated dampening of chronic liver injury, we developed a BM transplantation model. For that WT and *Trem2*$^{-/-}$ mice were lethally irradiated and reconstituted with WT and *Trem2*$^{-/-}$ BM cells that ubiquitously express green fluorescent protein (GFP), generating 4 different groups of mice: WT/WT, *Trem2*$^{-/-}$/*Trem2*$^{-/-}$, WT/*Trem2*$^{-/-}$ and *Trem2*$^{-/-}$/WT (recipient and donor, respectively). Interestingly, corroborating previous results, the transaminase levels were found increased in *Trem2*$^{-/-}$/*Trem2*$^{-/-}$, compared to the other genotypes. Of note, a significant damage was only observed when both infiltrating and resident cells were null for *Trem2* (**Figure R.8A-B**).

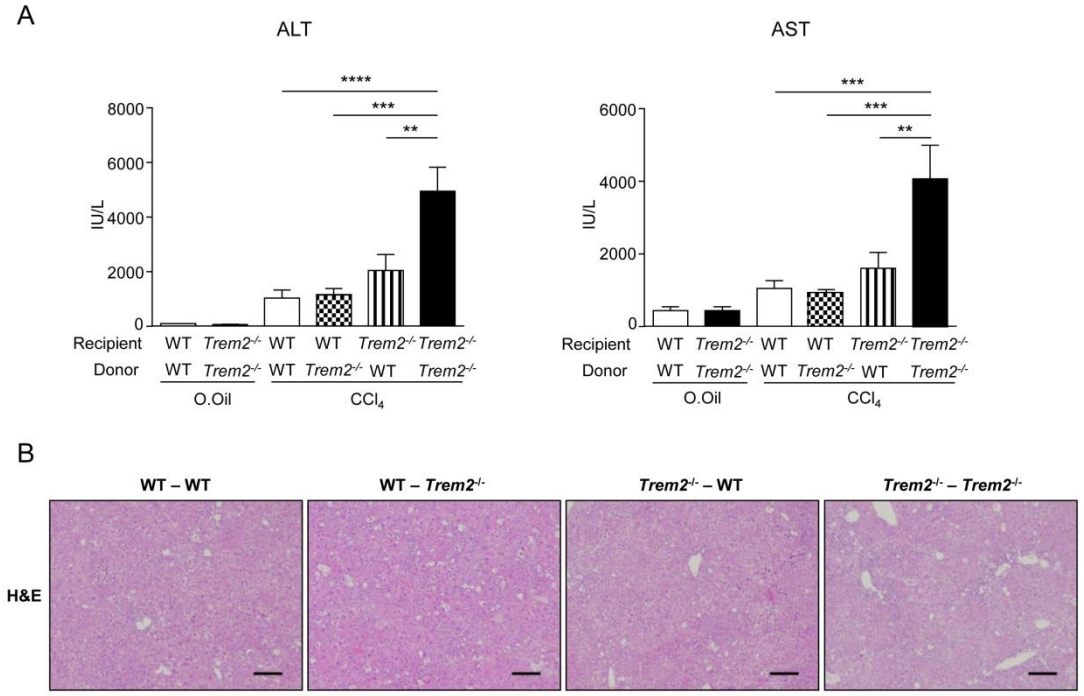

Figure R.8. **TREM2 expression within liver resident and infiltrating immune cells is necessary for the reduction of CCl_4 mediated chronic liver injury.** WT and *Trem2*$^{-/-}$ mice were lethally irradiated and reconstituted with WT-GFP^{+} BM (WT-WT) or *Trem2*$^{-/-}$-GFP^{+} BM (*Trem2*$^{-/-}$-*Trem2*$^{-/-}$), respectively. In addition, chimeric mice (WT-*Trem2*$^{-/-}$ and *Trem2*$^{-/-}$-WT) were also developed. These mice were treated for 8 weeks with CCl_4 and sacrificed 1 day after the last CCl_4 injection (n=3-5). Controls were treated with olive oil (n=3). (**A**) Serum ALT and AST levels were determined and (**B**) representative images of H&E staining are shown. One-way analysis of variance, followed by Tukey's posthoc test was used, data represent mean ± SEM and **, *** and **** denote a P value of <0.01, <0.001 and <0.0001 respectively. ALT, alanine aminotransferase; AST, aspartate aminotransferase; CCl_4, carbon tetrachloride; GFP, green fluorescent protein; H&E, haematoxylin and eosin; IU, international units; O.Oil, olive oil; *Trem2*, triggering receptor expressed on myeloid cells 2; WT, wild type.

Thus, we conclude that TREM2 protects from immune-mediated hepatocellular damage via its combined functions in liver resident and infiltrating immune cells.

Next, immune cell populations of the BM transplant model were analysed by flow cytometry (**Figure R.9**).

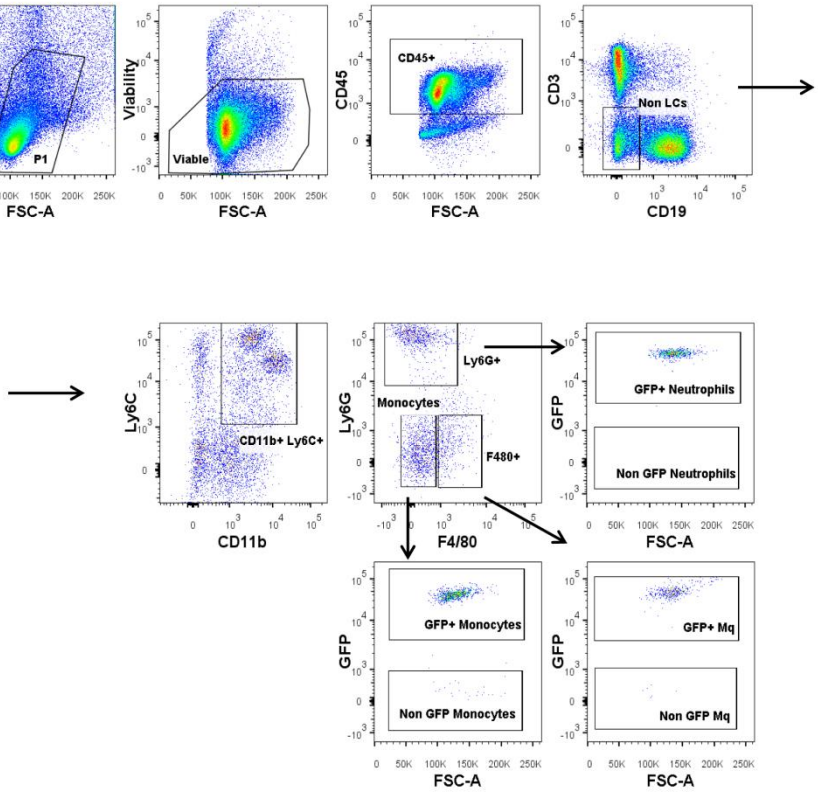

Figure R.9. Gating strategy used to determine liver neutrophil and macrophage numbers following BM transplantation and CCl_4 treatment. BM transplantation and CCl_4 treatment was performed as in **Figure R.8** and livers were isolated and analysed by flow cytometry. (**A**) Viable cells were gated for CD45 positivity, the non-lymphocyte ($CD19^-CD3^-$) fraction was selected and gated for $Ly6C^+$ and $Cd11b^+$. Infiltrating neutrophils were identified as $CD45^+CD11b^+Ly6C^+Ly6G^+F4/80^-GFP^+$ cells whereas monocyte derived macrophages were identified as $CD45^+CD11b^+Ly6C^+Ly6G^-F4/80^+GFP^+$ cells. CCl_4, carbon tetrachloride; GFP, green fluorescent protein; LCs, Leukocytes.

Importantly, successful reconstitution was obtained in all groups as shown by a nearly 100% of GFP positive blood leukocytes (**Figure R.10A**). When we monitored hepatic immune cell infiltration, recruited neutrophil numbers were not altered between the different groups of mice (**Figure R.10B**). However, there was an increase in the recruited monocyte derived macrophages in *Trem2*$^{-/-}$/*Trem2*$^{-/-}$ compared to the rest of the groups, correlating with the mRNA levels of the chemokine *Mcp1* (**Figure R.10C-D**).

These data demonstrates that TREM2 expression in both resident and infiltrating immune cells is necessary to dampen chronic CCl_4 induced liver injury.

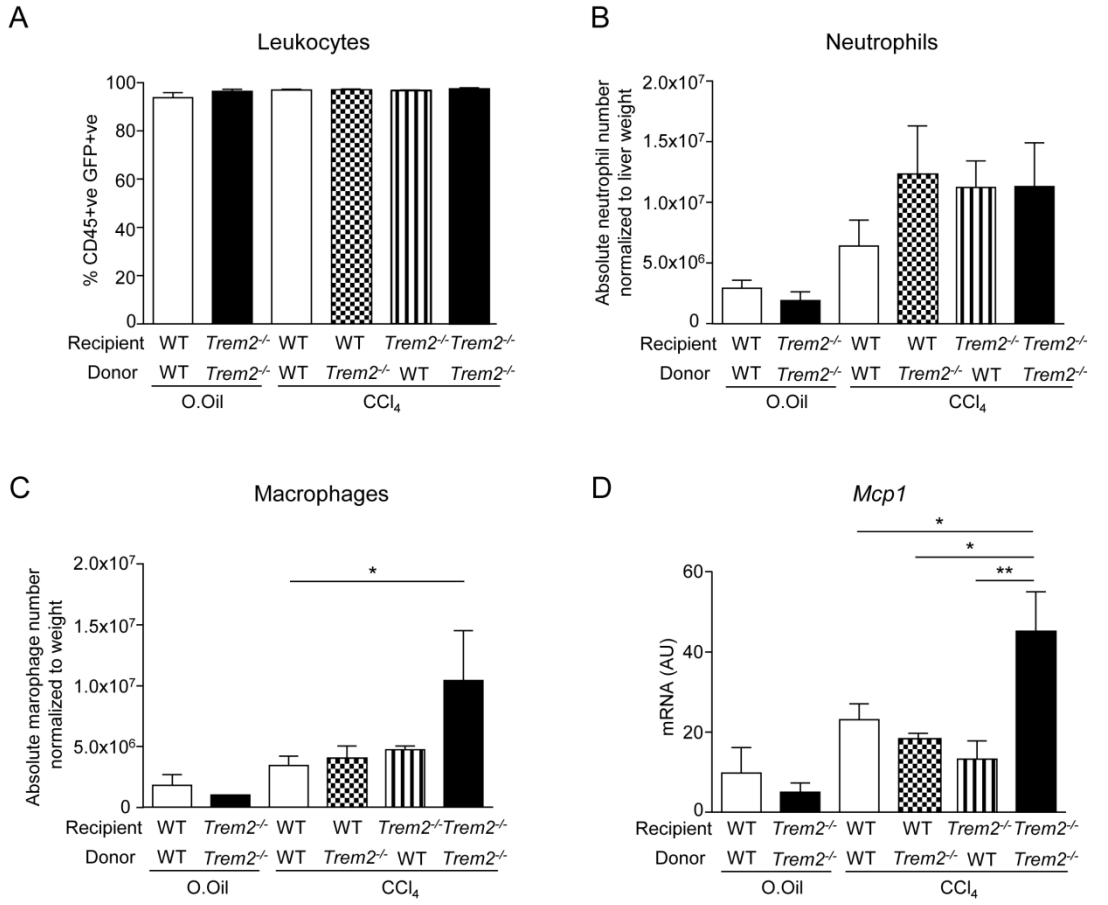

Figure R.10. Liver neutrophil and macrophage numbers following BM transplantation and CCl_4 treatment. BM transplantation and CCl_4 treatment was performed as in **Figure R.8** and livers were isolated and analysed by flow cytometry. (**A**) Blood was isolated and flow cytometry conducted for CD45 and GFP. Depicted is the % CD45+ cells that are GFP + within each group and represent mean ± SEM. n = 3 per genotype (olive oil) and 3-5 per genotype (CCl_4). (**B-C**) Livers were isolated and (**B**) hepatic neutrophil numbers were determined by gating on $CD45^+CD11b^+Ly6C^+Ly6G^+F4/80^-GFP^+$ cells and (**C**) monocyte derived macrophages were identified as $CD45^+CD11b^+Ly6C^+Ly6G^-F4/80^+GFP^+$ cells. Total number of (**B**) neutrophils and (**C**) macrophages normalised to liver weight are indicated. (**D**) *Mcp1* mRNA levels were analysed in the liver tissue of these animals. One-way analysis of variance, followed by Tukey's posthoc, data represent mean ± SEM and * and ** denote a P value of <0.05 and <0.01 respectively. AU, arbitrary units; CCl_4, carbon tetrachloride; GFP, green fluorescent protein; *Mcp1*, monocyte chemoattractant protein 1; O.Oil, olive oil; *Trem2*, triggering receptor expressed on myeloid cells 2; WT, wild type.

R.1.6 *TLR4-mediated inflammation is decreased by TREM2 in non-parenchymal liver cells*

As gut bacteria dysbiosis plays an important role in CCl_4-induced liver injury and inflammation (218, 219), we decided to uncover the role of TREM2 in non-parenchymal liver cells following TLR activation by LPS or *E. coli* stimulation. For that, we first analysed the inflammatory properties of WT and *Trem2*$^{-/-}$ KCs upon LPS or *E. coli* stimulation.

As shown in **Figure R.11**, LPS stimulated *Trem2*$^{-/-}$ KCs exhibited increased induction of the mRNA levels *Cxcl1*, *Il6*, *Tnf* and *Il1b* compared to WT KCs, as early as 1h post LPS treatment (**Figure R.11A**).

This was further confirmed when KCs were treated with the intestinal bacterium *E. coli* that also resulted in increased mRNA levels of pro-inflammatory cytokines in *Trem2*$^{-/-}$ KCs compared to WT (**Figure R.12A**). Moreover, these results were also confirmed at protein level by ELISA, and *Trem2*$^{-/-}$ KCs showed increased mRNA levels of *Cxcl1* and *Il6* compared to WT KCs after LPS or *E. coli* stimulation (**Figure R.11B and Figure 12B**). However, we could not observe any difference in LPS-induced *Mcp1* transcript levels within WT and *Trem2*$^{-/-}$ KCs (**Figure R.11C**).

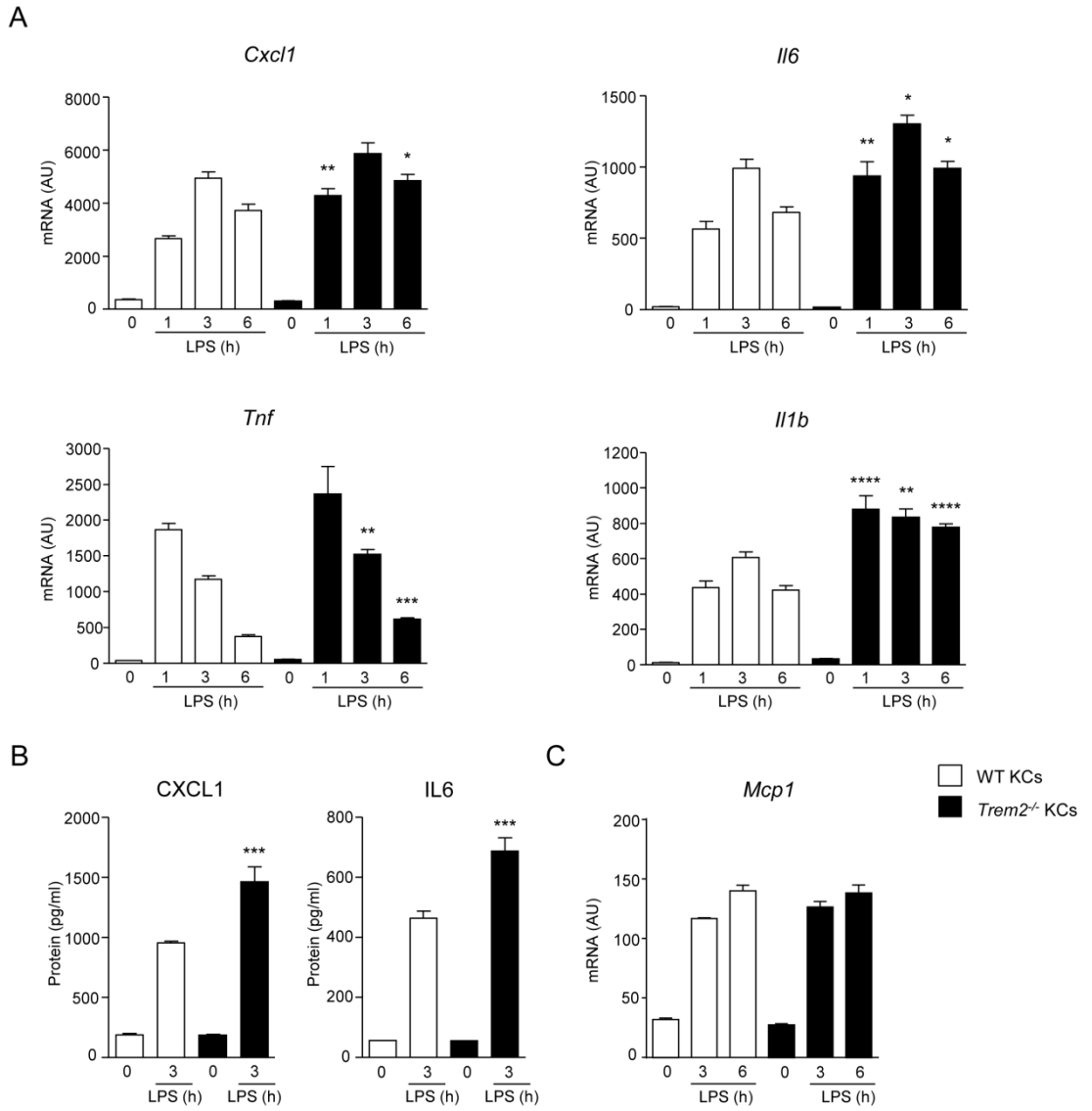

Figure R.11. Cytokine responses in WT and *Trem2*$^{-/-}$ KCs after TLR4 stimulation. (**A**) WT and *Trem2*$^{-/-}$ KCs were treated with LPS (100 ng/ml) for 1, 3 or 6 hours and levels of *Cxcl1*, *Il6*, *Tnf* and *Il1b* were determined by qRT-PCR (n=4-5). (**B**) WT and *Trem2*$^{-/-}$ KCs were treated with LPS (100 ng/ml) for 3 hours and protein levels of CXCL1 and IL6 were evaluated in the supernatant by ELISA (n=4-5). (**C**) WT and *Trem2*$^{-/-}$ KCs were treated with LPS (100 ng/mL) and mRNA levels of *Mcp1* were determined (n=4). One-way analysis of variance, followed by Tukey's posthoc test was used, data represent mean ± SEM and *, **, *** and **** denote a P value of <0.05, <0.01, <0.001 and <0.0001, respectively versus WT KCs. AU, arbitrary units; *Cxcl1*, C-X-C motif chemokine ligand 1; *Il*, interleukin; KCs, Kupffer cells; LPS, lipopolysaccharide; *Mcp1*, monocyte chemoattractant protein 1; *Tnf*, tumour necrosis factor; *Trem2*, triggering receptor expressed on myeloid cells 2; WT, wild type.

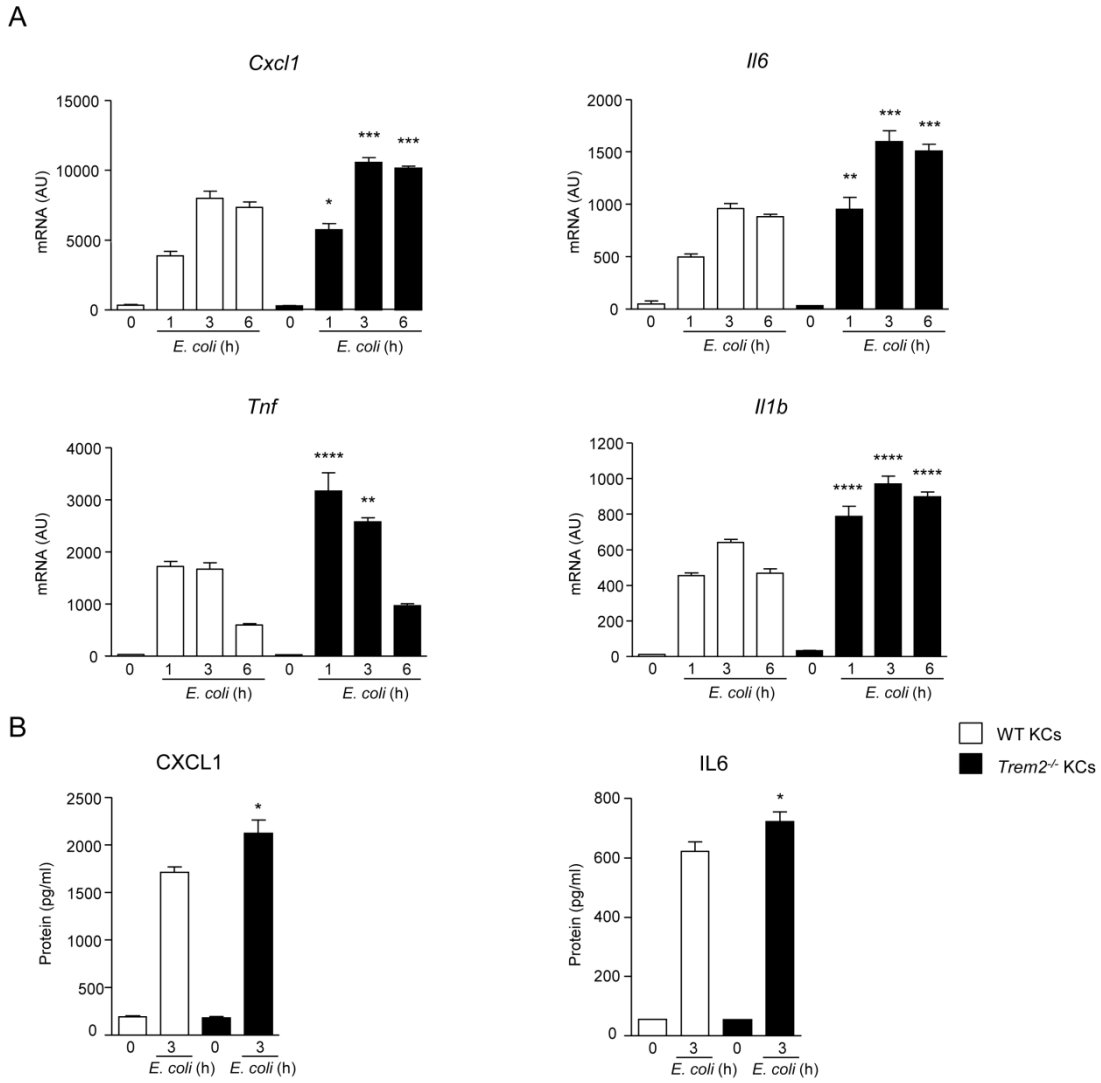

Figure R.12. Cytokine responses in WT and *Trem2*$^{-/-}$ KCs upon heat-killed *E.coli* treatment. (**A**) WT and *Trem2*$^{-/-}$ KCs were treated with heat-killed *E. coli* (2×10^7 CFU/ml) for 1, 3 or 6 hours and levels of *Cxcl1*, *Il6, Tnf* and *Il1b* were determined by qRT-PCR (n=4-5). (**B**) WT and *Trem2*$^{-/-}$ KCs were treated with heat-killed *E. coli* (2×10^7 CFU/ml) for 3 hours and protein levels of CXCL1 and IL6 were evaluated in the supernatant by ELISA (n=4-5). One-way analysis of variance, followed by Tukey's posthoc test was used, data represent mean ± SEM and *, **, *** and **** denote a P value of <0.05, <0.01, <0.001 and <0.0001, respectively versus WT KCs. AU, arbitrary units; CFU, colony-forming unit; *Cxcl1,* C-X-C motif chemokine ligand 1; *E. coli*, *Escherichia coli*; *Il*, interleukin; KCs, Kupffer cells; *Tnf*, tumour necrosis factor; *Trem2*, triggering receptor expressed on myeloid cells 2; WT, wild type.

As we had reported an increased mRNA expression of *Mcp1* during chronic liver injury *in vivo* (**Figure R.6A and Figure R.10D**) and that KCs were not the source of the increase in Mcp1 levels (**Figure R.11**) we speculated about other possible cellular sources of these chemokine. In this sense, HSCs could be a source of *Mcp1 in vivo*. Indeed when we treated WT and *Trem2*$^{-/-}$ HSCs with LPS or *E. coli*, we found increased levels of the *Cxcl1* and MCP1 chemokines in *Trem2*$^{-/-}$ HSCs compared to WT HSCs (**Figure R.13A-B**).

To corroborate this, we performed gain of function experiments on human LX-2 HSCs. Thus, LX-2 cells were transfected with a control plasmid or a TREM2 plasmid and were treated with LPS. As expected, TREM2 overexpression in LX-2 cells dampened LPS-induced *MCP1* and *IL6* mRNA levels (**Figure R.13C**).

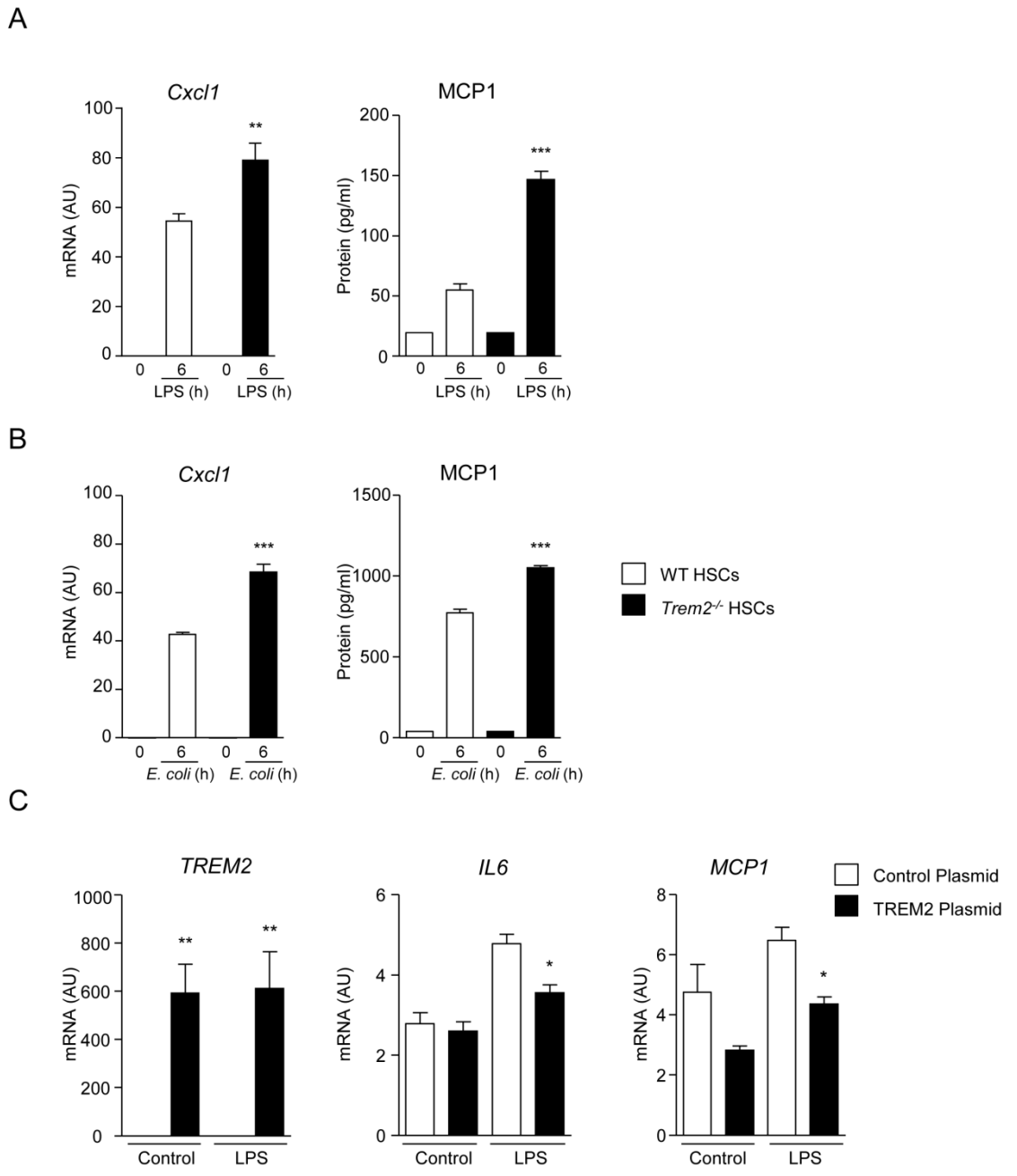

Figure R.13. Cytokine responses in WT and *Trem2*$^{-/-}$ HSCs upon LPS and heat-killed *E.coli* treatment. *Cxcl1* mRNA levels and MCP1 protein levels in WT and *Trem2*$^{-/-}$ activated mouse HSCs treated with 100 ng/ml LPS or (**A**) 2×10^7 CFU/ml heat-killed *E. coli (**B**)* (n=3-4). (**C**) Human HSC LX-2 cells were transfected with a control or *TREM2* overexpressing plasmid, 36 hours post-transfection were stimulated with 100 ng/ml LPS for 3 hours and levels of *TREM2*, *IL6* and *MCP1* were determined by qRT-PCR (n=4). One-way analysis of variance, followed by Tukey's posthoc test was used, data represent mean ± SEM and *, ** and *** denote a P value of <0.05, <0.01 and <0.001, respectively versus WT HSCs or control plasmid LX-2 cells. AU, arbitrary units; CFU, colony-forming unit; *Cxcl1*, C-X-C motif chemokine ligand 1; *E. coli*, *Escherichia coli*; HSCs, hepatic stellate cells; IL6, interleukin 6; LPS, lipopolysaccharide; MCP1, Monocyte chemoattractant protein 1; TREM2, triggering receptor expressed on myeloid cells 2; WT, wild type.

We also tested whether TREM2-mediated effects in inflammation were only specific for TLR dependent signalling or if other signalling pathways could also be involved. With that purpose, we treated isolated mouse WT and *Trem2*$^{-/-}$ KCs and HSCs with LPS, TNFα or IL1β. *Trem2*$^{-/-}$ KCs displayed increased pro-inflammatory gene expression compared to WT KCs only when cells were treated with LPS but not with TNFα or IL1β (**Figure R.14A**). Similarly, *Trem2*$^{-/-}$ HSCs showed increased levels of inflammation after LPS treatment, but not after IL1β treatment (**Figure R.14B**). These data further suggest that TREM2 receptor does not directly have an effect on TNFα or IL1β signalling pathways in non-parenchymal cells and ratifies the specificity for TLR4-mediated signalling.

We therefore conclude that TREM2 attenuates TLR4-mediated inflammatory responses in both KC and HSC.

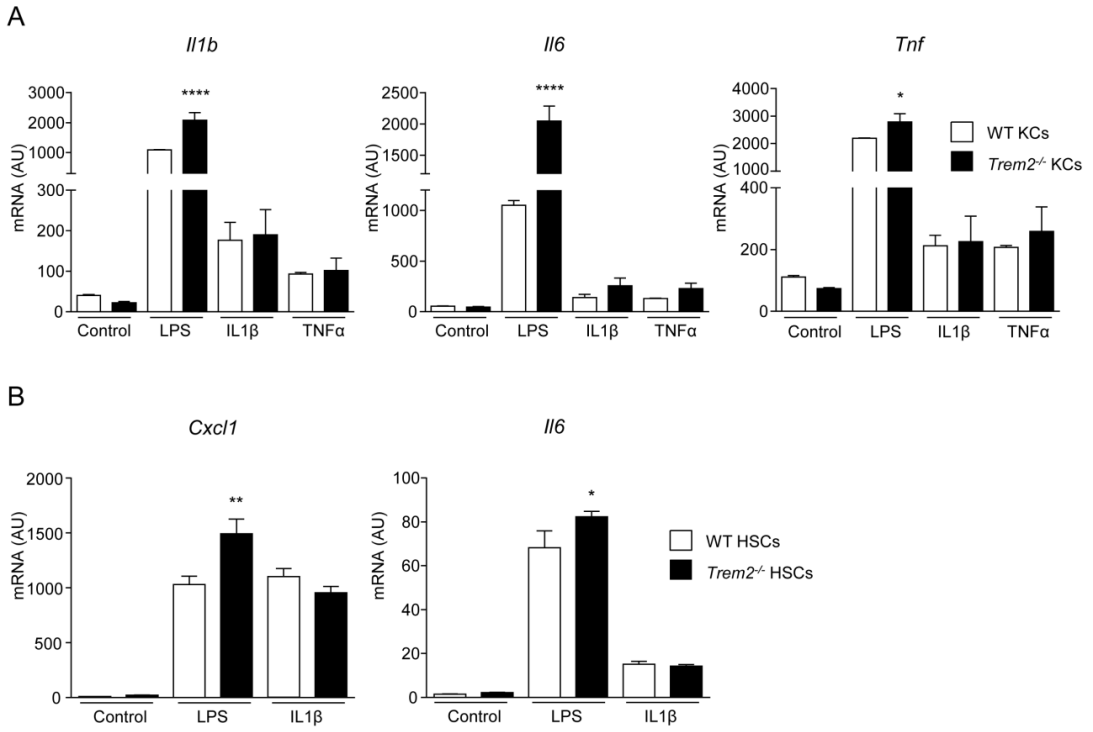

Figure R.14. Only LPS but not IL1β or TNFα treatment results in augmented inflammatory response in *Trem2*$^{-/-}$ KCs and HSCs. (**A**) WT and *Trem2*$^{-/-}$ KCs were treated with LPS (100 ng/ml), IL1β (10 ng/ml) and TNFα (10 ng/ml) for 3 hours and mRNA levels of *Il1b*, *Il6* and *Tnf* were evaluated (n=3-4). (**B**) WT and *Trem2*$^{-/-}$ HSCs were treated with LPS (100 ng/ml) and IL1β (10 ng/ml) for 3 hours and mRNA levels of *Cxcl1* and *Il6* were determined (n=4-5). One-way analysis of variance, followed by Tukey's post hoc test was used, data represent mean ± SEM and *, ** and **** denote a *P* value of <0.05, <0.01 and <0.0001 respectively versus WT KCs and HSCs. AU, arbitrary units; *Cxcl1*, C-X-C motif chemokine ligand 1; HSCs, hepatic stellate cells; *Il*, interleukin; KCs, Kupffer cell; LPS, lipopolysaccharide; *Tnf*, tumor necrosis factor alpha; *Trem2*, triggering receptor expressed on myeloid cells 2; WT, wild type.

Mechanistically, TREM2 has been reported to modulate the activation of MAPK signalling, including ERK, p38 and JNK phosphorylation, which are early and critical

signal transduction events in TLR4-induced cytokine production (185, 188, 220). We decided to check TREM2 effects on TLR4-mediated MAPK activation. Phosphorylation of p38 was potentiated in *Trem2*$^{-/-}$ KCs after *E. coli* treatment as well as ERK phosphorylation after both *E. coli* and LPS treatment. In addition, JNK phosphorylation after LPS and *E.coli* treatment was less pronounced in *Trem2*$^{-/-}$ KCs compared to WT KCs (**Figure R.15**). However, no differential effects were observed on TLR4-mediated NF-κB activation in WT and *Trem2*$^{-/-}$ KCs (**Figure R.15**).

We conclude that TREM2 dampening of TLR4-driven inflammation is associated with an early attenuation of MAPK phosphorylation, particularly ERK activation within KCs.

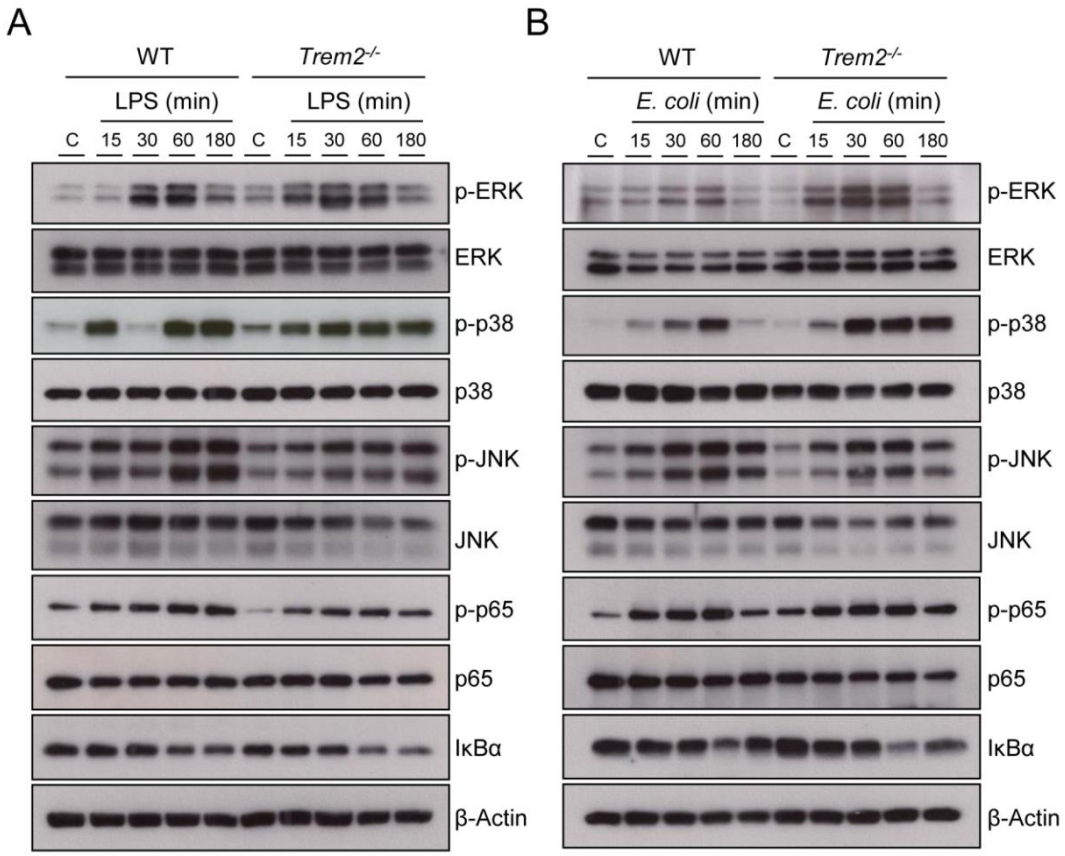

Figure R.15. TLR4-mediated MAPK signalling responses in WT and *Trem2*$^{-/-}$ KCs. WT and *Trem2*$^{-/-}$ KCs were treated with (**A**) LPS (100 ng/ml) or (**B**) 2×10^7 CFU/ml heat-killed *E. coli* for 15, 30, 60 and 180 minutes. Phosphorylation of ERK1/2, p38, JNK, p65 and IκB-α degradation was determined by immunoblot. CFU, colony-forming unit; ERK, extracellular regulated kinase; JNK, C-Jun N-terminal kinase; LPS, lipopolysaccharide; *Trem2*, triggering receptor expressed on myeloid cells 2; WT, wild type.

***R.1.7** TREM2 blunts CCl_4 and acetaminophen-induced liver injury and inflammation*

Given that TREM2 in non-parenchymal liver cells plays a key role in inflammation we wondered if this receptor could influence the response to acute liver injury. To answer

this question, we performed two acute liver injury models consisting in a single administration of CCl_4 or APAP.

Twelve hours after acute CCl_4 injury *Trem2*$^{-/-}$ mice displayed elevated ALT and AST levels compared to WT (**Figure R.16A-B**). This was associated with increased mRNA levels of the neutrophil chemoattractant *Cxcl1* and accompanied with increased liver neutrophil recruitment 24h post injury as determined by IHC (**Figure R.16C-D**). In accordance, we isolated inflammatory cells from the livers of WT and *Trem2*$^{-/-}$ mice 24h after CCl_4 injury and observed a strong tendency ($p=0.06$) for increased liver neutrophil numbers in *Trem2*$^{-/-}$ mice compared to WT controls by flow cytometry (**Figure R.16E**).

Thus, these data demonstrate that TREM2 is important for dampening CCl_4-mediated liver damage and inflammation.

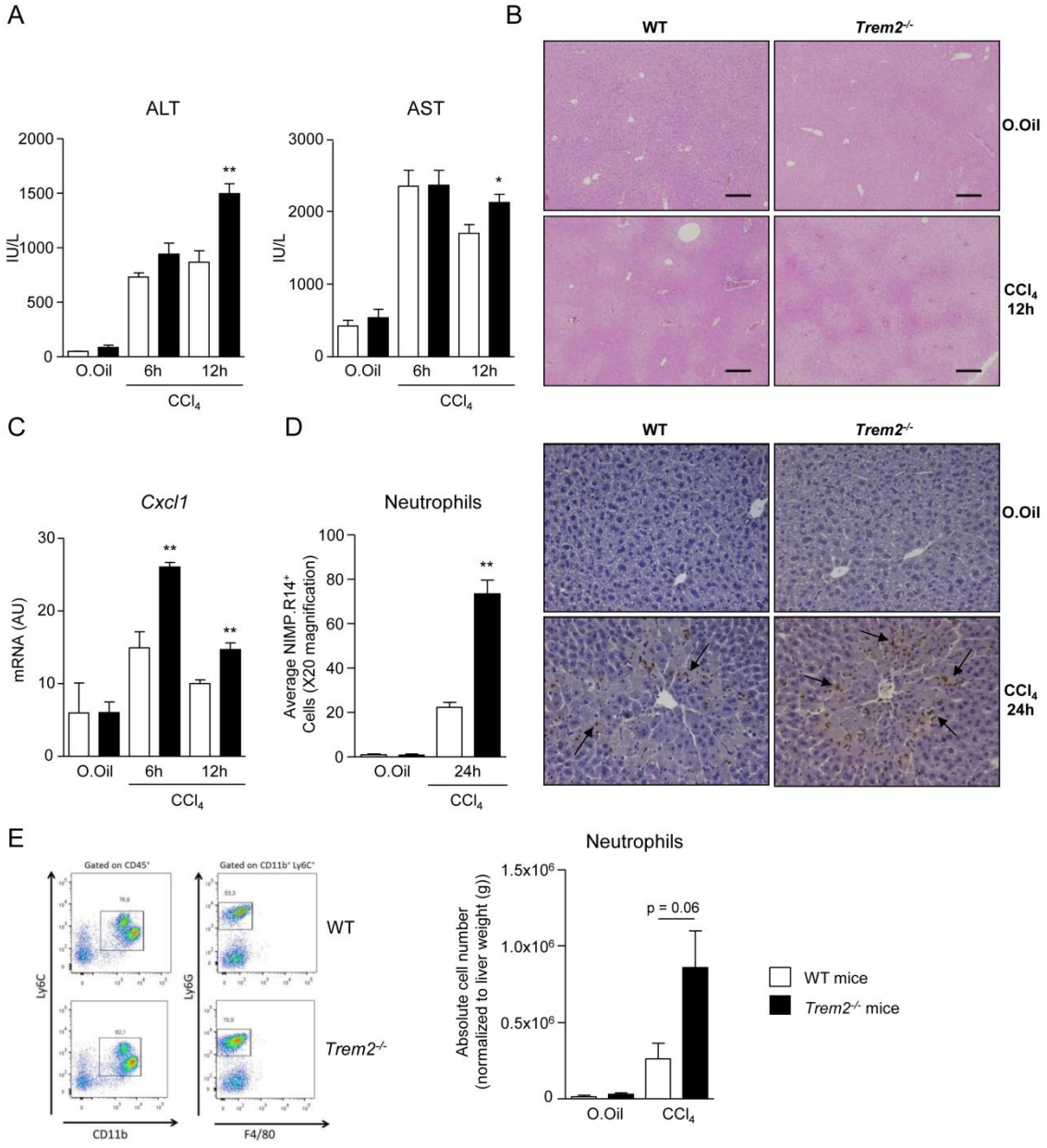

Figure R.16. CCl_4-mediated liver injury and inflammation is enhanced in *Trem2*$^{-/-}$ mice. (**A**) Serum ALT and AST levels, (**B**) representative H&E stains of liver tissue and (**C**) mRNA levels of liver *Cxcl1* 6 and 12 hours after CCl_4 treatment in WT and *Trem2*$^{-/-}$ mice (n=5) Scale bar in (**B**) indicates 200 μm. (**D**) Representative images of liver sections of WT and *Trem2*$^{-/-}$ mice 24 hours after acute CCl_4 treatment immunostained for neutrophils (NIMP.R14). Manual counts for NIMP-positive cells (n=6-10). Arrows denote positively stained cells. (**E**) Representative flow cytometry plot of hepatic neutrophils of WT and *Trem2*$^{-/-}$ mice 24 hours after CCl_4 treatment. Total number of neutrophils normalised to liver weight are shown (n=6-10). Parametric unpaired Student's t-test was used and data represent mean ± SEM and * and ** denote a P value of <0.05 and <0.01, respectively versus WT mice.. ALT, alanine aminotransferase; AST, aspartate aminotransferase; AU, arbitrary units; CCl_4, carbon tetrachloride; *Cxcl1*, C-X-C motif chemokine ligand 1; H&E, haematoxylin and eosin; IU, international units; *Trem2*, triggering receptor expressed on myeloid cells 2; WT, wild type.

Similarly, following sub-lethal APAP intoxication, *Trem2*$^{-/-}$ mice displayed augmented transaminase levels, more necrosis and increased neutrophil content compared to WT (**Figure R.17A-C**). In addition, in this model, *Trem2*$^{-/-}$ mice also exhibited increased macrophage content, which was also associated with elevated levels of *Mcp1* (**Figure R.17C-D**). All these data suggested that the driver for the increased liver damage could be an enhanced PAMP-driven inflammation from non-parenchymal liver cells in *Trem2*$^{-/-}$ mice. Therefore, to exclude a toxic effect of APAP on hepatocytes, we isolated WT and *Trem2*$^{-/-}$ hepatocytes, treated them with APAP and evaluated cell viability. APAP dose dependently killed hepatocytes; however, cell death was not elevated in *Trem2*$^{-/-}$ hepatocytes. In fact, there was a small although statistically significant tendency that viability was increased in *Trem2*$^{-/-}$ hepatocytes (**Figure R.17E**). As APAP overdose is a common cause of human acute liver failure that is associated with mitochondrial dysfunction, stress, lipid peroxidation and liver necrosis (221), we decided to administer a lethal dose of APAP (750 mg/kg) to WT and *Trem2*$^{-/-}$ mice and monitor survival. Strikingly, all *Trem2*$^{-/-}$ mice died within 25 hours, while as previously described, ~70% of WT mice survived 72h post APAP overdose (222, 223) (**Figure R.17F**).

We conclude that TREM2 is important for dampening acute liver damage and the associated inflammatory reaction, this immune receptor therefore being essential for preventing lethal APAP intoxication.

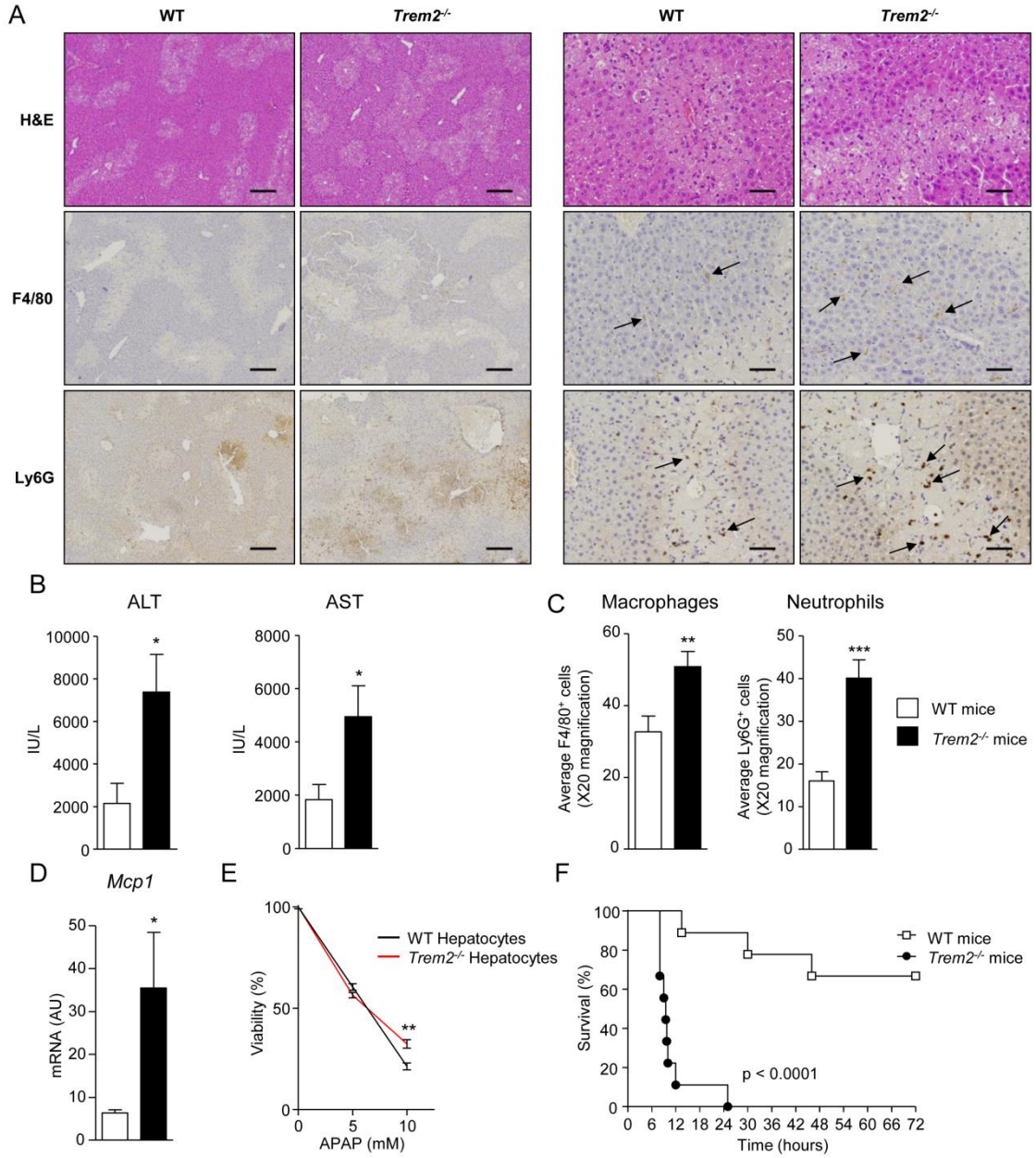

Figure R.17. **TREM2 dampens APAP-induced liver injury.** (**A-C**) 300 mg/kg APAP were injected in WT and *Trem2*$^{-/-}$ mice and (**A**) representative H&E, F4/80 and Ly6G stains from WT and *Trem2*$^{-/-}$ mice are depicted. Arrows denote positively stained cells (n=5). (**B**) ALT and AST levels 24 hours after APAP were determined (n=5). (**C**) Manual counts for F4/80 and Ly6G positive cells in WT and *Trem2*$^{-/-}$ mice livers after APAP injection (n=5). (**D**) 500 mg/kg APAP were injected in WT and *Trem2*$^{-/-}$ and mRNA levels of liver *Mcp1* were determined. (**E**) WT and *Trem2*$^{-/-}$ hepatocytes were treated with 0, 5 or 10 mM of APAP for 24 hours and cellular viability was evaluated (n=6). (**F**) 750 mg/kg APAP were injected and survival was monitored in WT and *Trem2*$^{-/-}$ mice (n=9-11). (**A-E**) Parametric unpaired Student's t-test and (**F**) Log-rank (Mantel-Cox) test were used and data represent mean ± SEM and *, ** and *** denote a P value of <0.05, <0.01 and <0.001, respectively versus WT mice. Scale bar in (**B**) indicates 50 µm (left panel) or 200 µm (right panel). ALT, alanine aminotransferase; AST, aspartate aminotransferase; APAP, acetaminophen; AU, arbitrary units; H&E, haematoxylin and eosin; IU, international units; *Mcp1*, monocyte chemoattractant protein 1; *Trem2*, triggering receptor expressed on myeloid cells 2; WT, wild type.

R.1.8 *Trem2$^{-/-}$ mice exhibit increased injury-induced hepatic lipid peroxidation*

TREM2 is able to modulate PPAR and nuclear receptor activities that regulate lipid-associated pathways (192). In addition, CCl_4 and APAP intoxication-mediated inflammation is associated with enhanced lipid peroxidation, which can result in hepatocyte death (224-226). Therefore, in search for a unified mechanism for the elevated liver injury of *Trem2$^{-/-}$* mice following chronic CCl_4 and acute APAP intoxication, we decided to monitor the levels of 4-hydroxynonenal (4-HNE), representative of lipid peroxidation (226). After chronic CCl_4 treatment and APAP intoxication, elevated 4-HNE levels were observed in the livers of *Trem2$^{-/-}$* mice (**Figure R.18A-C**). To confirm these data in an independent experiment, we also measured 4-HNE levels by ELISA in the livers of WT and *Trem2$^{-/-}$* mice 24 hours post APAP treatment. Indeed, with this approach we could also observe significantly elevated levels of 4-HNE in *Trem2$^{-/-}$* mice (**Figure R.18D**).

Interestingly, examining 4-HNE staining revealed that lipid peroxidation was most intense around hepatic venules, where inflammatory cells reside. These data suggest that resident or infiltrating immune cells could be responsible for the elevated lipid peroxidation through enhanced ROS levels (**Figure R.18A-C**). Supporting this idea, elevated lipid peroxidation after chronic CCl_4 treatment was only observed when both resident and infiltrating immune cells were deficient for TREM2 (**Figure R.18A**).

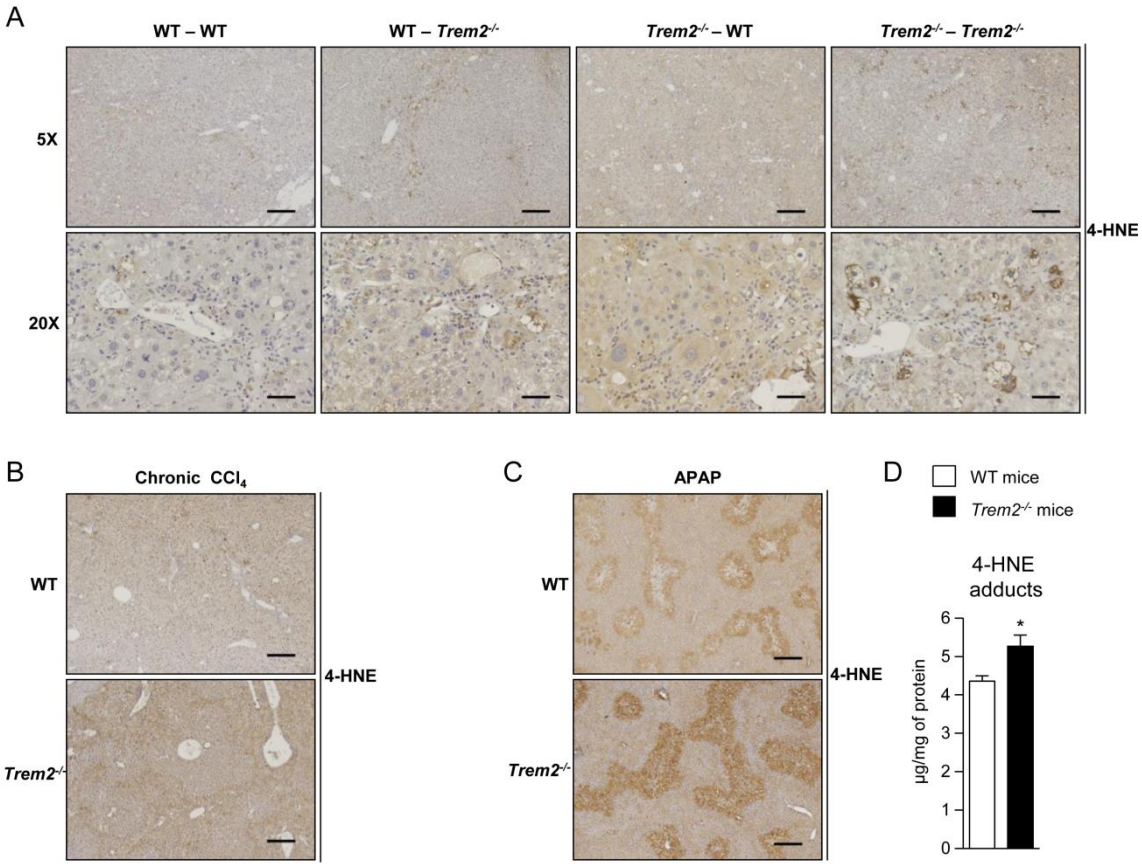

Figure R.18. TREM2 impacts hepatic lipid peroxidation. (**A**) Representative liver 4-HNE stain from WT mice reconstituted with WT-GFP^{+}BM (WT-WT), *Trem2*$^{-/-}$ mice reconstituted with *Trem2*$^{-/-}$-GFP^{+}BM (*Trem2*$^{-/-}$-*Trem2*$^{-/-}$) or chimeric mice (WT-*Trem2*$^{-/-}$) and (*Trem2*$^{-/-}$-WT) that were treated with CCl_4 chronically for 8 weeks and sacrificed 1 day after the last CCl_4 injection (n=3-5). Scale bar in 5X indicates 200 µm and in 20X indicates 50 µm. (**B**) Representative liver 4-HNE stain from WT and *Trem2*$^{-/-}$ mice that were chronically treated with CCl_4 for 8 weeks and sacrificed 1 day after the last CCl_4 injection (n=4-8 CCl_4, and n=3 O.Oil). (**C**) Representative liver 4-HNE stain from WT and *Trem2*$^{-/-}$ mice injected with 300 mg/kg APAP and sacrificed 24 hours after (n=5). Scale bar in (**B-C**) indicates 200 µm (**D**) 4-HNE content was determined by ELISA in livers of mice injected with 300 mg/kg APAP for 24 hours (n=5-7). Parametric unpaired Student's t-test was used and data represent mean ± SEM and * denote a P value of < 0.05 versus WT. 4-HNE, 4-hydroxynonenal; APAP, acetaminophen; CCl_4, carbon tetrachloride; TREM2, triggering receptor expressed on myeloid cells 2; WT, wild type.

As previously shown in the bone-marrow transplantation experiment, the ability of TREM2 to dampen liver damage after chronic CCl_4 treatment depended on TREM2 expression in both resident and infiltrating cells (**Figure R.8**), these data further linked elevated lipid peroxidation to injury and also suggested that this effect could be associated with enhanced ROS levels within *Trem2*$^{-/-}$ resident and/or liver infiltrating immune cells.

However, ROS levels in WT and *Trem2*$^{-/-}$ KCs revealed similar levels in both basal as well as in LPS-driven ROS (**Figure R.19A**). Considering that increased lipid peroxidation in *Trem2*$^{-/-}$ mice was associated with elevated MCP1 and newly recruited monocyte derived hepatic macrophage levels, we wondered if increased liver damage in *Trem2*$^{-/-}$ mice could be due to the differential ROS levels within injury-associated inflammatory monocytes that repopulate the liver. For that, we isolated BMDM and strikingly, *Trem2*$^{-/-}$ BMDM exhibited higher baseline and LPS-induced ROS levels (**Figure R.19B**). The production of ROS is mediated by oxidative phosphorylation as well as the nicotinamide adenine dinucleotide phosphate (NAPDH) oxidase complex in the mitochondria. Therefore, we determined the source for the elevated ROS in *Trem2*$^{-/-}$ macrophages. Interestingly, we observed that *Trem2*$^{-/-}$ BMDM exhibited higher baseline oxidative phosphorylation and maximal respiration, suggesting that this metabolic signature could be responsible for the enhanced ROS (**Figure R.19C**).

We conclude that TREM2 affects lipid peroxidation and subsequent damage of hepatocytes by skewing metabolic pathways and ROS generation within newly recruited liver macrophages following liver injury.

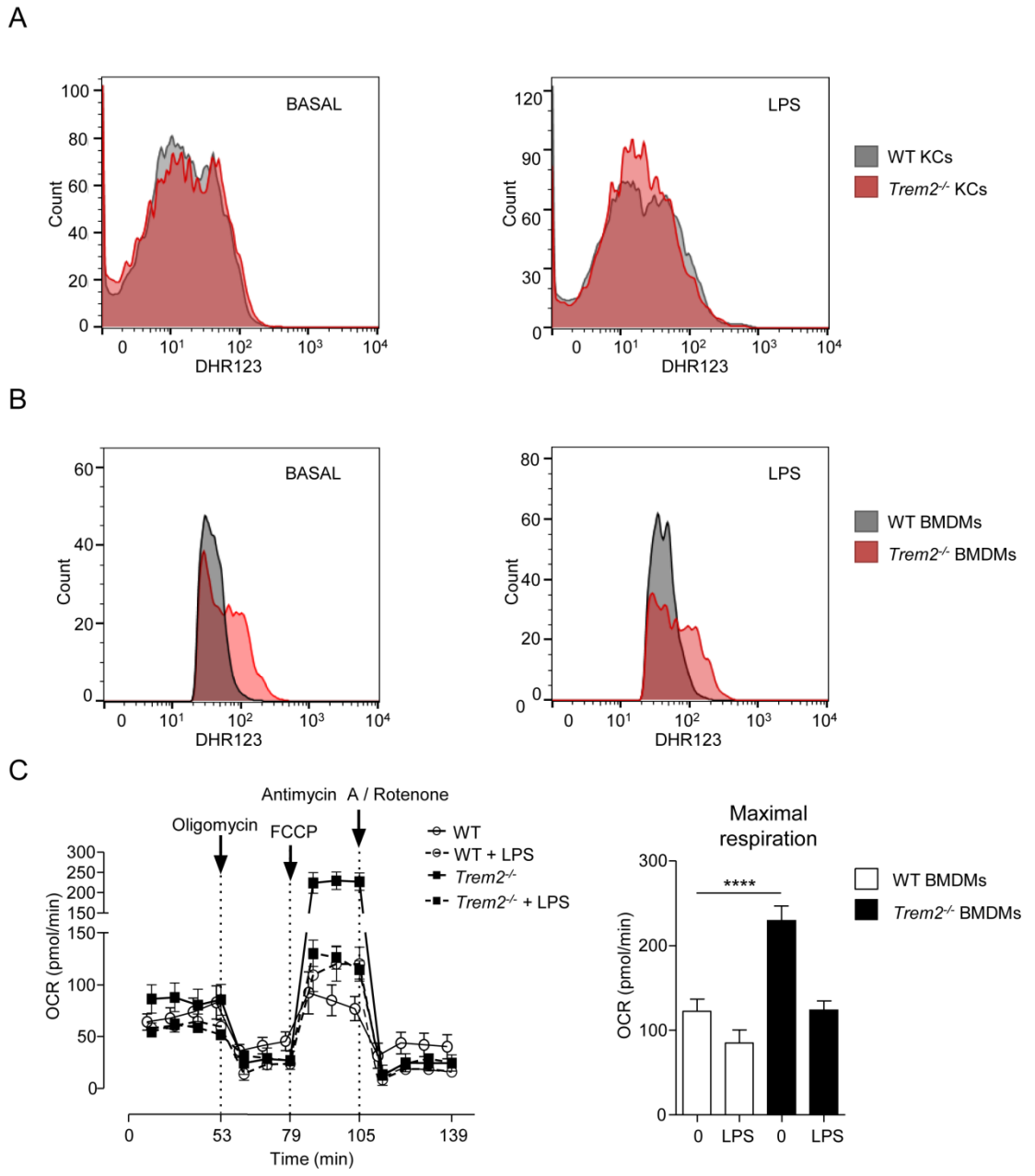

Figure R.19. TREM2 impacts ROS levels in BMDMs. WT and *Trem2*$^{-/-}$ (**A**) KCs or (**B**) BMDM were treated with 100 ng/ml LPS for 3 hour and total cellular ROS levels were determined using flow cytometry with dihydrorhodamine 123 and a representative histogram is shown (n=3-4). (**C**) Oxygen consumption rate and maximal respiration of naive and LPS-treated BMDM was evaluated (n=4-5). Parametric unpaired Student's t-test was used and data represent mean ± SEM and **** denotes a P value of <0.0001 versus WT. BMDM, bone marrow derived macrophages; DHR123, dihydrorhodamine 123; KCs, Kupffer cells; LPS, lipopolysaccharide; OCR, oxygen consumption rate; ROS, reactive oxygen species; *Trem2*, triggering receptor expressed on myeloid cells 2; WT, wild type.

R.1.9 *PAMPs are upstream of TREM2 during liver injury*

After showing the importance of TREM2 in dampening liver injury and inflammation we tried to elucidate whether the upstream driver of TREM2 were PAMPs associated to TLR4 signalling downstream of gut microbiota. With this aim, we administered WT and *Trem2*$^{-/-}$ mice antibiotics for 4 weeks, acute injured with CCl_4 and evaluated liver injury and inflammation compared to animals that did not receive antibiotics. We also evaluated intestinal permeability administering FITC-Dextran 4 hours before culling and sacrificed all animals 12 hours after CCl_4 administration. Serum FITC levels were unaltered in WT and *Trem2*$^{-/-}$ mice with or without antibiotics after CCl_4 treatment, showing no differences in intestinal permeability (**Figure R.20A**). Interestingly, *Trem2*$^{-/-}$ mice exhibited increased ALT and AST serum levels compared to WT after acute CCl_4 treatment, as previously observed (**Figure R.20B**), however, antibiotic treatment abolished these differences (**Figure R.20B**). In addition, antibiotic treatment also reverted the augmented liver inflammation levels of *Trem2*$^{-/-}$ mice compared to WT mRNA levels, as demonstrate the mRNA levels of *Il1b* and *Il6* (**Figure R.20C**).

Altogether, these data show that after acute liver injury, differences in altered intestinal permeability of *Trem2*$^{-/-}$ mice do not contribute to the enhanced liver damage and further support the concept that TREM2 dampens PAMP-derived signals from gut bacteria, perpetuating liver injury and inflammation.

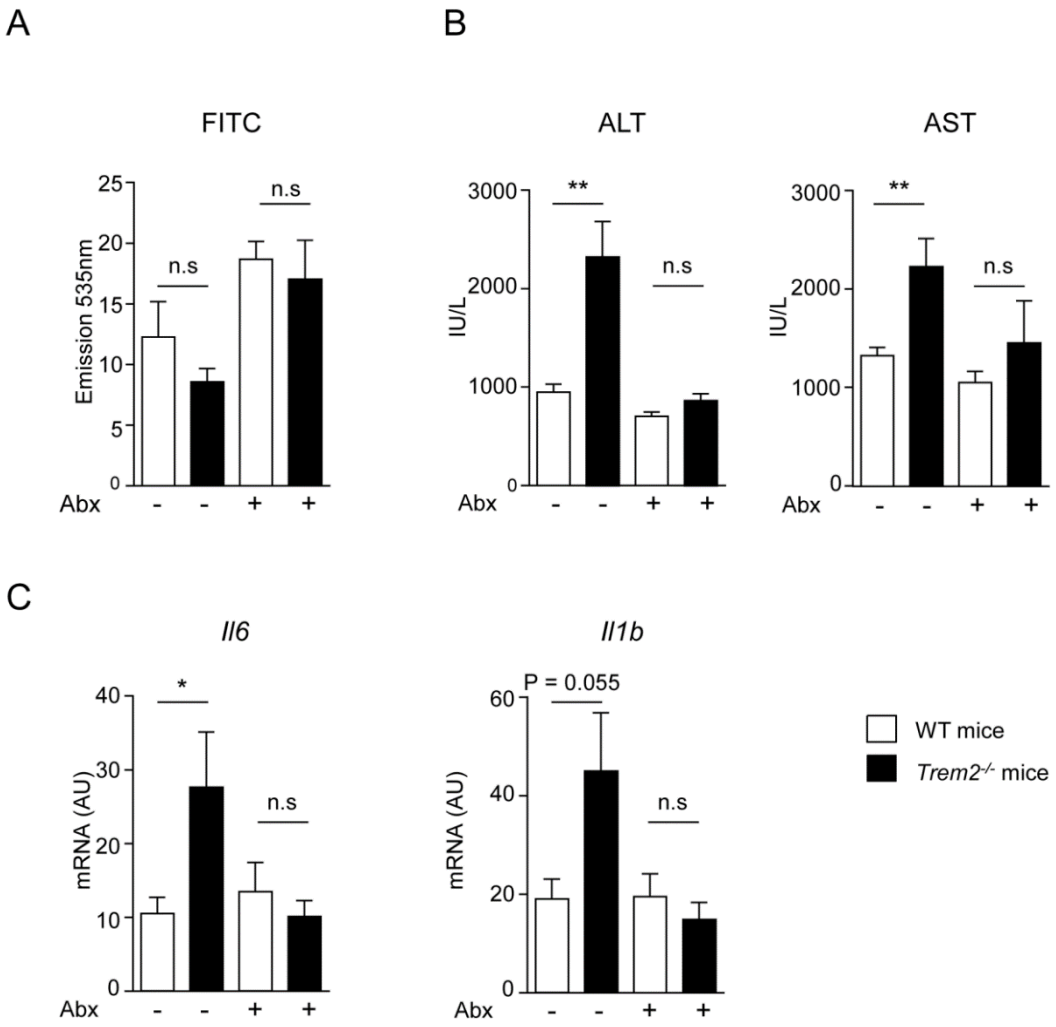

Figure R.20. **PAMPs are upstream of TREM2 during liver injury.** (**A-C**) Drinking water with or without antibiotics was administered to WT and *Trem2*$^{-/-}$ mice for 4 weeks. After that mice were injected with CCl_4 and 8 hours after were gavaged with 4KDa FITC Dextran and sacrificed 4 hours later (12 hours after CCl_4 administration) (n=8-9). Serum levels of (**A**) FITC Dextran, (**B**) ALT and AST were determined. (**C**) mRNA levels of liver *Il6* and *Il1b* were determined. Parametric Student's t-test was used, data represent mean ± SEM and * and ** denote a P value of <0.05 and <0.01, respectively versus WT mice. Abx, antibiotics; ALT, alanine aminotransferase; AST, aspartate aminotransferase; AU, arbitrary units; CCl_4, carbon tetrachloride; FITC, fluorescein isothiocyanate; *Il*, interleukin; IU, international units; n.s. non-significant; PAMPs, pathogen-associated molecular patterns; *Trem2*, triggering receptor expressed on myeloid cells 2; WT, wild type.

R.2 Role of TREM2 in liver regeneration after partial hepatectomy

R.2.1 *TREM2 mRNA expression is upregulated at different time points after PHx in mice.*

After tissue injury or loss of parenchymal mass due to PHx, regenerative mechanisms are activated in the liver. The fact that the expression of TREM2 was induced in cirrhotic human livers and acute and chronic liver injury models in mice, led us to investigate whether its induction in the damaged liver could be part of the regenerative response of the liver triggered during acute and chronic liver injury.

To directly test this hypothesis, we used the well-characterized mouse model of liver regeneration after two-thirds PHx. As shown in **Figure R.21**, *Trem2* mRNA expression was low in mouse liver in Sham operated mice, and progressively increased after 4, 24 and 48 hours after PHx, with its expression peaking at 48 hours post-surgery, and decreased after 72 hours (**Figure R.21**).

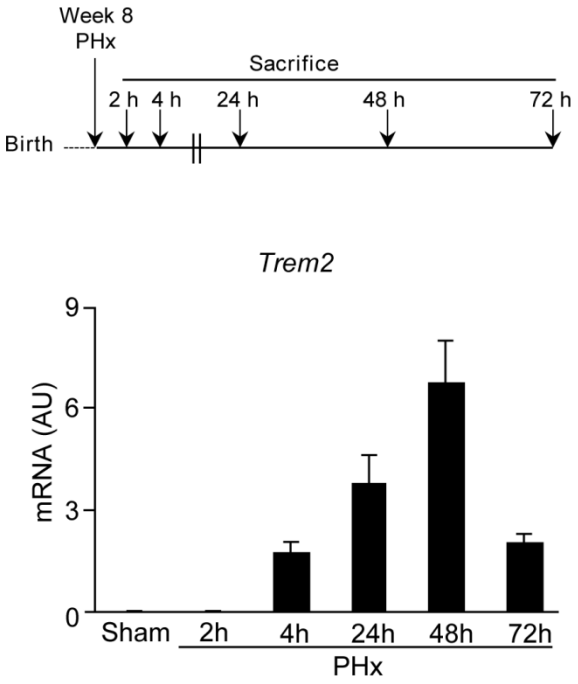

Figure R.21. TREM2 mRNA expression at different time points after PHx. *Trem2* mRNA expression was analysed in the remaining mouse liver parenchyma at different time points (2, 4, 24, 48 and 72 hours) after PHx or sham operation (n=3-4). AU, arbitrary units; PHx, partial hepatectomy; *Trem2,* triggering receptor expressed on myeloid cells 2.

R.2.2 *The initiation of liver regeneration and hepatocyte proliferation following PHx is accelerated in Trem2$^{-/-}$ mice*

With the aim of evaluating the significance of *Trem2* gene expression during liver regeneration after PHx, WT and *Trem*2$^{-/-}$ mice were used and these were subjected to ~70% PHx. First, the DNA synthetic response was analysed in WT and *Trem*2$^{-/-}$ mice at different times after PHx, by inmunohystochemical detection of BrdU incorporation into DNA, to determine the number of cells in S phase. Of note, 36 hours after surgery *Trem2*$^{-/-}$ mice displayed a marked tendency to exhibit increased, albeit not significant, hepatocyte proliferation. BrdU incorporation was significantly augmented in *Trem2*$^{-/-}$ mice 72 hours after PHx (**Figure R.22A**). In line with this observation, a significant elevation of PCNA expression in hepatocyte nuclei was observed 72 hours after PHx in *Trem2*$^{-/-}$ mice, when compared to WT mice (**Figure R.22B**). These results were also confirmed when PCNA expression levels were analysed by immunoblotting (**Figure R.22C**).

Since the restoration of liver mass is mediated by a network of cytokines, mitogens and growth factors in an orchestrated manner, we evaluated the mRNA levels of inflammatory and mitogenic genes. As shown in **Figure R.23A-B**, *Trem2*$^{-/-}$ mice exhibited a differential pro-inflammatory cytokine expression when compared to WT mice, as shown by increased levels of *Tnf* and *Il6* mRNAs as early as 1 hour and 6 hours after PHx, respectively. Similarly, in *Trem2*$^{-/-}$ livers augmented levels of *Hgf* were found 6 hours after PHx, when compared to WT mice (**Figure R.23B**).

Together these data suggest that TREM2 plays a key role modulating the early induction of inflammatory cytokine expression after PHx, and in its absence, liver regeneration is accelerated.

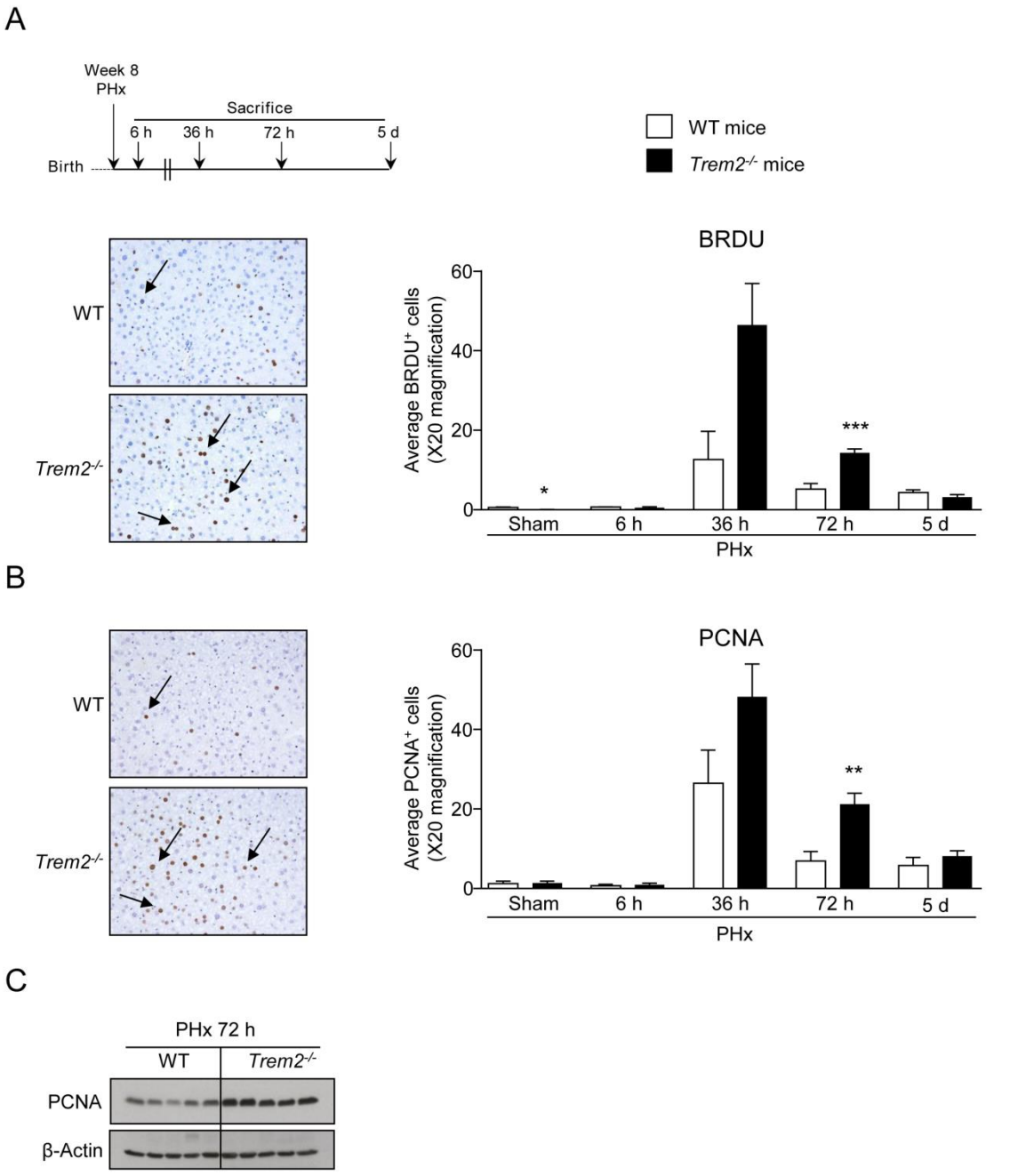

Figure R.22. Liver regeneration after partial hepatectomy is accelerated in *Trem2*$^{-/-}$ mice. (**A**) Representative immunohistochemical detection of BrdU in liver sections of WT and *Trem2*$^{-/-}$ mice at 36 hours after PHx (20X fields) and quantification of positively stained BrdU-labelled hepatocytes in liver sections of WT and *Trem2*$^{-/-}$ mice that were either sham operated or subjected to PHx and sacrificed 6, 36, 72 hours after (n=3-6). (**B**) Representative PCNA stains from WT and *Trem2*$^{-/-}$ mice at 36 hours after PHx (20X fields) and manual counts of positively stained PCNA hepatocytes in liver sections of WT and *Trem2*$^{-/-}$ mice that were either sham operated or 6, 36, 72 hours and 5 days after PHx (n=3-6). (**C**) Western blot analysis of PCNA 72 hours after PHx, β-actin was used as house-keeping control (n=5). Parametric Student's T test and non-parametric Mann-Whitney test were used. Data represent mean ± SEM and *, ** and *** denote a P value of <0.05, <0.01 and <0.001, respectively versus WT mice. AU, arbitrary units; BRDU, 5'-bromo-2'-deoxyuridine; PCNA, proliferating cell nuclear antigen; PHx, partial hepatectomy; *Trem2*, triggering receptor expressed on myeloid cells 2; WT, wild type.

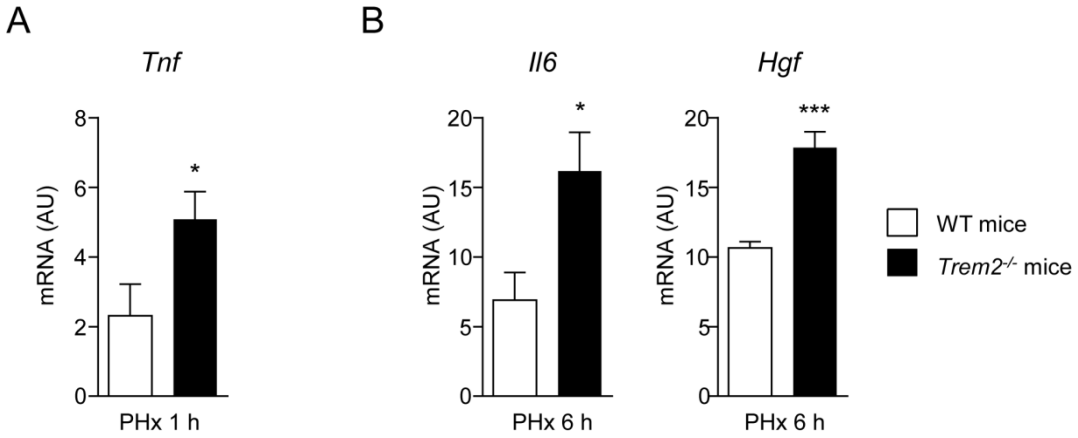

Figure R.23. Early inflammatory cytokine expression after partial hepatectomy is enhanced in *Trem2*$^{-/-}$ mice. (**A**) mRNA expression of the pro-inflammatory cytokine *Tnf* 1 hour after PHx (n=5-6) and (**B**) mRNA expression of the pro-inflammatory cytokine *Il6* and the growth factor *Hgf* 6 hours following PHx (n=6-11). Parametric Student's T test was used. Data represent mean ± SEM and * and *** denote a P value of <0.05 and <0.001 respectively. AU, arbitrary units; *Hgf*, hepatocyte growth factor; *Il6*, interleukin 6; PHx, partial hepatectomy; *Tnf*, tumour necrosis factor; *Trem2*, triggering receptor expressed on myeloid cells 2; WT, wild type.

R.3 Role of TREM2 in HCC

R.3.1 *TREM2 is upregulated in human HCC tissue*

We have previously reported that *TREM2* expression is upregulated in human liver cirrhosis and experimental mouse models of acute and chronic liver injury (**Figure R.1, Figure R.2 and Figure R.3**). This led us to evaluate whether the expression of *TREM2* was also elevated in the neoplastic liver. We first analysed *TREM2* expression data retrieved from the TCGA public repository. Interestingly, we observed that *TREM2* expression levels were significantly increased in HCC livers compared to controls in the TCGA cohort, consisting in 366 HCC samples and 49 surrounding normal tissue samples **(Figure R.24A**). Moreover, stratifying HCC samples according to tumour stage revealed that *TREM2* expression was upregulated in advanced T4 stage tumours compared to early T1 stage tumours.

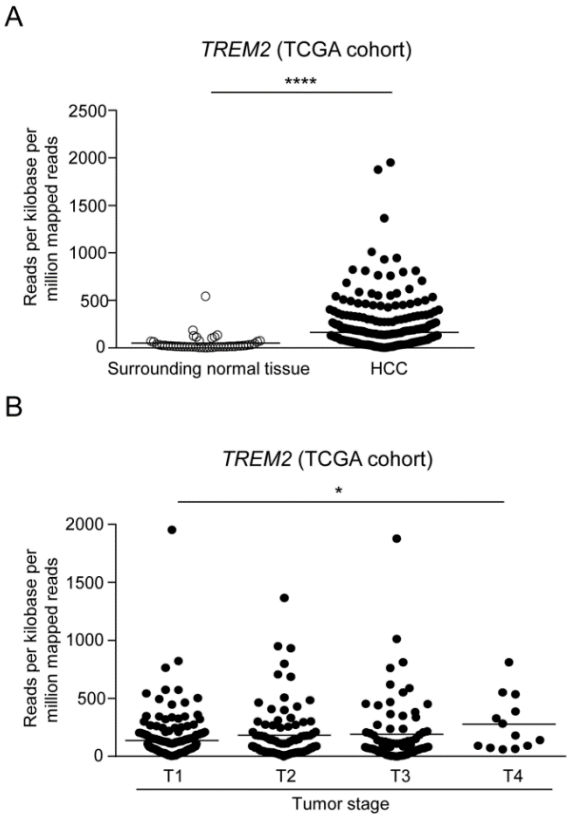

Figure R.24. *TREM2* expression in human HCC tissues. (**A**) RNA-seq analysis of *TREM2* expression in surrounding normal tissues and in HCC tissues (n=49 and 366 respectively) and (**B**) stratification of HCC tumors according to tumor stage (T1 n= 179, T2 n= 91, T3 n= 79 and T4 n= 13) in the TCGA database. Non-parametric Mann-Whitney test and Kruskal-Wallis test followed by Dunn's multiple comparison tests were used. Data represent mean ± SEM and * and **** denote a P value of <0.05 and <0.0001 respectively. HCC, hepatocellular carcinoma; TCGA, The cancer genome atlas; *TREM2*, triggering receptor expressed on myeloid cells 2.

Importantly, we also confirmed these results in an independent cohort of patients (**Table M.2**). *TREM2* mRNA expression was also induced in HCC samples compared to healthy liver tissue in the San Sebastian cohort of patients (**Figure R.25**).

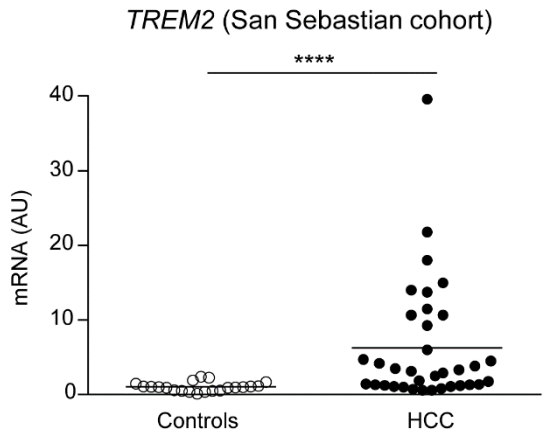

Figure R.25. *TREM2* expression in human HCC tissue. (**A**) *TREM2* mRNA expression in normal human livers (controls) and HCC samples (n=21 and 35, respectively) in the San Sebastian cohort of patients. Non-parametric Mann-Whitney test was used. Data represent mean ± SEM and **** denote a P value of <0.0001. AU, arbitrary units; HCC, hepatocellular carcinoma; *TREM2*, triggering receptor expressed on myeloid cells 2.

Next, correlation of fibrotic and inflammatory genes with *TREM2* expression was analysed in the HCC tissue samples of the San Sebastian cohort of patients and a positive correlation between *TREM2* expression and the expression levels of the fibrotic marker *COL1A1* was observed, whereas no correlation was evidenced with the fibrotic marker *ACTA2* (**Figure R.26A**). Furthermore, *TREM2* mRNA levels positively correlated with markers of inflammation, including the pro-inflammatory cytokines *IL1B*, *IL6*, *IL8* and *TNF* (**Figure R.26B**).

We conclude that *TREM2* mRNA expression is increased during human HCC and that *TREM2* levels correlate with inflammation markers and collagen levels in HCC.

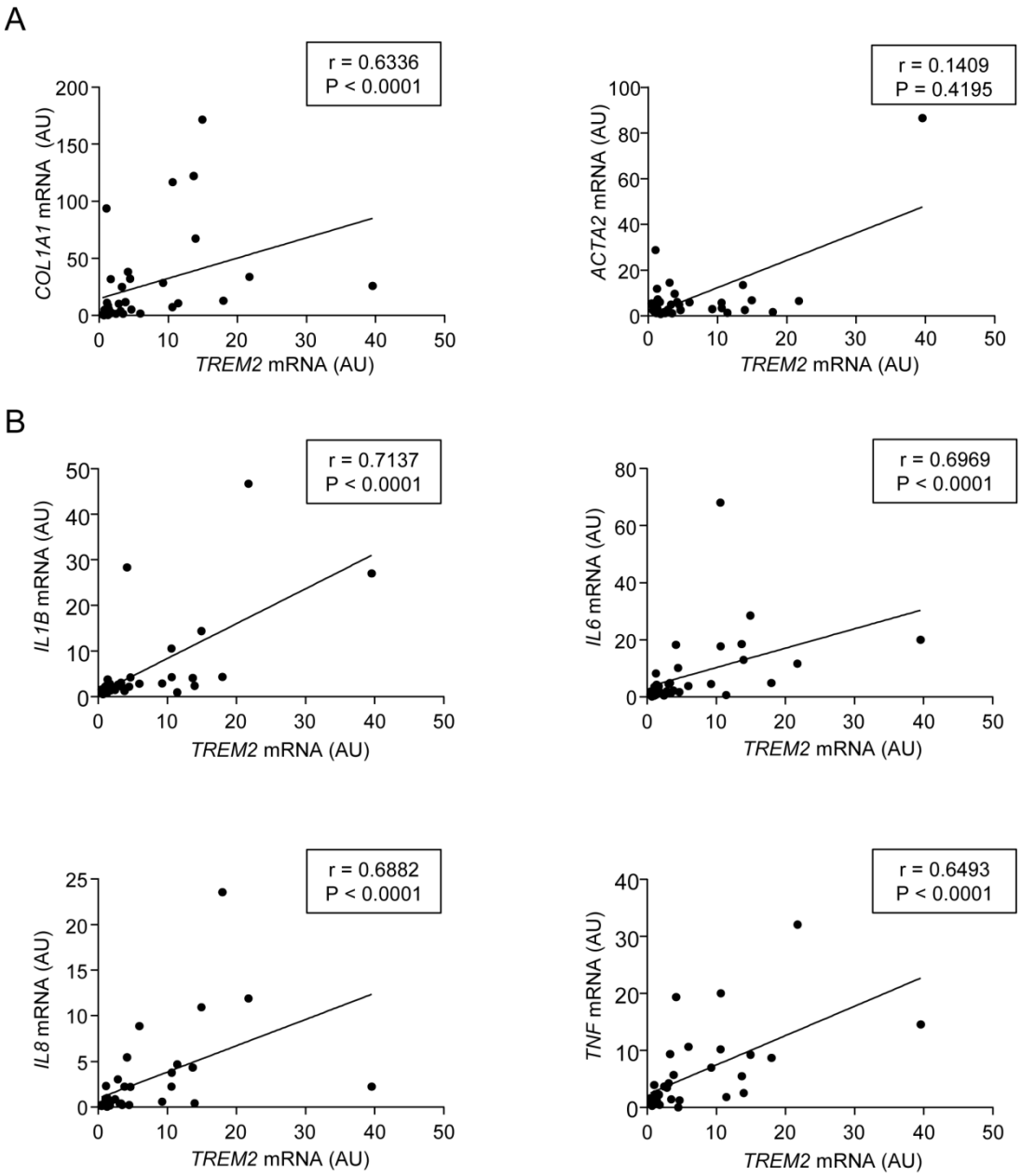

Figure R.26. *TREM2* mRNA expression in human HCC and its correlation with markers of fibrosis and inflammation. Correlation between *TREM2* mRNA levels and mRNA levels of the fibrosis and inflammation markers in HCC samples in the San Sebastian cohort of patients (n=35). (**A**) Correlation between *TREM2* mRNA levels and mRNA levels of the fibrotic markers *COL1A1* and *ACTA2*. (**B**) Correlation between mRNA levels of *TREM2* and markers of inflammation (*IL1B*, *IL6*, *IL8* and *TNF*) in HCC samples. Spearman's correlation test was used. *ACTA2*, Actin alpha 2, smooth muscle; AU, arbitrary units; *COL1A1*, collagen type I alpha 1 chain; HCC, hepatocellular carcinoma; *IL*, interleukin; *TNF*, tumour necrosis factor; *TREM2*, triggering receptor expressed on myeloid cells 2.

R.3.2 *Trem2$^{-/-}$ mice have increased levels of hepatocyte damage, inflammation and oxidative stress after acute DEN-induced liver injury in adult mice*

In order to clarify the role of TREM2 in the early stages of tumour development, we carried out a well-established *in vivo* approach that provides significant insight into the inflammatory mechanisms at play during HCC (163, 227). Thus, 8 week old WT or *Trem2$^{-/-}$* male mice were injected with 100 mg/kg of DEN and sacrificed 6, 24 or 72 hours later.

Histological analysis of H&E-stained liver sections revealed that the damaged area was significantly bigger in the *Trem2$^{-/-}$* mice, in comparison to WT mice (**Figure R.27A**). In addition, DNA damage was indirectly measured by phospho-histone H2A.X (γH2AX) staining, revealing increased number of damaged hepatocytes in the liver of *Trem2$^{-/-}$* mice, compared to WT mice (**Figure R.27B**). In agreement with these data, we found that the circulating levels of ALT were significantly elevated in the *Trem2$^{-/-}$* mice sera 6 and 72 hours after DEN injection compared to WT mice (**Figure R.27C**).

Importantly, in line with previous observations, we observed an increased accumulation of ROS in the liver tissue of *Trem2$^{-/-}$* mice 24 hours after DEN challenge, when compared with WT mice (**Figure R.27D**). Next, we analysed the mRNA expression of genes implicated in inflammation and oxidative stress. As previously shown in other acute and chronic toxic liver injury models, the mRNA levels of *Cxcl1* and *Mcp1* chemokines were also found upregulated in the *Trem2$^{-/-}$* mice 6 hours post-DEN administration (**Figure R.28A**). In addition, the mRNA expression of the pro-inflammatory cytokine *Tnf*, the hepatocyte growth factor *Hgf*, and the oxidative stress marker the inducible enzyme *heme oxigenase 1* (*Hmox1*) were also found increased in *Trem2$^{-/-}$* mice in comparison to WT mice (**Figure R.28A-C**).

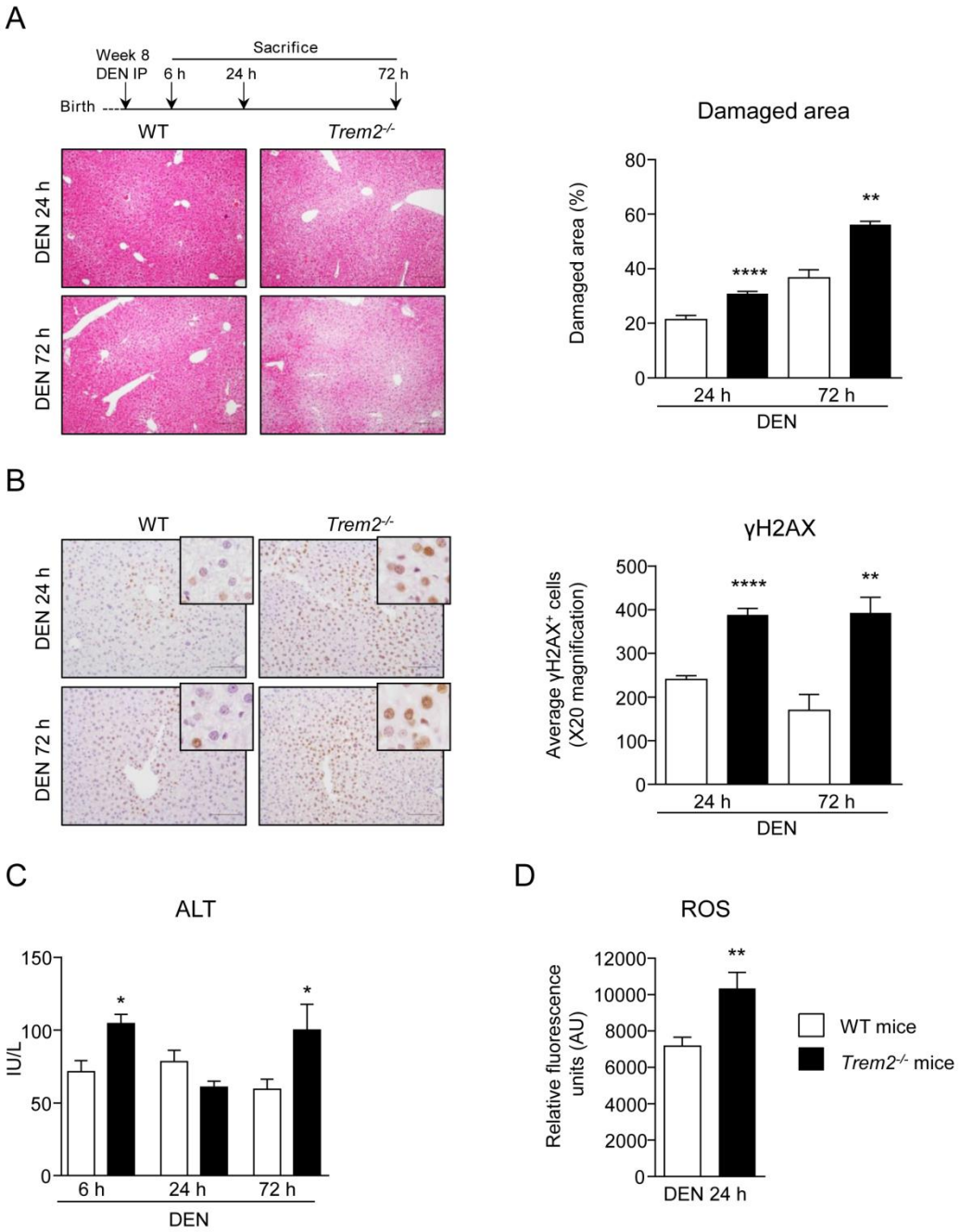

Figure R.27. TREM2 protects hepatocytes from DNA damage by attenuating inflammation and oxidative stress after acute DEN-induced liver injury. WT and *Trem2*$^{-/-}$ mice were injected with 100 mg/kg of DEN and were sacrificed 6, 24 and 72 hours post injury (n=6-10). (**A**) Representative H&E stains of liver sections post-acute DEN treatment and quantification of the damaged area (10X). (**B**) Representative images of liver sections immunostained for γH2AX and manual counts of positively stained hepatocyte nuclei (20X). (**C**) ALT levels were determined. (**D**) ROS was determined in liver tissue of WT and *Trem2*$^{-/-}$ mice 24 hours after DEN administration. Parametric Student's T test and non-parametric Mann-Whitney test were used. Data represent mean ± SEM and *, **, and **** denote a P value of <0.05, <0.01 and <0.0001, respectively versus WT mice. ALT, alanine aminotransferase; DEN, diethylnitrosamine; γH2AX, Phospho-Histone H2A.X; IU, international units; ROS, reactive oxygen species; *Trem2*, triggering receptor expressed on myeloid cells 2; WT, wild type.

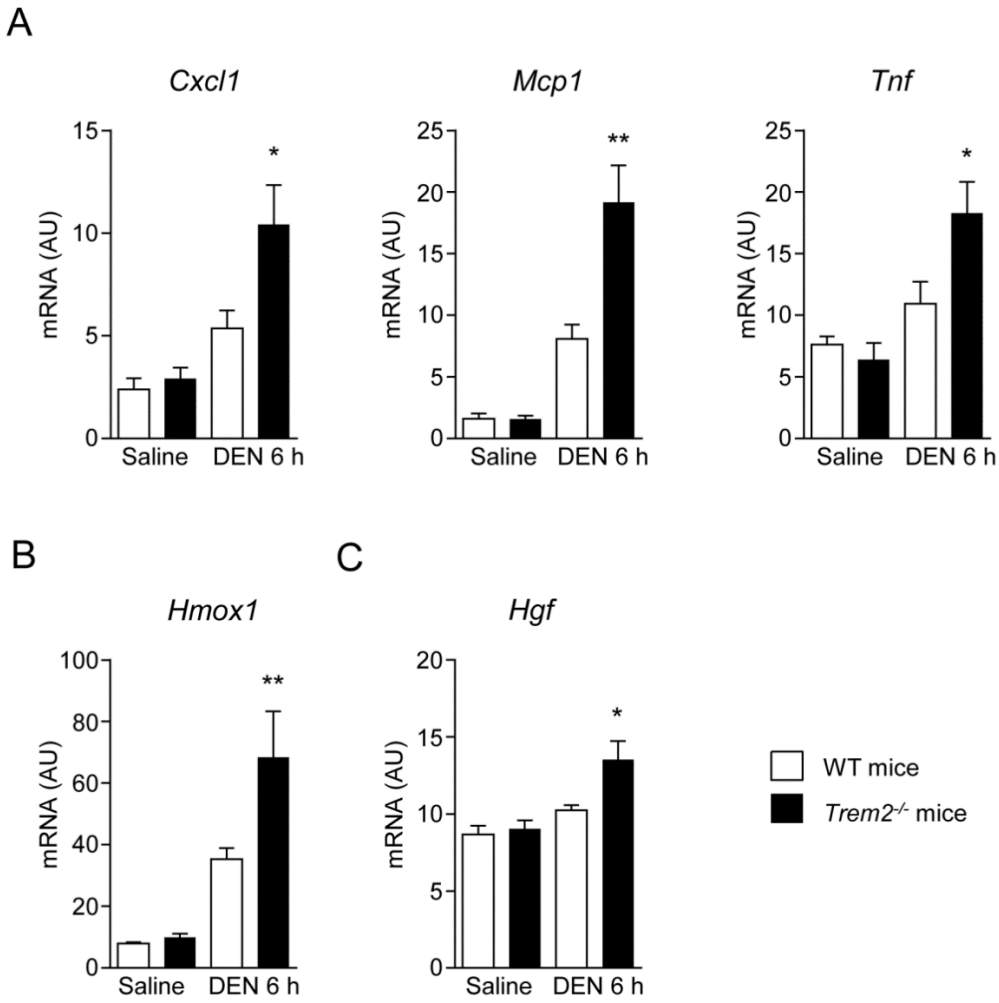

Figure R.28. mRNA expression analysis of key inflammatory, proliferative and injury mediators in WT and *Trem2*$^{-/-}$ mice after acute DEN administration. WT and *Trem2*$^{-/-}$ mice were injected with 100 mg/kg of DEN and were sacrificed 6 hours post injury (n=7). (**A**) mRNA levels of the pro-inflammatory chemokines *Cxcl1* and *Mcp1*, the cytokine *Tnf*, (**B**) the oxidative stress enzyme *Hmox1* and (**C**)the growth factor *Hgf* were determined. Parametric Student's T test and non-parametric Mann-Whitney test were used. Data represent mean ± SEM and * and ** denote a P value of <0.05 and <0.01, respectively versus WT mice. *Cxcl1*, C-X-C motif chemokine ligand 1; DEN, diethylnitrosamine; *Hgf*, hepatocyte growth factor; *Hmox1*, heme oxigenase 1; *Mcp1*, monocyte chemoattractant protein 1; *Tnf*, tumor necrosis factor; *Trem2*, triggering receptor expressed on myeloid cells 2; WT, wild type.

Given our previous observations showing that TREM2 modulates the immune cell recruitment after acute (**Figures R.16 and R.17**) and chronic liver injury (**Figure R.10**), we wondered if this receptor could also play a role in inflammatory cell recruitment to the liver in the DEN-induced injury model.

Thus, we evaluated T cell, neutrophil and macrophage content in the liver by performing immunohistochemical analysis. As shown in **Figure R29**, no relevant differences were observed in immune cells recruitment to the liver between genotypes.

In conclusion, these observations further support the concept that TREM2 might be protective in early stages after DEN challenge, as it attenuates liver damage, inflammation and oxidative stress.

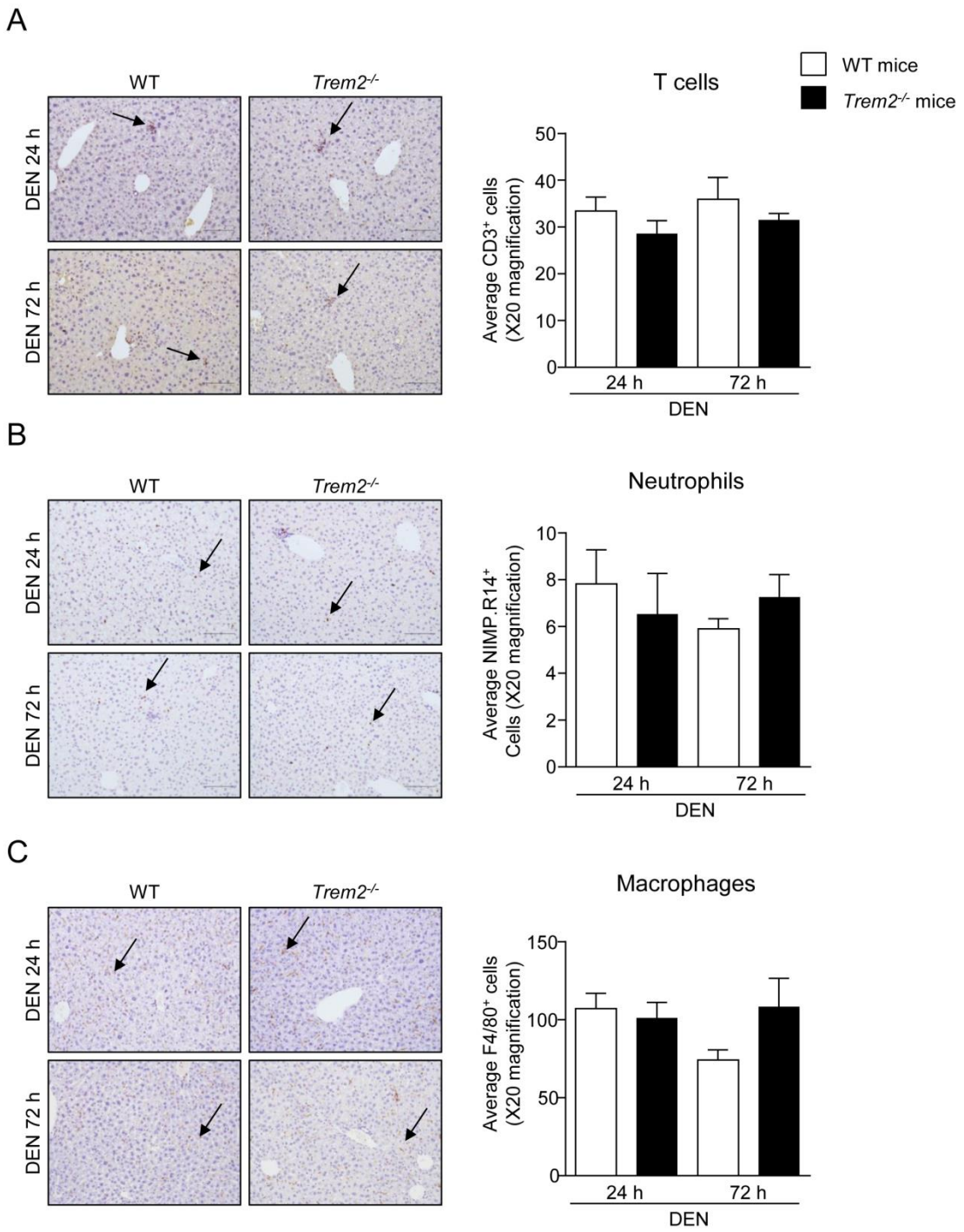

Figure R.29. No differences in immune cell recruitment after acute DEN-induced liver injury between livers of WT and *Trem2*$^{-/-}$ mice. Recruitment of immune cells to the liver was measured by IHC. Representative images of liver sections immunostained for (**A**) T cells (anti-T cell marker CD3), (**B**) neutrophils (anti-neutrophil marker NIMP.R14) and (**C**) macrophages (anti-macrophage marker F4/80) (20X). Arrows denote positively stained cells. Manual counts of positive cells in livers 24 and 72 hours post-DEN treatment are depicted. Scale bar represent 100 μm. Data represent mean ± SEM. Parametric Student's T test and non-parametric Mann-Whitney test were used. DEN, diethylnitrosamine; *Trem2*, triggering receptor expressed on myeloid cells 2; WT, wild type.

R.3.3 *TREM2 is upregulated in DEN-induced liver carcinogenic mouse model*

To formally investigate the role of TREM2 in hepatocarcinogenesis, we analysed *Trem2* expression in a chemically-induced mouse model of liver cancer. C57BL/6 male mice were administered the liver carcinogen DEN (30 mg/kg) 15 days after birth and sacrificed 30 or 40 weeks after. First, the mRNA expression levels of *Trem2* were measured in the liver of mice treated with DEN for 30 and 40 weeks. Interestingly, we were able to find a significant and progressive upregulation of *Trem2* expression in the liver tissue of these mice, comparing to saline-injected mice (**Figure R.30A**). In addition, mRNA levels of *Trem2* in non-tumour and tumour samples in this animal model were analysed and an upregulation of *Trem2* mRNA expression in tumours, compared to non-tumour tissue, particularly after 40 weeks of DEN administration was observed (**Figure R.30B**).

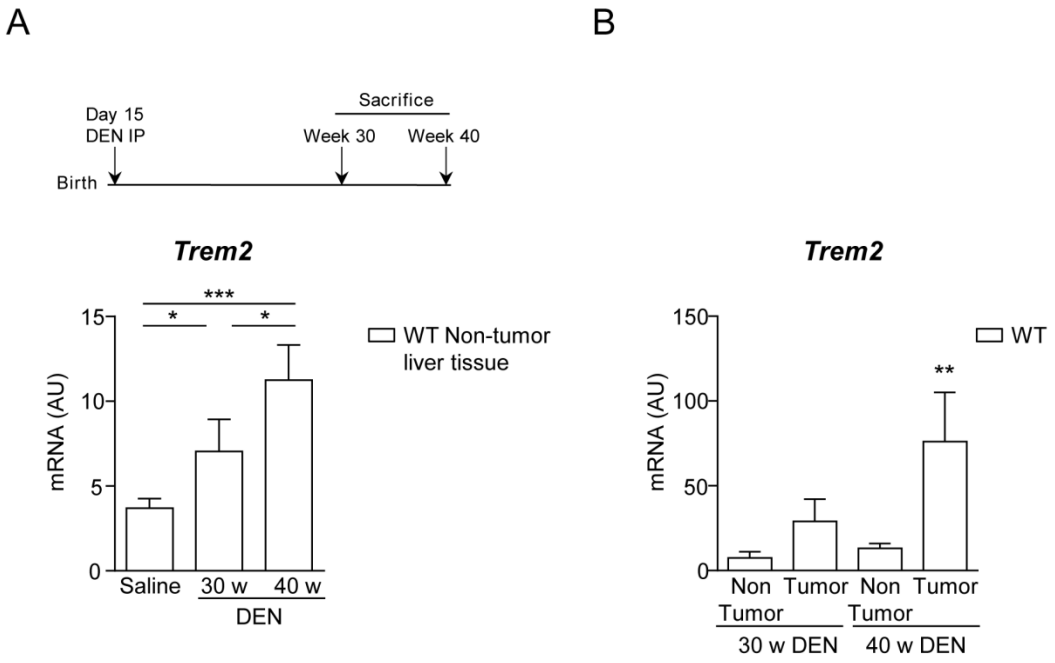

Figure R.30. *Trem2* mRNA expression is upregulated in experimentally induced HCC in mice. WT mice were injected with 30 mg/kg DEN and were sacrificed after 30 and 40 weeks (n=14-16). (**A**) qRT-PCR analysis of *Trem2* expression in the liver of 30 and 40 week DEN-injured mice and (**B**) qRT-PCR analysis of *Trem2* expression in non-tumour vs tumour tissue in the liver of 30 and 40 week DEN-injured mice (n=4-10). Parametric Student's T test and non-parametric Mann-Whitney test were used. Data represent mean ± SEM and *, ** and *** denote a P value of <0.05, <0.01 and <0.001, respectively versus saline or non-tumour tissue. AU, arbitrary units; DEN, diethylnitrosamine; *Trem2*, triggering receptor expressed on myeloid cells 2; WT; wild type.

Next, correlation studies between *Trem2* mRNA expression levels and fibrotic or inflammatory marker transcript levels were carried out both in the non-tumour tissue (**Figure R.31**) or tumour tissue (**Figure R.32**). Of note, *Trem2* mRNA expression levels correlated with markers of fibrosis *Col1a1* and *Acta2* in the non-tumour liver tissue of mice 30 and 40 weeks post-DEN administration (**Figure R.31A**). Similarly, in DEN-induced tumour tissue these fibrotic markers also positively correlated with the expression of *Trem2* (**Figure R.32A**). In addition, mRNA levels of *Trem2* and *Mcp1* positively correlated both in non-tumour tissue and in tumour tissue, whereas no correlation was observed between the expression levels of *Trem2* and the chemokine *Cxcl1* (**Figure R.31B and Figure R.32B**). Interestingly, no correlation was observed between the expression levels of *Trem2* and the pro-inflammatory cytokines *Il1b* and *Il6* in the non-tumour tissue, whereas *Tnf* expression levels correlated with *Trem2* expression levels (**Figure R.31C**). In addition, *Il6* expression levels correlated with *Trem2* expression levels in DEN-induced tumour tissue (**Figure R.32C**).

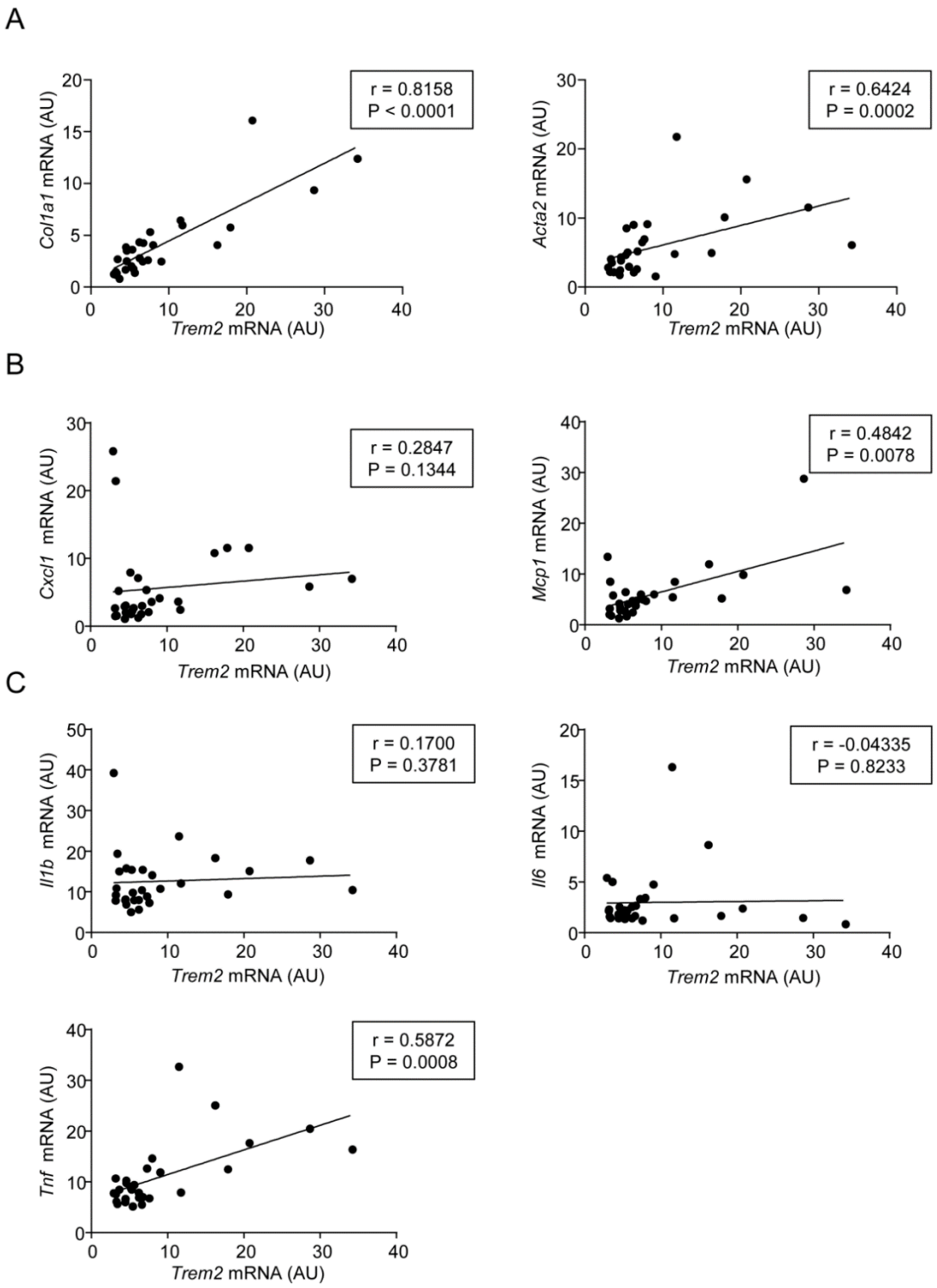

Figure R.31. Correlation between the expression levels of *Trem2* and markers of fibrosis and inflammation in the non-tumour liver tissue of DEN-induced mouse carcinogenic model. WT mice were injected with 30 mg/kg DEN and were sacrificed after 30 and 40 weeks (n=16 and n=14). (**A-C**) Correlation between the mRNA expression levels of *Trem2* and (**A**) markers of fibrosis *Col1a1* and *Acta2*, (**B**) the chemokines *Cxcl1* and *Mcp1* and (**C**) the cytokines *Il1b*, *Il6* and *Tnf*. Non-parametric Spearman's correlation test was used. *Acta2*, Actin alpha 2, smooth muscle; AU, arbitrary units; *Col1a1*, collagen type I alpha 1 chain; *Il*, interleukin; *Mcp1*, monocyte chemoattractant protein 1; *Tnf*, tumour necrosis factor; *Trem2*, triggering receptor expressed on myeloid cells 2; WT; wild type.

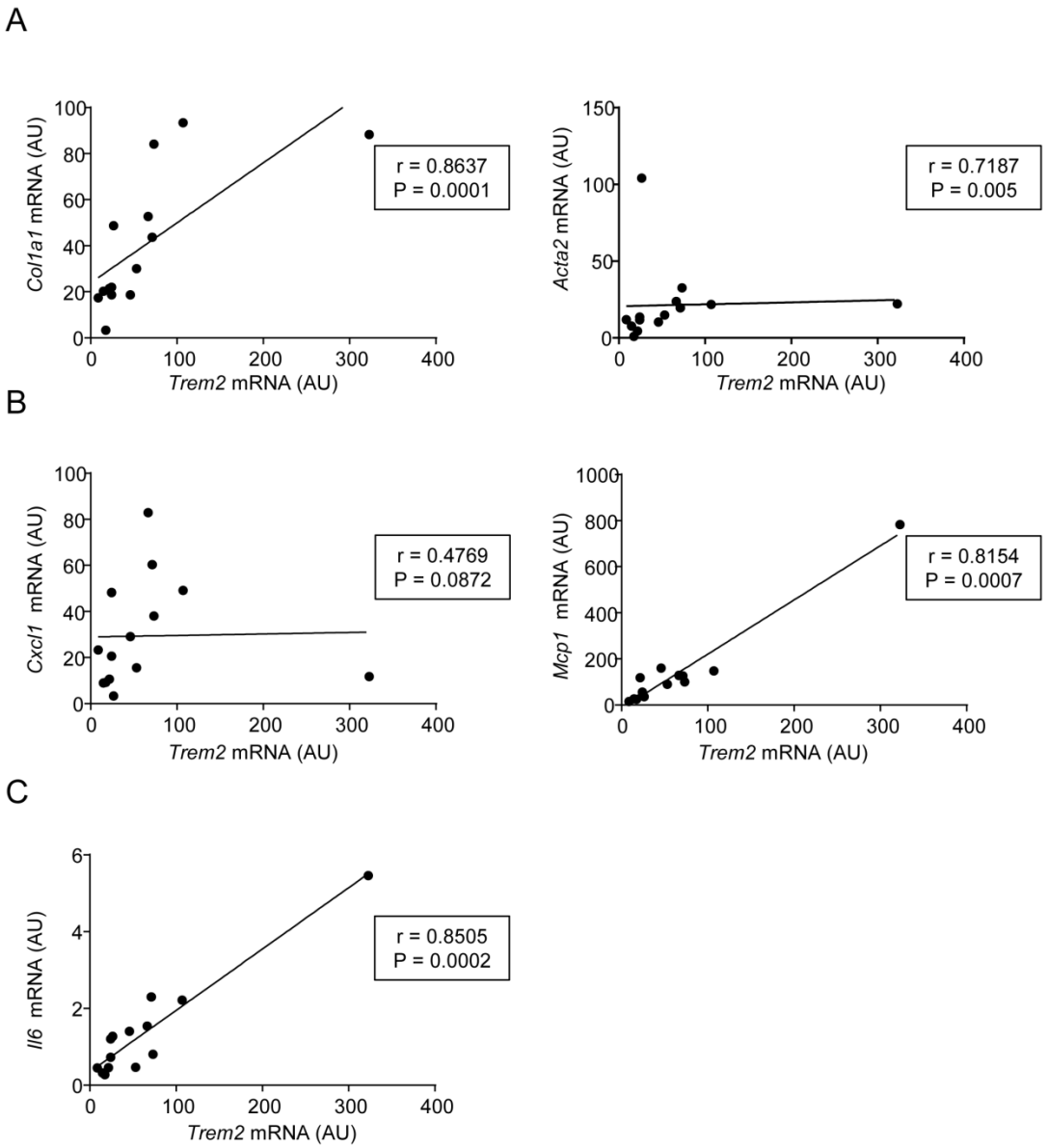

Figure R.32. Correlation between the expression levels of *Trem2* and markers of fibrosis and inflammation in the tumour liver tissue of DEN-induced mouse carcinogenic model. WT mice were injected with 30 mg/kg DEN and were sacrificed after 30 and 40 weeks (n=4 and n=10). (**A-C**) Correlation between the mRNA expression levels of *Trem2* and (**A**) markers of fibrosis *Col1a1* and *Acta2*, (**B**) the chemokines *Cxcl1* and *Mcp1* and (**C**) the cytokine *Il6*. Non-parametric Spearman's correlation test was used. *Acta2*, Actin alpha 2, *smooth muscle*; AU, arbitrary units; *Col1a1*, collagen type I alpha 1 chain; *Il*, interleukin*; Mcp1*, monocyte chemoattractant protein 1; *Trem2*, triggering receptor expressed on myeloid cells 2; WT; wild type.

R.3.4 *The number and size of tumours, hepatocyte proliferation and DNA damage in Trem2$^{-/-}$ mice is increased in the DEN-induced HCC model*

To investigate the relevance of TREM2 during hepatocarcinogenesis, 15 day old WT and *Trem2*$^{-/-}$ mice were injected with 30 mg/kg of DEN and tumourigenesis was assessed in the livers of these mice. Remarkably, *Trem2*$^{-/-}$ mice developed more tumours after both 30 and 40 weeks of DEN administration, compared to WT mice (**Figure R.33A**). We have so far demonstrated that lipid peroxidation is enhanced after acute and chronic liver injury models and that this was associated with higher levels of ROS in *Trem2*$^{-/-}$ BMDMs (**Figure R.18 and Figure R.19**). In line with this, we also observed increased ROS levels 24 hours after acute DEN challenge in *Trem2*$^{-/-}$ livers. Since exposure to DEN has been associated with accumulation of ROS within hepatocytes (90), we decided to perform in parallel to the DEN-model an additional experimental mouse model consisting on the administration of a normal diet supplemented with the antioxidant compound BHA for 15 weeks prior to the sacrifice of the animals 30 weeks after DEN administration. Remarkably, the administration of BHA in the diet resulted in an almost complete abrogation of tumour development in both, WT and *Trem2*$^{-/-}$ mice, compared to the DEN-injected mice fed with a normal diet. Importantly, the BHA diet lowered tumour burden to the same levels in both genotypes (**Figure R.33B**), supporting the concept that TREM2 protects in HCC by attenuating ROS levels. In addition, tumours in the DEN model were also analysed according to their size. *Trem2*$^{-/-}$ mice displayed increased number of small ($\leq$ 2mm) and big ($\geq$ 6mm) tumours after 30 weeks of DEN administration, whereas after 40 weeks of DEN administration *Trem2*$^{-/-}$ mice exhibited more small and medium size (2-6 mm) tumours, compared to WT livers (**Figure R.33C**).

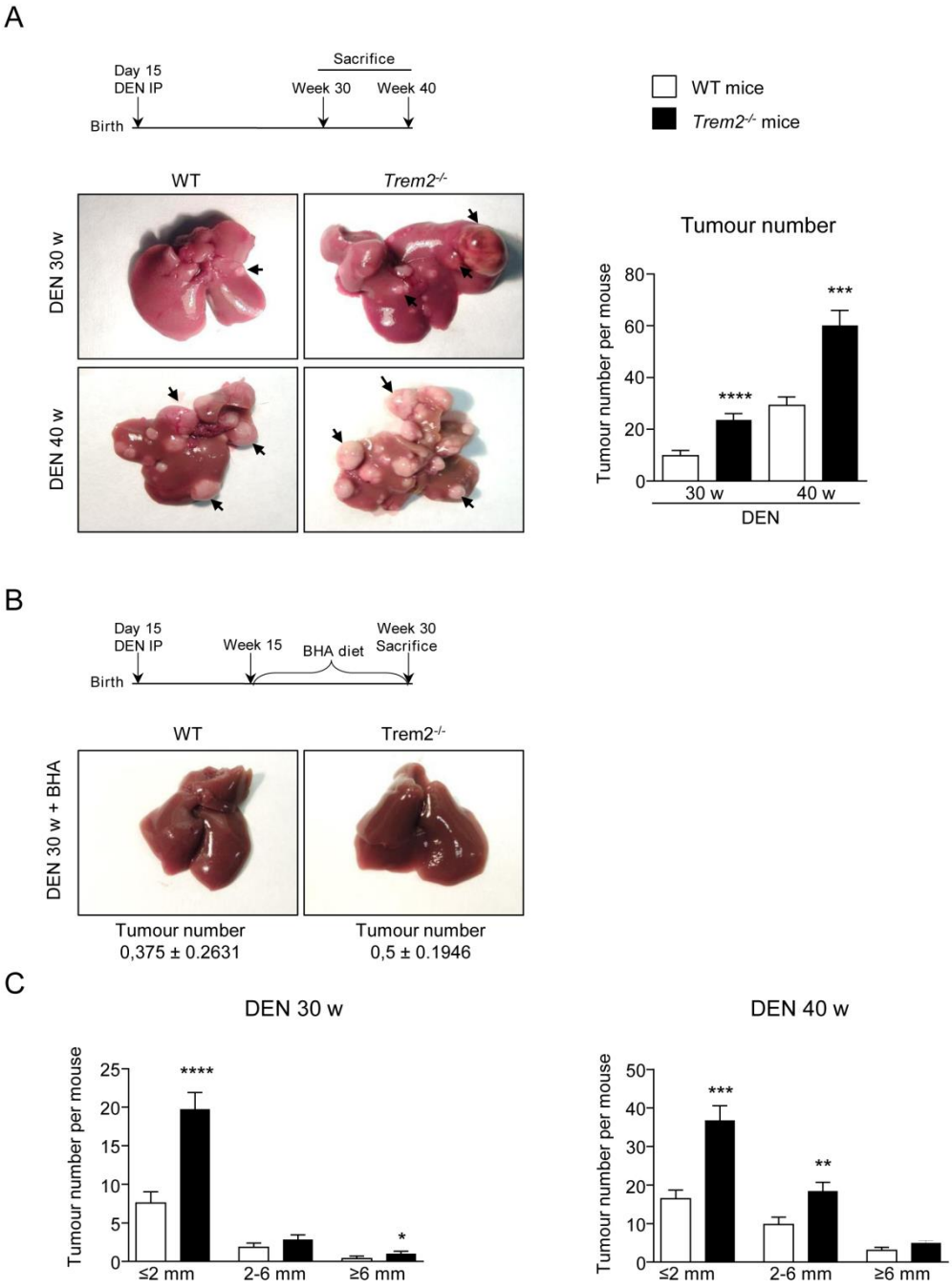

Figure R.33. *Trem2* null mice develop increased number of tumours after DEN treatment. (**A**) WT and *Trem2*$^{-/-}$ mice were injected with 30 mg/kg DEN and were sacrificed after 30 and 40 weeks (n=14-17). Representative pictures of the livers (arrows point to tumours) are depicted and total tumour number per mice is shown. (**B**) WT and *Trem2*$^{-/-}$ mice were injected with 30 mg/kg DEN, treated for 15 weeks with BHA diet and sacrificed after 30 weeks of DEN administration (n=7-12). Representative pictures of the livers (arrows point to tumours) are depicted and total tumour number per mice is shown. (**C**) Tumour number classified by size per mice in WT and *Trem2*$^{-/-}$ livers of 30 and 40 week DEN-injured mouse HCC models are shown. Parametric Student's T test and non-parametric Mann-Whitney test were used. Data represent mean ± SEM and *, **, *** and **** denote a P value of <0.05, <0.01, <0.001 and <0.0001, respectively versus WT mice. BHA, butylated hydroxyanisole; DEN, diethylnitrosamine; *Trem2*, triggering receptor expressed on myeloid cells 2; WT, wild type.

We further characterized the previously described carcinogenic mouse model by performing a microscopic analysis. Histologic analysis of H&E stains confirmed that *Trem2*$^{-/-}$ liver biopsies had increased number of HCC tumours compared to WT livers (**Figure R.34A**). In addition, we measured the expression of the hepatocyte proliferative marker PCNA by IHC in non-tumour liver tissue of these mice and we found that *Trem2*$^{-/-}$ livers displayed an increased number of PCNA positive nuclei both 30 and 40 weeks after DEN administration, compared with the respective WT livers (**Figure R.34B**). Similarly, DNA γH2AX IHC staining was performed in hepatocytes. Of note, *Trem2*$^{-/-}$ liver biopsies presented more positive hepatocyte nuclei compared to WT biopsies, at both time-points (**Figure R.34C**). Importantly, the protective effect of BHA diet shown in (**Figure R.33B**) was accompanied by a reduction of PCNA (**Figure R.34B**) positive and γH2A.X-stained (**Figure R.34C**) hepatocytes. Of note, the differences observed in WT and *Trem2*$^{-/-}$ mice after 30 weeks of DEN administration were reduced to the same level in both genotypes (**Figure R.34B-C**).

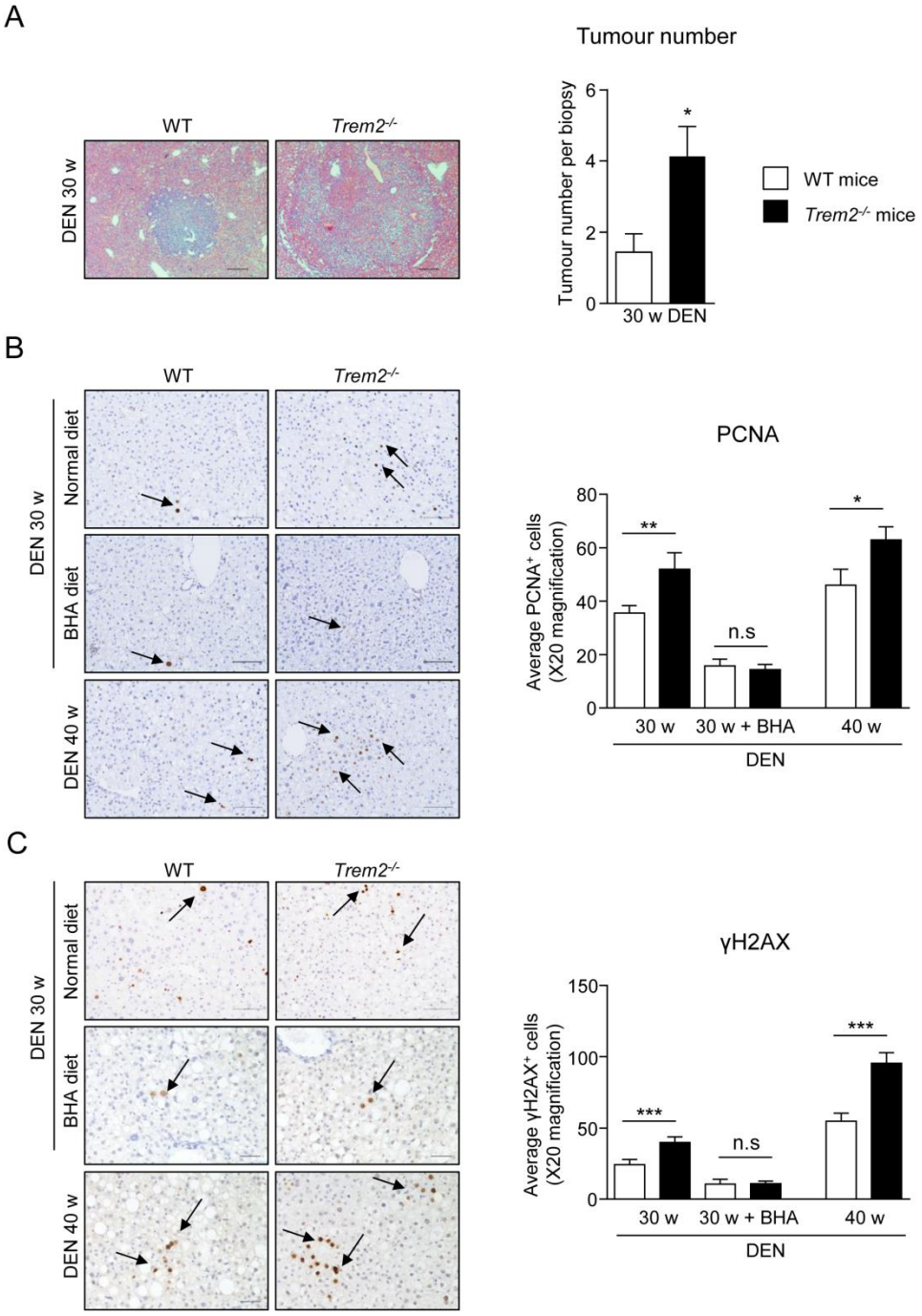

Figure R.34. *Trem2* null mice display an increased number of proliferative and damaged hepatocytes after DEN-induced liver carcinogenesis. Microscopic analysis of WT and *Trem2*$^{-/-}$ mice injected with 30 mg/kg DEN sacrificed after 30 and 40 weeks (n=14-17). (**A**) HCC tumour counting and representative H&E stained images after 30 weeks of DEN administration (4X). (**B**) Representative PCNA stained images and manual counts of positively stained hepatocytes (20X). (**C**) Representative γH2AX stained images and manual counts of positively stained hepatocytes (20X). Arrows denote positively stained cells. Parametric Student's T test and non-parametric Mann-Whitney test were used. Data represent mean ± SEM and *, ** and *** denote a P value of <0.05, <0.01 and <0.001 respectively. AU, arbitrary units; BHA, butylated hydroxyanisole; DEN, diethylnitrosamine; γH2AX, Phospho-Histone H2AX; HCC, hepatocellular carcinoma; n.s, non-significant; PCNA, proliferating cell nuclear antigen; *Trem2*, triggering receptor expressed on myeloid cells 2; WT; wild type.

In resemblance with our previous acute DEN-induced liver injury model, no significant difference was found in immune cell recruitment to the liver after chronic DEN-induced carcinogenic model (**Figure R.35A-C**).

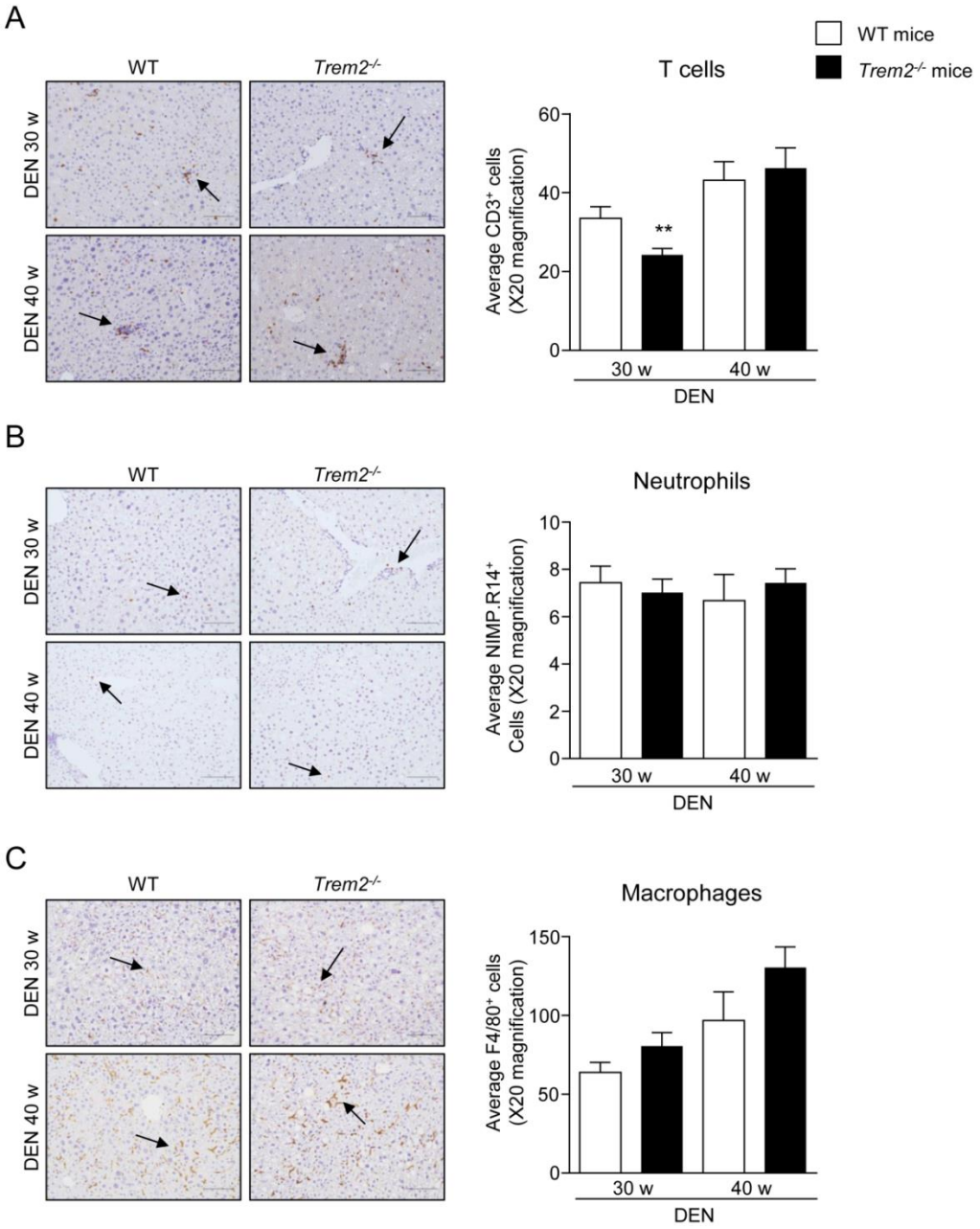

Figure R.35. No differences in immune cell recruitment after DEN-induced liver carcinogenesis between livers of WT and *Trem2*$^{-/-}$ mice. Recruitment of immune cells to the liver was measured by IHC. Representative images of liver sections immunostained for (**A**) T cells (anti-T cell marker CD3), (**B**) neutrophils (anti-neutrophil marker NIMP.R14) and (**C**) macrophages (anti-macrophage marker F4/80) (20X). Arrows denote positively stained cells. Manual counts of positive cells in livers 30 and 40 weeks post-DEN treatment are depicted. Scale bar indicates 100 μm. Parametric Student's T test and non-parametric Mann-Whitney test were used. Data represent mean ± SEM ** denote a P value of <0.01 versus WT mice. DEN, diethylnitrosamine; *Trem2,* triggering receptor expressed on myeloid cells 2; WT, wild type.

We further analyse the mechanisms by which TREM2 inhibits the hepatocarcinogenic process performing a proteomic analysis of DEN-induced WT and *Trem2*$^{-/-}$ mice liver tumour tissue.

Interestingly, 14 proteins were significantly and differentially expressed between WT and *Trem2*$^{-/-}$ liver tumours (**Figure R.36**)

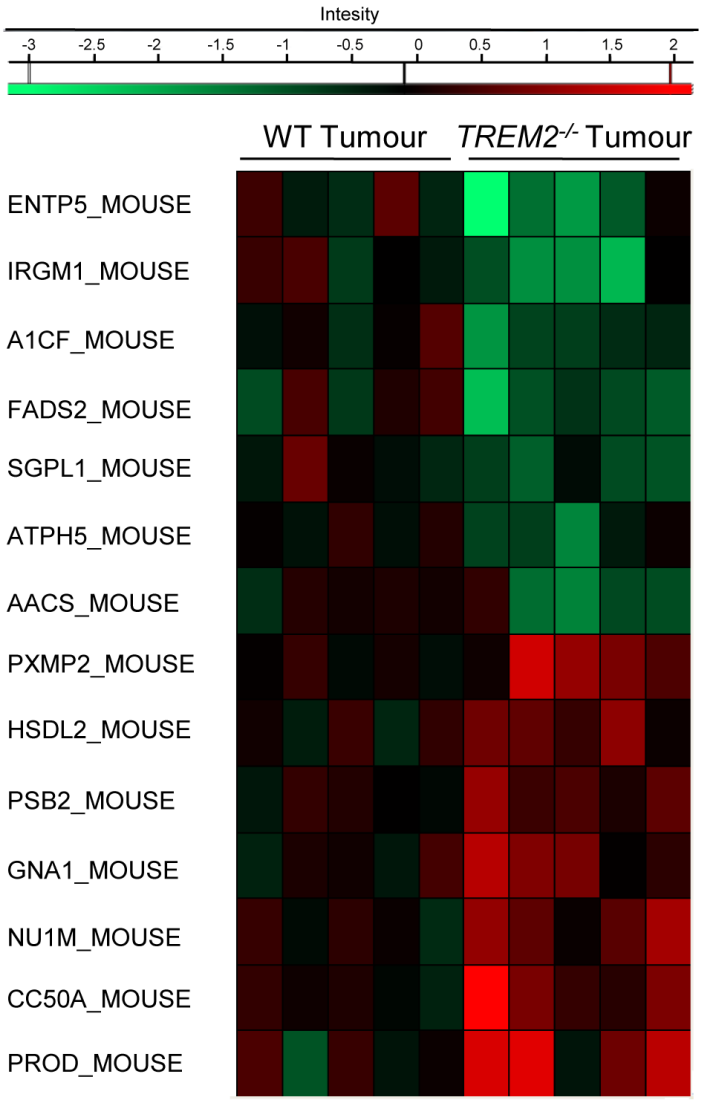

Figure R.36. Heatmap of differentially expressed proteins in DEN-induce HCC WT and *Trem2*$^{-/-}$ tumours (n=5). A1CF, APOBEC1 complementation factor; AACS, acetoacetyl-CoA synthetase; ATP5H, ATP synthase subunit d, mitochondrial; CC50A, cell cycle control protein 50A; ENTP5, ectonucleoside triphosphate diphosphohydrolase 5; FADS2, fatty acid desaturase 2; GNA1, glucosamine 6-phosphate N-acetyltransferase; HSDL2, hydroxysteroid dehydrogenase-like protein 2; IRGM1, immunity-related GTPase family M protein 1; NU1M, NADH-ubiquinone oxidoreductase chain 1; PROD, proline dehydrogenase 1, mitochondrial; PXMP2, peroxisomal membrane protein 2; proteasome subunit beta type-2; SGPL1, sphingosine-1-phosphate lyase 1; *Trem2*, triggering receptor expressed on myeloid cells 2; WT; wild type.

In accordance to an increased oxidative stress after acute DEN challenge, gene ontology analysis showed enriched processes including oxidoreductase activity and lipid metabolism (**Table R.1**). Similarly, Uniprot keywords analysis revealed that these processes were also enriched (**Table R.1**).

Table R.1. Gene ontology and Uniprot keywords enriched in the proteins differentially expressed in WT and *Trem2*$^{-/-}$ DEN-induced liver tumours.

Go Term	% of proteins	P value	Fold Enrichment
GO:0005783~endoplasmic reticulum	42.86	1.12E-03	6.37
GO:0014070~response to organic cyclic compound	21.43	1.24E-03	52.16
GO:0006631~fatty acid metabolic process	21.43	4.61E-03	26.75
GO:0016491~oxidoreductase activity	28.57	7.19E-03	8.89
GO:0055114~oxidation-reduction process	28.57	8.89E-03	8.23
GO:0016020~membrane	71.43	1.42E-02	2.01
GO:0010243~response to organonitrogen compound	14.29	1.52E-02	120.95
GO:0005739~mitochondrion	35.71	2.20E-02	4.08
GO:0005743~mitochondrial inner membrane	21.43	2.61E-02	10.89
GO:0046034~ATP metabolic process	14.29	2.62E-02	69.55
GO:0006629~lipid metabolic process	21.43	3.59E-02	9.09
UniProt Keyword	**% of proteins**	**P value**	**Fold Enrichment**
Oxidoreductase	28.57	5.15E-03	10.14
Endoplasmic reticulum	28.57	1.74E-02	6.5
Lipid metabolism	21.43	2.30E-02	11.66
Acetylation	42.86	2.44E-02	3.11

ATP, Adenosine triphosphate; GO, gene ontology.

Together, these data suggest that in the absence of *Trem2* the generation and development of HCC in mice is accelerated and is associated with enhanced hepatocyte damage and proliferation. In addition, this process can be inhibited by an antioxidant diet, providing a clear *in vivo* association between ROS levels, oxidative DNA damage and HCC development.

R.3.5 *HCC cell line spheroid growth is inhibited by TREM2 overexpressing HSC supernatant*

With the idea of translating our *in vivo* results to an *in vitro* system, we decided to perform gain of function experiments. As TREM2 is mainly expressed in non-parenchymal liver cells, is significantly induced during HSC activation (**Figure R.4**) and it is well established that activated HSCs infiltrate the tumour stroma, secrete ECM proteins and favour HCC tumourigenicity potentially through changes in their secretory phenotype (49, 228, 229). We decided to evaluate the impact of HSC expressed TREM2 as a potential regulator of HCC growth and translate these findings to the human situation by developing a humanized 3D spheroid model. Such models have proved to be invaluable for studying the interactions between cancer cells and their surrounding environment (230, 231). For that, first we confirmed TREM2 overexpression in LX-2 cells at mRNA and protein level (**Figure R.37A-B**).

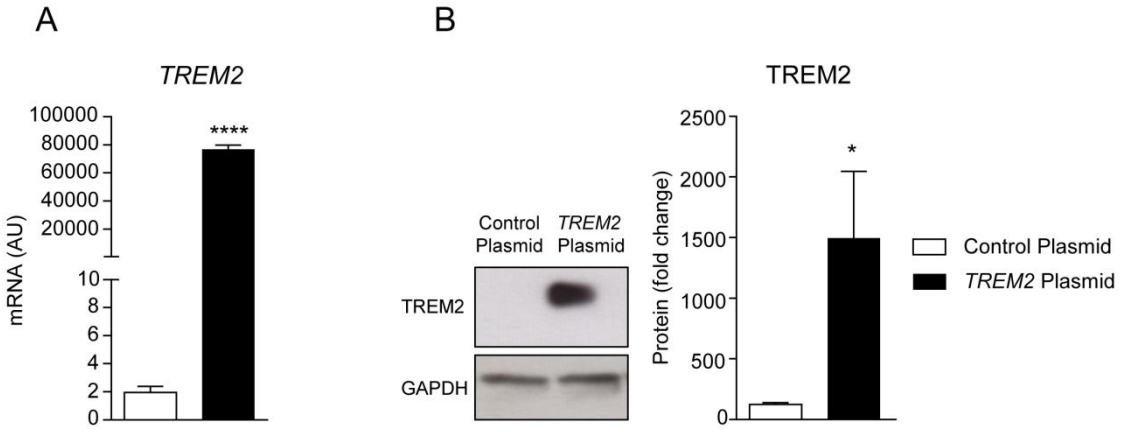

Figure R.37. TREM2 overexpression in the human LX-2 HSC cell line. Human LX-2 cells were transfected with a control or *TREM2* overexpressing plasmid and 24 hours post-transfection (**A**) *TREM2* mRNA and (**B**) TREM2 protein levels were determined. Parametric Student's T test was used. Data represent mean ± SEM and, *, **** denote a P value of <0.05 and <0.0001, respectively versus control plasmid LX-2 cells. AU, arbitrary units; GAPDH, glyceraldehyde 3-phosphate dehydrogenase; *TREM2,* triggering receptor expressed on myeloid cells 2.

Next, the role of TREM2 in the crosstalk between HSCs and HCC tumour cells was investigated *in vitro*. For that, we overexpressed *TREM2* in the human HSCs cell line LX-2 and carried out culture hanging droplet liver cancer spheroid growth experiments. Strikingly, the supernatant of TREM2 overexpressing LX-2 cells markedly reduced the 3-dimentional HCC (i.e., Hep3B and PLC/PRF5 HCC cell lines) spheroid growth *in vitro* compared to control conditions (media from LX-2 cells transfected with a control vector) (**Figure R.38A-B)**.

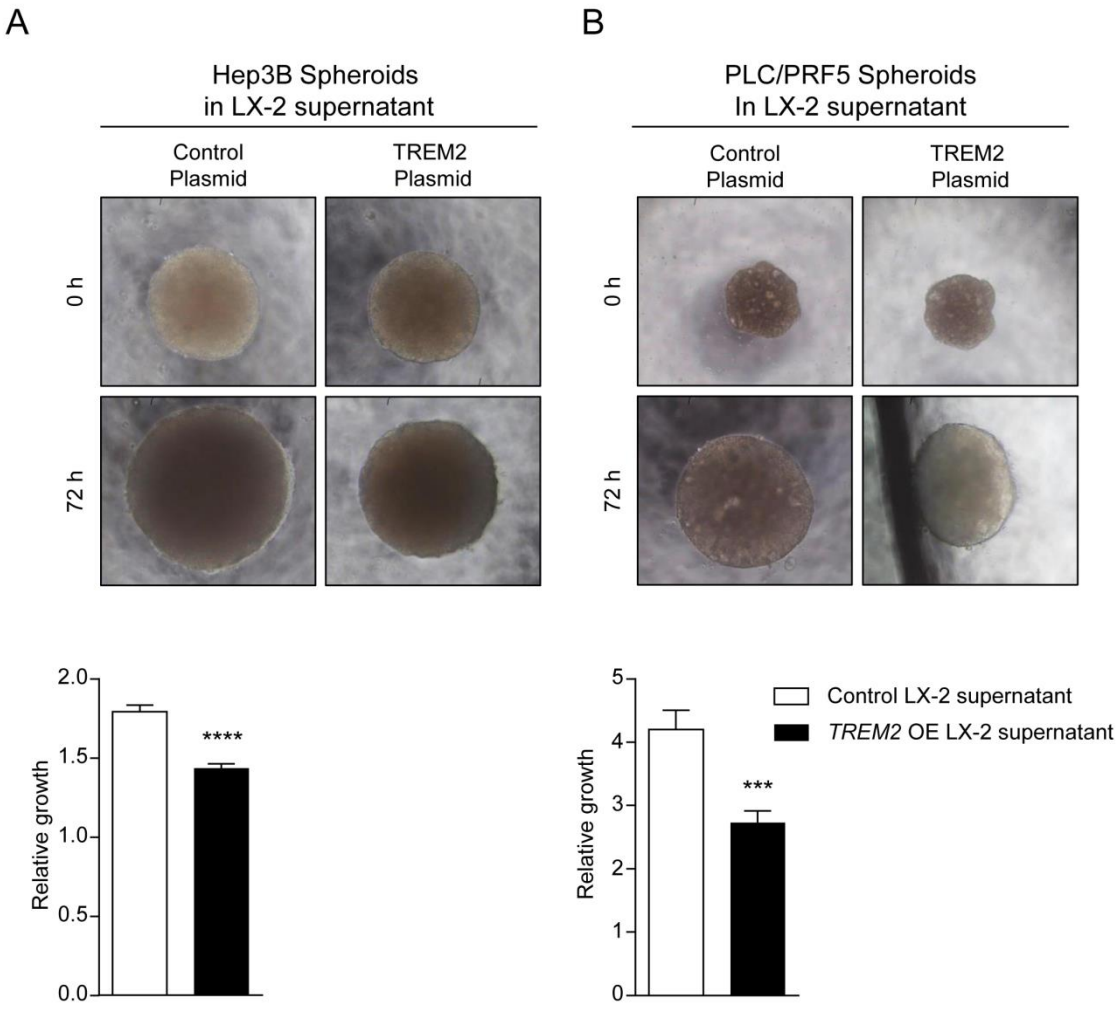

Figure R.38. HCC spheroid growth is inhibited in presence of TREM2 overexpressing LX-2 supernatant. (**A**) Hep3B or (**B**) PLC/PRF5 cells were seeded in hanging droplets for 7 days forming spheroids. Then, spheroids were treated with LX-2 supernatant (LX-2 overexpressing a control plasmid or *TREM2* plasmid) and spheroid size was recorded (20X). Non-parametric Mann-Whitney test was used. Data represent mean ± SEM and ***, **** denote a P value of <0.001 and <0.0001, respectively versus control LX-2 supernatant. AU, arbitrary units; OE, overexpression; *TREM2*, triggering receptor expressed on myeloid cells 2.

In view of these data, we next decided to perform the gene transcription analysis of key pro-inflammatory and HCC growth-related mediators in control or TREM2 overexpressing LX-2 cells. mRNA levels of *TNF* and *MCP1* were downregulated in *TREM2* overexpressing LX-2 cells compared to controls (**Figure R.39A**). We also verified these data by ELISA in the supernatant of LX-2. (**Figure R.39B**). In addition, the Wnt/β-catenin pathway plays a major role in cancer and particularly in HCC (232, 233), in this regard, TREM2 has been shown to modulate this pathwayin other cellular systems including the bone and brain (234, 235), we next decided to determine the potential effects of TREM2 on WNT signaling and HCC growth. Therefore, we checked for WNT ligand expression in control or TREM2 overexpressing LX-2 cells and observed that the canonical WNT ligands *WNT3, WNT7A* and *WNT8A* were downregulated upon TREM2 overexpression (**Figure R.39C)**.

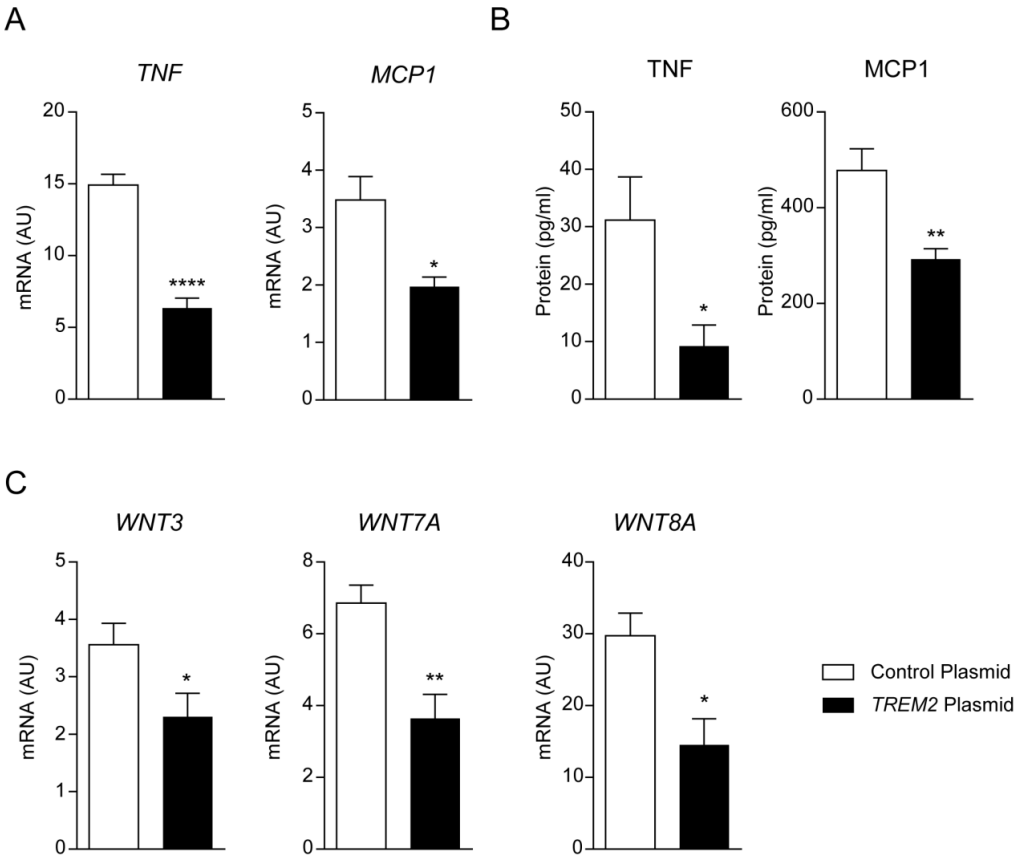

Figure R.39. Gene expression analysis in TREM2 overexpressing LX-2 cells. (**A**) mRNA levels of *TNF* and *MCP1* in cell extracts and (**B**) protein levels of TNF and MCP1 in the cell supernatant by ELISA were determined. (**C**) The mRNA levels of canonical WNT ligands *WNT3*, *WNT7A* and *WNT8A* were determined. Parametric Student's T test and non-parametric Mann-Whitney test were used. Data represent mean ± SEM and *, **, **** denote a P value of <0.05, 0.01 and <0.0001, respectively versus control plasmid LX-2 cells. AU, arbitrary units; *MCP1*, monocyte chemoattractant protein 1; OE, overexpression; *TNF*, tumour necrosis factor; *TREM2*, triggering receptor expressed on myeloid cells 2.

To mechanistically prove whether TREM2 mediated effects in HCC spheroid growth were Wnt/β-catenin pathway dependent, HCC spheroids were treated with the β-catenin inhibitor IWR-1. Consistent with the HSC expression of WNT ligands, HCC spheroid growth was dependent on Wnt/β-catenin signalling as it was substantially reduced upon IWR-1 treatment under control conditions (**Figure R.40A**). Notably, as these ligands were attenuated upon TREM2 overexpression (**Figure R.39C**), HCC spheroid growth attenuation in the presence of TREM2 overexpressing HSC supernatant was abolished upon IWR-1 treatment (**Figure R.40A**). These data suggest that TREM2 expression within HSCs attenuates HCC growth through Wnt/β-catenin signalling. To confirm this hypothesis we next blocked WNT ligand secretion in both sets of HSCs and could observe that blocking WNT ligand secretion abolished the differences associated with TREM2 overexpression (**Figure R.40B**). Additionally, to rule out direct autocrine effects of IWP-2 inhibitor treatment in the HCC spheroid growth, we directly added this inhibitor to spheroids. Of note, in presence of IWP-2 inhibitor, spheroid growth was still inhibited by TREM2 overexpressing LX-2 media compared to control plasmid overexpressing LX-2 media (**Figure R.40B**).

Thus, we demonstrate that TREM2 reduces HCC spheroid growth *in vitro* via HSC paracrine secretion of WNT ligands.

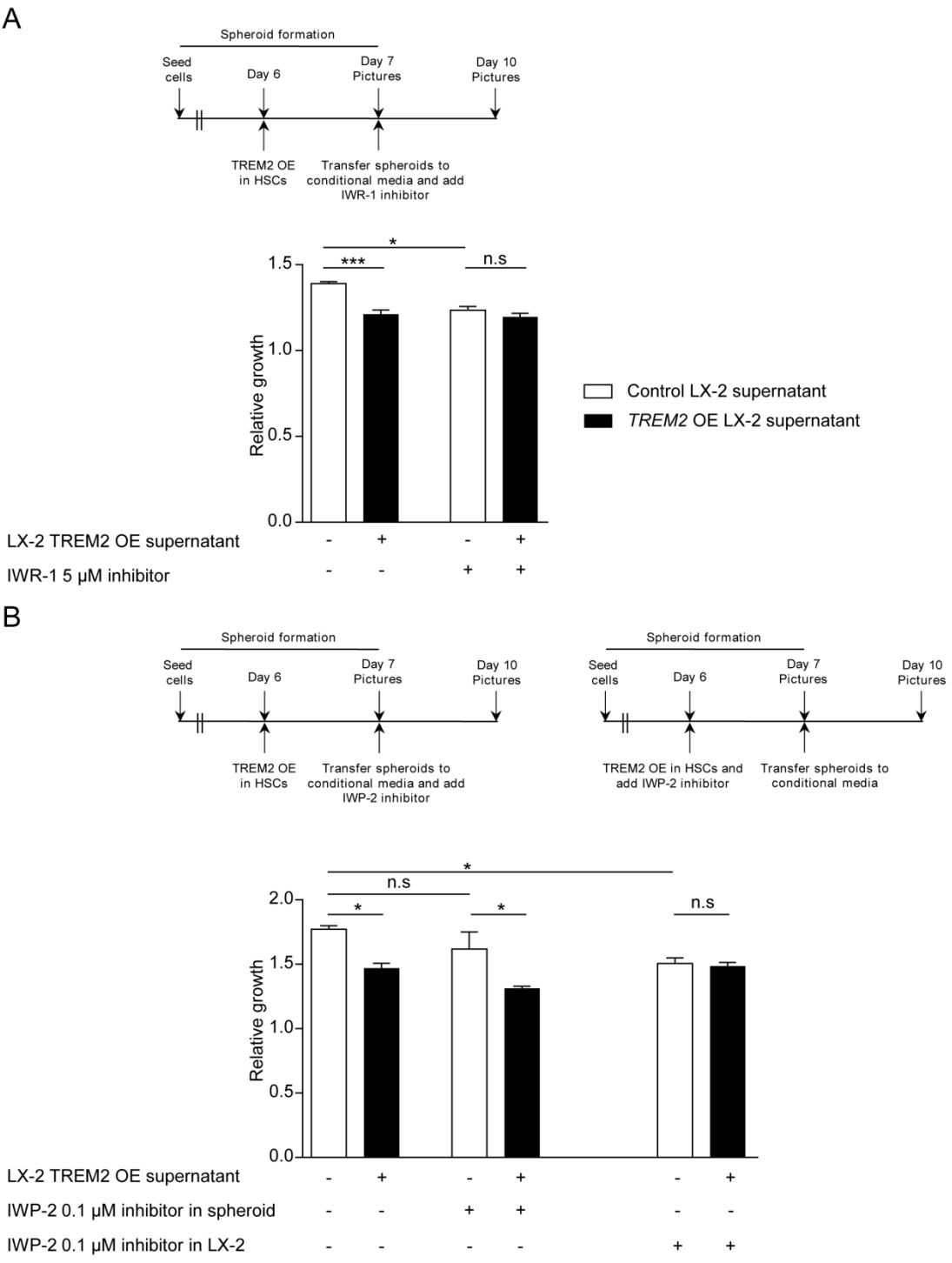

Figure R.40. TREM2 effects in HCC spheroid growth are mediated by LX-2 WNT ligand paracrine secretion. (**A**) Hep3B cells were treated with the Wnt/β-catenin inhibitor IWR-1 and (**B**) LX-2 cells or Hep3B spheroids were treated with the WNT ligand secretion inhibitor IWP-2, Hep3B spheroids were incubated in LX-2 conditioned media and spheroid growth was recorded. Parametric Student's T test and non-parametric Mann-Whitney test were used. Data represent mean ± SEM and ** and **** denote a P value of <0.01 and <0.0001 respectively. AU, arbitrary units; n.s, non-significant; OE, overexpression; *TREM2*, triggering receptor expressed on myeloid cells 2.

DISCUSSION

Unresolved inflammation is a pathogenic feature of liver disease occurring after chronic liver injury that contributes to liver damage and fibrosis. During liver injury, alterations in the intestinal permeability occur and cause the leakage of pathogens from the gut to the liver. In the liver, microbial molecules, also known as PAMPs, are recognized by non-parenchymal liver cells and recruited cells, among others. In turn, these cells release a diverse array of pro-inflammatory mediators, such as cytokines, chemokines and ROS, contributing to hepatocyte damage and death.

In line with this dogma, treatment of mice with antibiotics or probiotics attenuates various forms of liver injury including CCl_4, BDL and non-alcoholic steatohepatitis (NASH) (64, 146). Further, illustrating the importance of innate immunity during liver disease, mice deficient in key mediators of LPS signaling such as TLR4, CD14 and Myd88 are protected from different types of liver disorders (64, 146, 147, 236, 237) and cancer (145, 238). In addition, other members of TLR family such as TLR9 also play an important role liver disease, as TLR9 has been shown to promote steatohepatitis and HCC (237, 239).

Here, with the hypothesis that TREM2 could modulate TLR-mediated signaling in the liver and be involved in liver disease, we studied the role of this receptor during the progression of liver disease, from acute liver injury to chronic liver disease and the development of HCC.

D.1 Role of TREM2 in liver injury

In this work, we have shown that TREM2 expression significantly increases during liver injury both in humans and mice. Human TREM2 expression was augmented in cirrhotic patients compared to healthy controls and mouse *Trem2* expression was induced during both acute and repetitive CCl_4 injury and BDL. We have also demonstrated that hepatic mouse *Trem2* is expressed on non-parenchymal liver cells, KCs and HSCs. However, with our data we cannot exclude that in other species, including humans, TREM2 is not expressed in other cell types such us hepatocytes during liver injury. Importantly, although TREM2 expression was reported on different resident macrophages, including KCs, (151, 184, 192, 209) this is the first time demonstrating that TREM2 is expressed on quiescent and activated HSCs, which goes in line with previous studies showing that TREM1 is also expressed on HSCs (164). In addition, we show that *TREM2* is

dramatically induced during HSC activation, both *in vivo* after acute or chronic liver injury and during HSC transdifferentiation *in vitro*. Importantly, the upregulation of TREM2 expression during the activation of HSCs *in vitro* is conserved on different species, as shown in mouse, rat and human HSCs.

However, TREM2 did not impact the activation status of HSCs *in vitro,* as shown by undetectable differences in Acta2 and α1(I)procollagen mRNA levels in WT and *Trem2*$^{-/-}$ HSCs. These data suggest that TREM2 does not directly regulate the production of collagen. In agreement with no effects on collagen synthesis, during chronic liver injury, WT and *trem2*$^{-/-}$ mice displayed equal levels of TGFβ, a key mediator of fibrosis and a potent stimulus for collagen production (43, 240). Interestingly, *Mmp13* was elevated in *Trem2*$^{-/-}$ mice after chronic liver injury. Of note, this matrix metalloproteinase plays a crucial role in fibrosis resolution (241), indicating that upregulation of *Mmp13* in *Trem2*$^{-/-}$ mice may serve to attenuate liver fibrosis in these mice. Of note, TREM2 has been described as a phagocytic receptor that promotes clearance of bacterial cells and apoptotic bodies (63, 242, 243). Even though HSCs are not professional phagocytes, phagocytosis of apoptotic bodies by HSCs has been described and associated with HSC activation, survival and collagen deposition (187, 188, 190, 192). Therefore, impaired bacterial and apoptotic body clearance by *Trem2*$^{-/-}$ HSCs could also contribute to the absence of differences in fibrosis observed between WT and *Trem2*$^{-/-}$ mice after chronic CCl_4 injury.

Importantly, our data suggest that TREM2 inhibits hepatocellular injury primarily though the inhibition of inflammation. As it was previously reported in BMDMs (184), we have shown that TREM2 dampens TLR4-derived pro-inflammatory cytokine regulation in KCs and HSCs. Moreover, consistent with previous studies (185, 188), inflammation in *Trem2*$^{-/-}$ KCs correlates with TLR4-mediated effects on ERK activation and an absence of effects in NF-κB pathway. Besides the effects on classic pro-inflammatory cytokine expression, including *Il1b*, *Il6* and *Tnf*, we have also demonstrated a pivotal role of TREM2 negatively regulating the neutrophil chemoattractant chemokine *Cxcl1* expression. In agreement with this, during acute CCl_4-mediated injury, *Trem2*$^{-/-}$ mice displayed elevated liver injury and increased expression of *Cxcl1* compared to WT mice. This correlated with an elevated number of recruited neutrophils in *Trem2*$^{-/-}$ mice compared to WT mice. These observations are in line with other studies showing differences in neutrophil recruitment on *Trem2*$^{-/-}$ mice during pneumococcal infections (192). Likewise, after APAP challenge, increased neutrophil influx to the liver was also

observed in *Trem2*$^{-/-}$ mice compared to WT mice. However, in this model unlike in acute CCl_4-mediated injury, liver macrophage content was also elevated on *Trem2*$^{-/-}$ mice. Therefore, even though the relative contribution of each cell population to the models studied remains to be elucidated, we have demonstrated that i) TREM2 dampens liver injury in our models ii) gut-derived PAMPs are a driver for acute liver injury of *Trem2*$^{-/-}$ mice iii) After APAP lethal challenge *Trem2*$^{-/-}$ mice have a worsened survival outcome (**Figure D.1**).

In terms of mechanistic parallels between chronic CCl_4 injury and acute APAP challenge, both models are characterized by augmented *Mcp1* levels in *Trem2*$^{-/-}$ mice compared to WT mice, which is associated with increased macrophage content. In addition, in both models *Trem2*$^{-/-}$ mice exhibit more liver damage and increased lipid peroxidation. As mentioned, resident KCs have their origin in the yolk sac and/or in the foetal liver, however, during liver injury, circulating monocytes ($Ly6C^+$) are recruited to the liver by the MCP1 chemokine, and can contribute to injury (117-119). Interestingly, it has been reported that after APAP challenge, monocyte-derived macrophages are recruited to the liver and exert pro-inflammatory functions promoting liver injury. Hence, the reduction of monocyte recruitment via MCP1/CCR2 inhibition diminishes APAP-induced liver injury (244). Taken together, all these data point out that monocyte recruitment after hepatotoxic damage perpetuates parenchymal damage. In fact, there are studies supporting the concept that KCs are protective in APAP-induced liver injury in mice (133). With our data we add new information in this context emphasizing on the key role that TREM2 signalling plays suppressing the recruitment of macrophages to the liver and consequently reducing APAP-induced liver injury (**Figure D.1**).

Importantly, our data indicate that TLR4-dependent MCP1 production is inhibited by TREM2 in HSCs, which is associated with decreased macrophage recruitment to the liver. Moreover, ROS production is decreased by TREM2 in bone-marrow-derived macrophages and this may explain ROS-mediated increased lipid peroxidation and cell death in *Trem2*$^{-/-}$ mice. However, inhibition of ROS production in recruited macrophages by TREM2 might not be sufficient to dampen liver injury, as seen in the BM transplant experiment, where WT mice reconstituted with *Trem2*$^{-/-}$ BM cells do not display more liver damage compared to WT mice reconstituted with WT BM. Rather, our data points towards an important role of TREM2 in HSCs where it regulates the recruitment of macrophages to the liver via its effects on MCP1 production in a TLR4-dependent manner which is also influenced by ROS and cytokine production from the infiltrating immune

cells. Accordingly, liver steatosis is able to sensitize CCl_4 hepatotoxicity, partly through oxidative stress (245). In addition, purified $Cd11b^+F4/80^+Ly6C^+$ cells from CCl_4 treated mice can directly activate HSCs, showing more evidences of this cross-talk between HSCs and infiltrating cells in liver injury (40). Of note, infiltrating inflammatory $Ly6C^+$ macrophages decrease the expression of Ly6C after the uptake of apoptotic hepatocytes which is protective in alcohol induced liver injury (246). Even though the nature of the infiltrated macrophages in our model needs to be further studied, they seem to play an important role for TREM2 limiting the hepatocellular damage after APAP and chronic CCl_4 injury. Besides, in a context of liver injury, hepatocytes release DAMPS that can further enhance cell death, inflammation and macrophage content (224). Such a hepatotoxic feed forward loop could happen in the absence of TREM2, explaining the enhanced liver damage in *Trem2*$^{-/-}$ livers after acute APAP and chronic CCl_4 injury. Even more, other mechanisms such as the effect of TREM2 on liver lipid metabolism may play an important role too. In this sense, recent studies have shown that TREM2 is able to sense lipids and to alter lipid metabolism and purogenic signalling in the brain (189, 247). Importantly, highlighting the role of TREM2 in lipid metabolism, it was reported that TREM2 promotes adipogenesis, as mice overexpressing TREM2 fed with a high fat diet were more obese and developed more steatosis (248). Even though the authors of this study did not extensively address TREM2-mediated liver injury effects in these mice, the role of TREM2 in NAFLD-mediated liver injury seems to be complex, involving not only effects related to the immune system but also adipogenic and lipid regulatory functions (189, 248) (**Figure D.1**).

In conclusion, we demonstrated a role of TREM2 attenuating toxic liver injury that goes in line with published results in other organs and tissues. As in the colon, where it is important for the wound-healing process (203) or in the brain were TREM2 is key in the uptake of apoptotic neurons and in limiting microglial inflammation (187, 188).

In summary, we believe that TREM2 could be an attractive target to promote the resolution of inflammation during liver injury and also to prevent hepatocyte cell death.

D.2 Role of TREM2 in liver regeneration after partial hepatectomy

The regenerative mechanisms are activated in the liver after a liver injury or a hepatic parenchymal mass loss. Due to the fact that TREM2 plays an important role in acute and

chronic liver injury we decided to formally investigate the role of TREM2 in the context of liver regeneration after PHx.

In the early phases of liver regeneration after PHx, the expression of TNF and IL6 is increased. These inflammatory mediators are mainly produced by KCs and HSCs (26, 100). Of note, we show that after PHx, the levels of *Il6* and *Tnf* are upregulated in the *Trem2*$^{-/-}$ mice compared to WT mice during the priming phase, suggesting that inflammation after PHx is abnormally high in these mice. This was also accompanied with an upregulation of the hepatocyte proliferative factor *Hgf* 6 hours after PHx. Accordingly, hepatocyte proliferation was enhanced 72 hours after PHx in *Trem2*$^{-/-}$ mice (**Figure D.1**).

Thus, liver regeneration after PHx is accelerated in *Trem2*$^{-/-}$ mice, which was associated with an enhanced inflammation during the priming phase and augmented hepatocyte proliferation in the livers of these mice.

D.3 Role of TREM2 in HCC

HCC often arises in a setting of chronic liver injury caused by different aetiologies. Chronic liver injury is characterized by an enhanced inflammation, ROS production, DNA damage, hepatocyte death and necrosis. Consequently, compensatory proliferation of hepatocytes and liver progenitor cells is triggered, which may finally result in the development of HCC (75). Among other factors, gut-liver axis and bacterial translocation

are known to be involved in the progression of liver disease and HCC development (135). However, the molecular mechanisms that fine-tune the innate immune response involved in the negative regulation of the inflammatory response in the liver are still unknown and need to be studied in order to develop new therapeutic strategies for therapy.

Even though the role of TREM2 in several human disorders is being uncovered (151), there are only few studies that have started to shed light on the impact of TREM2 in cancer (204, 206, 207, 249). Thus, the role of this receptor in cancer is still largely unknown and regarding HCC, it needs to be fully elucidated. Here, we report novel data indicating that TREM2 in non-parenchymal cells functions as a natural brake on liver inflammation, regulating hepatocyte proliferation and damage, and consequently regulating HCC development and growth.

As aforementioned, *TREM2* is induced in cirrhotic patients compared to controls and that its expression correlated with markers of inflammation and its absence in murine models of liver injury was associated to increased liver damage and inflammation. These observations were also observed in HCC, since *TREM2* expression is also elevated in HCC patients compared to controls, correlating with inflammatory markers. In addition, experimental mouse models of hepatocarcinogenesis carried out in WT and *Trem2*$^{-/-}$ mice have demonstrated that *Trem2*$^{-/-}$ mice present a worsened liver phenotype, in terms of presenting higher number of tumours, increased liver damage and inflammation. Considering that HCC is a clear example of an inflammation-related cancer, as it usually arises and develops in a context of chronic liver inflammation (82) and that TREM2 is preferentially expressed in non-parenchymal cells within the liver, where it acts as a natural brake on inflammation during acute and chronic hepatotoxic injury, we believe that the upregulation of *TREM2* in HCC tissue is due to an accumulation of inflammatory cells in the liver, such as KCs and HSCs. We therefore postulate that TREM2 is upregulated during unresolved inflammation which is present during HCC in an attempt to counteract this inflammatory process.

The administration of the carcinogenic drug DEN inflicts death of hepatocytes which in turn results in enhanced proliferation of the intact hepatocytes (250). In this regard, TREM2 is able to protect from DEN-induced HCC as its absence enhances proliferation and DNA damage in hepatocytes. In other means, when DEN is administered 15 days after birth, *Trem2*$^{-/-}$ mice develop more and bigger liver tumours, both 30 and 40 weeks post-DEN injection. Accordingly, upon acute DEN administration, *Trem2*$^{-/-}$ mice exhibit increased number of damaged hepatocytes. Interestingly, this goes

in line with the results observed with the pro-inflammatory receptor TREM1. This receptor has been described to perform opposed functions to TREM2 (151) and is detrimental in HCC development, as *Trem1*$^{-/-}$ mice develop less liver tumours after DEN injection (163).

In addition, we observed increased pro-inflammatory gene (*Tnf*) and chemokine (*Mcp1* and *Cxcl1*) expression in the early phases after acute DEN administration. Furthermore, augmented transcript levels of the oxidative stress enzyme *Hmox1* and increased ROS levels were found in *Trem2*$^{-/-}$ liver tissues. Therefore, our results suggest that *Trem2*$^{-/-}$ mice display increased inflammation and ROS levels after DEN injury, which in turn, may help in the initiation and progression of HCC in these mice (**Figure D.1**).

Antioxidant intake has been postulated to overcome incipient carcinogenic processes. However, there is some controversy regarding the beneficial effects antioxidants may produce (251, 252) as they may promote the development of already formed tumours (253). Moreover, the balance between ROS and antioxidants needs to be optimal and the addition of antioxidants should be considered only in certain patients who may show beneficial effects due to high levels of oxidative stress and inflammation (253). In this regard, the use of antioxidant diets in mice has been shown to inhibit DEN-mediated hepatocarcinogenesis by reducing ROS and ROS-mediated DNA damage (90, 227). Considering that HCC is an inflammation-related cancer we decided to administer a diet supplemented with the antioxidant BHA in DEN-injected mice. This way we could test if lowering the levels of ROS would also lower the number of tumours in *Trem2*$^{-/-}$ mice to the same levels of WT mice. Indeed, tumour number in both genotypes decreased to the same level, indicating that TREM2 might protect from DEN-induced liver tumourigenesis by lowering the levels of ROS and inflammation. Of note, this diet was administered when the tumours were starting to develop (i.e. 15 weeks after DEN administration) and maintained until mice were sacrificed after 30 weeks of DEN injection. These results suggest that the activation of TREM2 in a setting of advanced chronic liver disease could be beneficial for patients with HCC.

On the other hand, to study the impact of TREM2 in HCC growth *in vitro*, we carried out sophisticated hanging droplet HCC spheroid growth experiments with the supernatant of TREM2 overexpressing HSCs. Of note, the conditioned media of TREM2 overexpressing HSCs inhibited the growth of HCC spheroids compared to controls and this event was associated with a reduction in the expression levels of TNF, MCP1 and

Wnt ligands. Interestingly, TREM2 reduces HCC tumourigenicity via paracrine mechanisms within HSCs that rely on Wnt signalling. Altogether, we believe that TREM2 inhibits inflammation, proliferative responses as well as HCC development and growth, which is indicative of a protective role of this receptor in HCC (**Figure D.1**).

In summary, this study provides novel insights into the important role of TREM2 in HCC. The tumorigenic drug DEN damages the hepatocytes causing mutations, inflammation and ROS. This is exacerbated in the absence of *Trem2* leading to hepatocyte DNA damage and proliferation, finally leading to increased liver tumourigenesis. In addition, liver regeneration is exacerbated in *Trem2*$^{-/-}$ mice. Taken together, non-parenchymal TREM2 is able to attenuate hepatocyte damage inhibiting ROS and inflammation, protecting the liver from hepatocyte proliferative responses, and the development of HCC.

In conclusion, TREM2 arises as a potential therapeutic target for HCC. Hence, in this regard it is important to describe and find TREM2 agonists that might have a significant impact on inflammation-driven cancer in humans. Altogether, these results provide pivotal findings about the key role of TREM2 in hepatocarcinogenesis, paving the way for new clinical strategies for HCC patients.

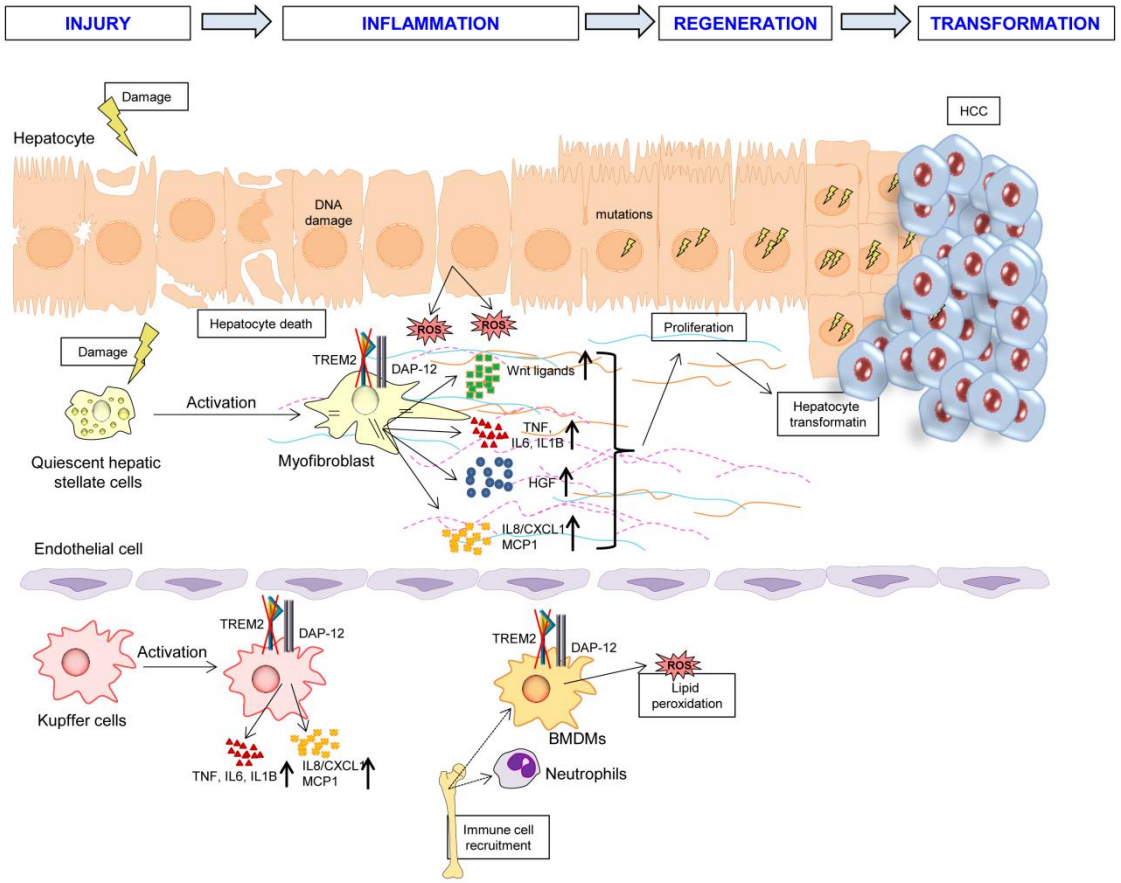

Figure D.1. Relevance of TREM2 in the liver disease. After liver injury, in the absence of *Trem2*, hepatocyte damage and death are increased. This is associated with increased ROS production, augmented cytokine, chemokine, growth factor and WNT ligand expression and DNA damage. In addition, immune cell recruitment is enhanced and ROS production in the absence of TREM2 in BMDMs is increased which is associatedwith an increased lipid peroxidation. On the other hand, during liver regeneration, in the absence of *Trem2*, increased inflammatory marker and growth factor expression is observed, which is in line with enhanced hepatocyte proliferation. The pro-inflammatory microenvironment may favour the appearance of mutations in the proliferating hepatocytes, promoting their transformation and the development of HCC. BMDMs, bone marrow derived macrophages, CXCL1, C-X-C motif ligand 1; DAP-12, DNAX-activation protein 12; HCC, hepatocellular carcinoma; HGF, hepatocyte growth factor; IL, interleukin; LPS, lipopolysaccharide; MCP1, monocyte chemoattractant protein 1; ROS, reactive oxygen species; TLR, toll-like receptor; TNF, tumor necrosis factor; TREM, triggering receptor expressed on myeloid cells.

CONCLUSIONS

1. TREM2 expression is upregulated in cirrhotic livers of various aetiologies compared to healthy controls in humans.
2. TREM2 is expressed on non-parenchymal liver cells (KCs and HSCs) and is induced during diverse forms of liver injury in mice, including acute and chronic CCl_4-induced liver injury and BDL-induced cholestatic liver injury models.
3. *Trem2*$^{-/-}$ mice exhibit increased liver damage and inflammation during acute and chronic CCl_4 treatment and APAP intoxication.
4. Effects of TREM2 in the context of chronic liver injury are dependent on both liver resident and infiltrating immune cells.
5. TREM2 promotes survival during drug-induced liver injury, upon APAP challenge.
6. KCs and HSCs that are deficient for *Trem2* display increased pro-inflammatory cytokine and chemokine production upon TLR4 stimulation.
7. TREM2 attenuates hepatic inflammation, liver injury and lipid peroxidation during APAP-induced acute and CCl_4-induced chronic liver injury. Effects of TREM2 on hepatic lipid peroxidation in these mouse models are associated with macrophage content and ROS production within infiltrating macrophages.
8. Liver regeneration following PHx is accelerated in the absence of *Trem2* through increased pro-inflammatory and growth-factor gene expression during the priming phase.
9. *TREM2* expression is induced in human HCC and its expression correlates with markers of inflammation.
10. *Trem2* is upregulated in DEN-induced HCC in mice. *Trem2*$^{-/-}$ mice exhibit increased liver tumourigenesis that is mediated by an enhanced hepatocyte DNA damage and proliferation.
11. The role of TREM2 in liver tumorigenesis is associated with protective effects in the early phases of HCC development after acute DEN challenge. These effects are linked with an attenuation of liver damage, inflammation and oxidative stress.
12. Enhanced liver carcinogenesis in the absence of *Trem2* can be inhibited by an antioxidant diet.

13. The supernatant of TREM2 overexpressing HSCs halts HCC spheroid growth *in vitro* in a Wnt/β-catenin dependent manner.

Therefore, TREM2 arises as a promising therapeutic target to tackle acute liver injury, progression to chronic liver disease and HCC.

SUMMARY IN SPANISH
(RESUMEN EN ESPAÑOL)

INTRODUCCIÓN

El hígado es un órgano vital y funcionalmente complejo y tiene un papel fundamental en la homeostasis metabólica del organismo. Además de participar en la síntesis, transporte y almacenamiento de una gran variedad de sustancias y hormonas, tiene una función muy importante en la detoxificación de compuestos que llegan desde el torrente sanguíneo a través de la vena porta (2). Por ello, el hígado se encuentra expuesto a diversos agentes potencialmente lesivos que participan en la progresión del daño hepático. Entre los factores etiológicos se incluyen la infección por los virus de la hepatitis B o C (HBV o HCV), el alcohol y otros tóxicos, respuestas inmunes exacerbadas, la esteatohepatitis no alcohólica (NASH) y determinadas alteraciones genéticas entre otros (19).

Al inicio de la lesión hepática la muerte de la célula parenquimal del hígado, el hepatocito, desencadena una respuesta inflamatoria con el objetivo de reparar el tejido dañado. La inflamación juega un papel esencial tanto en los procesos de regeneración como de cicatrización. (26, 28). Tras un daño hepático, uno de los eventos iniciales en respuesta al daño es la regeneración hepática. En este sentido, las células de Kupffer (KCs) juegan un papel muy importante secretando mediadores inflamatorios y factores de crecimiento para promover la proliferación hepatocitaria (25). Además de la proliferación hepatocitaria, también es necesario restaurar la estructura hepática, para lo cual se precisa de la participación de las células estelares hepáticas (HSCs), que son las responsables de remodelar la matriz extracelular (ECM) (39).

Estos procesos de regeneración hepática y cicatrización son procesos fisiológicos que se activan en respuesta al daño para una correcta reparación y cicatrización del hígado tras una lesión. Sin embargo, si la lesión hepática persiste en el tiempo y cronifica, se desarrolla una hepatitis crónica, en la cual el tejido hepático es progresivamente sustituido por tejido fibroso, desarrollándose así la fibrosis hepática (39). Además, si este proceso se mantiene en el tiempo, puede desarrollarse la cirrosis hepática, en la cual la estructura hepática se pierde y la función hepática se ve comprometida. Cabe destacar que la cirrosis hepática es el contexto ideal para el desarrollo de diversas complicaciones, tales como fallo renal, ascitis, encefalopatía hepática, fallo hepático agudo y finalmente, el desarrollo del carcinoma hepatocelular (HCC) (94). Por lo que la progresión del daño hepático sucede por una cronificación de los mecanismos de regeneración y cicatrización hepática.

El HCC es el tumor primario más común del hígado, representa el sexto cáncer más común y el tercero que más muertes causa a nivel mundial (76). El desarrollo del

HCC está estrechamente asociado a cirrosis, ya que el 80% de los HCC se desarrollan en el contexto de una cirrosis hepática (78). Además, el HCC presenta una elevada quimioresistencia, y los tratamientos actuales muestran una eficacia modesta (75), por lo que es necesario la búsqueda de nuevas dianas terapéuticas para el desarrollo de nuevas terapias para el HCC.

Recientemente se ha demostrado el papel que juegan la flora bacteriana y los receptores tipo Toll (TLRs) en la patogénesis de la fibrosis (52). El sistema inmune innato reconoce los microorganismos a través de un número limitado de receptores conocidos como receptores de reconocimiento de patrones (PRRs). Estos receptores, concretamente los TLRs, parece ser que tienen un papel central en la relación entre el sistema inmune y los agentes infecciosos. Los TLRs que están presentes en las células del sistema inmune innato pueden ser activados por macromoléculas liberadas por virus o bacterias (PAMPs o patrones moleculares asociados a patógenos) y provocar la producción de citoquinas. Los pacientes con cirrosis hepática presentan niveles elevados de lipopolisacárido (LPS) en la vena porta. La elevación de la presión portal puede dañar la mucosa intestinal y comprometer su función de barrera desencadenando la translocación bacteriana. El LPS derivado de la flora intestinal es un gran candidato como ligando de TLR4 en las KCs durante la fibrosis hepática (148) y un trabajo reciente ha demostrado que en las HSCs puede ser incluso más importante (64). Mediante la utilización de aproximaciones genéticas y moleculares se ha demostrado que el LPS a través de TLR4 es capaz de aumentar la actividad fibrogénica de transforming groth factor β (TGF β) en las HSCs (64). Los TLRs funcionan tanto como reguladores clave para el desarrollo de la fibrosis hepática como para el desarrollo del HCC puesto que modulan tanto funciones inflamatorias como fibrogénicas en las células hepáticas no parenquimales (KCs y HSCs) (64, 145). Sin embargo, hasta el momento se desconoce cuáles son los factores que tanto de forma positiva como negativa pueden estar regulando la función de estos TLRs. En este trabajo se pretenden dilucidar aspectos claves de la regulación de los TLRs.

En el año 2000, se descubrió la familia de los receptores TREM (triggering receptor expressed on myeloid cells), receptores que a través de la interacción ("cross-talk") positiva o negativa con los TLRs regulan la respuesta inmune. En términos generales, TREM1 se ha definido como un receptor que amplifica la respuesta inmune, mientras que TREM2 parece tener un papel en la regulación negativa de la inflamación mediada por TLR4 (151). En la actualidad se desconoce cuál puede ser el ligando que pueda activar estos receptores. Hasta el momento, existen datos en relación al posible papel que TREM1

pueda tener como modulador positivo de la hepatocarcinogénesis (163), sin embargo no se conoce el papel que el receptor TREM2 pueda desempeñar en la progresión del daño hepático crónico y en la hepatocarcinogénesis.

OBJETIVOS E HIPÓTESIS

Debido a que TREM2 juega un papel importante en varios tipos de daño, el interés de este estudio está centrado en el análisis del posible papel del receptor TREM2 en el hígado. Por lo cual, postulamos la hipótesis de que el receptor TREM2 puede jugar un papel importante en la regulación del daño hepático agudo y crónico, en la regeneración hepática y en el desarrollo del HCC. Para ello se han planteado los siguientes objetivos:

1. **Determinación del papel del receptor TREM2 en el daño hepático.**
   1.1. Estudio de la expresión génica del receptor TREM2 en muestras de hígado procedentes de pacientes control y pacientes cirróticos, así como en modelos experimentales murinos de daño hepático agudo y crónico.
   1.2. Determinación de la expresión y función de TREM2 en los distintos tipos celulares del hígado, tales como hepatocitos y células no parenquimales (KCs y HSCs).
   1.3. Evaluación de la contribución del receptor TREM2 en el desarrollo del daño hepático crónico.
   1.4. Estudio del papel de TREM2 en el daño hepático agudo.
   1.5. Determinación de los mecanismos moleculares por los que TREM2 media sus efectos en el daño hepático.

2. **Estudio de la contribución del receptor TREM2 en la regeneración hepática.**
   2.1. Caracterización del posible papel de TREM2 en el proceso regenerativo hepático y en la proliferación del hepatocito.

3. **Evaluación del papel del receptor TREM2 en el desarrollo del HCC.**
   3.1. Análisis de la expresión génica de TREM2 en muestras de hígado de pacientes control y de pacientes con HCC y su correlación con marcadores de inflamación y fibrosis.
   3.2. Estudio del papel del receptor TREM2 en el proceso de hepatocarcinogénesis.
   3.3. Determinación de los mecanismos moleculares por los que TREM2 regula el proceso hepatocarcinogénico.

MATERIALES Y MÉTODOS

Expresión génica del receptor TREM2 en muestras de tejido hepático de individuos control, pacientes con cirrosis y HCCs

La expresión de TREM2 se analizó tanto a nivel de mRNA como a nivel de proteína en muestras de tejido hepático sano, así como en muestras cirróticas y HCCs. Para ello se utilizaron muestras de pacientes que fueron obtenidas a través del Biobanco Vasco. Este estudio fue aprobado por el Comité de Ética de Investigación Clínica de Euskadi (CEIC-E) y el CEIC del Hospital Universitario Donostia. Además, la expresión de *TREM2* en muestras de HCC también se analizó en una segunda cohorte de pacientes del repositorio web perteneciente al *The Cancer Genome Atlas* (TCGA).

El análisis de la expresión génica a nivel de mRNA se llevó a cabo mediante PCR a tiempo real. Asimismo, la expresión de TREM2 a nivel de proteína fue analizada mediante mediante inmunohistoquímica (IHC).

Modelos experimentales murinos de daño hepático agudo y crónico, regeneración hepática y hepatocarcinogénesis

Se realizaron varios modelos experimentales en ratones para determinar el papel del receptor TREM2 en el daño hepático agudo y crónico, en la regeneración hepática y en el desarrollo del HCC. Para ello, utilizamos ratones nulos para *Trem2* (*Trem2*$^{-/-}$) y los correspondientes ratones salvajes. Todos los procedimientos fueron aprobados por los comités éticos de experimentación animal (CEEA) del Instituto de Investigación Biodonostia y por el comité de uso y cuidado animal de la Medical University of Viena y el Ministerio de Ciencia de Austria.

Modelos de daño hepático agudo y crónico inducido por la administración tetracloruro de carbono (CCl_4) y acetaminofeno (APAP)

Los modelos de daño hepático agudo y crónico se realizaron en ratones salvajes y ratones *Trem2*$^{-/-}$ de 8 semanas de vida. Para el modelo de daño hepático agudo inducido por la administración de CCl_4 utilizamos una dosis de 2 µl/g (CCl_4:aceite de oliva a una relación 1:1 [vol:vol]), mientras que para llevar a cabo un modelo de daño hepático crónico administramos el CCl_4 a una dosis de 2 µl/g (CCl_4:aceite de oliva a una relación 1:3 [vol:vol]), dos veces por semana, durante 8 semanas. Además, se realizó un modelo de trasplante de médula ósea en ratones salvajes y *Trem2*$^{-/-}$, de esta manera se generaron

ratones salvajes reconstituidos con médula ósea de ratones salvajes, ratones *Trem2*$^{-/-}$ reconstituidos con médula ósea de ratones *Trem2*$^{-/-}$ y ratones quiméricos. Además, a estos ratones se les indujo un daño crónico mediante la administración de CCl_4, tal y como se ha descrito previamente. Asimismo, también llevamos a cabo un modelo en el que eliminamos la flora bacteriana intestinal de los ratones a través de la administración de un cóctel de antibióticos en agua de bebida durante 4 semanas y posterior administración aguda de CCl_4 a una dosis de 2 μl/g (CCl_4:aceite de oliva a una relación 1:1 [vol:vol]).

Como otro modelo alternativo de daño hepático agudo, administramos APAP a una dosis de 300 mg/kg en ratones salvajes y *Trem2*$^{-/-}$. Además, también realizamos un modelo de fallo hepático agudo. Para ello, administramos una dosis letal de APAP (750 mg/kg) a ratones salvajes y nulos para *Trem2* y monitorizamos la supervivencia de los ratones durante 72 horas.

Modelo de regeneración hepática

Para estudiar la posible participación de TREM2 en los procesos de regeneración hepática, se llevó a cabo un modelo de regeneración hepática tras hepatectomía parcial (PHx) en ratones salvajes y *Trem2*$^{-/-}$ en los que se realizó una resección del 70% del hígado.

Modelo de carcinogénesis inducida por dietilnitrosamina (DEN)

Se desarrolló un modelo experimental de tumorigénesis *in vivo* en ratones salvajes y *Trem2*$^{-/-}$ inducido por la administración del carcinógeno DEN a una dosis de 30 mg/kg. El modelo consiste en una única administración del carcinógeno, a los 15 días de vida del ratón, y posterior sacrificio a las 30 o 40 semanas tras la administración de DEN. Además, se llevó a cabo un modelo de hepatocarcinogénesis en los que previo al sacrificio tras 30 semanas de la administración de DEN se administró una dieta suplementada con el antioxidante hidroxianisol butilado (BHA) durante 15 semanas.

Para poder dilucidar el papel que TREM2 juega en las fases tempranas del proceso carcinogénico se realizó un modelo de daño hepático agudo inducido por la administración de una dosis de 100 mg/kg de DEN en ratones salvajes y deficientes para *Trem2* de 6-8 semanas de edad. Los ratones fueron sacrificados 6, 24, y 72 horas tras la administración de DEN.

Una vez fueron llevados a cabo los modelos *in vivo*, se procedió al análisis de las muestras obtenidas de los ratones. El hígado se dividió en 3 fracciones. Dos de ellas se congelaron en nitrógeno líquido para realizar posteriores estudios de expresión génica a nivel de mRNA y proteína respectivamente, y la tercera fracción se utilizó para estudios histológicos en tejido fijado. Además, se extrajo la sangre de los ratones mediante punción cardiaca para analizar los niveles de transaminasas y otros marcadores bioquímicos en el suero.

El análisis de la expresión génica a nivel de mRNA se llevó a cabo tal y como se ha descrito previamente (214).

Las proteínas en estudio fueron detectadas mediante inmunoblot utilizando anticuerpos primarios específicos, y posteriormente anticuerpos secundarios conjugados con peroxidasa (Sigma-Aldrich). Las bandas de proteína se detectaron utilizando un sistema de detección mediante quimioluminiscencia (Amersham, GE Healthcare).

Para analizar la morfología del parénquima hepático, el daño hepático, así como el grado de fibrosis, se realizaron tinciones de Hematoxilina y Eosina (H&E) de Harris (Merck), y Rojo Sirio (Sigma-Aldrich) en hígado fijado en formalina y embebido en parafina, tal y como hemos descrito previamente (213). Además también se realizaron tinciones específicas para marcadores relacionadas con proliferación celular, daño y estrés oxidativo mediante IHC tal y como se ha descrito previamente (214).

Los niveles de especies reactivas del oxígeno (ROS) fueron analizados en lisados de tejido hepático de ratones salvajes y *Trem2*$^{-/-}$. El lisado fue sonicado e incubado con la sonda 2´,7´-diclorodihidrofluorescein diacetato (DCF) (Thermo fisher scientific) durante 30 min y los niveles de ROS fueron determinados mediante fluorescencia (Fluoroskan Ascent®).

Perfusión hepática, aislamiento y tratamiento de células primarias hepáticas

Las distintas poblaciones celulares del hígado fueron aisladas de ratones salvajes y *Trem2*$^{-/-}$. Los hígados de los ratones fueron perfundidos a través de la vena porta utilizando un catéter de 22G-15 mm (BD Insyte). Primeramente, con el objetivo de eliminar las células sanguíneas, se perfundió el hígado con una solución salina. A continuación se llevó a cabo una digestión secuencial *in situ* con soluciones que contienen las enzimas pronasa y colagenasa (Roche). Finalmente, las distintas poblaciones células hepáticas fueron aisladas *in vitro* llevando a cabo una centrifugación en gradiente de densidad con

Nycodenz (Axis-Shield). Posteriormente, las células fueron tratadas con ligandos que activan la señalización mediada por TLRs, como por ejemplo el LPS o bacterias como *Escherichia coli* (*E. coli*) y también con TNFα e IL1B.

Asimismo, también se aislaron BMDMs, que fueron obtenidos de las tibias y los fémures de los ratones salvajes y *Trem2*$^{-/-}$, llevando a cabo un protocolo previamente descrito (214).

En las distintas poblaciones celulares se realizaron estudios de expresión génica mediante PCR cuantitativa y proteica mediante inmunoblot o ELISA. Además, también se analizó la producción de ROS mediante citometría de flujo. Asimismo, se determinó el consumo de oxígeno mediante Seahorse (Seahorse Bioscience). Por último, también se realizaron ensayos de viabilidad celular.

Sobreexpresión de TREM2 en HSCs humanas y crecimiento de esferoides *in vitro*

La línea de HSCs humana LX-2 fue transfectada con un plásmido de TREM2 (Sino Biological Inc, HG11084-UT) o con el respectivo plásmido control (Sino Biological Inc, CV011) y se determinó al expresión génica de genes inflamatorios y pro-tumorigénicos mediante PCR cuantitativa. Además, la cantidad de proteína de TNF y MCP1 en el medio de estas células fue determinada mediante ELISA. Por último, las líneas de HCC humanas Hep3B y PLC/PRF5 fueron utilizadas para determinar el papel de TREM2 en el crecimiento de esferoides *in vitro*. Así, las líneas de HCC fueron plaqueadas en gotas en suspensión en placas de Petri y fueron incubadas durante 7 días para que se formaran los esferoides. Estos esferoides fueron posteriormente tratados con el sobrenadante procedente de células LX-2 que sobreexpresaban o no TREM2 y el crecimiento de los esferoides fue analizado durante 72 horas.

Análisis estadístico

Todos los parámetros cuantitativos del estudio fueron incluidos en tablas de MS Excell para su posterior análisis estadístico mediante el programa GraphPad Prism 6.00 (GraphPad Software). Para comparaciones entre dos grupos se utilizaron los tests estadísticos T de Student o Mann Whitney en el caso de que las variables de estudio cumplieran una distribución paramétrica o no paramétrica, respectivamente. Para comparaciones entre dos o más grupos se utilizaron el test paramétrico de análisis de varianza unidireccional seguido del test a posteriori de Bonferroni o del test no

paramétrico Kruskal Wallis seguido del test a posteriori Dunns. Para los análisis de correlación se utilizó el test de Spearman.

RESULTADOS Y DISCUSIÓN

Papel del receptor TREM2 en el daño hepático

Expresión de TREM2 durante la lesión hepática crónica y en las distintas poblaciones celulares hepáticas

Con el objetivo de estudiar el potencial papel de TREM2 durante el daño hepático, analizamos su expresión en muestras de pacientes cirróticos y sanos, así como en varios modelos murinos de daño hepático agudo y crónico. Así, pudimos observar que la expresión de TREM2 se encuentra inducida tras la lesión hepática crónica, ya que su expresión está aumentada en pacientes cirróticos en comparación con pacientes sanos. Asimismo, en modelos de daño hepático agudo y crónicos mediados por la administración única o repetitiva de CCl_4 o mediante la ligadura del conducto biliar, la expresión de *Trem2* también se encuentra aumentada en comparación con los respectivos controles. Además, se determinó la expresión de TREM2 en las distintas poblaciones de células hepáticas pudiéndose demostrar que su expresión estaba prácticamente restringida a las células no-parenquimales, tales como KCs y HSCs, mientras que su expresión en hepatocitos es prácticamente indetectable. Interesantemente, la expresión de *TREM2* aumenta tras la activación de las HSCs tanto *in vitro* como *in vivo* aunque no afecta al estado de activación de estas células, ya que los marcadores fibrogénicos no se ven alterados. Estos datos sugieren que TREM2 en las células no-parenquimales del hígado podría tener un papel importante durante el daño hepático crónico.

Papel del receptor TREM2 y contribución de las células residentes e infiltrantes en el daño hepático crónico

Para estudiar el papel de TREM2 en el daño hepático crónico realizamos un modelo de daño hepático crónico mediado por la administración repetitiva de CCl_4 durante 8 semanas en ratones salvajes y deficientes para *Trem2*. Así, pudimos observar que en ausencia de *Trem2* los ratones presentaban un mayor daño, necrosis y apoptosis en el parénquima hepático. Sin embargo, los ratones *Trem2*$^{-/-}$ no presentaban mayor fibrosis hepática. Además, estos ratones presentaban una elevada expresión hepática de citoquinas y quimiocinas inflamatorias y de genes relacionados con estrés oxidativo y apoptosis.

Con el objetivo de dilucidar el papel que juegan las células hepáticas residentes y las células inmunes infiltrantes y su potencial contribución en el daño hepático que se observa en los ratones *Trem2*$^{-/-}$ se realizó un modelo de trasplantes de médula ósea entre ratones salvajes y *Trem2*$^{-/-}$ seguido de la administración crónica de CCl_4 durante 8 semanas. De este modo pudimos observar que únicamente en situaciones en el que *Trem2*

está ausente tanto en las células residentes del hígado como en las inmunitarias infiltradas hay diferencias en el daño hepático, reclutamiento de macrófagos y expresión de genes pro-inflamatorios. Así, pudimos demostrar por un lado que *TREM2* frena el daño hepático crónico y que el efecto combinado de las células residentes del hígado y de las células inmunes infiltrantes es necesario para que TREM2 pueda frenar la lesión hepática crónica.

Efecto de TREM2 en las células no-parenquimales tras la activación de TLR4

A continuación se estudió el papel que juega TREM2 en las células no-parenquimales del hígado en respuesta a la activación de TLR4. Para ello se aislaron las células no parenquimales del hígado de ratones salvajes y deficientes para *Trem2* y se trataron con el ligando de TLR4, el LPS y *E. coli*. Así, pudimos observar que los niveles de mediadores inflamatorios y quimiocinas se encontraban elevados en los ratones *Trem2*$^{-/-}$ comparado con ratones salvajes, tanto en KCs como en HSCs. Interesantemente, tal y como se ha descrito en otros tipos celulares (188, 195), la vía de las MAP quinasas se encontraba aumentada en las KCs deficientes en *Trem2* mientras que no se observaron alteraciones en la vía de señalización NF-κB. Demostrando así que TREM2 frena la inflamación mediada por TLR4 en las células no-parenquimales del hígado y que además en KCs lo hace a través de la atenuación en la vía de las MAP quinasas.

Papel de TREM2 en modelos de daño hepático agudo

Posteriormente, decidimos estudiar el papel del receptor TREM2 en modelos de daño hepático agudo y daño hepático fulminante para lo cual desarrollamos modelos agudos basados en la administración de CCl_4 y APAP además de un modelo letal de daño hepático fulminante basado en la administración de APAP a una dosis letal. Así, pudimos observar que los ratones *Trem2*$^{-/-}$ presentaban mayor daño hepático, un aumento en la expresión de genes inflamatorios y un mayor reclutamiento de células inmunitarias comparado con ratones salvajes. Además, interesantemente los ratones deficientes en *Trem2* presentaron una menor superviviencia en comparación con los ratones salvajes tras la administración de una dosis letal de APAP. Concluyendo que TREM2 es importante para poder frenar el daño hepático agudo y que además es esencial para prevenir el daño hepático fulminante debido a la intoxicación con APAP.

Determinación de los mecanismos moleculares por los que TREM2 media sus efectos en la regulación del daño hepático

Para poder determinar el mecanismo por el cual TREM2 exacerba el daño hepático agudo y crónico en el hígado en primer lugar, se analizó la peroxidación lipídica en los tejidos los modelos agudos y crónicos estudiados, pudiendo observar una marcada elevación en los niveles de peroxidación lipídica en el tejido hepático de los ratones *Trem2*$^{-/-}$. Además, estos datos correlacionaron con una elevación en la producción de ROS en BMDMs. Interesantemente, esta elevación en los niveles de ROS parece ser debida a una mayor respiración metabólica, ya que los BMDMs deficientes en *Trem2* poseían una respiración máxima mitocondrial mayor en comparación con los ratones salvajes. Estos resultados demuestran que los efectos que TREM2 media en los macrófagos infiltrados en el hígado juegan un papel determinante en el daño hepático, afectando a la producción de ROS y peroxidación lipídica en el hígado.

Por último, analizamos si los efectos que media TREM2 en el hígado podrían estar mediados por su potencial papel en la regulación de la inmunidad innata debida a la translocación bacteriana. Para ello, se utilizó un modelo agudo de CCl_4 en el que previa administración del hepatotóxico se administró un coctel de antibióticos durante 4 semanas para eliminar la microbiota intestinal. Así, pudimos comprobar que los efectos que se observan en el daño hepático en ausencia de *Trem2* tras la administración de CCl_4 se revierten al eliminar la microbiota intestinal, demostrando así que TREM2 es capaz de frenar el daño hepático inhibiendo el efecto de los PAMPs debidos a la translocación bacteriana.

Papel del receptor TREM2 en la regeneración hepática

Efecto del receptor TREM2 en la regeneración hepática tras hepatectomía parcial

Debido a que los procesos de regeneración y proliferación hepatocitaria son mecanismos que se activan en respuesta al daño o debido a la pérdida de la masa hepática y además

juegan un papel determinante en el desarrollo del HCC (254, 255), decidimos llevar a cabo un modelo de regeneración hepática en el que realizamos una resección quirúrgica del ~70% del hígado tanto en ratones salvajes como *Trem2*$^{-/-}$. Tras PHx, observamos una aceleración en la proliferación hepatocitaria en los ratones *Trem2*$^{-/-}$ en comparación con los ratones salvajes. Además, este efecto se vio asociado con una inducción temprana de genes clave como *Tnf*, *Il6* y *Hgf* tras PHx en el hígado de los ratones *Trem2*$^{-/-}$. Indicándonos que TREM2 es clave durante la regeneración hepática.

Papel del receptor TREM2 en el desarrollo del HCC

Expresión de TREM2 en muestras de pacientes sanos y HCC

En primer lugar analizamos la expresión del receptor *TREM2* en 2 cohortes independientes de pacientes con HCC y pacientes sanos observando que su expresión estaba inducida en muestras de HCC. Además, pudimos observar que la expresión de *TREM2* correlaciona con marcadores inflamatorios y fibrogénicos, sugiriendo que TREM2 podría también jugar un papel importante en el desarrollo del HCC.

Papel de TREM2 en un modelo de HCC murino y en un modelo agudo mediados por la administración de DEN

Para poder determinar el papel que juega TREM2 en el desarrollo de HCC llevamos a cabo un modelo de tumorigénesis hepática basado en la administración de DEN. Así, pudimos observar cómo los ratones *Trem2*$^{-/-}$ desarrollan un mayor número de tumores en comparación con los ratones salvajes. Además, estos efectos se asociaron con la presencia de mayores niveles de daño en el DNA de los hepatocitos y una mayor proliferación en comparación con los ratones salvajes. Para poder dilucidar los mecanismos moleculares tempranos durante el desarrollo tumorigénico llevamos a cabo un modelo agudo basado en una única administración de DEN en ratones adultos. Así, en concordancia con los datos observados, los ratones *Trem2*$^{-/-}$ presentaban un mayor daño, una elevada expresión de marcadores inflamatorios, de factores de crecimiento y de enzimas de estrés oxidativo. Además, la producción de ROS también se encontraba elevada en los ratones deficientes de *Trem2* comparado con los ratones salvajes. Pudimos así demostrar que TREM2 juega un importante papel en el desarrollo tumorígenico, frenando el desarrollo de tumores, la proliferación y el daño hepatocitario, la inflamación y la producción de ROS. Por último,

para demostrar si los efectos que observamos en los ratones *Trem2*$^{-/-}$ están mediados, al menos en parte, por la regulación de los niveles de producción de ROS y de un elevado estrés oxidativo, desarrollamos un modelo tumorigénico basado en la administración de DEN al cual administramos una dieta antioxidante durante 15 semanas. De forma muy interesante observamos como el número de tumores y la proliferación hepatocitaria descendieron al mismo nivel en ratones salvajes y *Trem2*$^{-/-}$. Demostrando así que los efectos de TREM2 en el HCC son mediados a través de la regulación de los niveles de ROS.

Determinación de los mecanismos moleculares por los que TREM2 inhibe el proceso hepatocarcinogénico

A continuación intentamos trasladar nuestros resultados a un sistema *in vitro* y para ello sobreexpresamos TREM2 en la línea de HSCs humana LX-2, observando que los niveles de expresión génica de marcadores inflamatorios y ligandos de la familia de WNT se encontraban disminuidos tras la sobreexpresión de TREM2. Además, comprobamos que el sobrenadante de estas células contenía una disminución en la concentración de los mediadores pro-inflamatorios TNF y MCP1. A continuación desarrollamos un modelo de crecimiento de esferoides a partir de células de HCC. Para ello, se formaron los esferoides durante 7 días y éstos fueron tratados con el sobrenadante procedente de células LX-2 que sobreexpresaban TREM2 o un plásmido control. Interesantemente, pudimos observar que los esferoides tratados con el medio de cultivo procedente de LX-2 con sobreexpresión de TREM2 crecieron menos que los esferoides tratados con el sobrenadante de LX-2 transfectadas con un plásmido control. Además, pudimos observar que estos efectos eran dependientes de la secreción paracrina de ligandos de WNT de HSCs. Estos resultados demuestran que la expresión de TREM2 en las células no parenquimales tiene un papel importante en el crecimiento de los esferoides de HCC.

CONCLUSIONES

1. La expresión de *TREM2* se encuentra inducida en el hígado de pacientes cirróticos en comparación con controles sanos.
2. TREM2 se expresa en las células no-parenquimales hepáticas (KCs y HSCs) y su expresión se induce en el hígado durante el daño hepático crónico en modelos

experimentales en ratón inducidos por la administración de CCl_4 o por la ligadura del conducto biliar (BDL).

3. Los ratones *Trem2*$^{-/-}$ muestran un aumento en el daño hepático e inflamación tras los tratamientos agudo y crónico de CCl_4 e intoxicación por APAP.
4. Los efectos de TREM2 observados en el contexto de una lesión hepática crónica son dependientes tanto de las células hepáticas residentes como del infiltrado inflamatorio.
5. TREM2 promueve la supervivencia tras la administración letal de APAP.
6. Las KCs y las HSCs que carecen de *Trem2* muestran un aumento en la producción de citoquinas pro-inflamatorias y quimioquinas tras la estimulación del receptor TLR4.
7. TREM2 atenúa la inflamación hepática, la lesión hepática y la peroxidación lipídica durante la lesión crónica por CCl_4. Los efectos de TREM2 en la peroxidación lipídica durante la lesión hepática crónica se asocian con el contenido de macrófagos y los niveles de ROS en los macrófagos reclutados.
8. La ausencia de *Trem2* acelera la regeneración hepática tras la PHx a través de un aumento de la expresión génica de genes pro-inflamatorios y de la proliferación de hepatocitos.
9. La expresión de *TREM2* está inducida en muestras de HCC humano y su expresión correlaciona con marcadores de inflamación.
10. La expresión de *Trem2* se induce en el hígado en un modelo experimental de HCC inducido por la administración de DEN en ratones. La ausencia de *Trem2* promueve el desarrollo y la progresión de HCC, a través de la regulación de procesos de daño en el DNA y la proliferación de hepatocitos.
11. El papel protector de TREM2 en la tumorigénesis hepática están asociados con efectos tempranos durante el desarrollo del HCC tras la administración aguda de DEN. Estos efectos están relacionados con la atenuación de procesos de daño hepático, inflamación y estrés oxidativo.
12. El proceso de hepatocarcinogénesis que se encuentra potenciado en ausencia de *Trem2* puede ser inhibido con una dieta antioxidante.
13. La sobreexpresión de TREM2 en HSCs disminuye la expresión de marcadores inflamatorios y ligandos de WNT. Además, el sobrenadante procedente de HSCs que sobreexpresan TREM2 frena el crecimiento de esferoides de HCC *in vitro*.

Por lo tanto, estos resultados han permitido identificar al receptor TREM2 como una nueva diana terapéutica prometedora para abordar la lesión hepática aguda, la progresión de la enfermedad hepática y el HCC.

REFERENCES

1. Juza, R.M. & Pauli, E.M. Clinical and surgical anatomy of the liver: a review for clinicians. *Clin Anat* **27**, 764-9 (2014).
2. Mescher, A.L. Junqueira's Basic Histology : Text and Atlas (McGraw-Hill Medical, New York, N.Y., 2013).
3. O'Hara, S.P., Tabibian, J.H., Splinter, P.L. & LaRusso, N.F. The dynamic biliary epithelia: molecules, pathways, and disease. *J Hepatol* **58**, 575-82 (2013).
4. Tabibian, J.H., Masyuk, A.I., Masyuk, T.V., O'Hara, S.P. & LaRusso, N.F. Physiology of cholangiocytes. *Compr Physiol* **3**, 541-65 (2013).
5. Banales, J.M., Prieto, J. & Medina, J.F. Cholangiocyte anion exchange and biliary bicarbonate excretion. *World J Gastroenterol* **12**, 3496-511 (2006).
6. Tsuchida, T. & Friedman, S.L. Mechanisms of hepatic stellate cell activation. *Nat Rev Gastroenterol Hepatol* **14**, 397-411 (2017).
7. Jenne, C.N. & Kubes, P. Immune surveillance by the liver. *Nat Immunol* **14**, 996-1006 (2013).
8. Shetty, S., Lalor, P.F. & Adams, D.H. Liver sinusoidal endothelial cells - gatekeepers of hepatic immunity. *Nat Rev Gastroenterol Hepatol* (2018).
9. Sebastiani, G., Gkouvatsos, K. & Pantopoulos, K. Chronic hepatitis C and liver fibrosis. *World J Gastroenterol* **20**, 11033-53 (2014).
10. Suhail, M., Abdel-Hafiz, H., Ali, A., Fatima, K., Damanhouri, G.A., Azhar, E. et al. Potential mechanisms of hepatitis B virus induced liver injury. *World J Gastroenterol* **20**, 12462-72 (2014).
11. Osna, N.A., Donohue, T.M., Jr. & Kharbanda, K.K. Alcoholic Liver Disease: Pathogenesis and Current Management. *Alcohol Res* **38**, 147-161 (2017).
12. Ward, J., Kapadia, K., Brush, E. & Salhanick, S.D. Amatoxin poisoning: case reports and review of current therapies. *J Emerg Med* **44**, 116-21 (2013).
13. Tujios, S. & Fontana, R.J. Mechanisms of drug-induced liver injury: from bedside to bench. *Nat Rev Gastroenterol Hepatol* **8**, 202-11 (2011).
14. Lopez, A.M. & Hendrickson, R.G. Toxin-induced hepatic injury. *Emerg Med Clin North Am* **32**, 103-25 (2014).
15. Giachetti, C., Tenconi, A., Canali, S. & Zanolo, G. Simultaneous determination of atenolol and chlorthalidone in plasma by high-performance liquid chromatography. Application to pharmacokinetic studies in man. *J Chromatogr B Biomed Sci Appl* **698**, 187-94 (1997).
16. Brissot, P., Pietrangelo, A., Adams, P.C., de Graaff, B., McLaren, C.E. & Loreal, O. Haemochromatosis. *Nat Rev Dis Primers* **4**, 18016 (2018).
17. Hidvegi, T., Ewing, M., Hale, P., Dippold, C., Beckett, C., Kemp, C. et al. An autophagy-enhancing drug promotes degradation of mutant alpha1-antitrypsin Z and reduces hepatic fibrosis. *Science* **329**, 229-32 (2010).
18. Pellicoro, A., Ramachandran, P., Iredale, J.P. & Fallowfield, J.A. Liver fibrosis and repair: immune regulation of wound healing in a solid organ. *Nat Rev Immunol* **14**, 181-94 (2014).
19. Paradis, V. Histopathology of hepatocellular carcinoma. *Recent Results Cancer Res* **190**, 21-32 (2013).
20. Bernal, W. & Wendon, J. Acute liver failure. *N Engl J Med* **369**, 2525-34 (2013).
21. Bernal, W., Auzinger, G., Dhawan, A. & Wendon, J. Acute liver failure. *Lancet* **376**, 190-201 (2010).
22. Goldkind, L. & Laine, L. A systematic review of NSAIDs withdrawn from the market due to hepatotoxicity: lessons learned from the bromfenac experience. *Pharmacoepidemiol Drug Saf* **15**, 213-20 (2006).

23. Canbay, A., Chen, S.Y., Gieseler, R.K., Malago, M., Karliova, M., Gerken, G. et al. Overweight patients are more susceptible for acute liver failure. *Hepatogastroenterology* **52**, 1516-20 (2005).
24. Krahenbuhl, S., Brauchli, Y., Kummer, O., Bodmer, M., Trendelenburg, M., Drewe, J. et al. Acute liver failure in two patients with regular alcohol consumption ingesting paracetamol at therapeutic dosage. *Digestion* **75**, 232-7 (2007).
25. Michalopoulos, G.K. Liver regeneration. *J Cell Physiol* **213**, 286-300 (2007).
26. Taub, R. Liver regeneration: from myth to mechanism. *Nat Rev Mol Cell Biol* **5**, 836-47 (2004).
27. Luedde, T., Kaplowitz, N. & Schwabe, R.F. Cell death and cell death responses in liver disease: mechanisms and clinical relevance. *Gastroenterology* **147**, 765-783 e4 (2014).
28. Fausto, N., Campbell, J.S. & Riehle, K.J. Liver regeneration. *Hepatology* **43**, S45-53 (2006).
29. Forbes, S.J. & Newsome, P.N. Liver regeneration - mechanisms and models to clinical application. *Nat Rev Gastroenterol Hepatol* **13**, 473-85 (2016).
30. Palmes, D. & Spiegel, H.U. Animal models of liver regeneration. *Biomaterials* **25**, 1601-11 (2004).
31. Li, W., Liang, X., Leu, J.I., Kovalovich, K., Ciliberto, G. & Taub, R. Global changes in interleukin-6-dependent gene expression patterns in mouse livers after partial hepatectomy. *Hepatology* **33**, 1377-86 (2001).
32. Mao, S.A., Glorioso, J.M. & Nyberg, S.L. Liver regeneration. *Transl Res* **163**, 352-62 (2014).
33. Bohm, F., Kohler, U.A., Speicher, T. & Werner, S. Regulation of liver regeneration by growth factors and cytokines. *EMBO Mol Med* **2**, 294-305 (2010).
34. Mohammed, F.F. & Khokha, R. Thinking outside the cell: proteases regulate hepatocyte division. *Trends Cell Biol* **15**, 555-63 (2005).
35. Tsochatzis, E.A., Bosch, J. & Burroughs, A.K. Liver cirrhosis. *Lancet* **383**, 1749-61 (2014).
36. European Association for the Study of the, L. EASL clinical practice guidelines on the management of ascites, spontaneous bacterial peritonitis, and hepatorenal syndrome in cirrhosis. *J Hepatol* **53**, 397-417 (2010).
37. American Association for the Study of Liver, D. & European Association for the Study of the, L. Hepatic encephalopathy in chronic liver disease: 2014 practice guideline by the European Association for the Study of the Liver and the American Association for the Study of Liver Diseases. *J Hepatol* **61**, 642-59 (2014).
38. Fujiwara, N., Friedman, S.L., Goossens, N. & Hoshida, Y. Risk factors and prevention of hepatocellular carcinoma in the era of precision medicine. *J Hepatol* **68**, 526-549 (2018).
39. Friedman, S.L. Mechanisms of hepatic fibrogenesis. *Gastroenterology* **134**, 1655-69 (2008).
40. Karlmark, K.R., Weiskirchen, R., Zimmermann, H.W., Gassler, N., Ginhoux, F., Weber, C. et al. Hepatic recruitment of the inflammatory Gr1+ monocyte subset upon liver injury promotes hepatic fibrosis. *Hepatology* **50**, 261-74 (2009).
41. Ju, C. & Tacke, F. Hepatic macrophages in homeostasis and liver diseases: from pathogenesis to novel therapeutic strategies. *Cell Mol Immunol* **13**, 316-27 (2016).
42. Higashi, T., Friedman, S.L. & Hoshida, Y. Hepatic stellate cells as key target in liver fibrosis. *Adv Drug Deliv Rev* **121**, 27-42 (2017).

43. Friedman, S.L. Evolving challenges in hepatic fibrosis. *Nat Rev Gastroenterol Hepatol* **7**, 425-36 (2010).
44. Hernandez-Gea, V. & Friedman, S.L. Pathogenesis of liver fibrosis. *Annu Rev Pathol* **6**, 425-56 (2011).
45. McGuire, R.F., Bissell, D.M., Boyles, J. & Roll, F.J. Role of extracellular matrix in regulating fenestrations of sinusoidal endothelial cells isolated from normal rat liver. *Hepatology* **15**, 989-97 (1992).
46. Elpek, G.O. Cellular and molecular mechanisms in the pathogenesis of liver fibrosis: An update. *World J Gastroenterol* **20**, 7260-76 (2014).
47. Puche, J.E., Saiman, Y. & Friedman, S.L. Hepatic stellate cells and liver fibrosis. *Compr Physiol* **3**, 1473-92 (2013).
48. Marra, F., Romanelli, R.G., Giannini, C., Failli, P., Pastacaldi, S., Arrighi, M.C. et al. Monocyte chemotactic protein-1 as a chemoattractant for human hepatic stellate cells. *Hepatology* **29**, 140-8 (1999).
49. Kocabayoglu, P. & Friedman, S.L. Cellular basis of hepatic fibrosis and its role in inflammation and cancer. *Front Biosci (Schol Ed)* **5**, 217-30 (2013).
50. Friedman, S.L., Roll, F.J., Boyles, J. & Bissell, D.M. Hepatic lipocytes: the principal collagen-producing cells of normal rat liver. *Proc Natl Acad Sci U S A* **82**, 8681-5 (1985).
51. Xu, J., Liu, X., Koyama, Y., Wang, P., Lan, T., Kim, I.G. et al. The types of hepatic myofibroblasts contributing to liver fibrosis of different etiologies. *Front Pharmacol* **5**, 167 (2014).
52. Kisseleva, T. & Brenner, D.A. Mechanisms of fibrogenesis. *Exp Biol Med (Maywood)* **233**, 109-22 (2008).
53. Taura, K., Miura, K., Iwaisako, K., Osterreicher, C.H., Kodama, Y., Penz-Osterreicher, M. et al. Hepatocytes do not undergo epithelial-mesenchymal transition in liver fibrosis in mice. *Hepatology* **51**, 1027-36 (2010).
54. Scholten, D., Osterreicher, C.H., Scholten, A., Iwaisako, K., Gu, G., Brenner, D.A. et al. Genetic labeling does not detect epithelial-to-mesenchymal transition of cholangiocytes in liver fibrosis in mice. *Gastroenterology* **139**, 987-98 (2010).
55. Chu, A.S., Diaz, R., Hui, J.J., Yanger, K., Zong, Y., Alpini, G. et al. Lineage tracing demonstrates no evidence of cholangiocyte epithelial-to-mesenchymal transition in murine models of hepatic fibrosis. *Hepatology* **53**, 1685-95 (2011).
56. Novo, E. & Parola, M. Redox mechanisms in hepatic chronic wound healing and fibrogenesis. *Fibrogenesis Tissue Repair* **1**, 5 (2008).
57. Jarnagin, W.R., Rockey, D.C., Koteliansky, V.E., Wang, S.S. & Bissell, D.M. Expression of variant fibronectins in wound healing: cellular source and biological activity of the EIIIA segment in rat hepatic fibrogenesis. *J Cell Biol* **127**, 2037-48 (1994).
58. Myung, S.J., Yoon, J.H., Gwak, G.Y., Kim, W., Lee, J.H., Kim, K.M. et al. Wnt signaling enhances the activation and survival of human hepatic stellate cells. *FEBS Lett* **581**, 2954-8 (2007).
59. Corbett, L., Mann, J. & Mann, D.A. Non-Canonical Wnt Predominates in Activated Rat Hepatic Stellate Cells, Influencing HSC Survival and Paracrine Stimulation of Kupffer Cells. *PLoS One* **10**, e0142794 (2015).
60. Jiang, F., Parsons, C.J. & Stefanovic, B. Gene expression profile of quiescent and activated rat hepatic stellate cells implicates Wnt signaling pathway in activation. *J Hepatol* **45**, 401-9 (2006).

61. Canbay, A., Taimr, P., Torok, N., Higuchi, H., Friedman, S. & Gores, G.J. Apoptotic body engulfment by a human stellate cell line is profibrogenic. *Lab Invest* **83**, 655-63 (2003).
62. Jiang, J.X., Mikami, K., Venugopal, S., Li, Y. & Torok, N.J. Apoptotic body engulfment by hepatic stellate cells promotes their survival by the JAK/STAT and Akt/NF-kappaB-dependent pathways. *J Hepatol* **51**, 139-48 (2009).
63. Zhan, S.S., Jiang, J.X., Wu, J., Halsted, C., Friedman, S.L., Zern, M.A. et al. Phagocytosis of apoptotic bodies by hepatic stellate cells induces NADPH oxidase and is associated with liver fibrosis in vivo. *Hepatology* **43**, 435-43 (2006).
64. Seki, E., De Minicis, S., Osterreicher, C.H., Kluwe, J., Osawa, Y., Brenner, D.A. et al. TLR4 enhances TGF-beta signaling and hepatic fibrosis. *Nat Med* **13**, 1324-32 (2007).
65. Ramachandran, P., Iredale, J.P. & Fallowfield, J.A. Resolution of liver fibrosis: basic mechanisms and clinical relevance. *Semin Liver Dis* **35**, 119-31 (2015).
66. Troeger, J.S., Mederacke, I., Gwak, G.Y., Dapito, D.H., Mu, X., Hsu, C.C. et al. Deactivation of hepatic stellate cells during liver fibrosis resolution in mice. *Gastroenterology* **143**, 1073-83 e22 (2012).
67. Iredale, J.P., Benyon, R.C., Pickering, J., McCullen, M., Northrop, M., Pawley, S. et al. Mechanisms of spontaneous resolution of rat liver fibrosis. Hepatic stellate cell apoptosis and reduced hepatic expression of metalloproteinase inhibitors. *J Clin Invest* **102**, 538-49 (1998).
68. Yoshiji, H., Kuriyama, S., Yoshii, J., Ikenaka, Y., Noguchi, R., Nakatani, T. et al. Tissue inhibitor of metalloproteinases-1 attenuates spontaneous liver fibrosis resolution in the transgenic mouse. *Hepatology* **36**, 850-60 (2002).
69. Pellicoro, A., Aucott, R.L., Ramachandran, P., Robson, A.J., Fallowfield, J.A., Snowdon, V.K. et al. Elastin accumulation is regulated at the level of degradation by macrophage metalloelastase (MMP-12) during experimental liver fibrosis. *Hepatology* **55**, 1965-75 (2012).
70. Fallowfield, J.A., Mizuno, M., Kendall, T.J., Constandinou, C.M., Benyon, R.C., Duffield, J.S. et al. Scar-associated macrophages are a major source of hepatic matrix metalloproteinase-13 and facilitate the resolution of murine hepatic fibrosis. *J Immunol* **178**, 5288-95 (2007).
71. Zhou, W.C., Zhang, Q.B. & Qiao, L. Pathogenesis of liver cirrhosis. *World J Gastroenterol* **20**, 7312-24 (2014).
72. Poordad, F.F. Presentation and complications associated with cirrhosis of the liver. *Curr Med Res Opin* **31**, 925-37 (2015).
73. Zhang, D.Y. & Friedman, S.L. Fibrosis-dependent mechanisms of hepatocarcinogenesis. *Hepatology* **56**, 769-75 (2012).
74. Iwakiri, Y. Pathophysiology of portal hypertension. *Clin Liver Dis* **18**, 281-91 (2014).
75. Hernandez-Gea, V., Toffanin, S., Friedman, S.L. & Llovet, J.M. Role of the microenvironment in the pathogenesis and treatment of hepatocellular carcinoma. *Gastroenterology* **144**, 512-27 (2013).
76. Forner, A., Reig, M. & Bruix, J. Hepatocellular carcinoma. *Lancet* **391**, 1301-1314 (2018).
77. El-Serag, H.B. Hepatocellular carcinoma. *N Engl J Med* **365**, 1118-27 (2011).
78. Fattovich, G., Stroffolini, T., Zagni, I. & Donato, F. Hepatocellular carcinoma in cirrhosis: incidence and risk factors. *Gastroenterology* **127**, S35-50 (2004).
79. Llovet, J.M., Zucman-Rossi, J., Pikarsky, E., Sangro, B., Schwartz, M., Sherman, M. et al. Hepatocellular carcinoma. *Nat Rev Dis Primers* **2**, 16018 (2016).

80. Bertuccio, P., Turati, F., Carioli, G., Rodriguez, T., La Vecchia, C., Malvezzi, M. et al. Global trends and predictions in hepatocellular carcinoma mortality. *J Hepatol* **67**, 302-309 (2017).
81. de Lope, C.R., Tremosini, S., Forner, A., Reig, M. & Bruix, J. Management of HCC. *J Hepatol* **56 Suppl 1**, S75-87 (2012).
82. Berasain, C., Castillo, J., Perugorria, M.J., Latasa, M.U., Prieto, J. & Avila, M.A. Inflammation and liver cancer: new molecular links. *Ann N Y Acad Sci* **1155**, 206-21 (2009).
83. Zucman-Rossi, J., Villanueva, A., Nault, J.C. & Llovet, J.M. Genetic Landscape and Biomarkers of Hepatocellular Carcinoma. *Gastroenterology* **149**, 1226-1239 e4 (2015).
84. Nault, J.C. & Zucman-Rossi, J. TERT promoter mutations in primary liver tumors. *Clin Res Hepatol Gastroenterol* **40**, 9-14 (2016).
85. Nault, J.C., Calderaro, J., Di Tommaso, L., Balabaud, C., Zafrani, E.S., Bioulac-Sage, P. et al. Telomerase reverse transcriptase promoter mutation is an early somatic genetic alteration in the transformation of premalignant nodules in hepatocellular carcinoma on cirrhosis. *Hepatology* **60**, 1983-92 (2014).
86. Kelleher, F.C., Fennelly, D. & Rafferty, M. Common critical pathways in embryogenesis and cancer. *Acta Oncol* **45**, 375-88 (2006).
87. Monga, S.P. beta-Catenin Signaling and Roles in Liver Homeostasis, Injury, and Tumorigenesis. *Gastroenterology* **148**, 1294-310 (2015).
88. Waisberg, J. & Saba, G.T. Wnt-/-beta-catenin pathway signaling in human hepatocellular carcinoma. *World J Hepatol* **7**, 2631-5 (2015).
89. Wahid, B., Ali, A., Rafique, S. & Idrees, M. New Insights into the Epigenetics of Hepatocellular Carcinoma. *Biomed Res Int* **2017**, 1609575 (2017).
90. Paula Santos, N., Colaco, A., Gil da Costa, R.M., Manuel Oliveira, M., Peixoto, F. & Alexandra Oliveira, P. N-diethylnitrosamine mouse hepatotoxicity: time-related effects on histology and oxidative stress. *Exp Toxicol Pathol* **66**, 429-36 (2014).
91. Janku, F., Kaseb, A.O., Tsimberidou, A.M., Wolff, R.A. & Kurzrock, R. Identification of novel therapeutic targets in the PI3K/AKT/mTOR pathway in hepatocellular carcinoma using targeted next generation sequencing. *Oncotarget* **5**, 3012-22 (2014).
92. Li, L., Zhao, G.D., Shi, Z., Qi, L.L., Zhou, L.Y. & Fu, Z.X. The Ras/Raf/MEK/ERK signaling pathway and its role in the occurrence and development of HCC. *Oncol Lett* **12**, 3045-3050 (2016).
93. Ramesh, V., Selvarasu, K., Pandian, J., Myilsamy, S., Shanmugasundaram, C. & Ganesan, K. NFkappaB activation demarcates a subset of hepatocellular carcinoma patients for targeted therapy. *Cell Oncol (Dordr)* **39**, 523-536 (2016).
94. Thorgeirsson, S.S. & Grisham, J.W. Molecular pathogenesis of human hepatocellular carcinoma. *Nat Genet* **31**, 339-46 (2002).
95. Kawai-Kitahata, F., Asahina, Y., Tanaka, S., Kakinuma, S., Murakawa, M., Nitta, S. et al. Comprehensive analyses of mutations and hepatitis B virus integration in hepatocellular carcinoma with clinicopathological features. *J Gastroenterol* **51**, 473-86 (2016).
96. Banerjee, A., Ray, R.B. & Ray, R. Oncogenic potential of hepatitis C virus proteins. *Viruses* **2**, 2108-33 (2010).
97. Mathew, M.A., Kurian, S.C., Varghese, A.P., Oommen, S. & G, M. HBx Gene Mutations in Hepatitis B Virus and Hepatocellular Carcinoma. *Gastroenterology Res* **7**, 1-4 (2014).

98. Testino, G., Leone, S. & Borro, P. Alcohol and hepatocellular carcinoma: a review and a point of view. *World J Gastroenterol* **20**, 15943-54 (2014).
99. Barash, H., E, R.G., Edrei, Y., Ella, E., Israel, A., Cohen, I. et al. Accelerated carcinogenesis following liver regeneration is associated with chronic inflammation-induced double-strand DNA breaks. *Proc Natl Acad Sci U S A* **107**, 2207-12 (2010).
100. Li, H. & Zhang, L. Liver regeneration microenvironment of hepatocellular carcinoma for prevention and therapy. *Oncotarget* **8**, 1805-1813 (2017).
101. Stauffer, J.K., Scarzello, A.J., Jiang, Q. & Wiltrout, R.H. Chronic inflammation, immune escape, and oncogenesis in the liver: a unique neighborhood for novel intersections. *Hepatology* **56**, 1567-74 (2012).
102. Matsumoto, T., Takai, A., Eso, Y., Kinoshita, K., Manabe, T., Seno, H. et al. Proliferating EpCAM-Positive Ductal Cells in the Inflamed Liver Give Rise to Hepatocellular Carcinoma. *Cancer Res* **77**, 6131-6143 (2017).
103. Nio, K., Yamashita, T. & Kaneko, S. The evolving concept of liver cancer stem cells. *Mol Cancer* **16**, 4 (2017).
104. Worns, M.A. & Galle, P.R. HCC therapies--lessons learned. *Nat Rev Gastroenterol Hepatol* **11**, 447-52 (2014).
105. Bruix, J., Reig, M. & Sherman, M. Evidence-Based Diagnosis, Staging, and Treatment of Patients With Hepatocellular Carcinoma. *Gastroenterology* **150**, 835-53 (2016).
106. Sapisochin, G. & Bruix, J. Liver transplantation for hepatocellular carcinoma: outcomes and novel surgical approaches. *Nat Rev Gastroenterol Hepatol* **14**, 203-217 (2017).
107. Raoul, J.L., Kudo, M., Finn, R.S., Edeline, J., Reig, M. & Galle, P.R. Systemic therapy for intermediate and advanced hepatocellular carcinoma: Sorafenib and beyond. *Cancer Treat Rev* **68**, 16-24 (2018).
108. da Motta Girardi, D., Correa, T.S., Crosara Teixeira, M. & Dos Santos Fernandes, G. Hepatocellular Carcinoma: Review of Targeted and Immune Therapies. *J Gastrointest Cancer* (2018).
109. Llovet, J.M., Ricci, S., Mazzaferro, V., Hilgard, P., Gane, E., Blanc, J.F. et al. Sorafenib in advanced hepatocellular carcinoma. *N Engl J Med* **359**, 378-90 (2008).
110. Cheng, A.L., Kang, Y.K., Chen, Z., Tsao, C.J., Qin, S., Kim, J.S. et al. Efficacy and safety of sorafenib in patients in the Asia-Pacific region with advanced hepatocellular carcinoma: a phase III randomised, double-blind, placebo-controlled trial. *Lancet Oncol* **10**, 25-34 (2009).
111. Kudo, M., Finn, R.S., Qin, S., Han, K.H., Ikeda, K., Piscaglia, F. et al. Lenvatinib versus sorafenib in first-line treatment of patients with unresectable hepatocellular carcinoma: a randomised phase 3 non-inferiority trial. *Lancet* **391**, 1163-1173 (2018).
112. Bruix, J., Qin, S., Merle, P., Granito, A., Huang, Y.H., Bodoky, G. et al. Regorafenib for patients with hepatocellular carcinoma who progressed on sorafenib treatment (RESORCE): a randomised, double-blind, placebo-controlled, phase 3 trial. *Lancet* **389**, 56-66 (2017).
113. Yang, Y. Cancer immunotherapy: harnessing the immune system to battle cancer. *J Clin Invest* **125**, 3335-7 (2015).
114. Contratto, M. & Wu, J. Targeted therapy or immunotherapy? Optimal treatment in hepatocellular carcinoma. *World J Gastrointest Oncol* **10**, 108-114 (2018).

115. El-Khoueiry, A.B., Sangro, B., Yau, T., Crocenzi, T.S., Kudo, M., Hsu, C. et al. Nivolumab in patients with advanced hepatocellular carcinoma (CheckMate 040): an open-label, non-comparative, phase 1/2 dose escalation and expansion trial. *Lancet* **389**, 2492-2502 (2017).
116. Robinson, M.W., Harmon, C. & O'Farrelly, C. Liver immunology and its role in inflammation and homeostasis. *Cell Mol Immunol* **13**, 267-76 (2016).
117. Schulz, C., Gomez Perdiguero, E., Chorro, L., Szabo-Rogers, H., Cagnard, N., Kierdorf, K. et al. A lineage of myeloid cells independent of Myb and hematopoietic stem cells. *Science* **336**, 86-90 (2012).
118. Zimmermann, H.W., Trautwein, C. & Tacke, F. Functional role of monocytes and macrophages for the inflammatory response in acute liver injury. *Front Physiol* **3**, 56 (2012).
119. Zigmond, E., Samia-Grinberg, S., Pasmanik-Chor, M., Brazowski, E., Shibolet, O., Halpern, Z. et al. Infiltrating monocyte-derived macrophages and resident kupffer cells display different ontogeny and functions in acute liver injury. *J Immunol* **193**, 344-53 (2014).
120. Dixon, L.J., Barnes, M., Tang, H., Pritchard, M.T. & Nagy, L.E. Kupffer cells in the liver. *Compr Physiol* **3**, 785-97 (2013).
121. Willekens, F.L., Werre, J.M., Kruijt, J.K., Roerdinkholder-Stoelwinder, B., Groenen-Dopp, Y.A., van den Bos, A.G. et al. Liver Kupffer cells rapidly remove red blood cell-derived vesicles from the circulation by scavenger receptors. *Blood* **105**, 2141-5 (2005).
122. Li, P., He, K., Li, J., Liu, Z. & Gong, J. The role of Kupffer cells in hepatic diseases. *Mol Immunol* **85**, 222-229 (2017).
123. Zanoni, P., Velagapudi, S., Yalcinkaya, M., Rohrer, L. & von Eckardstein, A. Endocytosis of lipoproteins. *Atherosclerosis* **275**, 273-295 (2018).
124. Remmerie, A. & Scott, C.L. Macrophages and lipid metabolism. *Cell Immunol* (2018).
125. Matsuura, K., Ishida, T., Setoguchi, M., Higuchi, Y., Akizuki, S. & Yamamoto, S. Upregulation of mouse CD14 expression in Kupffer cells by lipopolysaccharide. *J Exp Med* **179**, 1671-6 (1994).
126. Shimazu, R., Akashi, S., Ogata, H., Nagai, Y., Fukudome, K., Miyake, K. et al. MD-2, a molecule that confers lipopolysaccharide responsiveness on Toll-like receptor 4. *J Exp Med* **189**, 1777-82 (1999).
127. Nenseter, M.S., Gudmundsen, O., Roos, N., Maelandsmo, G., Drevon, C.A. & Berg, T. Role of liver endothelial and Kupffer cells in clearing low density lipoprotein from blood in hypercholesterolemic rabbits. *J Lipid Res* **33**, 867-77 (1992).
128. Kamps, J.A., Kruijt, J.K., Kuiper, J. & Van Berkel, T.J. Uptake and degradation of human low-density lipoprotein by human liver parenchymal and Kupffer cells in culture. *Biochem J* **276 (Pt 1)**, 135-40 (1991).
129. Kunjathoor, V.V., Febbraio, M., Podrez, E.A., Moore, K.J., Andersson, L., Koehn, S. et al. Scavenger receptors class A-I/II and CD36 are the principal receptors responsible for the uptake of modified low density lipoprotein leading to lipid loading in macrophages. *J Biol Chem* **277**, 49982-8 (2002).
130. Bieghs, V., Verheyen, F., van Gorp, P.J., Hendrikx, T., Wouters, K., Lutjohann, D. et al. Internalization of modified lipids by CD36 and SR-A leads to hepatic inflammation and lysosomal cholesterol storage in Kupffer cells. *PLoS One* **7**, e34378 (2012).

131. Bieghs, V., Walenbergh, S.M., Hendrikx, T., van Gorp, P.J., Verheyen, F., Olde Damink, S.W. et al. Trapping of oxidized LDL in lysosomes of Kupffer cells is a trigger for hepatic inflammation. *Liver Int* **33**, 1056-61 (2013).
132. Biswas, S.K. & Mantovani, A. Macrophage plasticity and interaction with lymphocyte subsets: cancer as a paradigm. *Nat Immunol* **11**, 889-96 (2010).
133. Ju, C., Reilly, T.P., Bourdi, M., Radonovich, M.F., Brady, J.N., George, J.W. et al. Protective role of Kupffer cells in acetaminophen-induced hepatic injury in mice. *Chem Res Toxicol* **15**, 1504-13 (2002).
134. Ringelhan, M., Pfister, D., O'Connor, T., Pikarsky, E. & Heikenwalder, M. The immunology of hepatocellular carcinoma. *Nat Immunol* **19**, 222-232 (2018).
135. Yu, L.X. & Schwabe, R.F. The gut microbiome and liver cancer: mechanisms and clinical translation. *Nat Rev Gastroenterol Hepatol* **14**, 527-539 (2017).
136. Beutler, B.A. TLRs and innate immunity. *Blood* **113**, 1399-407 (2009).
137. Seo, Y.S. & Shah, V.H. The role of gut-liver axis in the pathogenesis of liver cirrhosis and portal hypertension. *Clin Mol Hepatol* **18**, 337-46 (2012).
138. Pinero, P., Juanola, O., Caparros, E., Zapater, P., Gimenez, P., Gonzalez-Navajas, J.M. et al. Toll-like receptor polymorphisms compromise the inflammatory response against bacterial antigen translocation in cirrhosis. *Sci Rep* **7**, 46425 (2017).
139. Liu, S., Gallo, D.J., Green, A.M., Williams, D.L., Gong, X., Shapiro, R.A. et al. Role of toll-like receptors in changes in gene expression and NF-kappa B activation in mouse hepatocytes stimulated with lipopolysaccharide. *Infect Immun* **70**, 3433-42 (2002).
140. Paik, Y.H., Schwabe, R.F., Bataller, R., Russo, M.P., Jobin, C. & Brenner, D.A. Toll-like receptor 4 mediates inflammatory signaling by bacterial lipopolysaccharide in human hepatic stellate cells. *Hepatology* **37**, 1043-55 (2003).
141. Gomez-Hurtado, I., Such, J. & Frances, R. Microbiome and bacterial translocation in cirrhosis. *Gastroenterol Hepatol* **39**, 687-696 (2016).
142. Bellot, P., Garcia-Pagan, J.C., Frances, R., Abraldes, J.G., Navasa, M., Perez-Mateo, M. et al. Bacterial DNA translocation is associated with systemic circulatory abnormalities and intrahepatic endothelial dysfunction in patients with cirrhosis. *Hepatology* **52**, 2044-52 (2010).
143. Shibolet, O. & Podolsky, D.K. TLRs in the Gut. IV. Negative regulation of Toll-like receptors and intestinal homeostasis: addition by subtraction. *Am J Physiol Gastrointest Liver Physiol* **292**, G1469-73 (2007).
144. Gomez-Hurtado, I., Such, J., Sanz, Y. & Frances, R. Gut microbiota-related complications in cirrhosis. *World J Gastroenterol* **20**, 15624-31 (2014).
145. Dapito, D.H., Mencin, A., Gwak, G.Y., Pradere, J.P., Jang, M.K., Mederacke, I. et al. Promotion of hepatocellular carcinoma by the intestinal microbiota and TLR4. *Cancer Cell* **21**, 504-16 (2012).
146. Li, Z., Yang, S., Lin, H., Huang, J., Watkins, P.A., Moser, A.B. et al. Probiotics and antibodies to TNF inhibit inflammatory activity and improve nonalcoholic fatty liver disease. *Hepatology* **37**, 343-50 (2003).
147. Rivera, C.A., Adegboyega, P., van Rooijen, N., Tagalicud, A., Allman, M. & Wallace, M. Toll-like receptor-4 signaling and Kupffer cells play pivotal roles in the pathogenesis of non-alcoholic steatohepatitis. *J Hepatol* **47**, 571-9 (2007).
148. Hua, J., Qiu, D.K., Li, J.Q., Li, E.L., Chen, X.Y. & Peng, Y.S. Expression of Toll-like receptor 4 in rat liver during the course of carbon tetrachloride-induced liver injury. *J Gastroenterol Hepatol* **22**, 862-9 (2007).

149. Pelham, C.J. & Agrawal, D.K. Emerging roles for triggering receptor expressed on myeloid cells receptor family signaling in inflammatory diseases. *Expert Rev Clin Immunol* **10**, 243-56 (2014).
150. Genua, M., Rutella, S., Correale, C. & Danese, S. The triggering receptor expressed on myeloid cells (TREM) in inflammatory bowel disease pathogenesis. *J Transl Med* **12**, 293 (2014).
151. Sharif, O. & Knapp, S. From expression to signaling: roles of TREM-1 and TREM-2 in innate immunity and bacterial infection. *Immunobiology* **213**, 701-13 (2008).
152. Kober, D.L. & Brett, T.J. TREM2-Ligand Interactions in Health and Disease. *J Mol Biol* **429**, 1607-1629 (2017).
153. Bouchon, A., Dietrich, J. & Colonna, M. Cutting edge: inflammatory responses can be triggered by TREM-1, a novel receptor expressed on neutrophils and monocytes. *J Immunol* **164**, 4991-5 (2000).
154. Bouchon, A., Facchetti, F., Weigand, M.A. & Colonna, M. TREM-1 amplifies inflammation and is a crucial mediator of septic shock. *Nature* **410**, 1103-7 (2001).
155. Zysset, D., Weber, B., Rihs, S., Brasseit, J., Freigang, S., Riether, C. et al. TREM-1 links dyslipidemia to inflammation and lipid deposition in atherosclerosis. *Nat Commun* **7**, 13151 (2016).
156. Schenk, M., Bouchon, A., Seibold, F. & Mueller, C. TREM-1--expressing intestinal macrophages crucially amplify chronic inflammation in experimental colitis and inflammatory bowel diseases. *J Clin Invest* **117**, 3097-106 (2007).
157. Saurer, L., Zysset, D., Rihs, S., Mager, L., Gusberti, M., Simillion, C. et al. TREM-1 promotes intestinal tumorigenesis. *Sci Rep* **7**, 14870 (2017).
158. Zhou, J., Chai, F., Lu, G., Hang, G., Chen, C., Chen, X. et al. TREM-1 inhibition attenuates inflammation and tumor within the colon. *Int Immunopharmacol* **17**, 155-61 (2013).
159. Zhang, G., Liu, H., Huang, J., Chen, S., Pan, X., Huang, H. et al. TREM-1low is a novel characteristic for tumor-associated macrophages in lung cancer. *Oncotarget* **7**, 40508-40517 (2016).
160. Yuan, Z., Mehta, H.J., Mohammed, K., Nasreen, N., Roman, R., Brantly, M. et al. TREM-1 is induced in tumor associated macrophages by cyclo-oxygenase pathway in human non-small cell lung cancer. *PLoS One* **9**, e94241 (2014).
161. Sigalov, A.B. A novel ligand-independent peptide inhibitor of TREM-1 suppresses tumor growth in human lung cancer xenografts and prolongs survival of mice with lipopolysaccharide-induced septic shock. *Int Immunopharmacol* **21**, 208-19 (2014).
162. Ho, C.C., Liao, W.Y., Wang, C.Y., Lu, Y.H., Huang, H.Y., Chen, H.Y. et al. TREM-1 expression in tumor-associated macrophages and clinical outcome in lung cancer. *Am J Respir Crit Care Med* **177**, 763-70 (2008).
163. Wu, J., Li, J., Salcedo, R., Mivechi, N.F., Trinchieri, G. & Horuzsko, A. The proinflammatory myeloid cell receptor TREM-1 controls Kupffer cell activation and development of hepatocellular carcinoma. *Cancer Res* **72**, 3977-86 (2012).
164. Liao, R., Sun, T.W., Yi, Y., Wu, H., Li, Y.W., Wang, J.X. et al. Expression of TREM-1 in hepatic stellate cells and prognostic value in hepatitis B-related hepatocellular carcinoma. *Cancer Sci* **103**, 984-92 (2012).
165. Duan, M., Wang, Z.C., Wang, X.Y., Shi, J.Y., Yang, L.X., Ding, Z.B. et al. TREM-1, an inflammatory modulator, is expressed in hepatocellular carcinoma

cells and significantly promotes tumor progression. *Ann Surg Oncol* **22**, 3121-9 (2015).
166. Washington, A.V., Schubert, R.L., Quigley, L., Disipio, T., Feltz, R., Cho, E.H. et al. A TREM family member, TLT-1, is found exclusively in the alpha-granules of megakaryocytes and platelets. *Blood* **104**, 1042-7 (2004).
167. Barrow, A.D., Astoul, E., Floto, A., Brooke, G., Relou, I.A., Jennings, N.S. et al. Cutting edge: TREM-like transcript-1, a platelet immunoreceptor tyrosine-based inhibition motif encoding costimulatory immunoreceptor that enhances, rather than inhibits, calcium signaling via SHP-2. *J Immunol* **172**, 5838-42 (2004).
168. Derive, M., Bouazza, Y., Sennoun, N., Marchionni, S., Quigley, L., Washington, V. et al. Soluble TREM-like transcript-1 regulates leukocyte activation and controls microbial sepsis. *J Immunol* **188**, 5585-92 (2012).
169. Washington, A.V., Gibot, S., Acevedo, I., Gattis, J., Quigley, L., Feltz, R. et al. TREM-like transcript-1 protects against inflammation-associated hemorrhage by facilitating platelet aggregation in mice and humans. *J Clin Invest* **119**, 1489-501 (2009).
170. Giomarelli, B., Washington, V.A., Chisholm, M.M., Quigley, L., McMahon, J.B., Mori, T. et al. Inhibition of thrombin-induced platelet aggregation using human single-chain Fv antibodies specific for TREM-like transcript-1. *Thromb Haemost* **97**, 955-63 (2007).
171. Gattis, J.L., Washington, A.V., Chisholm, M.M., Quigley, L., Szyk, A., McVicar, D.W. et al. The structure of the extracellular domain of triggering receptor expressed on myeloid cells like transcript-1 and evidence for a naturally occurring soluble fragment. *J Biol Chem* **281**, 13396-403 (2006).
172. Rivera-Chavez, F.A. & Minei, J.P. Soluble triggering receptor expressed on myeloid cells-1 is an early marker of infection in the surgical intensive care unit. *Surg Infect (Larchmt)* **10**, 435-9 (2009).
173. Yoon, S.H., Lee, Y.D., Ha, J., Lee, Y. & Kim, H.H. TLT-1s, alternative transcripts of triggering receptor expressed on myeloid cell-like transcript-1 (TLT-1), Inhibits the triggering receptor expressed on myeloid cell-2 (TREM-2)-mediated signaling pathway during osteoclastogenesis. *J Biol Chem* **287**, 29620-6 (2012).
174. Thomas, K.A., King, R.G., Sestero, C.M. & Justement, L.B. TREM-like transcript 2 is stored in human neutrophil primary granules and is up-regulated in response to inflammatory mediators. *J Leukoc Biol* **100**, 177-84 (2016).
175. Hashiguchi, M., Kobori, H., Ritprajak, P., Kamimura, Y., Kozono, H. & Azuma, M. Triggering receptor expressed on myeloid cell-like transcript 2 (TLT-2) is a counter-receptor for B7-H3 and enhances T cell responses. *Proc Natl Acad Sci U S A* **105**, 10495-500 (2008).
176. Kobori, H., Hashiguchi, M., Piao, J., Kato, M., Ritprajak, P. & Azuma, M. Enhancement of effector CD8+ T-cell function by tumour-associated B7-H3 and modulation of its counter-receptor triggering receptor expressed on myeloid cell-like transcript 2 at tumour sites. *Immunology* **130**, 363-73 (2010).
177. Leitner, J., Klauser, C., Pickl, W.F., Stockl, J., Majdic, O., Bardet, A.F. et al. B7-H3 is a potent inhibitor of human T-cell activation: No evidence for B7-H3 and TREML2 interaction. *Eur J Immunol* **39**, 1754-64 (2009).
178. Yan, R., Yang, S., Gu, A., Zhan, F., He, C., Qin, C. et al. Murine b7-h3 is a co-stimulatory molecule for T cell activation. *Monoclon Antib Immunodiagn Immunother* **32**, 395-8 (2013).

179. Halpert, M.M., Thomas, K.A., King, R.G. & Justement, L.B. TLT2 potentiates neutrophil antibacterial activity and chemotaxis in response to G protein-coupled receptor-mediated signaling. *J Immunol* **187**, 2346-55 (2011).
180. de Freitas, A., Banerjee, S., Xie, N., Cui, H., Davis, K.I., Friggeri, A. et al. Identification of TLT2 as an engulfment receptor for apoptotic cells. *J Immunol* **188**, 6381-8 (2012).
181. Schlepckow, K., Kleinberger, G., Fukumori, A., Feederle, R., Lichtenthaler, S.F., Steiner, H. et al. An Alzheimer-associated TREM2 variant occurs at the ADAM cleavage site and affects shedding and phagocytic function. *EMBO Mol Med* **9**, 1356-1365 (2017).
182. Wunderlich, P., Glebov, K., Kemmerling, N., Tien, N.T., Neumann, H. & Walter, J. Sequential proteolytic processing of the triggering receptor expressed on myeloid cells-2 (TREM2) protein by ectodomain shedding and gamma-secretase-dependent intramembranous cleavage. *J Biol Chem* **288**, 33027-36 (2013).
183. Hamerman, J.A., Jarjoura, J.R., Humphrey, M.B., Nakamura, M.C., Seaman, W.E. & Lanier, L.L. Cutting edge: inhibition of TLR and FcR responses in macrophages by triggering receptor expressed on myeloid cells (TREM)-2 and DAP12. *J Immunol* **177**, 2051-5 (2006).
184. Turnbull, I.R., Gilfillan, S., Cella, M., Aoshi, T., Miller, M., Piccio, L. et al. Cutting edge: TREM-2 attenuates macrophage activation. *J Immunol* **177**, 3520-4 (2006).
185. Bouchon, A., Hernandez-Munain, C., Cella, M. & Colonna, M. A DAP12-mediated pathway regulates expression of CC chemokine receptor 7 and maturation of human dendritic cells. *J Exp Med* **194**, 1111-22 (2001).
186. Correale, C., Genua, M., Vetrano, S., Mazzini, E., Martinoli, C., Spinelli, A. et al. Bacterial sensor triggering receptor expressed on myeloid cells-2 regulates the mucosal inflammatory response. *Gastroenterology* **144**, 346-356 e3 (2013).
187. Takahashi, K., Prinz, M., Stagi, M., Chechneva, O. & Neumann, H. TREM2-transduced myeloid precursors mediate nervous tissue debris clearance and facilitate recovery in an animal model of multiple sclerosis. *PLoS Med* **4**, e124 (2007).
188. Takahashi, K., Rochford, C.D. & Neumann, H. Clearance of apoptotic neurons without inflammation by microglial triggering receptor expressed on myeloid cells-2. *J Exp Med* **201**, 647-57 (2005).
189. Wang, Y., Cella, M., Mallinson, K., Ulrich, J.D., Young, K.L., Robinette, M.L. et al. TREM2 lipid sensing sustains the microglial response in an Alzheimer's disease model. *Cell* **160**, 1061-71 (2015).
190. N'Diaye, E.N., Branda, C.S., Branda, S.S., Nevarez, L., Colonna, M., Lowell, C. et al. TREM-2 (triggering receptor expressed on myeloid cells 2) is a phagocytic receptor for bacteria. *J Cell Biol* **184**, 215-23 (2009).
191. Gawish, R., Martins, R., Bohm, B., Wimberger, T., Sharif, O., Lakovits, K. et al. Triggering receptor expressed on myeloid cells-2 fine-tunes inflammatory responses in murine Gram-negative sepsis. *FASEB J* **29**, 1247-57 (2015).
192. Sharif, O., Gawish, R., Warszawska, J.M., Martins, R., Lakovits, K., Hladik, A. et al. The triggering receptor expressed on myeloid cells 2 inhibits complement component 1q effector mechanisms and exerts detrimental effects during pneumococcal pneumonia. *PLoS Pathog* **10**, e1004167 (2014).
193. Paloneva, J., Manninen, T., Christman, G., Hovanes, K., Mandelin, J., Adolfsson, R. et al. Mutations in two genes encoding different subunits of a receptor signaling

complex result in an identical disease phenotype. *Am J Hum Genet* **71**, 656-62 (2002).
194. Xing, J., Titus, A.R. & Humphrey, M.B. The TREM2-DAP12 signaling pathway in Nasu-Hakola disease: a molecular genetics perspective. *Res Rep Biochem* **5**, 89-100 (2015).
195. Cella, M., Buonsanti, C., Strader, C., Kondo, T., Salmaggi, A. & Colonna, M. Impaired differentiation of osteoclasts in TREM-2-deficient individuals. *J Exp Med* **198**, 645-51 (2003).
196. Jonsson, T., Stefansson, H., Steinberg, S., Jonsdottir, I., Jonsson, P.V., Snaedal, J. et al. Variant of TREM2 associated with the risk of Alzheimer's disease. *N Engl J Med* **368**, 107-16 (2013).
197. Guerreiro, R., Wojtas, A., Bras, J., Carrasquillo, M., Rogaeva, E., Majounie, E. et al. TREM2 variants in Alzheimer's disease. *N Engl J Med* **368**, 117-27 (2013).
198. Carmona, S., Zahs, K., Wu, E., Dakin, K., Bras, J. & Guerreiro, R. The role of TREM2 in Alzheimer's disease and other neurodegenerative disorders. *Lancet Neurol* **17**, 721-730 (2018).
199. Ulland, T.K., Song, W.M., Huang, S.C., Ulrich, J.D., Sergushichev, A., Beatty, W.L. et al. TREM2 Maintains Microglial Metabolic Fitness in Alzheimer's Disease. *Cell* **170**, 649-663 e13 (2017).
200. Song, W.M., Joshita, S., Zhou, Y., Ulland, T.K., Gilfillan, S. & Colonna, M. Humanized TREM2 mice reveal microglia-intrinsic and -extrinsic effects of R47H polymorphism. *J Exp Med* **215**, 745-760 (2018).
201. Benitez, B.A., Jin, S.C., Guerreiro, R., Graham, R., Lord, J., Harold, D. et al. Missense variant in TREML2 protects against Alzheimer's disease. *Neurobiol Aging* **35**, 1510 e19-26 (2014).
202. Zheng, H., Liu, C.C., Atagi, Y., Chen, X.F., Jia, L., Yang, L. et al. Opposing roles of the triggering receptor expressed on myeloid cells 2 and triggering receptor expressed on myeloid cells-like transcript 2 in microglia activation. *Neurobiol Aging* **42**, 132-41 (2016).
203. Seno, H., Miyoshi, H., Brown, S.L., Geske, M.J., Colonna, M. & Stappenbeck, T.S. Efficient colonic mucosal wound repair requires Trem2 signaling. *Proc Natl Acad Sci U S A* **106**, 256-61 (2009).
204. Yao, Y., Li, H., Chen, J., Xu, W., Yang, G., Bao, Z. et al. TREM-2 serves as a negative immune regulator through Syk pathway in an IL-10 dependent manner in lung cancer. *Oncotarget* **7**, 29620-34 (2016).
205. Zhang, X., Wang, W., Li, P., Wang, X. & Ni, K. High TREM2 expression correlates with poor prognosis in gastric cancer. *Hum Pathol* **72**, 91-99 (2018).
206. Wang, X.Q., Tao, B.B., Li, B., Wang, X.H., Zhang, W.C., Wan, L. et al. Overexpression of TREM2 enhances glioma cell proliferation and invasion: a therapeutic target in human glioma. *Oncotarget* **7**, 2354-66 (2016).
207. Zhang, H., Sheng, L., Tao, J., Chen, R., Li, Y., Sun, Z. et al. Depletion of the triggering receptor expressed on myeloid cells 2 inhibits progression of renal cell carcinoma via regulating related protein expression and PTEN-PI3K/Akt pathway. *Int J Oncol* **49**, 2498-2506 (2016).
208. Chen, L.C., Laskin, J.D., Gordon, M.K. & Laskin, D.L. Regulation of TREM expression in hepatic macrophages and endothelial cells during acute endotoxemia. *Exp Mol Pathol* **84**, 145-55 (2008).
209. Goncalves, L.A., Rodrigues-Duarte, L., Rodo, J., Vieira de Moraes, L., Marques, I. & Penha-Goncalves, C. TREM2 governs Kupffer cell activation and explains

belr1 genetic resistance to malaria liver stage infection. *Proc Natl Acad Sci U S A* **110**, 19531-6 (2013).
210. Gieling, R.G., Elsharkawy, A.M., Caamano, J.H., Cowie, D.E., Wright, M.C., Ebrahimkhani, M.R. et al. The c-Rel subunit of nuclear factor-kappaB regulates murine liver inflammation, wound-healing, and hepatocyte proliferation. *Hepatology* **51**, 922-31 (2010).
211. Higgins, G.M. & Anderson, R.M. Experimental pathology of the liver I Restoration of the liver of the white rat following partial surgical removal. *Archives of Pathology* **12**, 186-202 (1931).
212. Mann, J., Chu, D.C., Maxwell, A., Oakley, F., Zhu, N.L., Tsukamoto, H. et al. MeCP2 controls an epigenetic pathway that promotes myofibroblast transdifferentiation and fibrosis. *Gastroenterology* **138**, 705-14, 714 e1-4 (2010).
213. Perugorria, M.J., Wilson, C.L., Zeybel, M., Walsh, M., Amin, S., Robinson, S. et al. Histone methyltransferase ASH1 orchestrates fibrogenic gene transcription during myofibroblast transdifferentiation. *Hepatology* **56**, 1129-39 (2012).
214. Perugorria, M.J., Murphy, L.B., Fullard, N., Chakraborty, J.B., Vyrla, D., Wilson, C.L. et al. Tumor progression locus 2/Cot is required for activation of extracellular regulated kinase in liver injury and toll-like receptor-induced TIMP-1 gene transcription in hepatic stellate cells in mice. *Hepatology* **57**, 1238-49 (2013).
215. Wisniewski, J.R., Zougman, A., Nagaraj, N. & Mann, M. Universal sample preparation method for proteome analysis. *Nat Methods* **6**, 359-62 (2009).
216. Tyanova, S., Temu, T., Sinitcyn, P., Carlson, A., Hein, M.Y., Geiger, T. et al. The Perseus computational platform for comprehensive analysis of (prote)omics data. *Nat Methods* **13**, 731-40 (2016).
217. Huang da, W., Sherman, B.T. & Lempicki, R.A. Systematic and integrative analysis of large gene lists using DAVID bioinformatics resources. *Nat Protoc* **4**, 44-57 (2009).
218. Fouts, D.E., Torralba, M., Nelson, K.E., Brenner, D.A. & Schnabl, B. Bacterial translocation and changes in the intestinal microbiome in mouse models of liver disease. *Journal of hepatology* **56**, 1283-92 (2012).
219. Gomez-Hurtado, I., Santacruz, A., Peiro, G., Zapater, P., Gutierrez, A., Perez-Mateo, M. et al. Gut microbiota dysbiosis is associated with inflammation and bacterial translocation in mice with CCl4-induced fibrosis. *PLoS One* **6**, e23037 (2011).
220. Guha, M. & Mackman, N. LPS induction of gene expression in human monocytes. *Cell Signal* **13**, 85-94 (2001).
221. McGill, M.R., Williams, C.D., Xie, Y., Ramachandran, A. & Jaeschke, H. Acetaminophen-induced liver injury in rats and mice: comparison of protein adducts, mitochondrial dysfunction, and oxidative stress in the mechanism of toxicity. *Toxicol Appl Pharmacol* **264**, 387-94 (2012).
222. Ye, D., Wang, Y., Li, H., Jia, W., Man, K., Lo, C.M. et al. Fibroblast growth factor 21 protects against acetaminophen-induced hepatotoxicity by potentiating peroxisome proliferator-activated receptor coactivator protein-1alpha-mediated antioxidant capacity in mice. *Hepatology* **60**, 977-89 (2014).
223. Lin, Z., Wu, F., Lin, S., Pan, X., Jin, L., Lu, T. et al. Adiponectin protects against acetaminophen-induced mitochondrial dysfunction and acute liver injury by promoting autophagy in mice. *J Hepatol* **61**, 825-31 (2014).
224. Brenner, C., Galluzzi, L., Kepp, O. & Kroemer, G. Decoding cell death signals in liver inflammation. *J Hepatol* **59**, 583-94 (2013).

225. Manibusan, M.K., Odin, M. & Eastmond, D.A. Postulated carbon tetrachloride mode of action: a review. *J Environ Sci Health C Environ Carcinog Ecotoxicol Rev* **25**, 185-209 (2007).
226. Das, M., Boerma, M., Goree, J.R., Lavoie, E.G., Fausther, M., Gubrij, I.B. et al. Pathological changes in pulmonary circulation in carbon tetrachloride (CCl4)-induced cirrhotic mice. *PLoS One* **9**, e96043 (2014).
227. Wilson, C.L., Jurk, D., Fullard, N., Banks, P., Page, A., Luli, S. et al. NFkappaB1 is a suppressor of neutrophil-driven hepatocellular carcinoma. *Nat Commun* **6**, 6818 (2015).
228. Thompson, A.I., Conroy, K.P. & Henderson, N.C. Hepatic stellate cells: central modulators of hepatic carcinogenesis. *BMC Gastroenterol* **15**, 63 (2015).
229. Yang, J.D., Nakamura, I. & Roberts, L.R. The tumor microenvironment in hepatocellular carcinoma: current status and therapeutic targets. *Semin Cancer Biol* **21**, 35-43 (2011).
230. Khawar, I.A., Park, J.K., Jung, E.S., Lee, M.A., Chang, S. & Kuh, H.J. Three Dimensional Mixed-Cell Spheroids Mimic Stroma-Mediated Chemoresistance and Invasive Migration in hepatocellular carcinoma. *Neoplasia* **20**, 800-812 (2018).
231. Jung, H.R., Kang, H.M., Ryu, J.W., Kim, D.S., Noh, K.H., Kim, E.S. et al. Cell Spheroids with Enhanced Aggressiveness to Mimic Human Liver Cancer In Vitro and In Vivo. *Sci Rep* **7**, 10499 (2017).
232. Russell, J.O. & Monga, S.P. Wnt/beta-Catenin Signaling in Liver Development, Homeostasis, and Pathobiology. *Annu Rev Pathol* **13**, 351-378 (2018).
233. Nusse, R. & Clevers, H. Wnt/beta-Catenin Signaling, Disease, and Emerging Therapeutic Modalities. *Cell* **169**, 985-999 (2017).
234. Otero, K., Shinohara, M., Zhao, H., Cella, M., Gilfillan, S., Colucci, A. et al. TREM2 and beta-catenin regulate bone homeostasis by controlling the rate of osteoclastogenesis. *J Immunol* **188**, 2612-21 (2012).
235. Zheng, H., Jia, L., Liu, C.C., Rong, Z., Zhong, L., Yang, L. et al. TREM2 Promotes Microglial Survival by Activating Wnt/beta-Catenin Pathway. *J Neurosci* **37**, 1772-1784 (2017).
236. Yin, M., Bradford, B.U., Wheeler, M.D., Uesugi, T., Froh, M., Goyert, S.M. et al. Reduced early alcohol-induced liver injury in CD14-deficient mice. *J Immunol* **166**, 4737-42 (2001).
237. Miura, K., Kodama, Y., Inokuchi, S., Schnabl, B., Aoyama, T., Ohnishi, H. et al. Toll-like receptor 9 promotes steatohepatitis by induction of interleukin-1beta in mice. *Gastroenterology* **139**, 323-34 e7 (2010).
238. Naugler, W.E., Sakurai, T., Kim, S., Maeda, S., Kim, K., Elsharkawy, A.M. et al. Gender disparity in liver cancer due to sex differences in MyD88-dependent IL-6 production. *Science* **317**, 121-4 (2007).
239. Mohamed, F.E., Al-Jehani, R.M., Minogue, S.S., Andreola, F., Winstanley, A., Olde Damink, S.W. et al. Effect of toll-like receptor 7 and 9 targeted therapy to prevent the development of hepatocellular carcinoma. *Liver Int* **35**, 1063-76 (2015).
240. Friedman, S.L. Hepatic stellate cells: protean, multifunctional, and enigmatic cells of the liver. *Physiol Rev* **88**, 125-72 (2008).
241. Higashiyama, R., Inagaki, Y., Hong, Y.Y., Kushida, M., Nakao, S., Niioka, M. et al. Bone marrow-derived cells express matrix metalloproteinases and contribute to regression of liver fibrosis in mice. *Hepatology* **45**, 213-22 (2007).

242. Jiang, J.X., Mikami, K., Venugopal, S., Li, Y. & Torok, N.J. Apoptotic body engulfment by hepatic stellate cells promotes their survival by the JAK/STAT and Akt/NF-kappaB-dependent pathways. *Journal of hepatology* **51**, 139-48 (2009).
243. Canbay, A., Taimr, P., Torok, N., Higuchi, H., Friedman, S. & Gores, G.J. Apoptotic body engulfment by a human stellate cell line is profibrogenic. *Laboratory investigation; a journal of technical methods and pathology* **83**, 655-63 (2003).
244. Mossanen, J.C., Krenkel, O., Ergen, C., Govaere, O., Liepelt, A., Puengel, T. et al. Chemokine (C-C motif) receptor 2-positive monocytes aggravate the early phase of acetaminophen-induced acute liver injury. *Hepatology* (2016).
245. Donthamsetty, S., Bhave, V.S., Mitra, M.S., Latendresse, J.R. & Mehendale, H.M. Nonalcoholic fatty liver sensitizes rats to carbon tetrachloride hepatotoxicity. *Hepatology* **45**, 391-403 (2007).
246. Wang, M., You, Q., Lor, K., Chen, F., Gao, B. & Ju, C. Chronic alcohol ingestion modulates hepatic macrophage populations and functions in mice. *J Leukoc Biol* **96**, 657-65 (2014).
247. Cantoni, C., Bollman, B., Licastro, D., Xie, M., Mikesell, R., Schmidt, R. et al. TREM2 regulates microglial cell activation in response to demyelination in vivo. *Acta Neuropathol* **129**, 429-47 (2015).
248. Park, M., Yi, J.W., Kim, E.M., Yoon, I.J., Lee, E.H., Lee, H.Y. et al. Triggering receptor expressed on myeloid cells 2 (TREM2) promotes adipogenesis and diet-induced obesity. *Diabetes* **64**, 117-27 (2015).
249. Zhang, X., Wang, W., Li, P., Wang, X. & Ni, K. High TREM2 expression correlates with poor prognosis in gastric cancer. *Hum Pathol* (2017).
250. Maeda, S., Kamata, H., Luo, J.L., Leffert, H. & Karin, M. IKKbeta couples hepatocyte death to cytokine-driven compensatory proliferation that promotes chemical hepatocarcinogenesis. *Cell* **121**, 977-90 (2005).
251. Botterweck, A.A., Verhagen, H., Goldbohm, R.A., Kleinjans, J. & van den Brandt, P.A. Intake of butylated hydroxyanisole and butylated hydroxytoluene and stomach cancer risk: results from analyses in the Netherlands Cohort Study. *Food Chem Toxicol* **38**, 599-605 (2000).
252. Bjelakovic, G., Nikolova, D., Gluud, L.L., Simonetti, R.G. & Gluud, C. Antioxidant supplements for prevention of mortality in healthy participants and patients with various diseases. *Cochrane Database Syst Rev*, CD007176 (2012).
253. Poljsak, B., Suput, D. & Milisav, I. Achieving the balance between ROS and antioxidants: when to use the synthetic antioxidants. *Oxid Med Cell Longev* **2013**, 956792 (2013).
254. Shi, J.H. & Line, P.D. Effect of liver regeneration on malignant hepatic tumors. *World J Gastroenterol* **20**, 16167-77 (2014).
255. Shi, J.H., Huitfeldt, H.S., Suo, Z.H. & Line, P.D. Growth of hepatocellular carcinoma in the regenerating liver. *Liver Transpl* **17**, 866-74 (2011).

APPENDIX

Publications within the PhD

Esparza-Baquer A, Labiano I, Sharif O, Oakley F, Rodrigues PM, Hijona E, Jiménez-Agüero R, Lacasta A, Zaki MY, O'Rourke CJ, Munoz-Garrido P, Andersen JB, Knapp S, Mann DA, Bujanda L, Banales JM and Perugorria MJ. Non-parenchymal TREM2 Halts Hepatocarcinogenesis Through the Inhibition of Liver Inflammation and DNA damage. In revision.

Perugorria MJ, Olaizola P, Labiano I, **Esparza-Baquer A**, Marzioni M, Marin JJG, Bujanda L, Banales JM. Wnt–β-catenin signalling in liver development, health and disease. Nat Rev Gastroenterol Hepatol 2018. Accepted. Review.

Perugorria MJ, **Esparza-Baquer A**, Oakley O, Labiano I, Korosec A, Jais A, Mann J, Tiniakos D, Santos-Laso A, Arbelaiz A, Gawish R, Sampedro A, Fontanellas A, Hijona E, Jiménez-Agüero R, Esterbauer H, Stoiber D, Bujanda L, Banales JM, Knapp S, Sharif O, and Mann DA. Non-parenchymal TREM-2 protects the liver from immune-mediated hepatocellular damage. Gut 2018. pii: gutjnl-2017-314107.

\# Nature Reviews Gastroenterology and Hepatology did an editorial about this paper: Ray K. Liver: A protective role for TREM2 in liver injury. Nat Rev Gastroenterol Hepatol. 201815(3):130-131. Editorial

Merino-Azpitarte M, Lozano E, Perugorria MJ, **Esparza-Baquer A**, Erice O, Santos-Laso A, O'Rourke CJ, Andersen JB, Jiménez-Agüero R, LaCasta A, Briz O, Jalan-Sakrikar N, Huebert RC, Thelen KM, Gradilone SA, Aransay AM, Lavín JL, Fernández-Barrena MG, Matheu A, Marzioni M, Gores GJ, Bujanda L, Marin JJG, and Banales JM. SOX17 Regulates Cholangiocyte Differentiation and Acts as a Tumor Suppressor in Cholangiocarcinoma. Journal of Hepatology 2017 J Hepatol. pii: S0168-8278(17)30114-9.

Perugorria MJ, Labiano I, **Esparza-Baquer A**, Marzioni M, Marin JJ, Bujanda L, Banales JM. Bile Acids in Polycystic Liver Diseases: Triggers of Disease Progression and Potential Solution for Treatment. Dig Dis. 2017;35(3):275-281.

Esparza-Baquer A, Labiano I, Bujanda L, Perugorria MJ, Banales JM. MicroRNAs in cholangiopathies: Potential diagnostic and therapeutic tools. Clin Res Hepatol Gastroenterol. 2016 40(1):15-27. Review.